IN VITRO ANALYSES OF MERKEL CELL POLYOMAVIRUS CELL BIOLOGY

by

Anna Guastafierro

Bachelors of Science in Biological Science, Holy Names University, 2007

Submitted to the Graduate Faculty of

University of Pittsburgh School of Medicine

Program in Integrative Molecular Biology

in partial fulfillment of the requirements for the degree of

Doctor of Philosophy

University of Pittsburgh

2013

UNIVERSITY OF PITTSBURGH

SCHOOL OF MEDICINE

This dissertation was presented

by

Anna Guastafierro

It was defended on

August 13th, 2013

and approved by

Jeffrey L. Brodsky, Ph.D., Professor, Department of Biological Sciences

James M. Pipas, Ph.D., Professor, Department of Biological Sciences

Frank J. Jenkins, Ph.D., Associate Professor, Department of Pathology

Anthony Schwacha, Ph.D., Associate Professor, Department of Biological Sciences

Dissertation Advisor: Patrick S. Moore, MD, MPH, Professor, Department of Microbiology and Molecular Genetics

IN VITRO ANALYSES OF MERKEL CELL POLYOMAVIRUS CELL BIOLOGY

Anna Guastafierro

University of Pittsburgh, 2013

The work described in this dissertation was initiated in 2008, shortly after the discovery of Merkel cell polyomavirus (MCV). MCV was discovered as clonally integrated in 80% of Merkel cell carcinoma (MCC) and tumor-derived viral genomes were found to harbor individual large T antigen (LT) truncating deletions. The work presented in this thesis focuses on two main features associated with MCV cell biology: (1) Viral replication requirements that promote viral origin replication in the context of full length MCV LT (chapter 3) and (2) cellular targets that enhance human fibroblast proliferation in the presence of tumor-derived full length LT (chapter 4). As part of these studies, the novel MCV-positive MCC cell line MS-1 was generated, and its cellular and viral features are presented here (chapter 2). MCC cell lines are useful tools that can be used to study MCV biology, and test therapeutic compounds *in vitro*, as well as in a xenograft setting *in vivo* as described in the appendix of this thesis. Within the past 6 years, 8 new human polyomaviruses have been identified through basic biological approaches, highlighting the possibility that other human malignancies may be associated with polyomaviral infections. The identification of MCV in association with an aggressive human cancer also underscores the relevance of basic research in understanding human disease.

TABLE OF CONTENTS

LIST OF TABLES

LIST OF FIGURES

ACKNOWLEDGMENTS

First and foremost, I would like to thank my mentors Dr. Patrick Moore and Dr. Yuan Chang. I am in deep gratitude to you for providing me with the opportunity to grow in my profession and establish myself as an independent scientist in your lab. I appreciate your patience and insightful advice on scientific matters. My graduate student experience in your lab has been invaluable for my future career. Thank you!

Next, I want to thank the current and past members of the Chang-Moore lab, who have provided me not only with a professional environment that was very supportive in my development as a scientist, but also have become a family away from home. I appreciate your guidance and will cherish memories of our times together in and outside of the lab for the rest of my life. I especially want to thank Masa for being a great mentor to me. I have learned so much from you.

I would like to thank my thesis committee members for your valuable advice throughout the past years. I have benefited from your scientific expertise, and I appreciate the time you have taken out of your busy schedules to serve on my thesis committee.

Last but not least, I would like to thank family and friends who have been a strong support of mine throughout the years. I want to thank my parents, Lena, Ciro, Luisa and Kensington for always believing in me and supporting me in whatever I

decided to do. You are my foundation in life, without which I could not have done any of this. I love you guys! Thank you Gene for being my best friend and confidant extraordinaire. You keep my spirits lifted and I appreciate every minute we spend together. I will miss you, but I know this is not the end of the road for us. You have a friend in me for life. I would like to thank Alex, Nathalie and Sarah for being my friends throughout the years and keeping in touch even when we are far away from each other. I also want to thank my PIMB friends, for a great graduate school experience. I especially want to thank Jelena and Reety for being awesome friends during my stay in Pittsburgh. I could not have made it without your advice and friendship. I will miss you!

1.0 INTRODUCTION

1.1 VIRUSES AND CANCER

1.1.1 History of tumor viruses

The field of tumor virology dates back to the 1911 discovery of the Avian Rous sarcoma virus (RSV) by Francis Peyton Rous (*1, 2*). Rous discovered that a chicken sarcoma could be transmitted from one chicken to another using a filtered cell-free tumor extract (*3*). This novel finding of an infectious agent that induces cancer represented an unrecognized concept in the field of cancer research at the time. Even though it was known since the 19th century that cancer was a cellular disease, its specific etiology was still unclear. The theory of an infectious cause was disregarded for over fifty years due to a failure to experimentally verify microbial pathogens as cancer causing agents. Even after Rous reported his findings of RSV-induced sarcomas in chickens, the scientific community at the time was not convinced that tumor viruses existed, or that they represented the causative agent for a number of human cancers. Opponents of this theory claimed that the cell-free extracts used by Rous to transmit sarcomas in chickens, were in fact not cell-free, or that chickens are not an appropriate model system to study human cancer.

However, Ludwik Gross' discoveries of the acutely transforming mouse leukemia retrovirus and the mouse polyomavirus (PyV), which causes many (poly) tumors (oma) in newborn mice (*4, 5*), lead to wider acceptance of the concept of viral tumorigenesis in the 1950s. In 1966 Rous finally received recognition for his groundbreaking work, and was awarded the Nobel Prize. Since then, studies centered around RSV and PyV, as well as other subsequently discovered tumor viruses, have contributed to major scientific advances including the discoveries of reverse transcriptase, as well as a number of cellular oncogenes and tumor suppressors.

1.1.2 Viruses and human cancer

Since the 1911 discovery of the avian tumor virus RSV, a total of seven tumor viruses have been discovered to cause human cancer. Viruses cause a total of 10-15% of cancers worldwide, including cancers of diverse cellular origins. Viral etiology of a cancer provides the unique opportunity to develop preventative, diagnostic and therapeutic tools that target viral proteins specifically. This has been utilized in developing vaccines against hepatitis B virus (HBV) and human papillomavirus (HPV) infections, resulting in a decrease of respective liver and cervical tumor incidents. Anthony Epstein, Yvonne Barr, and Bert Anchong discovered the first human tumor virus called Epstein-Barr virus (EBV) in 1964 (*6*). EBV is a herpesvirus found by electron microscopy of cell lines derived from Burkitt's lymphoma (Table 1). Burkitt's lymphoma is a cancer which predominately affects children from equatorial Africa and it is more common in immunosuppression, which is often related to malaria in this geographically confined area. Subsequent serological studies revealed the seemingly

contradictory fact that persistent EBV infection is ubiquitous, yet asymptomatic in adults worldwide. This posed the question of how such a common viral infection could cause a rare, geographically confined cancer (*7, 8*). In addition, a small number of Burkitt's lymphoma arising in developed countries are not associated with EBV (*9*). Shortly after its discovery, the research team surrounding Gertrude and Werner Henle demonstrated that EBV is capable of transforming primary B-cells (*10*). Nevertheless, it was not until 1997 that the International Agency for Research on Cancer (IARC) officially declared EBV as a human carcinogen (*7*). To understand the debate that resulted in a 30-year time delay until EBV was finally recognized as a human carcinogen, one must understand which criteria are used in order to demonstrate disease association.

To evaluate causality of an infectious agent in the context of a disease state, there are several standards that are used to examine the evidence at hand. These include Koch's postulates published in 1890 as well as Hill's criteria published in the 1960's. Koch's postulates originate from his work on bacterial pathogens including anthrax and tuberculosis (*11*). They include the following requirements: 1) The infectious agent has to occur in every case of the disease, 2) it does not occur in any other disease, and 3) it can be isolated as pure cultures in vitro, and when re-introduced into susceptible laboratory animals results in the same disease outcome (*11*). Koch's postulates cannot be applied in the case of EBV or other tumor viruses, since it is not always possible to isolate them as pure cultures or introduce them into experimental animals and always observe the same disease state. Hill's criteria to evaluate the observed association of a pathogen with a disease state include 1) strength, 2) consistency, 3) specificity, 4) temporality, 5) biological gradient, 6) plausibility, 7)

coherence, and 8) experimental evidence of association (*12*). Hill's criteria were established to evaluate the relationship between smoking cigarettes and lung cancer, but in the field of tumor virology some aspects are not applicable.

With our current knowledge of cancer being a multi-step disease that results from a combination of cellular changes and environmental factors, we can explain how a common viral infection may cause a rare cancer in a subset of individuals. In the case of EBV and other tumor viruses, the immune status of the infected individual plays a major role in determining disease state. In immunocompetent individuals, the viral infection is contained and regulated by the immune cells. However, in the case of immunosuppression, as seen in elderly people, as well as transplant and AIDS patients, the virus is able to re-emerge, and viral protein expression may lead to cell transformation and consequent tumorigenesis.

As more human tumor viruses were discovered over time **(Table 1)**, it became apparent that tumor viruses usually do not replicate as virions within the tumor cells, but instead exist either as latent episomes or integrate into the host cell genome. To date, 7 human tumor viruses have been identified using different experimental techniques **(Table 1)**. They belong to different classes of viruses, and cause tumors in a number of different cell types **(Table 1)**. The following paragraphs will provide a brief description of each tumor virus discovered subsequent to EBV.

Shortly after the discovery of EBV, Blumberg and colleagues identified a new antigen named Australia (Au) antigen in the serum of an Australian aborigine (*13*). They found the Au antigen to be present in the sera of patients with acute or chronic hepatitis (*14*), and in 1968 Alfred Prince demonstrated that Au is the surface antigen of HBV (*15*),

the virus that causes serum hepatitis. Due to persistent, yet asymptomatic HBV infection in healthy individuals, linking HBV infection to hepatocellular carcinoma (HCC) proved to be difficult once again. In 1975 Blumberg and colleagues described a link between HBV infection and HCC development, and proposed vaccination against HBV using the Au antigen (*16*). Merck eventually started producing an HBV vaccine commercially using recombinant Au subunit produced in yeast, which is still used today. Vaccination efforts worldwide have reduced HBV-induced acute and chronic hepatitis, as well as HCC incidents (*17, 18*). HBV-induced liver disease causes > 300,000 deaths each year, but expanding routine vaccination regimens during early childhood worldwide will likely reduce this death toll further in the future. Previous to the identification of HBV, Feinstone and colleagues identified the picornavirus hepatitis A virus (HAV) in 1973 as an infectious agent that induces acute hepatitis (*19*). However, in contrast to HBV, HAV infection is not persistent, and not involved in HCC (*20*).

The mechanism by which HBV contributes to HCC is not exactly clear. Lack of an appropriate experimental model system that mimics the human host has hindered research progression in this field. However, it is well known that chronic viral infection with HBV leads to active viral replication in liver cells and viremia. The production of viral proteins in chronically infected hepatocytes leads to a persistent immune response and destruction of these cells. This leads to a much more rapid turnover of liver cells, which are usually long-lived with half-lives of 6-12 months (*21*). Some studies have indicated the HBV protein HBx as a potential viral oncogene, but studies utilizing different experimental systems have failed to yield reproducible results (*21, 22*).

Table 1. Human Tumorviruses

Virus	Genome	Method of Identification	Associated cancers	Year identified	Reference
Epstein-Barr virus (EBV)*	Double-stranded DNA herpesvirus	Electron microscopy	Burkitt's lymphoma	1964	Epstein et al., 1964
Hepatitis B virus (HBV)	Single- and double-stranded DNA hepadenovirus	Serology	Some hepatocellular carcinoma	1965	Blumberg et al., 1965
Human T-lymphotropic virus-I (HTLV-I)	Positive-strand, single-stranded RNA retrovirus	Tissue culture	Adult T cell leukemia	1980	Poiesz et al., 1980
High-risk human papillomaviruses (HPV) 16 and 18	Double-strandedDNA papillomavirus	DNA cloning	Most cervical and penile cancers; some other anogenital and head and neck cancers	1983-84	Durst et al., 1983 Boshart et al., 1983
Hepatitis C virus (HCV)	Positive-strand, single-stranded RNA flavivirus	cDNA cloning	Some hepatocellular carcinoma and some lymphomas	1989	Choo et al., 1989
Kaposi's sarcoma herpesvirus (KSHV)*	Double-stranded DNA herpesvirus	Representational difference analysis	Kaposi's sarcoma, primary effusion lymphoma; some multicentric Castleman's disease	1994	Chang et al., 1994
Merkel cell polyomavirus (MCV)	Double-stranded DNA polyomavirus	Digital transcriptome subtraction (DTS)	Most Merkel cell carcinoma	2008	Feng et al., 2008

* EBV is also known as human herpesvirus 4 (HHV4) and KSHV is also known as human herpesvirus 8 (HHV8)

Yet another hypothesis that could explain HCC development in the context of HCV infection is the presence of harmful environmental co-factors such as aflatoxin, which may result in G-to-T transversions. In 80-90% of HCC that have mutated p53 (~50%) residue 249 is changed from G to T (*21, 23, 24*).

In 1989, Choo et al. found that in addition to HBV and HAV associated hepatitis, they were able to distinguish a third form, non-A, non-B hepatitis (NANBH) (*25*). They screened a cDNA library from chimpanzee serum containing the NANBH agent with serum from a patient diagnosed with NANBH, and they were able to identify an unknown antigen belonging to a new RNA flavivirus, which was named hepatitis C virus (HCV) **(Table 1)**. Subsequently, HCV was established as a causal agent in chronic hepatitis, liver cirrhosis, as well as HCC. HCV infection affects more than 170 million individuals worldwide, of whom approximately 20% are at risk of developing HCV-induced HCC. In contrast to HAV and HBV, a vaccine that protects against HCV is not available at this point, and attempts to develop a vaccine have been challenging due to the high mutation rate in the HCV RNA genome, resulting in the presence of many different HCV strains. Nevertheless, research is ongoing in this field, and the company Inovio is currently testing a plasmid DNA vaccine against HCV in a clinical phase II trial (www.inovio.com).

Human T-lymphotropic virus-1 (HTLV-1) is the only known human tumor virus that belongs to the family of retroviruses **(Table 1)**. Its discovery depended heavily on the identification of reverse transcriptase (RT) in 1970 in independent studies by Howard Temin, and David Baltimore, who were both able to demonstrate RNA-dependent DNA polymerase activity in RSV (*26, 27*). The discovery of RT was awarded

with a Nobel price in 1975, and represents one of many examples in which the study of tumor viruses resulted in a major discovery that influenced science across all disciplines. In 1979, Bernard Poiesz, a postdoctoral fellow in Robert Gallo's lab at the time, was able to detect RT activity in cell lines derived from adult T-cell lymphoma/leukemia patients and electron microscopy confirmed the presence of budding HTLV-1 virions (*28*). Shortly after, Gallo and his team were able to demonstrate that HTLV-1 was not only able to infect T-cells, but also transformed them *in vitro* (*29, 30*), and that proviral DNA could be found integrated into the host cell genome (*31*). In addition, they were able to isolate HTLV-1 from additional patient ATL samples and detect specific antibodies against the virus in patient sera (*32*). Subsequent studies from research teams worldwide confirmed HTLV-1 association with ATL (*33-35*). However, as is the case with other human tumor viruses, only a small percentage of individuals infected with HTLV-1 develop ATL throughout their lifetime. Cellular transformation is associated with expression of the viral oncoprotein Tax, which induces T cell proliferation and survival (*36*).

Another groundbreaking, and recently deemed Nobel prize-worthy discovery in tumor virology is the identification of high-risk papillomaviruses that cause human cancers. In 1983-84, a research team led by Harald zur Hausen at the University of Heidelberg identified human papillomavirus (HPV) types 16 and 18 by cross-hybridizing DNA from other papillomaviruses to DNA from cervical carcinoma biopsies (*37, 38*). Cervical cancer is one of the most common cancers in women worldwide, and the identification of its viral etiology has lead to the successful development of a vaccine within recent years (*39, 40*). This vaccine utilizes recombinant HPV capsid proteins L1,

and exists in bivalent (protection against HPV 16 and 18) and quadrivalent (protection against HPV 16, 18, 6, and 11) forms (*41*). In addition to cervical carcinoma, various types of HPVs are also linked to genital warts, other anogenital cancers as well as close to 20% of oropharyngeal cancers in both women and men (*42*).

With regards to cervical carcinoma, 15 high-risk HPV types have been identified that are individually necessary, however not sufficient to induce tumorigenesis (*43*). Of these, both HPV types 16 and 18 are most commonly associated with squamous cell carcinoma, whereas HPV 18 shows strong association with adenocarcinoma of the cervix. High-grade neoplastic lesions and invasive disease are characterized by viral integration of high-risk HPV types 16 and 18, with integration events that disrupt the E2 gene favoring tumorigenesis due to E2's repressive effect on E6 and E7 oncogene expression (*43*). However, even though the majority of women get infected with HPV, only a small percentage will actually suffer from invasive neoplastic disease. This indicates that progression to high-grade cervical neoplasia requires additional changes within the cervical epithelium, which may include genetic and epigenetic changes that have to be taken into consideration when tackling this disease. Non-viral risk factors that contribute to HPV-induced malignant disease progression include a high number of sexual partners, mutagens, smoking, hormones, immunosuppression, and genetic predisposition (*39*).

Most recent efforts to discover new tumor viruses associated with human cancers have focused on human malignancies that are more prevalent in immunosuppressed individuals including AIDS and transplant patients as well as the elderly. Patrick Moore and Yuan Chang have lead the way in scientific endeavors that

identified the human tumor viruses Karposi's sarcoma herpesvirus (KSHV) or Human herpesvirus 8 (HHV-8) in 1994 as well as Merkel cell polyomavirus (MCV) in 2008 (**Table 1**). Kaposis's sarcoma (KS) is an angioproliferative malignancy first reported in 1872 by Moritz Kaposi, who described KS lesions as 'idiopathic multiple pigmented sarcomas of the skin' (*44*). Even though KS was initially described as endemic in the Mediterranean and in Africa, the HIV epidemic in Europe and the US in the 1980's coincided with increased cases of AIDS-related KS in homosexual men (*45*). The elevated occurrence of KS in immunosuppressed individuals initiated a search for an infectious etiology. KSHV was discovered in 1994 using a PCR-based technique called representational difference analysis (RDA) (*46*). Briefly, DNA sequences unique to AIDS-KS lesions were isolated following PCR amplification and subtractive hybridization (*46*). Within a year of its discovery, KSHV had also been indicated in multicentric Castleman's disease (MCD), as well as AIDS-related primary effusion lymphoma (PEL) (*47-49*).

Merkel cell carcinoma (MCC) is an aggressive skin cancer that arises from mechanoreceptor Merkel cells in the basal layer of the epidermis (*50, 51*). It is more prevalent in immunosuppressed (13.4 fold higher incidence in AIDS patients) as well as older individuals (*52, 53*), which prompted the search of an infectious agent that may be associated with this cancer. In 2008, Feng et al. performed a direct sequencing-based technique called digital transcriptome subtraction (DTS) analysis (*54*) on cDNA libraries derived from four MCC tumors (*55*). Annotated human sequences were subtracted from the MCC cDNA libraries to identify candidate reads of non-human origin. Alignment of non-human reads with viral genome databases identified one transcript with high

homology to polyomavirus sequences (*55*). Subsequently, the whole MCV genome was sequenced and its association with MCC was confirmed in multiple studies (*55-57*). Detailed descriptions of MCV discovery, its viral features and association with MCC can be found in section 1.4 Merkel cell polyomavirus.

1.2 POLYOMAVIRUS BIOLOGY

1.2.1 History and phylogeny

Polyomaviruses are small, non-enveloped viruses that have double-stranded DNA genomes of ~5.0-5.4 kb. They have icosahedral capsids of 40-45nm diameter, and have been shown to infect various species including humans, monkeys, rodents, rabbits and birds. They can be divided into three major subgroups including the mammalian species containing groups *Wukipolyomaviridae* and *Orthopolyomaviridae*, and the avian group *Avipolyomaviridae*. Polyomaviruses encode for viral proteins called tumor (T) antigens, which have been associated with oncogenic transformation in cell culture experiments as well as tumor formation in animal models (*58*).

The first polyomavirus, murine polyomavirus (MPyV), was discovered as a filterable agent from mouse leukemia cells in 1953. Subsequently, MPyV was shown to cause cancers in newborn mice, rats, as well as hamsters (*59-61*), which led the way to investigating the oncogenic potential of polyomaviruses discovered ever since. Shortly after the identification of MPyV, simian vacuolating virus 40 (SV40) was discovered between 1959-1960, and it also was capable of inducing tumors in hamsters during

initial experiments (*62, 63*). SV40's natural host is the rhesus macaque, and many lots of poliovirus vaccine produced in rhesus cells between 1955 and 1963 were found contaminated with SV40 (*64*). It is estimated that 10-30 million individuals received a polio vaccine that contained SV40 during that time period, and studies to evaluate the potential oncogenic risk of SV40 in humans were initiated afterwards.

1.2.2 Association with human cancer

PCR-based studies reported the presence of SV40 DNA in non-Hodgkin lymphomas (*65*), osteosarcomas (*66*), brain tumors (*67*) as well as meotheliomas (*68*). However, subsequent studies failed to repeat these results and they were indicated as false positives due to PCR template contamination from 293FT cell DNA (HEK293 cells that were stably transduced to express SV40 T antigen) or common laboratory plasmids containing SV40 sequences (*69, 70*). Serologic studies to investigate the presence of SV40-specific antibodies in the general population as well as in patients with supposedly SV40-linked cancers, provide more consistent results due to a high specificity of this assay, and less chances for false positive results. The results indicate that there is no difference in seroreactivity between the general population and individuals with supposedly SV40–linked cancers (*71-73*). Low levels of seroprevalence across all groups tested can be attributed to cross reactivity of antibodies from human polyomaviruses BKV and JCV with SV40 peptides (*74*). In conclusion, there is no convincing or repeatable evidence linking SV40 exposure to human cancer to this date (*58, 70*).

The human polyomaviruses BKV and JCV (described in more detail in section 1.2.3) have recently been classified as “possibly carcinogenic to humans” by a WHO International Agency for Cancer Research Monograph Working Group (*75*). Single case reports link BKV infection to renal tubular as well as urothelial tumors in the context of renal transplantation (*76-78*). However, other studies failed to detect BKV in these malignancies, and a causal relationship is still under debate (*79, 80*). Some reports indicate the presence of BKV DNA in lymphomas, colorectal, pancreatic, prostate and brain tumors, but these associations are still controversial (*81*). *In vitro* and *in vivo* experiments clearly support an oncogenic potential of both BKV and JCV. Inoculation of either BKV or JCV into newborn rodents induces the formation of tumors in various tissues, as has been observed in the cases of MPyV and SV40 (*82*).

1.2.3 Human polyomaviruses

The first human polyomaviruses BKV and JCV (BK and JC stand for the initials of the patients from which they were isolated) were identified in 1971, and are closely related to SV40 by phylogenetic analysis of T antigen sequences. BKV was isolated from the urine sample of a renal transplant patient (*83*), whereas JCV was isolated from human brain tissue with progressive multifocal leukoencephalopathy (*84*). BKV infection is wide-spread throughout healthy individuals, with an early and rapid seroconversion of over 50% in children 2 years of age, and over 90% in > 10 year old age groups (*82*). In contrast, JCV seroconversion in the general, healthy population can be detected at later stages in life. Compared to BKV seroreactivity, it increases much slower but steadily over time, reaching 50-70% among older individuals (*82*).

In 2007, the two closely related human polyomaviruses KIV and WUV were discovered in children with acute respiratory tract infections (*85, 86*). Their names indicate the institutions at which they were identified: Karolinska intitute (KIV) and Washington University (WUV). NCBI genome database analyses of deep sequencing derived cDNA lbraries were used to detect non-human sequences and identify these two novel viral genomes. Serologic studies have detected both KIV and WUV in a large percentage of healthy individuals, with seroprevalence ranging from 55-98% depending on age groups evaluated in various geographic locations (*87-89*). A slightly higher prevalence is observed in immunosuppressed individuals, but thus far, experimental evidence links neither KIV nor WUV to any disease phenotypes, and infection seems to be asymptomatic (*82*).

Shortly after the identification of KIV and WUV, MCV was discovered in association with MCC in 2008. MCV biology is the focus of this thesis and literature reviews on MCC and MCV are described in subsequent sections 1.3 and 1.4. Schowalter et al. investigated the presence of MCV on human skin by taking forehead skin swabs, and not only revealed that MCV is frequently shed from healthy skin, but also identified two novel human polyomaviruses also present on the skin, HPyV6 and 7 (*90*). Both of these viruses were less prevalent than MCV in the 35 skin samples tested by rolling circle amplification (RCA) in this study (MCV = 14/35; HPyV6 = 5/35; HPyV7 = 4/35), and serologic evaluation of 95 serum samples revealed a seroprevalence of 69% for HPyV6 and 35% for HPyV7 (*90*). Interestingly, a study testing the presence of HPyV6 and 7 in MCV-negative MCCs did not find any association (*91*). At this point, no

disease development has been linked to HPyV6 or 7 infections, and further experimental analyses are necessary.

RCA was also used to identify the 8th human polyomavirus called trichodysplasia spinulosa-associated polyomavirus (TSV) in nose spicules collected from a transplant patient suffering from trichodysplasia spinulosa (TS) (*92*), and this viral association was subsequently confirmed (*93*). Seroprevalence of TSV was determined in 528 healthy individuals, and ranges from 10% in children to 80% in older adults, with an average seroreactivity of 70% (*94*). TSV viral protein expression is specifically associated with affected hair follicles, suggesting a possible role of this virus in TS development (*95, 96*). Other disease associations have not been reported, yet, and require further investigation.

In 2011, the 9th human polyomavirus (HPyV9) was identified by generic PCR utilizing primers designed against conserved VP1 regions of known polyomaviruses. Screening of 597 clinical samples not only detected the above-described human polyomaviruses in 84 cases, but also identified HPyV9 in the serum of an immunosuppressed kidney transplant patient (*97*). HPyV9 shares high homology with the African green monkey lymphotropic polyomavirus (LPV), which may explain human seroreactivity to LPV due to cross reactivity (*98*). Seroprevalence of HPyV9 lies between 21-53% in healthy individuals, and disease associations have not been reported at this point (*98, 99*).

In 2012, three independent studies identified the 10th human polyomavirus referred to as Malawi polyomavirus (MWPyV) (*100*), human Polyomavirus 10 (HPyV10) (*101*), or MX polyomavirus (MXPyV) (*102*). Siebrasse et al. identified this new

polyomavirus by shotgun pyrosequencing of DNA from virus particles isolated from a stool sample from a healthy child from Malawi, and named it MWPyV (*100*). Subsequently, they screened 514 diarrhea samples from children in the United States, and found MWPyV present in 12 (2.3%) cases. The MWPyV viral genomes isolated in the United States varied from the Malawi viral genome by 5.3% by nucleotide sequence comparison (*100*).

In the same year, Buck et al. published the identification of HPyV10, which was found to share 95-99% nucleotide identities with the MWPyV viral strains, and therefore is considered the same virus (*82, 101*). HPyV10 was discovered by RCA on DNA isolated from virions purified from condyloma samples from a patient suffering from a genetic disorder known as warts, hypogammaglobulinemia, infections, and myelokathexis (WHIM) syndrome (*101*). It is not clear whether HPyV10 infection contributed to the development of warts in this patient, since papillomavirus 6 infection was also found, which is known to cause genital warts.

Yet another group identified the 10th human polyomavirus in acute diarrheal samples from children in the United States, Mexico and Chile in 2012 (*102*). The virus was named MXPyV and its genome was found to contain almost identical nucleotide sequence to MWPyV and HPyV10, confirming that these three independent viral discoveries describe geographic variants of the same new member of the human polyomavirus family (*82, 102*). MXPyV was found in 23 (3.4%) out of 834 fecal samples, but not in blood or urine samples of immunocompromised individuals (*102*). Whether or not the tenth human polyomaviruses is associated with diarrhea or other disease phenotypes in humans remains to be elucidated.

In 2013, 454 pyrosequencing identified a novel polyomaviral genome in a stool sample from a healthy child from Malawi (*103*), which was named STL polyomavirus (STLPyV). It encodes for a 229 amino acid long T antigen splice variant (229T), which utilizes distinct splice donor and acceptor sites downstream of the LT splicing sites (*103*). STLPyV is closely related to MWPyV and subsequent PCR analysis indicates the presence of this novel polyomavirus in pediatric stool samples from St. Louis as well as Gambia. However, neither MWPyV nor STLPyV were detected in 237 fecal samples from adult transplant patients. Disease associations with this novel human polyomavirus remain to be explored.

Finally, HPyV12 represents the latest human polyomavirus identified to date (July 2013). It was identified by PCR using generic polyomavirus primers targeting the VP1 region (*104*). 242 specimens from various body sites were tested and a novel polyomavirus genome with low homology (51-67%) to known polyomaviruses was identified in 4 liver samples (*104*). Subsequent re-evaluation of the 242 samples by PCR using HPyV12 specific primers revealed viral genome presence in 11% of liver samples and to a lesser extent in organs of the gastrointestinal tract and feces (*104*). Seroprevalence of HPyV12 lies at 12% in young children (2-5 years) with a rising seroreactivity of 15-33% in older adults (*104*). Interestingly, HPyV12 is the first human polyomavirus identified that lacks an LXCXE Rb family targeting domain. Disease associations have to be evaluated in future studies.

Overall, it is noteworthy to mention that the past 6 years have brought about a new era of human polyomavirus research with the discovery of 10 new human polyomaviruses in addition to BKV and JCV. Two of the newly identified polyomaviruses

(MCV and TSV) have been convincingly linked to human disease. A great contribution to these discoveries was the completion of the human genome project in 2003. It allowed for the development of new techniques to identify non-human sequences in diseased tissue, which ultimately lead to the identification of novel viral agents. Studies that center on the epidemiology of polyomavirus infections in humans have revealed that humans are frequently infected with multiple polyomaviruses from an early age (*74, 87, 88, 94, 98, 99, 105*). Multiple common human polyomaviruses are chronically shed from the skin of healthy individuals (*90*), and have been identified in human serum, urine, and cerebrospinal fluid, as well as nasopharyngeal, respiratory, and fecal samples thus far (*97, 100-102, 106, 107*). Most human polyomaviral infections seem to be asymptomatic, but further studies are needed to investigate possible disease phenotypes. It is apparent that immunosuppression poses a risk factor in the development of polyomavirus-induced malignancies such as MCC and TS. Given that polyomaviruses seem to be part of normal human flora, it is likely that more human polyomaviruses will be discovered in the future. Careful investigations are needed to identify human diseases associated with common polyomaviral infections most likely in the context of immunosuppression.

1.2.4 Genome organization

Polyomaviral genomes are composed of circular, covalently closed, double-stranded DNA, and range from 4.6 kb to 5.4 kb in length. They are divided into three distinct regions, which contain genome features common to all polyomaviruses: the non-coding regulatory region (NCRR), as well as the early and late transcript regions. Early and late designations refer to the timely expression of transcripts during the viral infectious cycle. The NCRR, which divides early and late regions, contains the viral origin of replication as well as early and late promoter elements. Early transcripts include T antigen

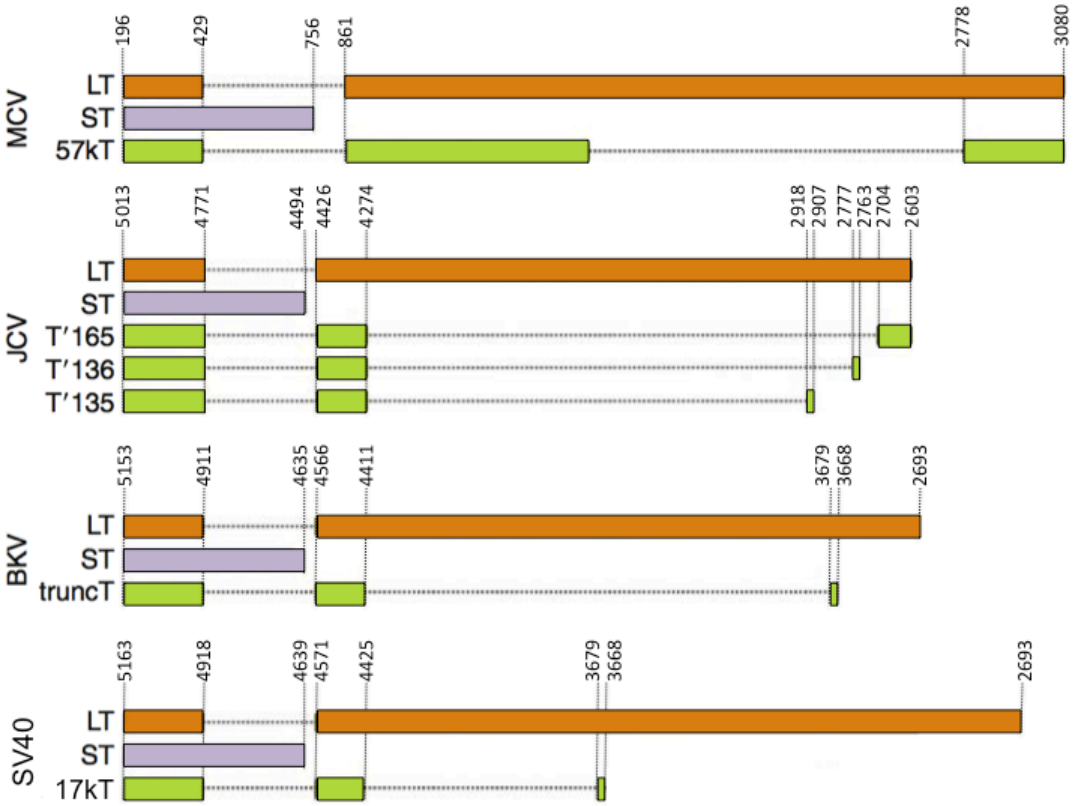

Figure 1. MCV, JCV, BKV , and SV40 T antigen splice isoforms
The splicing patterns of JCV, BKV , and SV40 early regions are compared to MCV T antigen splice variants. Different colors represent individual T antigen isoforms: Orange (LT), Lavender (sT), and Green (additional virus unique isoforms). Dottet lines represent intronic regions and nucleotide positions are indicated with respect to genome position for each respective virus. (Modified from Gjoerup and Chang, 2010)

isoforms, which are expressed before the onset of viral replication. Late transcripts are expressed afterwards and encode VP gene products involved in viral genome packaging and capsid formation.

The early region encodes between 2 to 5 differentially spliced T antigen isoforms that differ between individual polyomaviruses **(Figure 1)**. Open reading frame analysis predicts Large (LT) and small T (sT) antigen expression for all known polyomaviruses. LT and sT protein expression has been confirmed for a great number of polyomaviruses including MPyV, SV40 BKV, JCV and MCV. Additional T antigen isoforms can be found in various polyomaviruses and include: middle and tiny T from MPyV (*108, 109*), 17kT from SV40 (*110*) **(Figure 1)**, truncT from BKV (*81*) **(Figure 1)**, T'135, T'136 and T'165 from JCV (*111*) **(Figure 1)** as well as 57kT from MCV (*56*) **(Figure 1)**. While the N-terminal region is shared among T antigens from a given polyomavirus, alternative splicing creates T antigen isoforms with unique C-terminal domains **(Figure 1)**. Polyomavirus T antigens are not only essential for viral genome replication (described in more detail in section 1.2.5), but also have been shown to interact with many cellular proteins to alter signaling pathways in ways that benefit the viral lifecycle (described in more detail in section 1.2.7). Due to their small genome size, polyomaviruses are depended on multi-functional T antigen proteins that are involved in many different aspects of the viral life cycle.

The late region encodes for the viral capsid proteins VP1, VP2 and VP3, which are also generated through alternative splicing. SV40 is the only polyomavirus that is known to encode a VP4 isoform, which creates pores in the cell membrane to promote viral release (*112*). Viral capsids are comprised of 72 VP1 pentamers, with VP2 and

VP3 buried internally (*113, 114*). When expressed alone, the major capsid protein VP1 forms virus-like particles (VLPs) that are successfully used in serological studies to determine the prevalence of a given polyomavirus in a population.

1.2.5 Viral life cycle

The infectious cycle of polyomaviruses can be divided into 8 distinct phases (**Figure 2**). The first step involves the interaction of the major capsid protein VP1 with the host cell membrane. Host cell specificity depends on the receptors utilized by polyomaviruses, which include ganglioside receptors with differentially linked sialic acids. SV40 has been shown to bind to ganglioside GM1 (*115, 116*), whereas MPyV specifically interacts with GD1a and GT1b (*116*). BKV utilizes GD1b as well as GT1b gangliosides (*117*), and JCV has been shown to require both the $5HT_{2A}$ family of serotonin receptors as well as gangliosides with alpha 2-6–linked sialic acids to successfully infect cells (*118*). The MCV mode of entry is still controversial. A 2009 report indicated that MCV VP1 binds to GT1b, with the unique feature of binding sialic acids on both branches of this ganglioside (*119*). However, subsequent studies refute the requirement of sialylated glycans for MCV attachment to cultured cells (*120, 121*), and identified a linear Neu5Ac-α2,3-Gal disaccharide as a specific MCV binding motif (*120*).

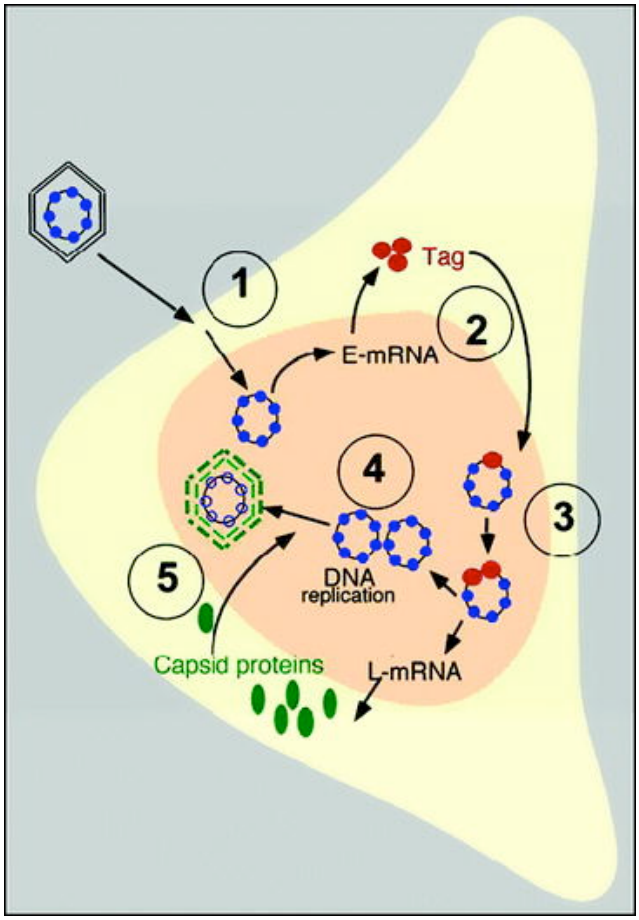

Figure 2. The polyomavirus lifecycle
The stages of the polyomavirus life cycle in a permissive host cell are indicated at each step of this simplified diagram. (1) Virus attachment, endocytosis and transport to nucleus. (2) T antigen (Tag) expression. (3) Tag mediated re-programming of the cellular environment and late gene expression. (4) Viral DNA replication. (5) Virion assembly and release. (Modified from Fanning et al., 2009 (*122*))

Following attachment to host cell receptors, polyomaviruses enter the cell via specific endocytosis mechanisms. Most polyomaviruses utilize caveolae-mediated endocytosis, while JCV requires the formation of clathrin-coated pits (*123*). Once the virus has entered the cell, it depends on the cellular cytoskeletal machinery for transport through the cytosol to the nucleus, a process that requires intact microtubules (*123*). Once the nucleus is reached, uncoating of the viral genome begins, followed by transcription of the early region. Early gene expression is vital for providing a cellular milieu that supports viral genome replication by driving the cell into S-phase through

interactions with various cellular proteins (described in detail in section 1.2.7). LT assembles into a hexameric helicase unit that initiates bi-directional replication from the viral origin in the NCRR (*124*). After complete viral DNA replication, LT subsequently inhibits early gene expression, while promoting late gene transcription. Capsid protein expression leads to capsid assembly and viral genome encapsidation. The new viral progeny then lyses the cell and exits to infect more cells. A simplified diagram of the polyomavirus lifecycle is depicted in **Figure 2**.

1.2.6 Permissive vs. non-permissive infection

The successful completion of the viral life cycle depends on several host cell factors, and can therefore only be accomplished in the appropriate cell type of the species that is considered the natural host for the virus (permissive cell). Factors that influence species tropism include available receptor molecules on the cell surface (as described in section 1.2.5) as well as the appropriate DNA replication machinery to facilitate viral DNA synthesis. Viral DNA replication requires the cooperation of T antigen with cellular replication factors including replication protein A (RPA) and DNA polymerase alpha primase (polα) (*125*). The Pol interaction in particular has been shown to be functional in a species-specific manner (*126*). SV40 genome replication for example cannot successfully proceed in rodent cells (non-permissive), due to insufficient primosome assembly and primer synthesis on SV40 origin DNA (*126*). Therefore, only infection of a permissive cell leads to virion production followed by cell lysis **(Figure 3A)**.

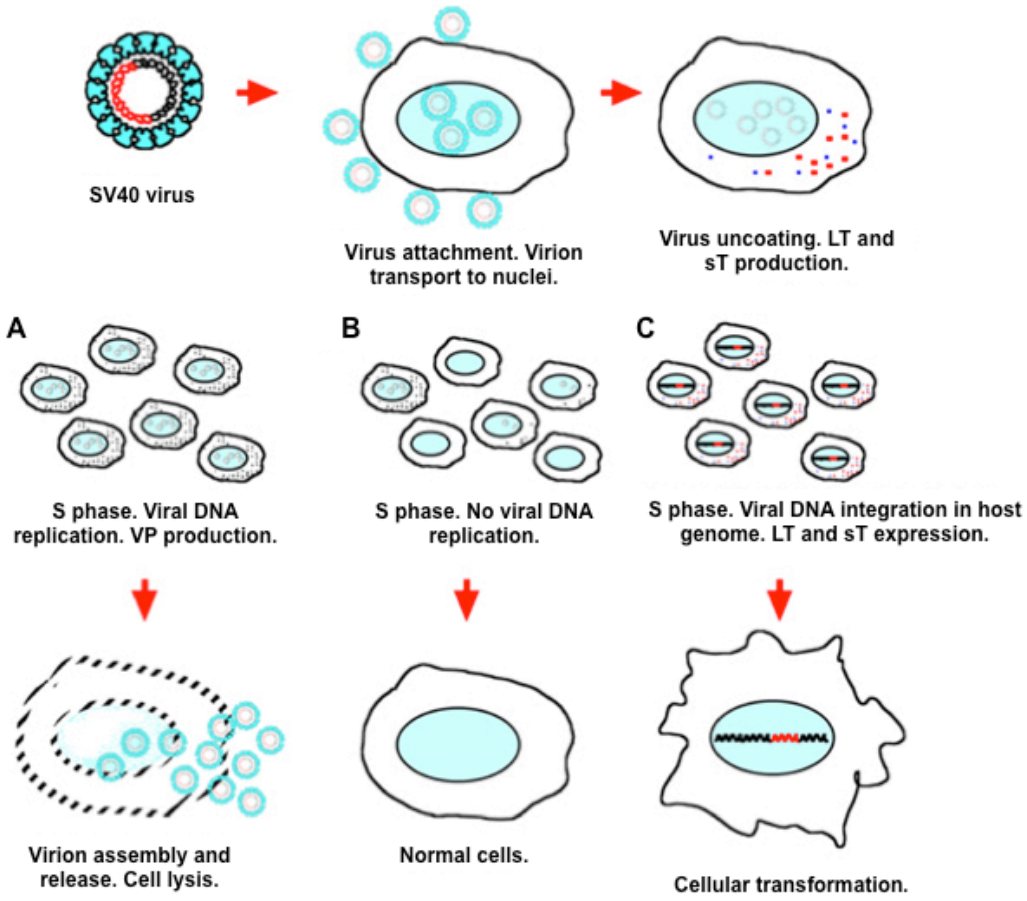

Figure 3. Possible outcomes of SV40 infection in different cell types
(A) Infection of a permissive cell results in virus particle production and cell lysis. (B) SV40 infection of some rodent cells fails to support viral DNA replication or virion production and eventually leads to loss of the viral genome. (C) Infection of a non-permissive cell rarely leads to integration of the viral genome into the host genome generating a stably transformed clone. (Modified from Ahuja et al., Oncogene 2005)

There are two possible outcomes upon infection of a non-permissive cell type **(Figure 3 B-C)**. SV40 infection of rodent cells for example results in expression of the early region T antigens, while the late transcripts and virion production are missing. T antigen expression leads to an increase S-phase entry followed by mitosis, which promotes cell proliferation even in quiescent mouse fibroblasts. Since the viral genome cannot be replicated, the majority of rodent cells infected with SV40 will initially go through increased rounds of proliferation, but eventually lose the viral DNA through

step-wise dilution or degradation, and revert to their normal state (*127*) **(Figure 3B)**. Various cell types allow for polyomavirus entry upon infection, but fail to support the late phase of the infectious cycle resulting in what is called an abortive infection.

Infection of a non-permissive host cell can also involve the integration of viral genomic DNA into the host cell DNA, which provides a mechanism to pass on the viral genome to daughter cells even after multiple cell division cycles **(Figure 3C)**. During this process, which is considered a "biological accident" because it is a dead end scenario for the virus, the viral DNA integrates randomly with regards to the cellular as well as the viral genome. Integration events that preserve intact T antigen sequences promote T antigen driven cell proliferation, and in the context of a replication defective environment can result in the outgrowth of transformed clones (*128*). With regards to MCV induced tumorigenesis, viral genome integration is a signature feature in MCC, indicating that even though humans are considered the natural host for MCV, Merkel cells may not be a permissive cell type and therefore are susceptible to transformation. Details about MCV genome integration in MCC can be found in section 1.5.4.

1.2.7 Cell transformation assays

Polyomaviruses provide excellent tools for studying the molecular basis of neoplastic transformation, which is characterized by the extended proliferation potential or increased survival of a cell (*127*). In cell culture systems it is possible to evaluate the effects that viral proteins have on the host cell, and determine specific cellular pathways that contribute to the transformation phenotype. The SV40 interactions with host cell proteins described in section 1.3.1 have been useful in identifying genes that are altered

in many human cancers (for example p53), highlighting the relevance of studying tumorviruses like SV40. Cellular pathways perturbed by SV40 (described in section 1.3.1) have been assessed for their contributions to oncogenic transformation by a number of different *in vitro* and *in vivo* assays described below.

1.2.7.1 Loss of contact inhibition

Focus formation assays demonstrate the loss of contact inhibition that can be observed in cancer cells of diverse origins. Upon oncogenic signaling, adherent cells that usually would grow in a one cell-thick monolayer start to pile-up and grow on top of each other, forming visual foci on the dish. SV40 transformed rodent fibroblast cells readily form foci when co-cultured with, or plated on top of a monolayer of non-transformed, growth-arrested cells (*127*). In addition to focus formation, saturation density measurements can also indicate loss of contact inhibition. Transformed cells exceed the maximum number of cells per unit area and fail to undergo growth arrest upon contact with adjacent cells.

1.2.7.2 Immortalization

Primary cells cannot be passaged in culture indefinitely. After a certain number of population doublings, they undergo growth arrest and senesce irreversibly. Rodent fibroblasts that are infected with SV40, however, are capable of dividing indefinitely, and are considered immortalized (*127*). Human fibroblasts on the other hand do not behave this way upon expression of SV40 T antigens, and require additional expression of human telomerase reverse transcriptase (hTERT) to maintain telomere length and escape senescence (*127*).

1.2.7.3 Anchorage-independent growth

Soft agar growth has been established as another *in vitro* technique that tests the oncogenic potential of cells. In this assay cells are plated in a semi-solid agar medium in which non-transformed cells cannot grow. Cancer cells however, are able to grow anchorage-independently in this soft agar environment, forming sphere-like clumps called colonies. Cell transformation studies using rodent fibroblast cells have identified several polyomaviruses that are capable of inducing soft agar growth in addition to focus formation and immortalization (*127, 129-131*).

1.2.7.4 Growth under nutrient deprivation

In addition to focus formation and soft agar assays, serum starvation through culture medium provides insight into another characteristic specific to cancer cells, which is growth under nutrient deprivation. Non-cancerous cells usually stop dividing when they are placed in an environment with decreased serum growth factors (growth conditions are typically changed from 10% to 1 or 0.1% serum). Transformed cells however still continue to proliferate, overcoming environmental signals that would normally indicate growth arrest.

1.2.7.5 Tumor formation in animal hosts

The ultimate experimental evidence that supports the presence of a cellular transformed state is growth after xenograft transplantation into an immunocompromised host. In mouse experiments, cell lines are often injected subcutaneously and monitored for tumor formation at the site of the injection. However, transformed cells do also metastasize and form nodules at other body sites indicating an increased

aggressiveness of the transformed clone. Non-transformed cells do not grow in a xenograft setting due to a competitive environment for nutrients and blood supply with the host's cells that has to be overcome to settle into a niche and support the growth of a colony of cells. Xenograft experiments are especially useful in pre-clinical studies (such as described in Appendix A and B), to test drug efficacy and dosing regimens for cancers where a transgenic model is not available. Transgenic models that have been established for SV40 T antigen expression are described in detail in section 1.3.2.

1.3 SV40 EARLY REGION

1.3.1 SV40 T antigen interactions with cellular proteins

SV40 is one of the most well studied tumor viruses, and since its discovery in the late 1950's a wealth of information has been collected that has uncovered important pathways involved in basic cell biology. In its natural host the rhesus macaque, SV40 infects quiescent epithelial cells in the kidney, which enter the cell cycle upon SV40 T antigen expression (*127*). An important feature of SV40 T antigen expression therefore includes its effect on cellular S-phase entry to create an environment that allows for viral genome replication. Highlights from studies of SV40 interactions with cellular proteins include the discovery of the important cellular tumor suppressor p53 and dissection of the retinoblastoma protein (pRB) pathway (*132-135*). In addition, SV40 LT has been shown to interact with a number of other cellular targets including p107, p130, p300/CBP, Hsc70, Cul7, Bub1, IRS1, and FBW7 **(Figure 5)** (*136-145*).

1.3.1.1 SV40 LT interaction with Rb family

It is well established that SV40 as well as all other polyomaviral large T antigens contain an LXCXE consensus motif, which targets the Rb family proteins pRB, p107 and p130. Other oncoproteins from various tumorviruses (HPV E7, Adenovirus E1A, or KSHV LANA2) also share this common motif, emphasizing the importance of the Rb pathway in regulating cellular growth (*146, 147*). Rb family members control the cell cycle by

inhibiting the E2F transcription factors including E2F1, E2F2, and E2F3a (activating factors) as well as E2F4 and E2F5 (repressive factors). E2F-responsive genes are involved in many pathways including cell cycle control, apoptosis, DNA repair and replication as well as nucleotide synthesis.

The repressive E2F factors 4 and 5 preferentially bind p130 within a large complex called the DREAM complex that inhibits responsive promoters during G0 and in quiescent cells (*148*). The E2F4/5-p130 complex is also thought to recruit histone deacetylase (HDAC) to promoters, which additionally represses transcription through chromatin remodeling (*149*). SV40 LT can disrupt this repressive complex by targeting p130 for degradation, which allows for activation of genes involved in cell cycle entry (*150*) **(Figure 4A)**. The ubiquitination and consequent degradation of p130 depends on chaperone functions mediated by the DnaJ domain of LT, which recruits cellular Hsc70 (*151, 152*).

In addition to mitigating E2F repressive effects, LT also induces transcription of E2F target genes by releasing activating E2Fs. E2F1/2/3a factors are usually bound to hypophosphorylated pRb until cyclin/cyclin dependent kinase complexes phosphorylate Rb (*153*). LT binding to pRb releases E2F1/2/3a resulting in E2F-mediated transcription of genes involved in S-phase entry, which contributes to LT mediated cell proliferation and transformation **(Figure 4A)**. The exact role of p107 in cell cycle progression is less well understood.

1.3.1.2 SV40 LT interaction with p53

To prevent abnormal S-phase entry and maintain genome integrity, cells have established mechanisms to intervene with aberrant up regulation of E2F targets. This

process usually involves an increase in p53 protein level, which is generally low in cells due to p53 ubiquitination by Mdm2 (*154*). Activation of p53 by DNA damage, oxidative stress, or oncogene signaling leads to p53 stabilization and phosphorylation/acetylation, which allows for the transcriptional activation of genes involved in apoptosis and senescence (*155*). SV40 LT binds the p53 DNA binding domain through a bipartite site

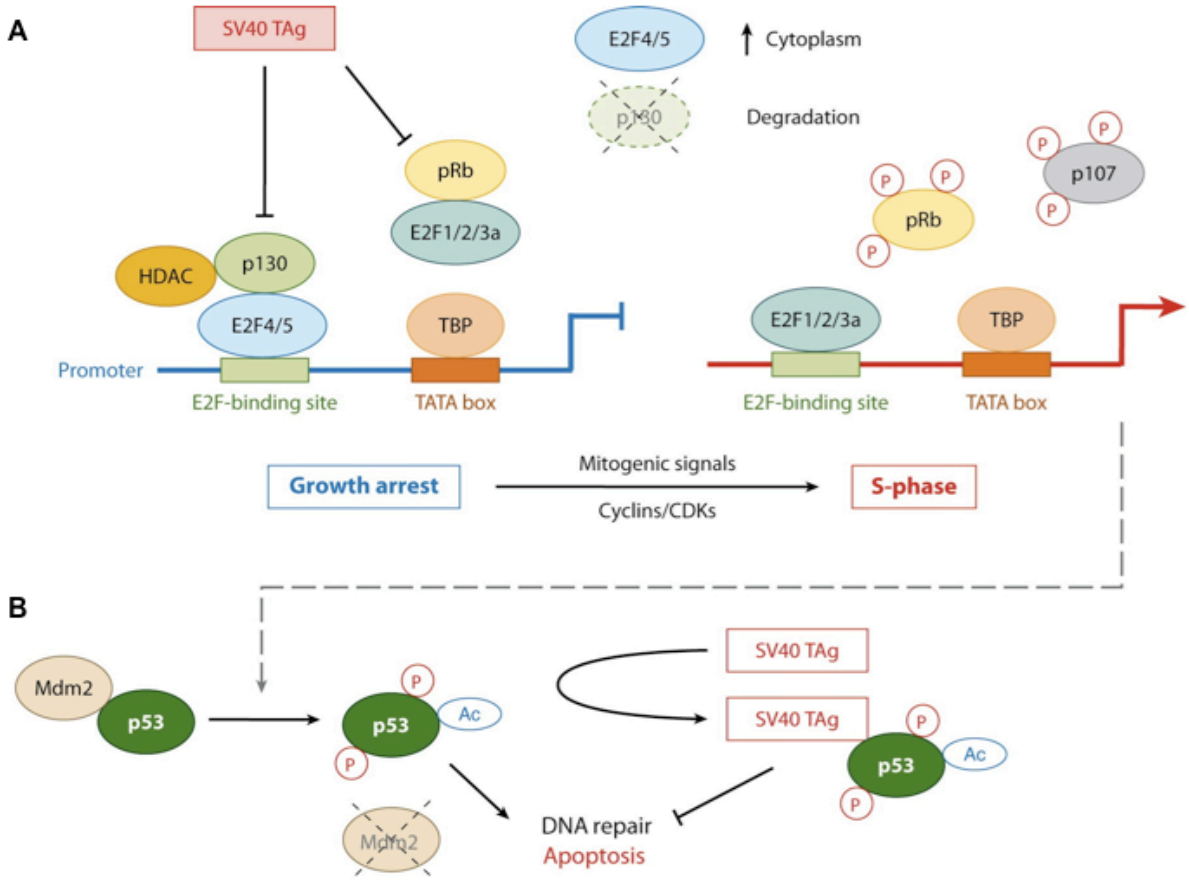

Figure 4. Targeting of the Rb-E2F and p53 pathways by SV40 LT
(A) SV40 LT inhibits Rb-family pocket proteins pRb, p107 and p130 through its LXCXE motif. This leads to release of E2F transcription factors, which activate genes that induce S-phase entry. (B) Aberrant cell cycle entry leads to p53 activation to facilitate DNA repair or induce apotosis. SV40 LT counteracts this by binding to p53 and inhibiting activation of p53 responsive genes. (Modified from Sáenz Robles and Pipas, Ann. Rev. Microbiology, 2013)

in its C-terminal ATPase domain (residues 351-450 and 533-626), which prevents tetramerization of p53, and therefore prohibits its transcriptional activity (*156*) **(Figure 4B)**. In contrast to other viral oncoproteins that either target p53 for proteasomal degradation (i.e. HPV E6) (*157*) or repress its transcription (i.e. adenovirus E1B 55k) (*158*), SV40 LT stabilizes p53 levels in the cell, while inactivating its transcriptional activity (*159*). In 1979, p53 was discovered in complex with SV40 LT (*135, 160*), and it was initially mistaken for an oncogene due to its increased protein level in SV40 transformed cells.

Even though it is clear that SV40 inactivates p53-mediated apoptosis in response to aberrant S-phase entry, the complete extent of the LT-p53 interaction still remains to be worked out. p53 has a diverse range of downstream targets, some of which may be involved in different aspects of the SV40 cellular reprogramming (*161*). Studies that evaluated the growth promoting effects of SV40 LT in rodent cells discovered that transformation efficiency was markedly reduced in the absence of wildtype p53, indicating a gain-of-function modality for the SV40 LT interaction with p53 (*162*). Results from a transgenic model of SV40 LT induced beta cell carcinogenesis (Rip1Tag2) support this data, with lower tumor volumes observed in mice crossed to p53 deficient mice (*163*). The possible role of a gain-of-function by redirecting wildtype p53 activity may also explain why SV40 LT does not degrade p53 protein, but instead stabilizes it. One explanation that has been proposed is that LT binds wildtype p53 to recruit the CREB binding protein (CBP)/p300 coactivators to allow for posttranscriptional modification (acetylation) on LT (*164*). The significance of this modification or other functions achieved by the LT-p53 complex remains to be identified.

1.3.1.3 Other SV40 LT cellular targets

In addition to the pRb family proteins and p53, SV40 LT interacts with a number of other cellular proteins, demonstrating its multifunctional nature **(Figure 5)**. Several of these interactors have been implicated in LT-mediated transformation. The following paragraphs provide a brief overview of the additional SV40 LT cellular targets.

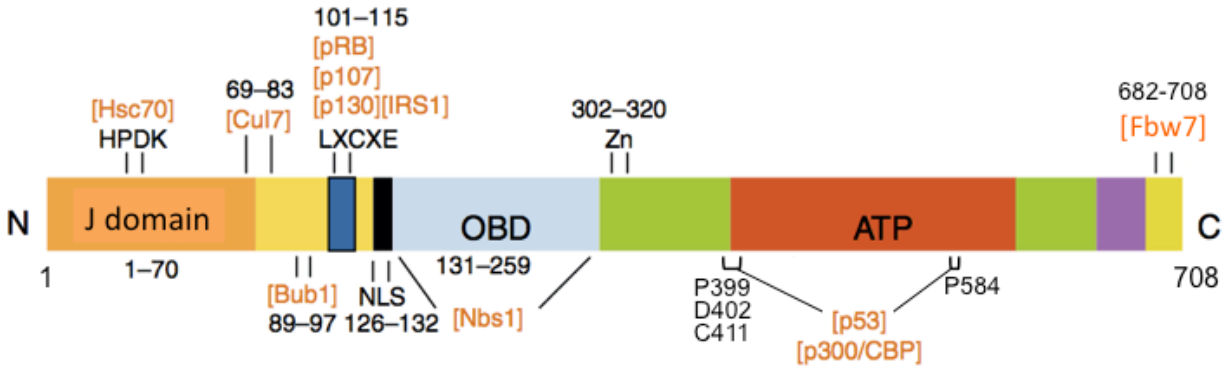

Figure 5. SV40 LT domains and cellular interactors
SV40 LT is a multifunctional protein that binds to a variety of cellular interactors through conserved motifs. Cellular binding partners are indicated in brackets (orange letters) and their respective amino acid binding sites on LT are shown (black numbers). (Modified from Gjoerup and Chang, 2010)

J Domain

The N-terminal region of SV40 T antigen, shared by both LT and sT, contains a J-domain ranging from amino acids 1 to 82 (*165*), which is functionally conserved in all polyomavirus T antigens. The J domain is similar to that of molecular chaperones called DnaJ proteins, which interact with cellular heat shock (Hsc) proteins to mediate chaperone functions including protein folding and transport. The J domain of SV40 and other polyomaviral T antigens consists of a conserved HPDKGG motif and the CR1-like

region (*141*). The CR1 motif is similar to that found in adenovirus E1A and contributes to cellular transformation. E1A targets pRb and p300 through its CR1 (*166*) but this has not been confirmed for polyomavirus T antigens, for which the cellular target of this region remains to be discovered.

Both LT and sT bind to the cellular DnaK family member Hsc70 through the HPDKGG motif and this interaction is important for both viral replication as well as transformation functions of T antigen (*141*). The ATPase activity of Hsc70 is required for LT binding to pRb, p107 or p130 by releasing heterodimeric E2F-DP complexes, which are then freed to facilitate cell cycle progression (*141, 142, 152*). The sT interaction with Hsc70 facilitates sT binding to the heterotrimeric protein phosphatase 2A (PP2A) by replacing its regulatory B subunit (*141*). Mutations of the HPDKGG motif reveal the importance of this domain for viral replication and transformation. D44N and H24Q are two classic mutants that are used in molecular studies to study the significance of this motif. The D44N mutant does not bind Hsc70, is defective for viral replication, and shows decreased transforming activity (*141*).

CBP/p300

Cyclic AMP response element binding (CREB)- protein (CBP) as well as p300 are cellular tumor suppressors that possess intrinsic histone acetylase (HAT) activity through which they mediate a wide range of cellular processes involved in cell growth and transformation (*167*). SV40 LT binds to the co-activators CBP/p300 (*168*) and this interaction contributes to the transforming activity of LT (*137*) through an unknown mechanism (*150*). The association of LT with CBP/p300 leads to acetylation of LT on

residue K697 through CBP and is dependent on LT binding to p53 (*164, 169*). The significance of K697 acetylation remains to be elucidated. Adenovirus E1A also binds CBP/p300 resulting in a changes in histone modification patterns (*170*) and global re-localization of RB family members and CBP/p300 on cellular promoters (*150*). This leads to a change in the cellular transcriptional program that results in cell cycle entry and progression (*150, 171*). SV40 LT can rescue non-transforming E1A mutants that are incapable of binding to CBP/p300 (*143*), indicating a similar role for SV40 LT on chromatin remodeling and transcriptional reprogramming.

p400

The chromatin remodeling ATPase p400 is a member of the SWI2/SNF2 family of proteins. Adenovirus E1A binds to p400 as well as the scaffolding protein TRRAP, which results in stable association of p400 with c-Myc and subsequent stabilization of c-Myc protein levels (*172*). This increase of c-Myc protein results in transcriptional activation of c-Myc target genes in the presence of E1A (*172*). SV40 LT has been shown to bind to p400 as well (*144*), but the significance of this interaction with regards to T antigen mediated transformation is not well understood.

Cul7

The molecular scaffold cullin 7 (Cul7) is part of an SCF (Skp1, cullin, F-box) E3 ubiquitin ligase complex containing Skp1, ROC1 and Fbw8, which targets specific cellular proteins for proteasomal degradation (*173*). Cul7 was first identified in association with SV40 LT (amino acids 69-83) and LT mutants incapable of binding Cul7 are defective in

transformation assays even though binding to pRB and p53 remains unchanged (*138, 174*). Cellular proteins that are targeted for degradation through Cul7-SCF complexes include cyclin D1 (*175*) as well as insulin receptor substrate 1 (IRS1) (*176*). Further studies are needed to determine whether or not alterations in the degradation of these two known Cul7-SCF targets is essential in LT mediated transformation.

Bub1

The mitotic checkpoint kinase Bub1 ensures appropriate attachment of kinetochores to microtubules during the metaphase to anaphase transition (*177*). A yeast two-hybrid screen discovered Bub1 as a cellular binding partner of SV40 LT and genetic mapping experiments revealed LT amino acid residues 89-97 as the responsible interaction domain (*139*). Other polyomaviral T antigens that share the Bub1 binding site include JCV, BKV, and bovin polyomavirus LTs. Bub1 inactivation by SV40 LT de-regulates the cellular DNA damage response (*178*) and results in cellular senescence in the absence of pRb and p53 targeting by LT (*179*).

IRS1

Insulin receptor substrate 1 (IRS1) is a docking protein for both insulin and insulin growth factor-I receptor (IGF-IR) (*180*) whose downstream signaling involves PI3K/Akt activation (*181*). SV40 LT binds to IRS1 and this interaction is required for efficient transformation by LT (*180*). While LT is incapable of transforming IRS1 deficient cells, its transforming activity can be restored by exogenous expression of wildtype IRS1; however, IRS1 that is mutated in its PI3K binding site does not restore transformation.

Both SV40 as well as JCV LTs have been shown to interact with and translocate IRS1 from the cytoplasm to the nucleus (*182, 183*).

Nbs1

The Nijmegen breakage syndrome 1 (Nbs1) protein is part of the MRN complex, which is composed of Mre11, Rad50 and Nbs1. This complex has been implicated in DNA double-strand break repairs (*184*) and its dysfunction due to Nbs1 mutations in the Nijmengen breakage syndrome leads to chromosomal instability, which in turn increases cancer incidence. SV40 LT binds to Nbs1 through its origin-binding domain, which facilitates unlicensed firing of the viral origin (*185*). Whether or not the LT-Nbs1 interaction is important for transformation remains to be uncovered.

Fbw7

The F-box protein Fbw7 is the substrate recognition component of the SCF-Fbw7 ubiquitin ligase complex that targets specific proteins for degradation by the proteasome. Known targets of this complex include cyclin E (*186*), c-Myc (*187*), c-Jun (*188*), and Notch (*189*). SV40 LT binds to Fbw7 through a conserved Cdc4 phospho-degron (CPD) site that usually binds cellular target proteins (*190*). Despite binding to this site LT does not get degraded and is thought to compete with cellular targets such as cyclin E (*190*), which are stabilized in the presence of LT due to decreased targeting by the SCF-Fbw7 complex. Given that Fbw7 regulates the proteolysis of a number of oncoproteins, SV40 LT targeting of the SCF-Fbw7 complex likely plays a role in its transformation activity.

1.3.1.4 SV40 sT

SV40 sT shares the N-terminal portion (82 amino acids) with LT, which includes a functional J domain (described in section 1.3.1.3). sT is a 147 amino acid long protein that can be found in both the nucleus as well as the cytoplasm. The C-terminal region is unique to sT and contains two Zinc-binding CXCXXC domains that provide conformational stability (*191*) **(Figure 6)**.

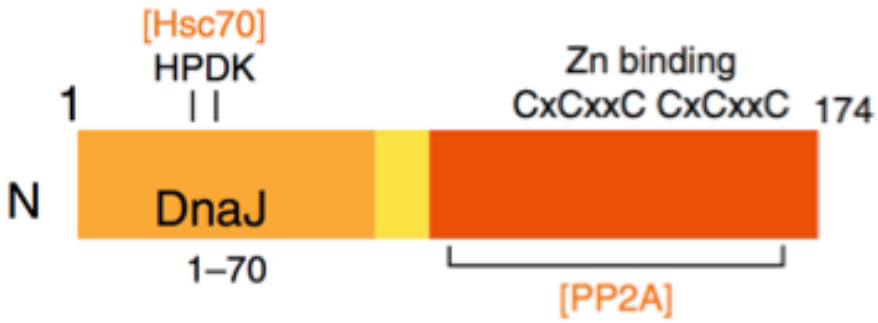

Figure 6. SV40 sT domains and cellular interactors
Cellular binding partners of SV40 sT are indicated in brackets (orange letters) and their respective amino acid binding sites are shown (black numbers). (Modified from Gjoerup and Chang, 2010)

SV40 sT cooperates with LT to fully transform cells. Rodent cells that only express LT acquire lack of contact inhibition and form foci, but they do not grow anchorage independently without the presence of sT (*192, 193*). Human cells require oncogenic signaling events in addition to LT and sT expression to become transformed. Hahn et al. demonstrated that BJ fibroblast cells that expressed LT and sT were anchorage independent and grew in immuocompromised mice only in the presence of

human telomerase reverse transcriptase (hTERT) as well as mitogenic hRas (V12 mutant) (*194*). The contribution of sT to transformation depends on sT's interaction with the protein phosphatase 2A (PP2A).

PP2A is a ubiquitously expressed heterotrimeric serine-threonine protein phosphatase that is involved in various proliferation and apoptosis related signaling pathways within the cell. It is composed of a scaffold subunit A, a regulatory subunit B, and a catalytic subunit C. The PP2A holoenzyme can be composed of different variations of splice isoforms of the individual subunits. Subunit A and C each have two splice variants α and β, whereas at least 20 different B subunits have been identified thusfar (*195*). Combinations of the different subunits can assemble into over 100 different complexes, with the B subunits conferring substrate specificity (*195, 196*).

SV40 sT binds to the scaffolding subunit A through sT-unique residues 97-103 (*197*). This interaction inhibits binding of the B subunit in a concentration dependent manner, and compromises PP2A activity (*195, 198*). In addition to the direct interaction of sT with PP2A through residues 97-103, the J domain of sT, located in the N-terminal region of sT, directly contributes to PP2A B subunit displacement and sT binding to the A subunit (*198*). sT preferentially inhibits certain subsets of PP2A complexes but the nature of how this selection process occurs is still poorly understood (*199*). Cellular targets that are altered by PP2A inhibition by sT include c-Myc, which is stabilized through S62 dephosphorylation (*200*), as well as Akt, which gets phosphorylated leading to mTOR pathway activation and increased cap dependent translation (*201, 202*). sT targets a variety of cellular kinases involved in cell proliferation that are controlled by PP2A. Examples of these in addition to Akt include MAP kinase signaling

(*203*) and PKCξ activation, which in turn leads to NFκB activation (*204*). The fact that PP2A regulates more than 30 kinases in the cell indicates that sT may have access to control a wide range of signaling pathways, which are likely to contribute to sT-mediated transformation.

1.3.2 SV40 transgenic mouse models

Transgenic mouse models are powerful tools to study the contribution of specific genetic elements to tumor formation in an animal host. They provide the opportunity to analyze transgene expression in specific tissue types and at different stages during development. The SV40 early region has been expressed in a variety of tissues in the mouse. Depending on the specific tissue environment, expression of LT, sT, or both can lead to the development of hyperplasia, dysplasia, carcinoma, or even malignant metastatic disease (*127, 205*). On the other hand, some tissues show no proliferative stimulation at all, underscoring the importance of the specific cell type for tumorigenesis (*199*). A well-characterized SV40 transgenic mouse model targets LT expression to the choroid plexus epithelium (CPE) in the brain, which leads to rapid tumor formation (*206*). The aggressiveness of this particular tumor development is emphasized by the short life expectancy of only 1-2 months in this mouse model.

Functional dissection of LT domains responsible for tumor development in this model revealed that expression of a N-terminal fragment including amino acids 1 through 121 (LT1-121) is sufficient for tumor development; however, tumors progress much slower compared to full length LT (*207, 208*). This observation can be attributed to the p53 targeting domain, which is present in full length LT but not in LT1-121. p53

targeting by full length LT prevents the induction of apoptosis by LT expression, and therefore promotes more rapid tumor development (*209, 210*). Consequently, in a p53 deficient mouse strain, expression of LT1-121 is able to induce tumor development at the same rate as full length LT (*210*). The LXCXE Rb family-targeting domain is essential for tumor development in the context of LT1-121 expression, highlighting the importance of pocket protein inhibition for malignant progression *in vivo*. These results point out that while Rb family targeting is required for cell proliferation through promoting cell cycle entry and progression, p53 targeting prevents subsequent apoptosis induction due to checkpoint activation in response to abnormal cell cycle entry. Therefore, full malignant tumor development in the CPE requires both, the Rb as well as p53 targeting domains of LT. This was confirmed in the mammary gland, where expression of LT1-121 induces tumors to a lesser extend than full length LT due to p53 mediated apoptosis induction (*211*). In addition, p53 targeting by full length LT is also required for the formation of B and T cell lymphomas in respective transgenic model systems (*207, 208*).

Interestingly, the requirement of p53 inactivation for tumorigenesis highly depends on the specific cell type that is targeted for transgenic LT expression. In intestinal enterocytes for example, LT1-121 or LT1-136 expression induces hyperplastic development that progresses to dysplasia with age (*212*) and this is unchanged in a p53 deficient background (*213, 214*). Hyperplasia development in enterocytes is however dependent on an intact LXCXE Rb family-targeting motif as well as a functional J domain, both of which collaborate to bind to pocket proteins and release E2F transcription factors, which in turn promote cell cycle entry and progression. Microarray

analysis in the context of full length LT and LT1-136 expression in enterocytes revealed that the transcriptional profile was almost identical, emphasizing the essential role of the Rb-E2F axis for hyperplastic development in the intestine (*153*). Other cell types in which p53 targeting by full length LT is dispensable include astrocytes, the pancreatic epithelium as well as hepatocytes. In astrocytes, induction of apoptosis by LT expression is mediated through PTEN. Expression of LT1-121 in the context of PTEN loss accelerates astrocytomas in this transgenic model (*215*). Similar results can be observed in the pancreas, where tumor evolution is associated with PTEN loss and does not depend of p53 inactivation by LT (*216*). In a liver specific transgenic model, a functional J domain and intact Rb family-targeting domain are sufficient to induce hepatocellular carcinomas upon expression of LT1-121 (*217*).

Overall, it is clear that SV40 LT targeting of the Rb-E2F pathway is necessary for tumor formation in all cell types tested thus far. In contrast, p53 inactivation by LT is dispensable in some cell types. There are several possibilities that could explain heterogeneous requirements for tumor formation in different cell types. It may be possible that LT interacts with diverse sets of proteins in different cell types, which in turn have differential affects on tumor formation (*205*). On the other hand, it is also possible that LT interacts with the same cellular proteins in all cell types, but that the signaling pathways that these proteins are involved in are regulated differently in each cell type (*205*). Either way, SV40 T antigen transgenic mouse models undoubtedly recapitulate the heterogeneity of the disease they are modeling, which is cancer.

1.4 MERKEL CELL CARCINOMA

1.4.1 Origin and pathology

The first description of Merkel cells (MCs) dates back to 1875, when the German pathologist Friedrich Sigmund Merkel identified them as “Tastzellen” or “touch cells” (*51*). Merkel’s early observations already predicted the mechanoreceptor function of MCs and their role in sensory sensation in the skin, which was established much later (*218*). Located in the basal layer of the epidermis and hair follicle bulges, MCs are closely associated with nerve endings, which is essential in their function of transmitting mechanical stimuli (*219*) **(Figure 7)**.

For a long time, the exact cellular origin of MCs was a topic heavily debated, but recent lineage-tracing studies indicate that MCs arise from epidermal stem cells rather than neuronal progenitors (*220*). MCs give rise to Merkel cell carcinoma (MCC), an aggressive, cutaneous neoplasm, which resembles both basal cell carcinoma and small cell lung carcinoma (SCLC) in its morphology (*221, 222*). Interestingly, MCC is positive for both epithelial as well as neuroendocrine markers. The most distinguishing immunohistochemical markers that are used in the identification of MCC in the clinic include perinuclear staining of cytokeratin 20 (CK20) **(Figure 8B)**, and negative staining for thyroid transcription factor-1 (TTF-1) as well as leukocyte common antigen (LCA) (*223*).

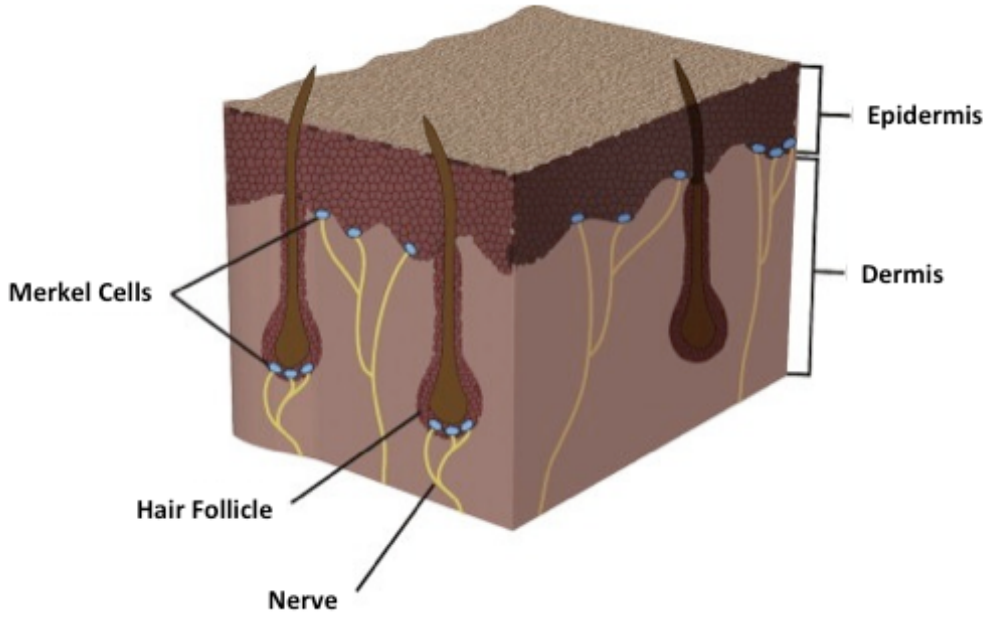

Figure 7. Location of Merkel cells
Merkel cells (in light blue) are located in the basal layer of the epidermis as well as hair follicle bulges, where they make connections with nerve endings. (Modified from Spurgeon and Lambert, Virology, 2013)

1.4.2 Incidence and clinical manifestation

MCC is more common in immunosuppressed individuals such as AIDS and transplant patients as well as the elderly (*53*). The chance of developing MCC is increased 13-fold in AIDS patients compared to the general population (*52*). Ultraviolet (UV) exposure poses an additional risk factor for developing MCC, as is seen in melanoma and other skin cancers (*224*). The majority of MCC patients are Caucasian with a slightly higher frequency in males (*225*). MCC incidence has risen within the past two decades reaching approximately 1,500 cases per year in the United States (*226*). Elevated UV exposure in many parts of the world as well as increasing older populations may result in even more MCC cases in the future. Potentially due to its association with UV

radiation, MCC often arises in the extremities including legs, arms, and the head. **Figure 8C** depicts a MCC lesion on the arm of a patient.

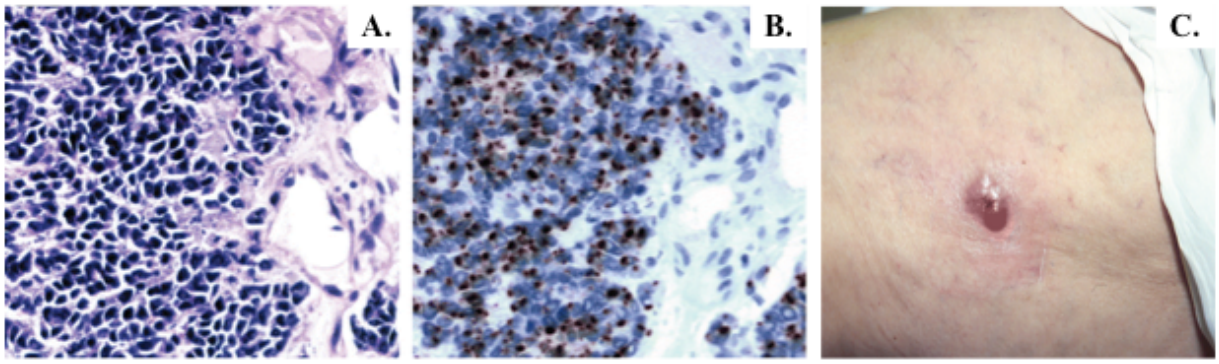

Figure 8. Pathology and clinical manifestation of MCC
(A) Hematoxylin and Eosin (H&E) and (B) diagnostic cytokeratin (CK) 20 perinuclear stain of MCC tumor tissue (C) Red MCC nodule on a patient arm. (Modified from Chang and Moore, Annual Review of Pathology, 2012)

Clinically, MCC is divided into four stages classifying disease severity and prognosis (*227*). Stages I and II include cases that present as local lesions at the primary site on the skin. Stage I encompasses lesions up to 2 cm in diameter, and stage II includes lesions that exceed this 2 cm mark (*228*). MCC cases that involve metastasis to local lymph nodes are classified as stage III. Stage IV, the most severe form, consists of metastatic MCC beyond the lymph nodes (*228*). Staging at diagnosis predicts disease outcome, and determines the treatment regimen. Survival of MCC patients depends on the stage of the tumor at diagnosis. Patients that are diagnosed with stage I MCC have a 5-year survival average of 60%, whereas only 18% of stage IV patients survive 5 years (*229*). These statistics highlight the aggressiveness of MCC as well as the limited treatment options of progressed disease stages.

1.4.3 Treatment

The standard treatment regimen for local MCC primary tumors includes wide surgical excision followed by adjuvant radiotherapy. In addition, sentinel lymph node biopsies are necessary to evaluate regional metastases, which are treated by complete lymph node resection followed by radiation therapy (*227*). There is a high recurrence rate of 30-40%, and primary tumors frequently metastasize to distant sites (*230*). Distant metastatic MCC as well as inoperable primary tumors are often treated with chemotherapeutic regimens used for SCLC patients. Chemotherapeutics used for MCC include a combination therapy with doxorubicin, cisplatin, and vincristine, or with platinum and etoposide (*231*). These treatment regimens yield a good response only within the first 8 months, resulting in a poor survival prognosis (*231*). The median survival time for patients with advanced disease is only 10 months. For a long time, the lack of knowledge about the molecular pathways involved in MCC hindered the design of a more targeted chemotherapeutic treatment regimen. However, with the 2008 discovery of MCV as the causative agent of the majority of MCC (*55*), new studies have already utilized this viral etiology as a target for therapy in pre-clinical studies (*232*) (detailed description in Appendix A and B).

1.4.4 Molecular features

Several studies have found karyotypic abnormalities in MCC. These include deletions or rearrangements in chromosomes 3p, 4, 5q, 7, 10q, 13q and 17q, as well as amplifications of 1q, 3q, 5p, 6 and 8q (*233-235*). Even though chromosomal aberrations

are not consistent across MCC cases, genetic elements that may potentially play a role in tumorigenesis include L-Myc as well as pRB1 (*235*). However, studies linking these abnormalities to the development of MCC are missing.

Gene mutations involved in oncogenic or tumor suppressor signaling have also been evaluated as potential links to MCC. The tumor suppressor p53, which is frequently mutated in skin cancers due to UV exposure (*236*), is mutated only in a subset of MCC, with a large number of MCC tumors having wildtype p53 sequence (*237, 238*). Both Ras (Ha-, Ki- and N-Ras) and CDKN2A (INK4a-ARF locus encoding p14 and p16) point mutations have been implicated in skin tumorigenesis including squamous cell carcinoma (SCC) and melanoma (*239-241*). In the case of MCC however, neither could be detected thus far (*237, 242*).

Activating B-raf mutations, which can be observed in melanoma as well as other human cancers (*243*), were not present in a study that tested 49 MCC cases; in contrast, classical MAP kinase signaling was reported as silenced in this set of MCC (*244*). Additionally, the Wnt/βcatenin pathway as well as c-Kit expression have been evaluated in MCC for possible mutations; however neither show consistent de-regulation that could explain tumorigenic development (*245, 246*). Finally, expression of the anti-apoptotic protein Bcl-2 was reported in 15 out of 20 MCC cases (*247, 248*), which may explain evasion from apoptotic cell death, but does not indicate pathways involved in cell proliferation in MCC.

Up until 2007, many studies identified pathways that are not involved in MCC tumorigenesis; however, the molecular signaling that does play a role in MCC was still a

mystery (*226*). This all changed with the 2008 discovery of an infectious agent associated with MCC.

1.5 MERKEL CELL POLYOMAVIRUS

1.5.1 Discovery of MCV

In 2008, Feng et al. reported the discovery of a clonally integrated polyomaviral genome present in 8 out of 10 MCC samples tested (*55*). In this study, DTS was used to screen MCC cDNA libraries for the presence of non-human sequences, which could indicate the presence of a viral agent. Two MCC cDNA libraries were created from a total of 4 MCC tumor samples and pyro-sequencing generated a total of 216,599 and 179,135 cDNA sequences of ~150 to 200 bp each (*55*). A high-fidelity (HiFi) dataset of 382,747 sequences from both libraries was generated and subjected to DTS analysis (*55*) **(Figure 9)**. *In silico* subtraction of annotated RefSeq RNA, mitochondrial, assembled chromosomes and immunoglobulin sequences from National Center for Biotechnology Information (NCBI) databases, yielded a total of 2394 non-human sequences, which represented candidates for viral genome sequences (*55*) **(Figure 9)**.

Utilizing the Basic Local Alignment Search Tool (BLAST), one candidate cDNA sequence DTS1 indicated high homology to T antigen sequences from both African green monkey lymphotropic polyomavirus (LPyV) as well as human BK polyomavirus (*55*) (**Figure 9**). The novel polyomavirus was called Merkel cell polyomavirus (MCV) due to its connection with MCC. DTS analysis also identified a second cDNA sequence DTS2 aligning with the MCV genome, which showed no homology to any other known

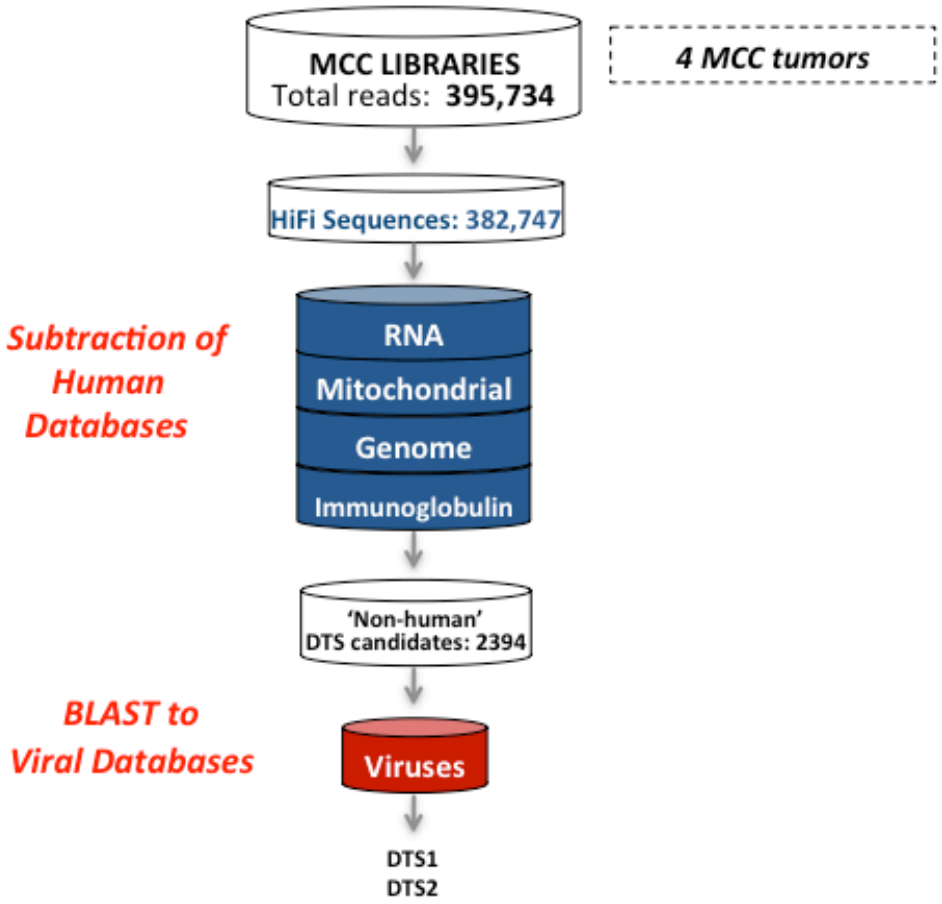

Figure 9. Digital transcriptome subtraction
In silico DTS pipeline applied to MCC cDNA libraries comprised of 4 MCC tumor samples. (Modified from Feng et al., AACR meeting presentation)

polyomaviruses (*55*). Subsequent experiments including Rapid amplification of cDNA ends (3'RACE) and genome walking generated the first complete MCV prototype genomes MCV350 and MCV339 (Accession numbers EU375803 and EU375804 respectively) (*55*). PCR analysis and Southern blotting identified MCV positivity in 80% (8 out of 10) of MCC tumor samples as well as one metastasis. In contrast, PCR analysis with 13 MCV-specific primer pairs revealed only 8% positivity in 59 control tissues from various body sites (from individuals without MCC) and 16% positivity in non-MCC skin samples from both immunocompetent and immunosuppressed individuals (including KS and AIDS patient samples) (*55*).

1.5.2 MCV genome organization

MCV is a double-stranded DNA virus with a genome length ranging from 5.2 to 5.4 kb. Like other polyomaviral genomes, the MCV genome can be divided into an early and a late region divide by a non-coding regulatory region (NCRR) **(Figure 10)**. This NCRR contains the MCV origin of replication (described in detail in Chapter 3 of this thesis), as well as a bi-directional early and late promoter element. The early region transcribes

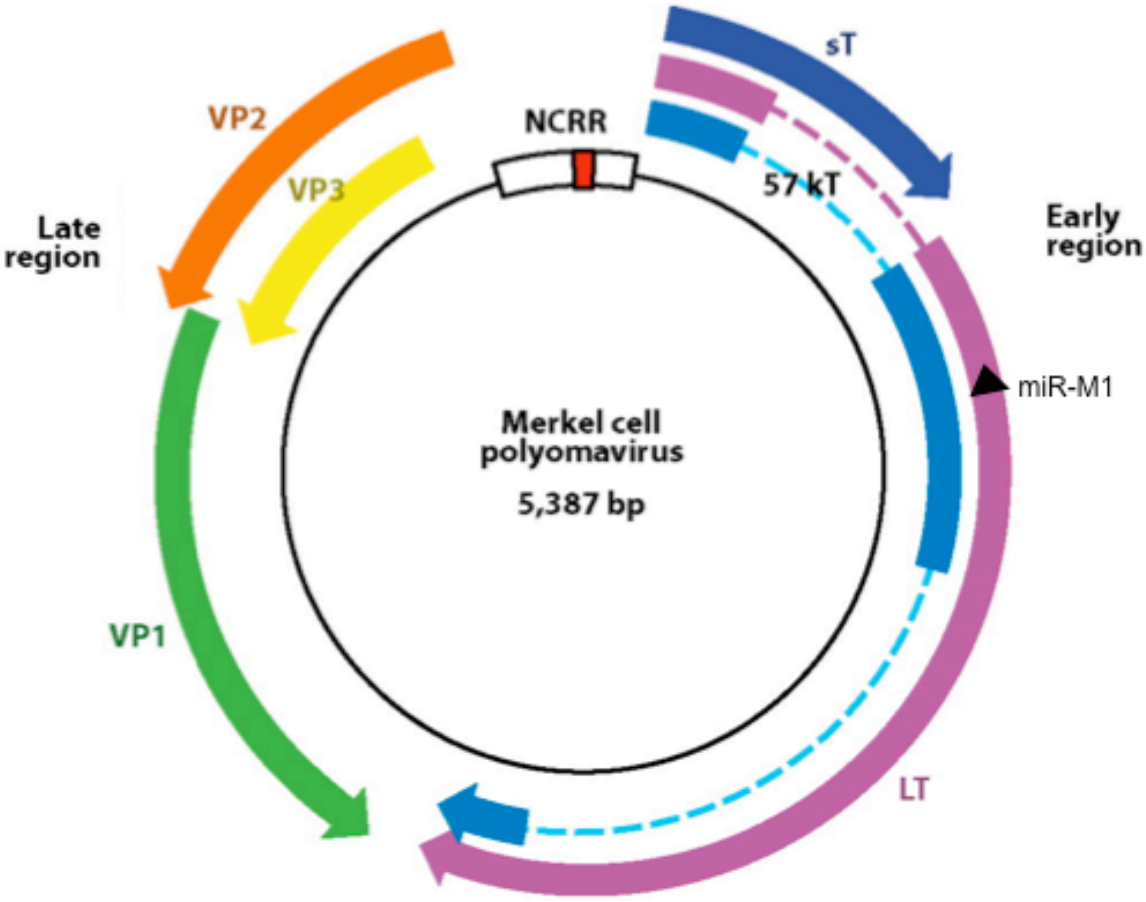

Figure 10. MCV 350 prototype genome organization
MCV350 has a circular double stranded-DNA (5387 bp) genome including a non-coding regulatory region (NCRR), which includes the viral replication origin and a bi-directional early and late promoter element. The early region includes T antigen transcripts (LT, sT and 57kT); the late region includes viral proteins 1, 2, and 3 (VP1-3). The MCV encoded miRNA miR-M1 is indicated with a black arrowhead. (Modified from Chang and Moore, Annual Review of Pathology, 2012)

alternatively spliced T antigen sequences encoding large T (LT) and small T (sT) antigens similar to other polyomaviruses. In addition, MCV encodes a 57 kT splice isoform comparable to SV40 17kT (*110*) **(Figure 10 and 11)**. Initially it was thought that neither the middle T (MT) antigen transcript observed in murine polyomavirus (*249*), nor an agnoprotein as seen in other polyomaviruses (*250, 251*) were encoded by MCV. A recent report however describes a novel MCV MT-like T antigen isoform named ALTO, which is translated from an internal start codon in LT exon 2 with an alternative ORF (*252*).

The MCV late region encodes for the 3 capsid proteins VP1, VP2 and VP3, which are capable of self assembly into virus-like particles (VLPs) of icosahedron structure (*253*). Late gene expression has been linked to active replication of viral DNA. A tumor-derived point mutation in the origin of the MCV-HF molecular clone abolishes viral replication and diminishes late gene expression (*254*). The viral origin of replication is described in detail in chapter 3 of this thesis.

Members of the polyomavirus family including PyV, SV40, BK and JC have been shown to encode viral micro RNAS (miRNAs) that regulate early gene expression (*255, 256*). In the case of MCV, the miRNA miR-M1 **(Figure 10)** has been demonstrated to regulate LT expression in vitro as well as in MCV-positive MCC tumors (*257, 258*). Therefore, its function may involve regulation of LT expression to evade immune surveillance. Cellular targets of miR-M1 have not been identified at this point.

1.5.3 Large T antigen truncations in MCC tumors

Sequencing of additional LT genomes from MCC tumors revealed a consistent pattern of C-terminal truncations due to pre-mature stop codons generated by deletion, substitution, frame shift, or missense mutations (*56, 259-261*). This feature is unique to tumor-derived LT genomes, and LT sequences isolated from asymptomatically infected tissues (i.e. LT206 derived from appendix) are full length (*56*). All sT sequences isolated from MCC tumors thus far are unaffected by truncation mutations. **Figure 11** indicates the C-terminal genomic region in LT that harbors tumor specific truncation mutations. The LT domain that is eliminated in MCC tumors includes the ATPase/helicase domain, which is essential in facilitating viral DNA replication. Thus, tumor-derived truncated LT proteins are defective in initiating viral origin replication (*56*). Recently, the C-terminal exon 3 of LT has been shown to have a growth-inhibitory function independent of viral replication features (*260*). Both the viral replication function as well as the growth inhibitory effect of the C-terminal portion of LT may explain the selective pressure to mutate and eliminate this domain during the process of tumorigenesis. Additionally, mutations in the viral origin as well as VP1 region have been observed, both of which prevent viral particle formation in tumor cells (*254, 262*).

Tumor-derived MCV genomes conserve N-terminal domains that are shared with other members of the polyomavirus family as well as other DNA tumor viruses. These include the conserved region 1 (CR1), DnaJ domain, PP2A binding site in sT, as well as the pocket protein (Rb, p107, p130) binding (LXCXE) motif **(Figure 11)** (*56*). In addition, the MCV unique region immediately N-terminal to the LXCXE contains an hVam6p binding site, which sequesters hVam6p to the nucleus, consequently disrupting

lysosome clustering (*263*). The functional importance of this interaction has not been addressed yet. All tumor LT truncating mutations described thus far appear after the LXCXE motif (*56, 259, 260*), which indicates that this interaction domain is important in facilitating tumorigenic development and maintenance.

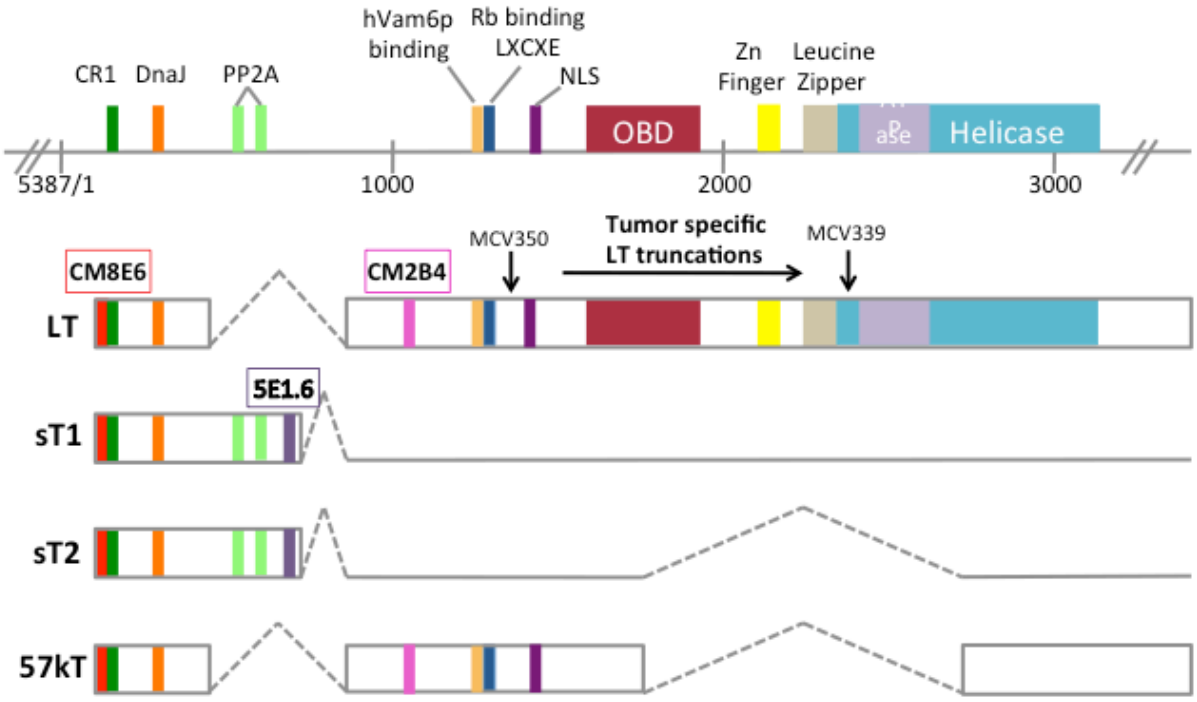

Figure 11. MCV T antigen locus
Alternatively spliced transcripts from the MCV early region include LT, sT1, sT2 and 57kT. mRNA splicing is indicated by the dotted line. Conserved protein interaction domains CR1 (conserved region 1), DnaJ, Rb (retinoblastoma) binding, hVam6p binding and a nuclear localization signal are located in the N-terminal portion of LT. The C-terminal region, which is affected by tumor truncations (indicated by arrows for prototypes MCV350 and MCV339) contains an origin binding domain (OBD), Zinc finger, leucine zipper and ATPase/helicase domain required for viral replication. MCV sT has a PP2A (protein phosphatase 2A) binding motif as seen in other polyomaviral sT proteins. The positions of antibody epitopes CM8E6, CM2B4, and 5E1.6 are shown within different T antigen isoforms.

1.5.4 MCV genome copy number and integration

When MCV was initially discovered, it was found clonally integrated in MCC tumors (*55*), indicating that MCV infection and genome integration precedes carcinogenesis. MCV T antigen copies per cell are usually detected at a level of >1 by qPCR, with some MCCs having more than 10 copies per cell (*55, 57, 264*). VP region copy number determinations repeatedly yield higher copy numbers by qPCR than assays targeting the T antigen region (*57, 265*). At this point the significance of this is unknown, but important experimental limitations that have to be taken into account include potential differences in primer efficiencies for either VP or T antigen amplification. Viral MCV genome copies >1 per cell indicates either multiple cellular integration sites, or viral concatenation in a single integration site. Southern blotting analyses have shown that viral concatamers are present in some MCV-positive MCC cell lines (*56, 265*).

A common cellular integration site in MCC would indicate the interruption or activation of a cellular gene by the viral genome as a factor contributing to MCC tumorigenesis. Multiple groups have mapped integration sites in MCC, but no consistent gene location has been identified (*259, 266, 267*). This indicates that viral protein expression in fact is a key mediator of tumor development. Further details regarding viral copy number and genome integration in MCC cell lines are described in Chapter 2 of this thesis.

1.5.5 MCV Serology and transmission

The fact that low copies of MCV DNA could be detected in healthy tissues of non-MCC patients raised the question whether or not MCV infection is ubiquitous in humans, as seen with other human tumor viruses. Rolling circle amplification (RCA) as well as nested PCR on DNA isolated from skin swabs of healthy individuals revealed that MCV is part of the normal human skin flora (*90, 268*), and serologic studies confirmed 25-88% seroprevalence in healthy individuals (*87, 253, 269, 270*). However, when comparing healthy individuals to MCV-positive MCC patients, it is clear that MCC patients have significantly higher antibody titers against MCV (**Figure 12B**) (*269*). The wide range of MCV seroprevalence in healthy individuals observed between different studies could in part be contributed to differences in antigens used. Analyses utilizing GST-VP1 fusion proteins detect 25-59% seroprevalence (*87, 270*), whereas the use of VLP-derived VP1 epitopes as antigens detects MCV antibodies with higher sensitivity of 60-88% in individuals (*105, 269, 271*). Antibodies against MCV can be detected in children as young as 2 years of age, and a study comparing sera from Langerhans cell histiocytosis (LCH) patients of different age groups reveals an increase of seroprevalence over time, with 80% of people 50 years and older testing positive for MCV exposure (*269*) (**Figure 12A**).

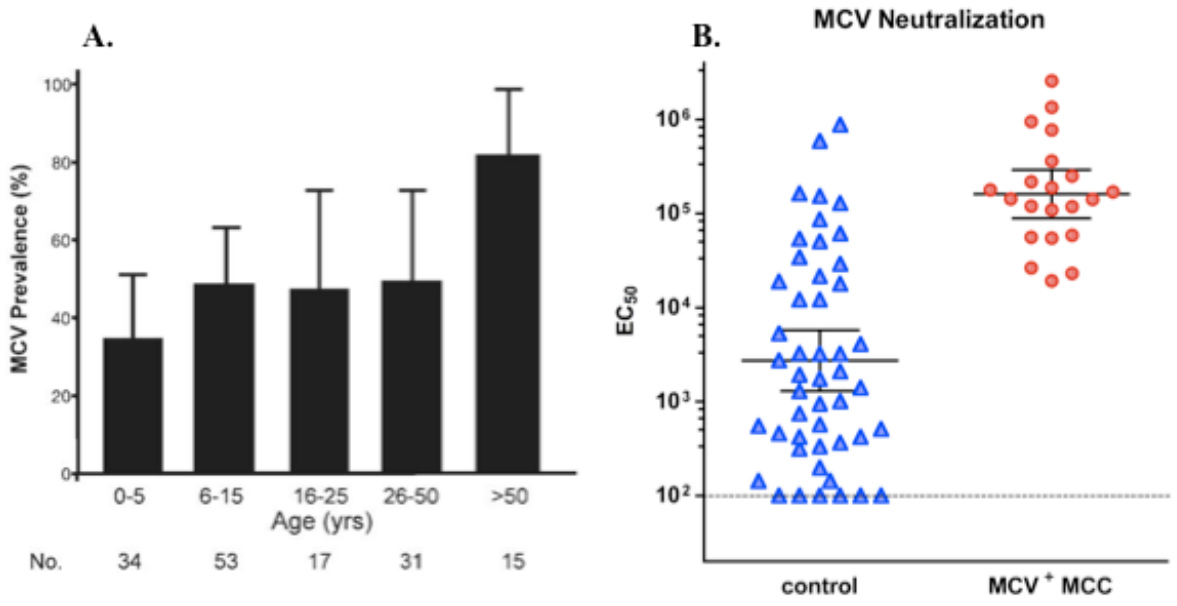

Figure 12. MCV Seroprevalence
(A) MCV seroprevalence can be detected early in life, and increases with age in Langerhans cell histiocytosis (LCH) patients. (Reproduced from Tolstov et al., International journal of cancer, 2009) (B) Neutralization assays reveal significantly higher anti-MCV antibody levels in MCV+MCC patients compared to healthy controls. (Adapted from Pastrana et al., PLOS Pathogens, 2009)

No children under the age of 1 showed any MCV seroprevalence, indicating that vertical transmission is not likely; yet the fact that young children between the ages of 2-5 have detectable levels of antibodies against MCV, suggests a casual route of transmission (*269*). MCV, as well as KIV and WUV, may be transmitted by respiratory route since DNA from these viruses can be detected in the respiratory tract (*272-274*). In addition, MCV is also found in sewage samples (*275*), but the possible role of this in transmission remains to be elucidated.

1.5.6 T antigen expression in MCC

Immunohistochemical analyses of 51 MCC tumors using either the LT specific antibody CM2B4 or an antibody against sT 5E1.6, reveal that 73% of tumors express both T antigens (*129*) (antibody epitopes indicated in **Figure 11**). In this particular study 75% of tumors were positive for LT, whereas 92% were positive for sT expression (*129*). MCC tumor cells uniquely express T antigens, which cannot be detected in healthy tissue adjacent to the tumor (**Figure 13 A-B**) (*129*). MCV-positive MCC cell lines express both individually truncated versions of LT as well as sT protein (see chapter 2). MCC tumors specifically express MCV T antigens, and immunohistochemical staining with an antibody recognizing SV40 LT shows no positivity (**Figure 13C**).

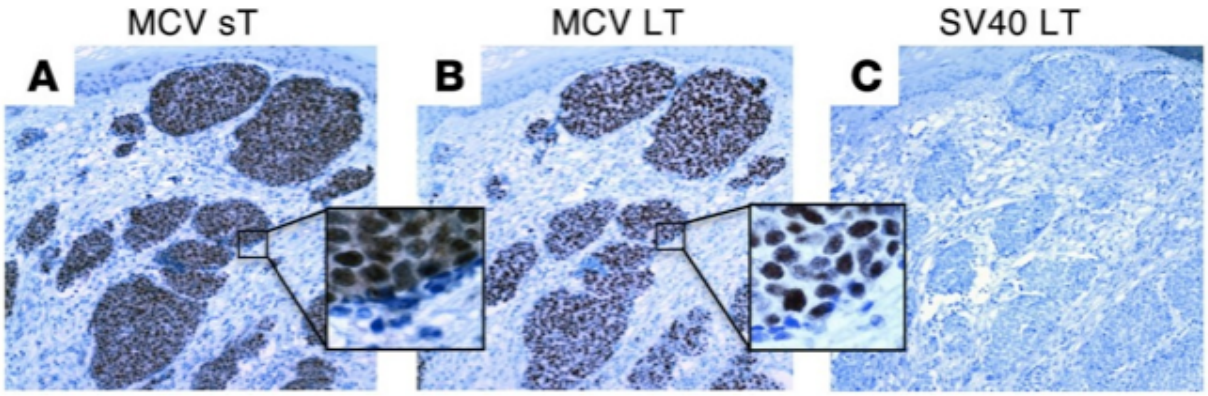

Figure 13. MCV T antigen expression in MCC
Immunohistochemical evaluation of a MCC tumor tissue demonstrates (A) MCV sT expression using 5E1.6 and (B) MCV LT expression using CM2B4 in tumor cells but not normal adjacent tissue. MCC specifically expresses MCV T antigens; (C) SV40 LT expression cannot be detected using the antibody Pab419. Original magnification x100; insets x1000. (Modified from Shuda et al., Journal of clinical investigation, 2011)

To elucidate whether or not MCV-positive MCC cancer cell lines are dependent on T antigen protein expression, knockdown studies were performed that evaluated the effect of simultaneous knockdown of LT and sT (panT), or sT knockdown alone. panT knockdown results in non-apoptotic cell death as well as markedly reduced cell cycle entry of MCV-positive MCC cell lines (*129, 276*). The mechanism of cell death is still unknown. On the other hand, sT knockdown alone (targeting the sT unique region in intron 1) does not induce cell death, but rather results in growth arrest with moderate inhibition of cell cycle entry (*129*). It is difficult to knockdown LT independently of sT, due to an overlap of mRNA sequence of these two transcripts (**Figure 11**). However, one report describes the successful knockdown of LT alone by targeting the splice site between exons 1 and 2 (*277*). LT-specific knockdown results in growth retardation of MCV-positive MCC cell lines *in vitro*, and in a mouse xenograft experiment. Ectopic shRNA-insensitive LT expression rescues this phenotype in an LXCXE-dependent manner, highlighting the importance of this domain in MCC tumors.

1.5.7 MCV T antigen interactions with cellular proteins

Like SV40 and other tumor viruses, the MCV genome contains an LXCXE-pocket protein-binding motif in LT, which is essential for interactions with Rb family members pRB, p107 and p130 as well as other LXCXE-motif containing proteins. Tumor-derived as well as full length MCV LT bind pRB in an LXCXE-dependent manner, and mutation of this motif to LXCXK abolishes the interaction (*56*). As seen with other tumor viruses, this interaction is thought to induce cell cycle entry and therefore is probably important in MCV induced tumorigenesis. MCV LT has been shown to indirectly target the inhibitor

of apoptosis protein (IAP) family member survivin, most likely via E2F transcriptional activation of the survivin promoter as this effect is LXCXE motif-dependent (*232*). MCV-positive MCC cells are dependent on survivin expression and a survivin inhibitor shows promising effects in mouse xenograft studies (*232*) (details can be found in Appendix B and C).

Interestingly, neither full length, nor tumor-derived LT binds to p53, a common cellular target of polyomaviruses and other tumor viruses (*260*). The C-terminal domain, which is responsible for p53 interaction with SV40 LT, is deleted in tumor-derived MCV LT indicating that MCV-induced tumorigenesis is either independent of p53 status or requires additional cellular mutations in the p53 signaling pathway.

A study aimed to discover MCV exclusive interactions utilized the MCV unique region (nt. 861-1565) in a tandem affinity purification (TAP) assay, and identified human Vam6p (hVam6p) bound to MCV LT in close proximity to the LXCXE motif (*263*). This interaction re-localizes hVam6p from the cytoplasm to the nucleus in the presence of MCV LT proteins with an intact NLS, including full length LT and the majority of tumor-derived LTs. One of the observed effects of hVam6p sequestration to the nucleus is the disruption of lysosome clustering in the cytoplasm. Whether or not hVam6p exhibits a gain-of-function in the nucleus, and whether or not this interaction is significant in MCV-positive MCC cancers remains to be uncovered.

As seen with SV40, MCV T antigen interacts with Hsc70 through its HPDK motif in the DnaJ domain, and this interaction is important for viral replication (described in detail in chapter 3 of this thesis) (*278*). MCV sT contains a consensus PP2A binding site found in other polyomaviral small T antigens that inhibit PP2A activity. Neither the PP2A

nor the DnaJ interaction domains of MCV sT contribute to its transforming activity in rodent cells (described in section 1.5.8) (*129*).

1.5.8 Cellular transformation by MCV T antigens

The strong dependency of MCV-positive MCC cells on T antigen expression for survival posed the question whether or not MCV T antigens are capable of transforming cells. *In vitro* assays revealed that MCV sT is able to transform rodent cell lines and promote serum-free human cell proliferation (*129*). Transforming activities were measured by anchorage-independent growth (growth in soft agar) and loss of contact inhibition (focus formation). Neither full-length, nor truncated MCV LT however, showed any transforming activity in these assays. This was a rather surprising result, given the model of SV40-induced cell transformation in which LT is the dominant contributor to the transformation phenotype, and sT alone has no transforming activities. These results highlight unique molecular interactions of MCV T antigens with cellular proteins in comparison to the well-studied SV40 T antigens.

Interestingly, MCV sT transformation is independent of its PP2A interaction domain, which has been implicated as essential in SV40 sT contribution to transformation in the context of SV40 LT. A feature that is necessary for MCV sT-induced transformation is sT downstream targeting of the mammalian target of rapamycin (mTOR) signaling pathway. sT induces mTORC1/mTORC2 independent hyper-phosphorylation and subsequent inactivation of the 4E binding protein 1 (4E-BP1), which results in de-regulation of cap-dependent translation (*129*). In the presence of a constitutively active mutant of 4E-BP1, which cannot be phosphorylated, the

transformation phenotype is diminished. This molecular pathway remains to be explored with regards to potential clinical applications in MCC management.

In vitro human fibroblast transformation by MCV T antigens has not been reported. However, in the context of SV40 T antigen defined human fibroblast. transformation, the additional expression of both hTERT as well as mutated HRas (HRasV12) is required. Chapter 4 of this thesis will present data assaying human fibroblast transformation in the context of MCV T antigens with the addition of defined oncogenic elements. Recently published results by Cheng et al. show that expression of tumor-derived MCV LT and sT in human fibroblasts induces growth proliferation, and that full-length LT contains a growth inhibitory domain in the C-terminal exon 3 (*260*). Expression of a 100 bp exon 3 fragment inhibited cell growth of MCV-positive MCC cell lines and reduced soft agar colony formation of transformed human fibroblasts expressing SV40 LT + sT, hTERT, and HRasV12 (*260*). This data has implications with regards to the tumor evolution model for MCV-positive MCC. It indicates that LT truncations are not only selected for because of the replication function of LT, which lies within the C-terminus, but also because there is an anti-proliferative domain in this region. This is further supported by the fact that the MCV tumor genome MCV350, which has a point mutation in the viral origin that abolishes origin replication, still contains a C-terminal truncation of LT (*278, 279*). In addition, Cheng et al. demonstrated that unlike SV40 LT, MCV LT does not bind to the tumor suppressor p53, providing further evidence for differences in molecular targets between MCV and SV40 (*260*). Characterization of the functional pathways involved in the growth promoting effect of truncated MCV T antigens is described in chapter 4 of this thesis.

1.5.9 Evidence for causality

A vast amount of scientific evidence can be used to argue for a causal relationship between MCV infection and the development of MCV-positive MCC. Applying Hill's criteria (*12*) to this scenario reveals that all of Hill's criteria are met, with exception of his 3rd criterion of 'specificity'. MCV infection is not specifically associated with MCC patients, since healthy individuals are also infected; however, our current knowledge of the cancer phenotype as a multi step process explains how MCV can be required, but may not be sufficient to induce MCC tumorigenesis. Additional factors including immunosuppression, as well as viral genome mutations and integration, possibly induced by UV radiation, are needed. Therefore, Hill's criterion of 'specificity' may not be useful in establishing causal relationships with regards to cancer development associated with tumor viruses.

Hill's 1st criterion 'strength of association' has been established by the detection of MCV DNA in ~80 % of MCC tumors (*55*). His 2nd criterion of 'consistency' is met by repeated results that confirm the presence of MCV in MCC from different groups worldwide (reviewed by Coursaget et al., 2013 (*280*)). The 4th criterion of 'temporality' is supported by the fact that MCV genomes are clonally integrated in MCC (*55*), indicating that MCV infection precedes tumor cell outgrowth. Presence of a 'biological gradient', Hill's 5th criterion, can be observed in immunohistochemical evaluations of MCC tumors, which show that only MCC tumor cells are positive for viral protein expression, but not the adjacent healthy tissue (*281*). The 6th criterion asks for biological 'plausibility', which is provided by the fact that other polyomaviruses are capable of transforming cells and inducing tumors in respective animal models. MCV, which shares many protein

interaction domains that are functionally important for polyomavirus transformation, is therefore a plausible agent for tumorigenic development. The 7th criterion of 'coherence' asks that the causal association under evaluation be in agreement with biological and epidemiological aspects already known about the disease. In the case of MCV association with MCC, it is coherent for MCC to have a viral etiology, since it is a cancer associated with immunosuppression, which suggests an infectious cause. Finally, the 8th criterion of experimental evidence has been strengthened by various studies that show the transforming activity of sT in rodent cells (*129*), dependency of MCV-positive MCC cell lines on T antigen expression (*276*), as well as growth promoting activities of both tumor LT as well as sT in rodent and human fibroblasts (chapter 4) (*129, 260*).

Overall, the collective evidence strongly supports a causal link between MCV infection and MCC development, but additional factors are needed for clinically presented MCC to emerge. MCV-negative MCC arise from an unknown etiology, and therefore should be classified as a distinct type of tumor with a differential chemotherapeutic treatment regimen. MCV T antigen status in MCC therefore could prove useful as a diagnostic marker that can be utilized to distinguish different MCC types, and it may even be used to make prognostic evaluations about disease outcome (*282, 283*).

2.0 CHARACTERIZATION OF AN EARLY PASSAGE MERKEL CELL POLYOMAVIRUS-POSITIVE MERKEL CELL CARCINOMA CELL LINE, MS-1, AND ITS GROWTH IN NOD SCID GAMMA MICE

Work described in this chapter was published in the Journal of Virological Methods

J Virol Methods. 2013 Jan;187(1):6-14.

with authors Guastafierro A, Feng H, Thant M, Kirkwood JM, Chang Y, Moore PS, and Shuda M.

A. Guastafierro, H. Feng and M. Shuda contributed equally to this work.
A. Guastafierro and M. Shuda performed qPCR and RT-qPCR experiments and analyses. A. Guastafierro performed immunoblotting, xenograft experiments and CM2B4 immunohistochemistry of xenograft tumors. M. Shuda performed Southern blotting. H.Feng performed MCV genome sequencing and T antigen transcript mapping. H. Feng and M.Thant determined MCV integration sites in MS-1 and MCC tumors by Phage library screening and RACE analysis. Ms. Marie Acquafondata, Ms. Susan Sharp and the UPMC Presbyterian Clinical IPEX Laboratory performed immunohistochemical staining for MCC cell lines. A. Guastafierro, M.Shuda, Y. Chang and P.S. Moore conceived the project, analyzed results and wrote the manuscript.

This chapter describes the characterization of an early passage MCV-positive MCC cell line MS-1, and compares its cellular, immunohistochemical, and virological features to previously derived MCV-negative (UISO, MCC13, and MCC26) and MCV-positive cell lines (MKL-1 and MKL-2). The MS-1 cellular genome harbors integrated MCV, which preserves an identical viral sequence from its parental tumor. Neither VP2 gene transcripts nor VP1 protein are detectable in MS-1 or other MCV-positive MCC cell lines tested. Mapping of viral and cellular integration sites in MS-1 and MCC tumor samples demonstrates no consistent viral or cellular gene integration locus. All MCV-positive cell lines show cytokeratin 20 (CK20) positivity and grow in suspension. When injected subcutaneously into NOD scid gamma (NSG) mice, MS-1 forms a discrete macroscopic tumor. Immunophenotypic analysis of the MS-1 cell line and xenografts in mice show identical profiles to the parental tumor biopsy. Hence, MS-1 is an early passage cell line that provides a useful *in vitro* model to characterize MCV-positive MCC.

2.1 INTRODUCTION

Due to the limited availability of patient samples and the lack of an animal model, MCC cell lines are critical in investigating MCV-dependent Merkel cell carcinogenesis *in vitro* (*264, 276, 279, 284*). Historically, MCC cell lines have been divided into classic and variant subtypes based on the expression of immunohistochemical markers including neuron specific enolase (NSE) and chromogranin A, as well as their neurosecretory granule status (*285, 286*). Further division of MCC into subtypes I-IV has been based on SCLC morphology, aggregation, and colony shape in culture (*287*). Subtypes I and II grow in dense, floating, spherical aggregates, with type I showing central necrosis (*287*). Type III cells are aggregated loosely with a 2-dimensional appearance, and type IV cells grow in an adherent monolayer (*284, 285*). Most MCV-positive cell lines studied to date are of the classic phenotype and have class III growth morphology in culture, while MCV-negative cell lines mostly fall into the variant class IV phenotype (*284*). However, some MCC cell lines diverge from this grouping, and the discovery of MCV in 2008 has provided a more meaningful classification of MCC cell lines to approach the molecular study of MCC.

Although a number of MCC cell lines have been established from MCC tumors (*264, 287-289*), detailed characterization of features associated with virus positivity, e.g. integration sites, viral sequence and truncation patterns, as well as viral protein expression in MCV-positive cell lines, has not been performed. In addition, many previously derived cell lines are adapted to cell culture conditions as a result of

extended passages, which could lead to the accumulation of spontaneous mutations in the viral or cellular genomes. Such culture-derived changes can only be detected if the sequence of the parental tumor biopsy is known. The establishment of a new cell line allows the comparison of viral sequences as well as protein expression data from the MS-1 cell line to the patient tumor tissue from which it was derived. This aids in determining whether or not this cell line is an appropriate surrogate for its *in vivo* tumor. Comparison of MS-1 phenotypic and genotypic features to previously derived MCV-positive as well as MCV-negative MCC cell lines in this study supports that MCV-positive MCC cell lines are distinct from MCV-negative cell lines in their immunohistochemical profile as well as cell culture morphology. Additionally, MS-1 is tumorigenic in immunocompromised mice, forming xenograft tumors that retain T antigen expression as well as phenotypic markers of the cell line *in vivo*.

In summary, the MS-1 cell line is a well-characterized early passage MCC cell line, which manifests characteristics of the parental MCC tumor tissue, providing a valuable tool for studying MCV-induced MCC carcinogenesis *in vitro*. We describe MCV genome copy number, viral and host cell integration sites, as well as the LT antigen truncation pattern and viral protein expression in this cell line. The establishment of a MS-1 xenograft model that recapitulates features of the original tumor biopsy provides a novel tool for *in vivo* studies of MCV-positive MCC.

2.2 MATERIALS AND METHODS

2.2.1 Preparation of tumor biopsy and cell culture conditions

The MCC tumor biopsy (R08-05) was minced in RPMI 1640 with (filtered) 10% FBS, 1% Pen-Strep, 1% L-Glutamine, and 1% MEM Hepes buffer. Digestion media (0.1% Hyaluronidase, 0.02% DNase, 1.0% Collagenase in PBS, Sigma-Aldrich, St. Louis, MO) was added, and the specimen was placed at 37°C for 30-40 min. After incubation, the suspension was passed through a cell strainer to remove undigested tissue. Cells were initially cultured in RPMI medium with 20% human serum, 0.01% Pen Strep, 0.01% Fungison, 0.01% Insulin-transferrin-selenous-acid, 50 uM bathocuproine disulfate, and 1 M L-Cystein. After 5 passages, serum was switched from 20% human to 20% fetal bovine (FBS), and following passage 10, serum concentration was reduced to 10% FBS in RPMI for culture. Experimental analyses in this this study were performed using MS-1 cells of passage <40.

2.2.2 Real time quantitative PCR

Quantitative PCR was performed using primers amplifying the MCV T antigen promoter region (pTAg 98-184 nt; forward primer: 5'-CCC AAG GGC GGG AAA CTG-3', reverse primer: 5'-GCA GAA GGA GTT TGC AGA AAC AG-3') and VP2 locus (4563–4472 nt, forward primer: 5'-AGT ACC AGA GGA AGA AGC CAA TC-3', reverse primer: 5'-GGC CTT TTA TCA GGA GAG GCT ATA TTA ATT-3') with internal TaqMan probes (pTAg: 5'-CCA CTC CTT AGT GAG GTA GCT CAT TTG C-3', VP2: 5'-GCA GAG TTC CTC-3')

labeled with FAM and BGH quencher for pTAg (Biosearch Technologies, Carlsbad, CA), and MGB quencher for VP2 (Applied Biosystems, Novato, CA). Standard curves for copy number calculations were generated for TAg and VP2 primers separately using values from serial dilutions of known copy numbers of the full-length MCV-HF genomic clone (*254*). Water was used as control and no evidence of PCR template contamination was observed. An RNase P primer probe mixture (Applied Biosystems) was used to determine cell genome copy number. qPCR reaction was performed in triplicates as described previously (*281*). Results are expressed as numbers of viral copies per cell calculated from Ct values of viral and cellular gene standards. To determine T antigen and VP2 mRNA expression levels, the expression of the human RNase P gene was used as a reference, and RNAs from MCV-negative cell lines were used as controls.

2.2.3 MCV genome sequencing

Genomic DNA from MCV-positive MCC cell lines as well as the MS-1 tumor biopsy R08-05 was extracted by the standard phenol chloroform extraction method. 13 PCR primer sets (contig 1- contig 13) were used for PCR amplification of the MCV genome as described before. All PCR reactions were performed with High Fidelity Platinum Taq DNA polymerase (Invitrogen, Carlsbad, CA). Standard Sanger sequencing of PCR products was performed using DNA analyzers from Applied Biosystems.

2.2.4 Phage library screen of MCV integration site

Ten micrograms of genomic DNA extracted from MKL-1 and MS1 cells were digested with *EcoRI* (New England Biolabs, Ipswich, MA), and ligated into Lambda Zap II predigested *EcoRI*/CIAP-treated vector using the Gigapack III Gold Packaging Extract (Stratagene, Santa Clara, CA) to construct the phage library. After titer optimization, 7 µl of a 1:10 dilution of phage library mixed with 600 µl MRF' cells at an OD_{600} of 0.500 were plated on NZY agar, and incubated at 37°C overnight. Two rounds of screens of virus-positive clones were performed with a ^{32}P dCTP-labeled MCV DNA probes according our previously published protocol (*55*). Positive clones were isolated, and inserts were sequenced.

2.2.5 RACE analysis

Both 5'-RACE and 3'-RACE were used to identify integration sites in MCC cases with GeneRacer Kit (Invitrogen) according to the manufacturer's instructions. For MCC347/348 tumor cases, primer sequences were described previously (*55*). For MCC350, 5'-GCT AGA TTT TGC AGA GGT CCT G-3' and 5'-TTT CCT TGG GAA GAA TAT GGA A-3' primers were used to identify a viral integration site by 3'-RACE analysis. For MCC345, 5'-AAA CAA CAG AGA AAC TCC TGT TCC-3' and 5'-TGA TCT TTC TGA TTA TCT TAG CCA TGC TG-3' primers were used in 3'-RACE analysis. For MCC352, 5'-GGG AGG CTC AGG GGA GGA AA-3' and 5'-TCC AGA GGA TGA GGT GGG TTC C-3' primers were used in 5'-RACE analysis. PCR fragments were isolated

from 1.2% agarose gel, extracted with QIAEX II Gel Extraction Kit (Qiagen, Valencia, CA), and ligated into pCR2.1 vector (Invitrogen) for DNA sequencing.

2.2.6 Southern blot

Genomic DNA was extracted by the standard phenol chloroform extraction method. Fifteen micrograms of genomic DNA from cell lines were digested with MCV genome single cut enzymes *EcoRI* and *BamHI* separately or together. Digested DNA was separated on 0.7 % agarose-TBE gel, followed by denaturation for 45 min (1.5M NaCl, 0.5M NaOH), and neutralization for 1h (3.0M NaCl, 0.5M Tris-HCl pH7.4). RNA was extracted using Trizol (Invitrogen). Genomic DNA was transferred onto a Hybond-C nitrocellulose membrane (GE Healthcare) with 10X SSC. To generate a ^{32}P dCTP-labeled probes for Southern hybridization, five MCV DNA fragments (contig1, contig3, contig6, contig9 and contig12) described previously (*55*) were used as templates for the Amersham Rediprime II Random Prime Labeling kit (GE Healthcare). Hybridization was performed as described previously (*279*).

2.2.7 Immunoblotting

Cells were lysed in radioimmunoprecipitation assay (RIPA) buffer containing 50mM Tris, 150 mM NaCl, 0.1% SDS, 0.5% Na Deoxycholate, 1% NP40, and protease inhibitors (Complete cocktail, Roche, Indianapolis, IN). Lysates were kept on ice for 15 minutes, and then centrifuged 20,000 x g for 10 minutes at 4°C. Supernatants were mixed with 5X sodium dodecyl sulfate (SDS) loading dye, and denatured at 100°C for 5 minutes.

Proteins were separated by SDS-polyacrylamide gel electrophoresis **(**PAGE), and transferred onto a Hybond-C nitrocellulose membrane (GE Healthcare). Proteins were detected using CM2B4, CM8E6, CM5E1 and 9B2 antibodies as described before (*129, 254, 281, 290*)

2.2.8 Xenograft model

Triple immunodeficient NOD scid gamma (NSG) mice (Jackson laboratories, Bar Harbor, MN) were housed in a specific pathogen-free area at the Division of Laboratory Animal Research (DLAR) facility at the Hillman Cancer Center, University of Pittsburgh according to University of Pittsburgh Institutional Animal Care and Use Committee (IACUC) regulations (IACUC protocol #1102226). At 6 weeks of age, mice were injected in the flank with 2x10^7 cells in 100 ul PBS subcutaneously. For MS-1 and MKL-1 cell lines, 5 mice were injected each. Mice were sacrificed when tumors reached a diameter of 2 cm. Tumor volumes were calculated according to the following formula: $(\text{width})^2 \times (\text{length}/2)$.

2.2.9 Immunohistochemistry

For immunohistochemical staining of paraffin embedded xenograft tumor tissues, epitope retrieval was performed using 1mM EDTA buffer pH 8.0 at 125°C for 3:15 min after deparaffinization and hydrogen peroxide treatment. After blocking with Protein Block (Dako, Carpinteria, CA), primary antibody was applied for 30 min at room temperature with dilutions described below. After washing, samples were incubated with

Mouse Envision Polymer (Dako) for 30 min at room temperature for subsequent deaminobenzidine (DAB) reaction. Antibodies and dilutions used for immunohistochemistry were: CM2B4 (1:1000; Santa Cruz, Santa Cruz, CA), CK20 (1:50; Dako), CK7 (1:50; Dako), Chromogranin A (1:600; Dako), TTF-1 (1:50; Dako), AE1/3 (1:100; Dako), CAM5.2 (1:10; Becton Dickinson, Franklin Lakes, NJ), Synaptophysin (1:100; Biogenex, Fremont, CA), NSE (pre-dilute; Ventana, Tucson, AZ), and LCA (pre-dilute; Ventana). Each cell line was stained once for every marker, and negative human control tissue was stained with the same antibody dilutions for each marker to ensure minimal background reactivity.

2.3 RESULTS

2.3.1 MS-1 cell culture morphology and immunohistochemistry

The MS-1 tumor biopsy was obtained from a MCC metastasis to the right adrenal gland of a 59-year-old woman. In culture, the cells form floating aggregates of 3-dimensional cell clusters similar to other MCV-positive MCC cell lines including MKL-1, and MKL-2 (**Figure 14 and Table 2**). In contrast, the MCV-negative MCC cell lines UISO, MCC13, and MCC26 grow in an adherent monolayer (**Figure 14 and Table 2**).

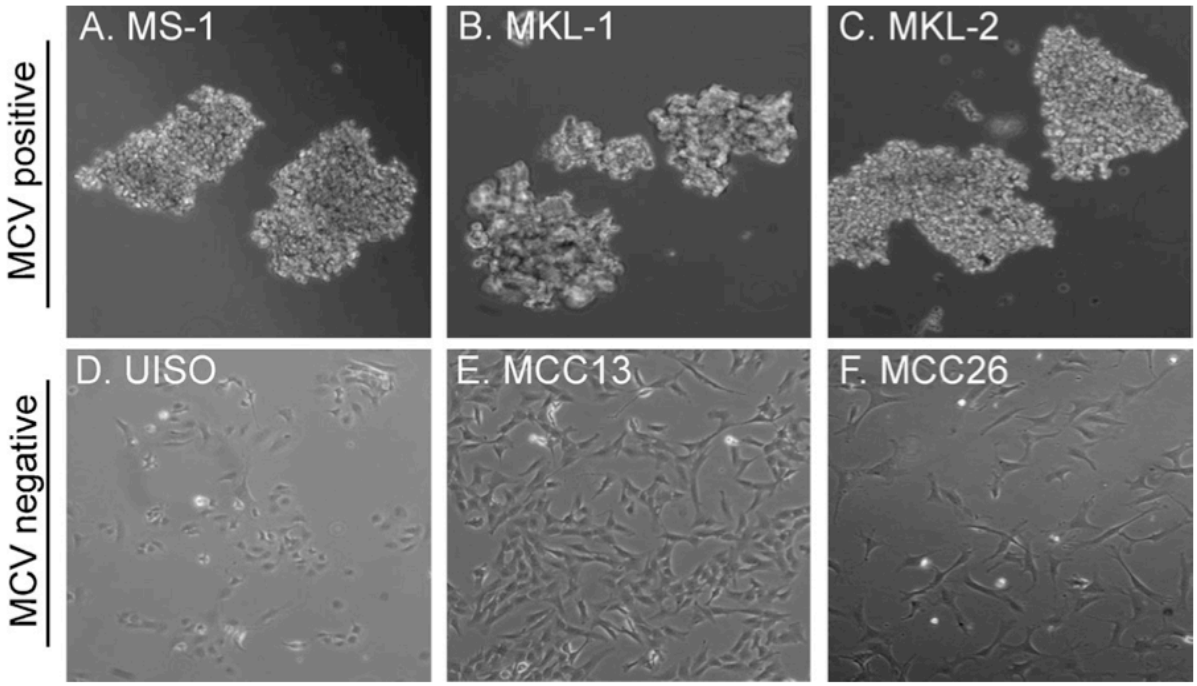

Figure 14. Morphological features of MCC cell lines
MCV-positive cell lines MS-1 (A), MKL-1 (B), and MKL-2 (C) grow in floating aggregates in cell culture, whereas MCV-negative cell lines UISO (D), MCC13 (E), and MCC26 (F) are adherent cells.

Table 2. Immunohistochemical features of MCC cell lines

Markers	MCC diagnostic Profile[a b]	MCV positive			MCV negative		
		MS-1	MKL-1	MKL-2	UISO	MCC13	MCC26
CK20	+	+	+	+	-	-	-
AE1/AE3	+	+	+	+	-	+	-
CAM5.2	+	+	+	+	-	+	-
CK7	-	-	-	-	-	+	-
Chromogranin A	+/-[c]	-	-	+	-	-	-
Synaptophysin	+/-[c]	+	-	+	-	-	-
NSE	+	+	+	+	+	+	-
LCA	-	-	-	-	-	-	-
TTF-1	-	-	-	-	-	-	-

Abbreviations: CK20, cytokeratin 20; AE1/AE3, pan-cytokeratin; CAM5.2, pan-cytokeratin; CK7, cytokeratin 7; NSE, neuron-specific enolase; LCA, leucocyte common antigen; TTF-1, thyroid transcription factor 1

[a] Koljonen, 2006
[b] Goessling et al., 2002
[c] +/- mostly positive

As described before (*276*), immunohistochemical analyses of MCC cell lines reveal differences in various markers diagnostic for MCC between MCV-positive and -negative cell lines (**Table 2**). In comparison to data published previously (*276*), this immunohistochemical analysis of MCC cell lines is expanded to include MCC 26, as well as the negative markers CK-7, TTF-1, and LCA. Cytokeratin 20 (CK 20) is a low molecular weight cytokeratin with perinuclear distribution in MCC, which is used to distinguish MCC from other small cell carcinomas (*291*). MCV-positive cell lines MS-1, MKL-1 and MKL-2 are positive for CK20 by immunohistochemistry, whereas the MCV-negative cell lines UISO, MCC13 and MCC26 are not (**Table 2**). MS-1, MKL-1, MKL-2 and MCC13 are positive for the pan-keratin markers, AE1/3 (anion exchanger 1/3), and CAM5.2 (cytokeratin 8 and 18). Cytokeratin 7 (CK7), which has been reported to stain

negative in MCC (*292*), is positive only in MCC 13 tumor cells. All MCV-positive and –negative cell lines except MCC26 express neuron-specific enolase (NSE), and only MKL-2 expresses chromogranin A (**Table 2**). All cell lines are negative for leukocyte common antigen (LCA) and thyroid transcription factor 1 (TTF-1) (**Table 2**), markers that have been described as negative in MCC biopsies (*292, 293*).

2.3.2 MCV status

MCV copy number per cell was determined by qPCR in three separate experiments (**Table 3**) for the MCV-positive cell lines MS-1, MKL-1, and MKL-2. MS-1 harbors an average of 2.1 copies of T antigen per cell, whereas MKL-1 and MKL-2 harbor 3.5 and 1.7 copies per cell respectively. No positivity was detected in the three MCV-negative MCC cell lines UISO, MCC13, and MCC26 used as controls. VP2 specific primers consistently detect higher genomic copy numbers than T antigen specific primers with MS-1 containing an average of 3.6 VP2 copies per cell. MKL-1 and MKL-2 contain 8.6 and 3.0 copies, respectively (**Table 3**).

Table 3. MCV genome copy number and viral RNA expression

		MCV genome copies per cell		Relative MCV RNA expression[a]	
	MCC cell line	TAg	VP2	TAg	VP2
MCV +ve	MS-1	2.1 ± 0.1[b]	3.6 ± 0.9[b]	0.069[a]	ND[c]
MCV +ve	MKL-1	3.5 ± 0.4[b]	8.6 ± 1.2[b]	0.073[a]	ND[c]
MCV +ve	MKL-2	1.7 ± 0.5[b]	3.0 ± 0.6[b]	0.014[a]	ND[c]
MCV –ve	UISO	ND[c]	ND[c]	ND[c]	ND[c]
MCV –ve	MCC13	ND[c]	ND[c]	ND[c]	ND[c]
MCV –ve	MCC26	ND[c]	ND[c]	ND[c]	ND[c]

[a] normalized to RNase P RNA expression
[b] standard deviation of three independent experiments
[c] not detected

To determine whether there is any correlation between viral DNA load and viral mRNA expression in the MCV-positive cell lines, total RNA was extracted from the MCC cell lines and treated with DNase to eliminate genomic DNA amplification. Quantitative RT-PCR was performed with the same primers used to determine T antigen and VP2 copy numbers per cell. All three MCV-positive cell lines express T antigen mRNA transcripts at different levels, whereas none of them express VP2 transcripts (**Table 3**). MS-1 mRNA levels are 0.069-fold RNaseP expression, whereas MKL-1 and MKL-2 are 0.073-, and 0.014-fold respectively (**Table 3**). There is no apparent evidence for a linear correlation between DNA copy number and mRNA levels.

Southern blot analysis using previously described MCV probes that cover the entire viral genome (*55*), reveals a ~1.6 kb band in the MCV-positive cell lines MS-1, MKL-1, and MKL-2, when digested with the restriction enzymes *BamHI* and *EcoRI*. Both enzymes are single cutters within the MCV genome sequence, and double digestion cleaves a ~1.6 kb internal virus sequence (**Figure 15A**). Consistent with qPCR results (**Table 3**), the intensities of viral internal 1.6 kb bands were similar between MS-1 and MKL-2, whereas MKL-1 shows a 1.6 kb band of higher intensity. Single digestions with either *BamHI* or *EcoRI* generate multiple MCV-related bands in MS-1 (*BamHI*), MKL-1 (*EcoRI*), and MKL-2 (*EcoRI*) consistent with random clonal integration in different cell lines, as has been shown in MKL-1 previously (*279*). Single digestion with either *BamHI* or *EcoRI* yields a 5.4 kb band representing the whole MCV genome in MKL-1 and MKL-2, demonstrating virus concatenation in these cell lines.

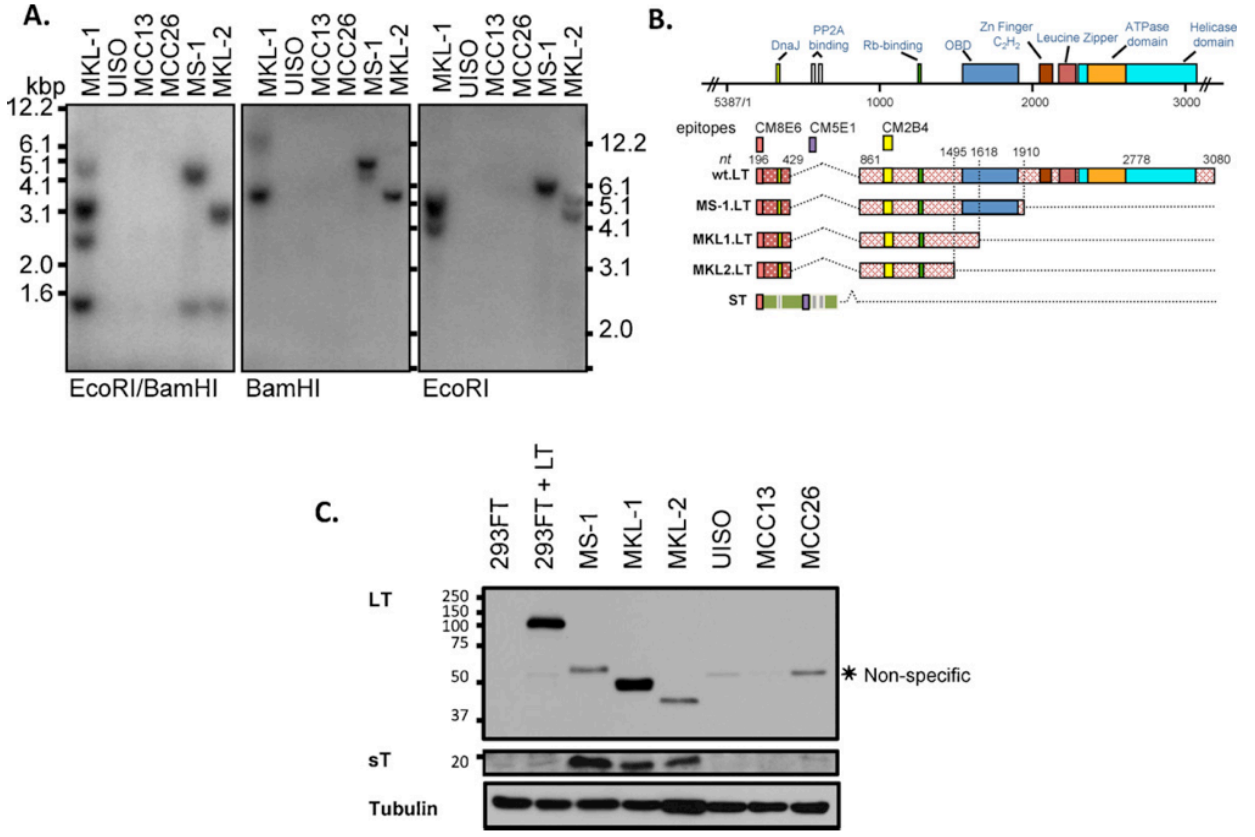

Figure 15. MS-1 harbors clonally integrated MCV and expresses viral T antigens
(A) Southern blot analysis of MCV-positive cell lines shows clonally integrated viral genomes. (B) The MCV-positive MCC cell lines MS-1, MKL-1 and MKL-2 have C-terminal LT truncations as determined by direct sequencing performed on genomic DNA. LT protein sizes correspond to 428 aa, 330 aa, and 275 aa, respectively. (C) Western blotting using antibodies CM2B4 for LT and CM8E6 as well as CM5E1 for sT shows differences in size of LT proteins from different MCV-positive MCC cell lines, whereas sT size is the same. The CM2B4 antibody picks up a faint non-specific band in MCV-negative MCC cell lines (marked *).

2.3.3 T antigen truncations and corresponding protein sizes

Next, we sought to determine the T antigen truncation pattern in MS-1 as well as MKL-2. The MKL-1 LT truncation (GenBank accession no. FJ173815.1) has been mapped previously (*279*). Genomic DNA was isolated from MS-1, MKL-1 and MKL-2, and subjected to direct sequencing using MCV contiguous primer pairs spanning the whole

MCV genome (*55*). Sequencing of the PCR products revealed premature stop codons in all three cell lines (**Figure 15B**). MS-1 LT terminates at nucleotide position 1910, whereas the MKL-1 and MKL-2 LT truncations can be found at positions 1618 and 1495 respectively (**Figure 15B**).

The differential LT truncation patterns of MCV-positive cell lines are reflected by varying LT migration speeds by immunoblotting (**Figure 15C**). MS-1 expresses the largest LT protein among the MCV-positive MCC cell lines in this study, with the truncation occurring after the origin-binding domain (OBD) of LT, yielding a 428 amino acid (aa) long protein. MKL-1 (330 aa) and MKL-2 (275 aa) LT truncations are N-terminal to the MS-1 truncation mutation, while all three truncated LT proteins maintain the LXCXE Rb binding motif (**Figure 15B**). This truncation pattern and conservation of the N-terminal motifs is consistent with LT sequences derived from MCC tumor tissues in various studies (*279, 294, 295*). In agreement with the truncation patterns in **Figure 15B**, MS-1 expresses a 60 kDa truncated LT protein as compared to a 105 kDa full length LT expressed exogenously in 293 FT cells (**Figure 15C** compare lane 3 to lane 2). MKL-1 and MKL-2 also express shorter forms of LT, which migrate at 50 kDa and 40 kDa, respectively. Even though sequencing results reveal intact splice donor and acceptor sites for the 57 kT isoform, neither MS-1 nor MKL-2 express a 57 kT protein that is detectable by immunoblotting (**Figure 15C**). MKL-1 has already been reported to have a deletion in the second splice donor site of 57 kT (*279*), which explains the absence of this isoform. All MCV-positive cell lines consistently express an intact 19 kDa sT protein (**Figure 15C**). While sT protein size does not differ between cell lines (**Figure 15B-C**), sequencing results reveal one single nucleotide polymorphism, which

results in a difference in amino acid 20 of sT between cell lines. MS-1 and MKL-1 have an alanine at this position, whereas MKL-2 has a serine.

Viral sequence comparison between the MS-1 cell line and its parental tumor biopsy (R08-05) reveals the same pre-mature stop codon mutation of LT as well as an identical MCV genome sequence with a deletion from nucleotide 1912 to 1951 and a 5 base pair insertion at position 5218 (**Figure 16**). As described previously, the MKL-1 viral genome has a deletion at nucleotide position 1612-1657 (FJ173815.1). The MKL-2

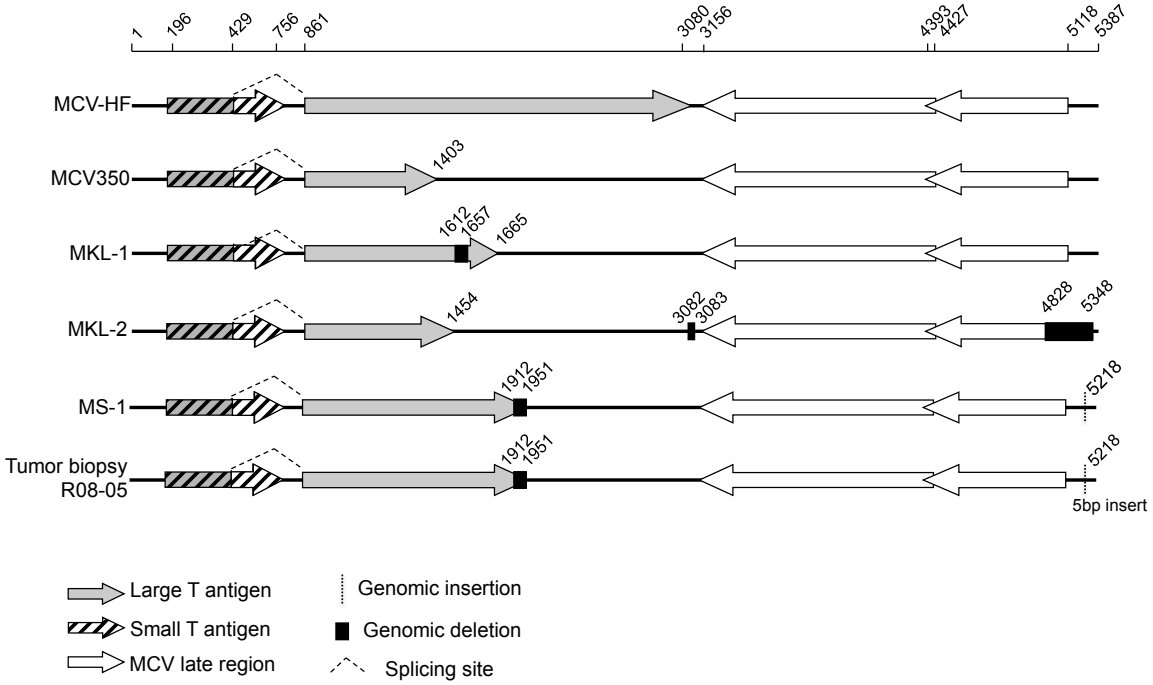

Figure 16. MCV genome comparison
MCV genomes from published clones MCV-HF, MCV 350 and MKL-1 were compared to MCV genomes from MKL-2, MS-1 and the R08-05 tumor biopsy based on genomic sequence alignments. Genomic deletions (black box) as well as insertions (vertical dotted line) are indicated for early (gray) and late (white) regions.

genome has two deletions at nucleotide positions 3082-3083 and 4828-5348 (**Figure 16**). MCV viral genome sequences have been deposited to GenBank with corresponding accession numbers JX045709 (MS-1) and JX045708 (MKL-2).

2.3.4 Viral genome integration site

To determine the integration site of the MCV genome within the cellular genome of MS-1, a lambda phage library was constructed from MS-1 genomic DNA and used for library screening. The MCV genome integration in MS-1 maps to a non-coding DNA region on human chromosome 5 (5q11.2). In the MCV genome, the integration event occurs after base pair 2843, which maps to the ATPase/helicase domain of LT (**Table 4**). Four MCC tumor samples (347/348, 345, 350, and 352), identified previously as MCV-positive (*55*), were tested for MCV integration sites by RACE, and no common cellular or viral integration sites were found (**Table 4**), consistent with previous studies (*259, 294, 296*).

Table 4. Chromosomal integration sites in MCC

MCC	Type	Methods	Chromosome	Locus[a]	Gene	MCV breakpoint
MS-1	cell line	Phage library	5q11.2	2,282,589	Non-coding region	2843
347/348	tumor tissue	3'RACE	3p14.2	61,561,985	PTPRG (intron1)	2140
345	tumor tissue	3'RACE	6p24.3	9,842,760	MRDS1 (intron6)	1836
350	tumor tissue	3'RACE	3q26.33	88,824,524	Non-coding region	596
352	tumor tissue	5'RACE	10q23.1	36,041,150	Unidentified ORF	491

[a]GRCh37.5

2.3.5 Tumorigenicity of MS-1 cells *in vivo*

The MCV-positive cell line MKL-1 (*288*) has been shown to induce tumors in immunocompromised mice. The established MS-1 cell line was tested in NSG mice for *in vivo* growth. After injecting MS-1 cells subcutaneously in the flank, tumor formation was observed at injection sites after 30 days (**Figure 17A**). This represents a 14-day delay in tumor onset as compared to MKL-1, and a slower growth behavior subsequently (**Figure 17A**). The mice did not develop metastasis during the 80-day observation period, and were killed when the tumor reached a diameter of 2cm. LT and

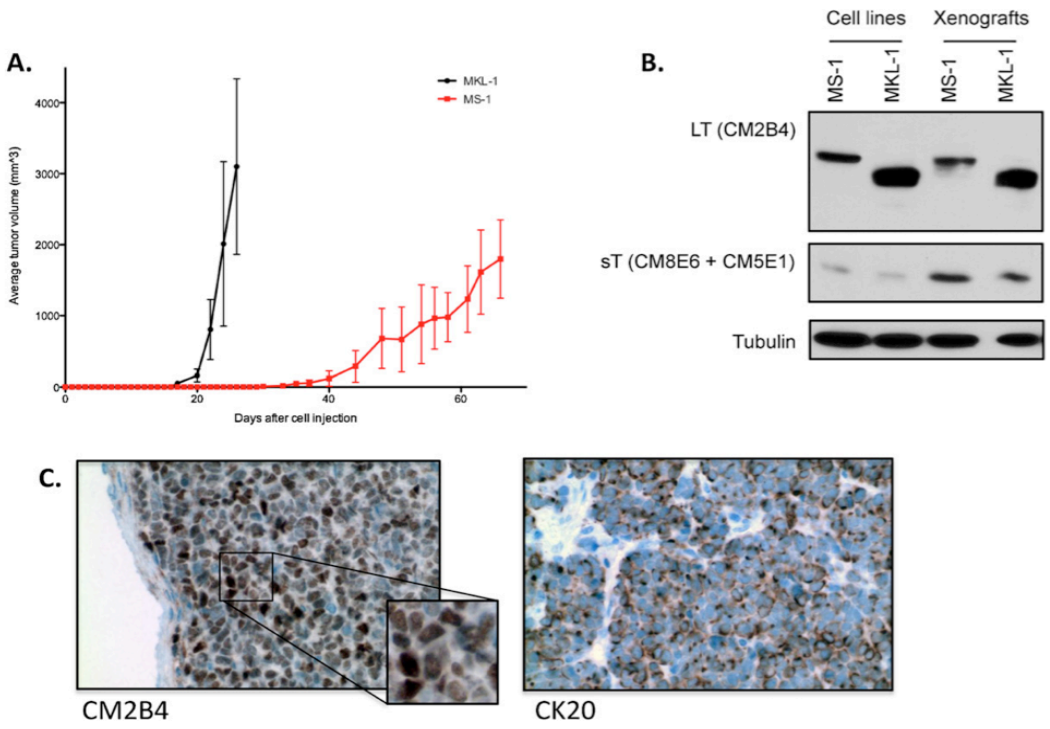

Figure 17. MS-1 xenograft model
(A) Tumor volume graph represents average tumor volumes of 5 animals for each MS-1 and MKL-1 cell lines. (B) Immunoblot analysis of MS-1 and MKL-1 xenograft tumors shows LT as well as sT protein expression *in vivo*. Three separate xenograft tumor lysates were prepared for each cell line; one representative is shown here. (C) Immunohistochemical analysis of MS-1 xenograft tumors validates LT protein expression and nuclear localization (CM2B4), as well as CK20 positivity *in vivo.*

sT protein sizes were unchanged *in vivo* as demonstrated by immunoblot (**Figure 17B**). Nuclear localization of LT protein expression was maintained, as shown by immunohistochemistry (**Figure 17C**), as was perinuclear distribution of CK 20 in the MS-1 xenograft tissue (**Figure 17C**).

2.4 DISCUSSION

Tumor-derived MCV-positive MCC cell lines represent a valuable tool for *in vitro* analyses of MCV related MCC carcinogenesis. For example, Houben *et al.* demonstrated that T antigen knockdown in MCV-positive MCC cell lines results in growth arrest and cell death (*297*) underscoring the critical role of viral T antigen expression in MCC tumorigenesis.

The MS-1 cell line is a newly established MCC cell line that has been maintained in culture for few passages (<40 passages). MS-1 is positive for MCV, and displays a tumor specific C-terminal LT truncation pattern. Using RNase P as a cellular reference gene, T antigen copy number in MS-1 was determined by qPCR, to be 2.1 copies per cell, which could be explained by either multiple viral integration events or virus concatenation. At this point however, we do not have experimental evidence that would suggest multiple integration events nor virus concatenation in MS-1. MCV-positive MCC cell lines MKL-1 and MKL-2 also have T antigen copy numbers >1 **(Table 3**), and southern blot data (**Figure 15A**) supports the presence of concatenated viral genomes in these cell lines. In addition, southern blot analysis confirms higher genome copies in MKL-1 cells than MS-1 and MKL-2 cells, which is consistent with qPCR results. In agreement with our results, Fischer *et al.* have also described variations in MCV copy number per cell in other MCC cell lines (*264*). However, the use of different reference genes for qPCR copy number determination has to be taken into account since cancer cells often harbor chromosomal aberrations. In MCC, specific chromosomal aberrations

for chromosomes 1, 3-8, 10, 13, and 17 have been reported (*234, 235*). However, there is no reported data that suggests deletion or amplification of the RNase P reference gene, located on chromosome 14, in MCC.

T antigen copy number per cell corresponds to LT protein expression by immunoblot, which shows a stronger protein band for MKL-1 LT as compared to MS-1, which has a lower copy number of T antigen per cell compared to MKL-1. One explanation for the variations in LT expression levels observed between cell lines may be due to a difference in protein stability caused by different truncations. However, further studies are needed to investigate this. Even though VP2 copy numbers in the three MCV-positive MCC cell lines are higher than the T antigen, neither VP1 protein immunoblot (data not shown) nor quantitative RT-PCR on VP2 transcripts (**Table 3**) detect expression of late gene products. These results do not support one reported observation of viral particle production in MCC by electron microscopy (*298*). Instead, our data suggests that late gene expression or viral particle production of MCV is absent in MCC tumors.

LT proteins expressed in the MCV-positive MCC cell lines migrate at higher molecular weights than the predicted sizes from their individual truncations. MS-1 LT is truncated after 428 amino acids and has a predicted molecular weight of 48 kDa, but it migrates at ~60 kDa on SDS-PAGE (**Figure 15B-C**). MKL-1 and MKL-2 LT protein have predicted molecular weights of 37 kDa and 31 kDa, respectively, but they migrate at ~ 50 kDa, and ~ 40 kDa. Explanations for this difference in migration may include aberrant migration due to charge as well as post-translational modifications of LT such as phosphorylation or acetylation, both of which have been reported previously for T

antigens of other polyomaviruses including murine polyomavirus middle T antigen and SV40 LT (*299, 300*). Phosphorylation of LT in MKL-1 has been confirmed experimentally (data not shown), and results in higher molecular weight of LT on SDS-PAGE. Other modifications are likely, and require further experimental analyses.

The MCV integration site within the cellular genome of MS-1 as well as several other MCC tumor samples was determined. A common integration site could point toward the disruption of a cellular gene as a factor in MCC tumorigenesis. However, the MCC tumor samples including MS-1, did not show any common integration sites nor any interruptions of tumor suppressor genes (**Table 4**). Therefore, it is less likely that the interruption of a common host cell gene by viral integration contributes to tumorigenesis in most MCV-associated MCC.

Sequence comparison between the MS-1 cell line and its parental tumor biopsy reveals identical viral sequences and LT truncation patterns (**Figure 16**). This suggests that additional mutations of the viral genome acquired during cell culture are not necessary to maintain the tumorigenic phenotype of MS-1 neither in culture nor in an *in vivo* xenograft setting. All three MCV-positive cell lines conserve the LXCXE Rb binding motif in LT as observed in other MCC tumor-derived LT (*279*). Experimentally, the importance of LT binding to Rb has been demonstrated by Houben *et al*. *in vitro* and in an *in vivo* xenograft model using the MCV-positive MCC cell lines WaGa and MKL-1 (*297*). However, another report demonstrates that MCV LT cannot transform rodent NIH 3T3 and Rat-1 cells in contrast to MCV sT, which alone is sufficient to transform rodent cells (*129*). Therefore, LT's Rb-targeting function may play an essential role in human

cell transformation in concert with sT's oncogenic function, which is expressed intact in all three MCC cell lines (**Figure 15C**).

Morphological comparison between MCV-positive and -negative cell lines demonstrates a significant difference in appearance as has been described before (*276*). Immunohistochemical analysis of the MCV-positive and MCV-negative MCC cell lines shows that only the MCV-positive lines conform to diagnostic criteria that distinguish MCC tumors from other neuroendocrine cancers (**Table 2**). These results are in concordance with published data (*276*) for CK20, pan-CK as well as NSE markers in the MCC cell lines studied. In contrast, the immunohistochemical data for chromogranin, as well as synaptophysin presented in this study, show differences from published results (*276*) for the cell lines MS-1, MKL-1, and MCC13. These differences may be a result of different experimental techiques used, as Houben *et al*. determined their results by qPCR instead of immunohistochemistry.

Despite a report by Fischer *et al*. of the adherent MCV-positive MCC cell line MCCL12 (*264*), all MCV-positive MCC cell lines tested in this report demonstrate a suspension growth pattern in culture. The MCV-negative cell lines used in this study are not only immunophenotypically different from MCC they also grow adherently *in vitro*. In SCLC, adherent cell growth is associated with loss of neuroendocrine marker expression and adherent growth (*286*). Despite the data on UISO, MCC13 and MCC26, the MCV-negative cell line MaTi, was found to grow in suspension similar to MCV-positive cell lines. However, MaTi neither expresses CK20 nor other cytokeratin markers similar to the MCV-negative cell lines studied by us. Among the MCV-negative MCC cell lines analyzed, one cell line, MCC26, lacks expression of all neuroendocrine

markers examined. Those markers could be attenuated by de-differentiation of cells associated with tumor progression. However, the difference in growth morphology and the lack of CK20 positivity in UISO, MCC13, MCC26, and MaTi raises concern whether they were originally derived from correctly diagnosed MCC tumors. Alternatively, outgrowth of another cell population during the process of culturing is possible, and could explain the difference in morphology as well as phenotypic markers by immunohistochemistry. This is an important factor to take into account when using MCV-negative putative MCC cell lines as controls for MCV-positive MCC cell lines.

In vivo analysis of the MS-1 cell line confirms its tumorigenic growth potential by forming tumors in immunocompromised mice as has been shown in other MCC xenograft studies before (*277, 301, 302*). MS-1 cells maintain viral T antigen expression and LT nuclear localization, as well as CK20 positivity *in vivo*, demonstrating the validity of this xenograft model with regard to MCC tumorigenesis. *In vivo*, MS-1 xenografts are less tumorigenic compared to MKL-1, with a 14-day delayed onset of tumor growth as well as a slower growth rate after tumor onset. In concurrence, xenograft models described in the literature for different cancer cell lines show varying onsets of tumor growth as well as differential levels of metastasis (*303, 304*). It is possible that higher protein expression of LT in MKL-1 compared to MS-1 (**Figure 15C**) is a factor contributing to increased tumorigenicity *in vivo.* Surprisingly, no metastatic growth was observed in mice injected with MS-1 despite the aggressive nature of MCC in humans, and the fact that MS-1 was derived from a metastasis.

The data presented in this study emphasizes that MS-1 and MCV-positive MCC cell lines in general, represent important tools to understand MCV biology and potential

mechanisms of viral tumorigenesis in MCC. MS-1 in particular is a good cell culture model due to its low passage number, and well-characterized viral features. Importantly, MS-1 has identical features to the parental MCC tumor from which it was derived. To conduct translational research focusing on the viral etiology of MCC, having an accurate model system that reproduces the virus-associated features of clinical disease is essential. MS-1 is a cell line that provides these benefits and shows great potential in pre-clinical applications including drug screening of chemotherapeutic agents.

3.0 THE MINIMUM REPLICATION ORIGIN OF MERKEL CELL POLYOMAVIRUS HAS A UNIQUE LARGE T-ANTIGEN LOADING ARCHITECTURE AND REQUIRES SMALL T-ANTIGEN EXPRESSION FOR OPTIMAL REPLICATION

Work described in this chapter was published in the Journal of Virology

J Virol. 2009 Dec;83(23):12118-28.

with authors Kwun HJ, Guastafierro A, Shuda M, Meinke G, Bohm A, Chang Y, and Moore P.S.

H.J. Kwun, A. Guastafierro, and M. Shuda contributed equally to this work.
H.J. Kwun, A. Guastafierro, and M. Shuda performed plasmid construction and cloning. A. Guastafierro performed origin replication experiments and analyses. H.J. Kwun performed immunoblotting, immunoprecipitation and ChIP experiments. M. Shuda performed knockdown studies and immunoblotting. Dr. Mary Ann Accavitti produced antibodies. G. Meinke performed molecular modeling. H.J. Kwun, A. Guastafierro, M.Shuda, Y. Chang and P.S. Moore conceived the project, analyzed results and wrote the manuscript.

This chapter describes the genomic mapping of the 71 bp minimal MCV replication core origin that is sufficient for initiating eukaryotic DNA replication in the presence of wild-type MCV large T (LT) protein. The origin includes a poly (T) rich tract and eight variably oriented, GAGGC-like pentanucleotide sequences (PS) that serve as LT recognition sites. Mutation analysis shows that only four of the eight PS are required for origin replication. A single point mutation in one origin PS from a naturally occurring, tumor-derived virus reduces LT assembly on the origin and eliminates viral DNA replication. Tumor-derived LT having mutations truncating either the origin-binding domain or the helicase domain also prevent LT-origin assembly. Optimal MCV replication requires co-expression of MCV small T (sT) protein together with LT. An intact DnaJ domain on the LT is required for replication but is dispensable on the sT. In contrast, PP2A targeting by sT is required for enhanced replication. The MCV origin provides a novel model for eukaryotic replication from a defined DNA element and illustrates the selective pressure within tumors to abrogate independent MCV replication.

3.1 INTRODUCTION

Unlike human cellular DNA replication origins, polyomavirus replication origins are discrete and well-defined yet retain many features of eukaryotic cellular origins. For this reason, polyomavirus replication origins, particularly the SV40 origin, have been used as easily tractable models to define eukaryotic replication requirements (*305*).

Polyomaviruses are small, double-stranded DNA viruses with circular genomes functionally divided into coding and noncoding regions (*306*). The early coding region for all polyomaviruses encodes large tumor (LT) and small T (sT) antigens that serve as viral oncoproteins and a late coding region that produces viral structural proteins. Aside from LT and ST, other T antigen isoforms, such as middle T antigen (MT) and 17kT/57kT, may be present and are virus-specific. LT has pleiotropic functions that include initiation and maintenance of viral DNA replication, regulation of early and late genes transcription, and virion assembly (*307-313*). Expression of LT also leads to the transformation of susceptible cell lines mediated in part by functional regions such as the DnaJ, pocket protein binding, and p53 binding domains that target growth-suppressing and cell cycle regulatory proteins (*314*). Additionally, sT has been shown to play an important role in LT mediated cell transformation in SV40 (*315-319*) and has been reported to increase virus replication efficiency in JCV (*320*).

Polyomavirus origins are situated within a noncoding site, located between early and late viral coding regions, which also contains promoters for early and late transcriptional units and enhancers that mediate cis-activation of early gene

transcription (*306*). Polyomavirus replication origins contain a central region, referred to as Site 1/2 in murine polyomavirus (Py) and Site II in SV40, with variable numbers of LT-binding pentanucleotide sequences. Since MCV is more closely related to Py, we will use the Py nomenclature in this chapter. Site 1/2 is flanked by AT-rich regions: the homopolymeric T tract on the late side of MCV Site 1/2 is called the AT-rich tract and is an initial site for polyomavirus DNA melting during replication (*321*). For SV40, the AT-rich region on the opposite, early side of Site 1/2 is palindromic and referred to as the early palindrome (EP). While this region is also AT-rich in the MCV origin, no palindrome is present (*55*).

An initial step in polyomavirus DNA replication is seeding of LT at consensus DNA 5'-G(A/G)GGC-3' pentanucleotide sequences (PS) in the LT binding site 1/2 region followed by oligomerization of double LT hexamers in a head-to-head orientation (*306*). Three structural domains of SV40 LT, the DnaJ domain, the origin-binding domain (OBD), and the helicase domain, have all been subjects of structural studies (*322, 323*). Although precise mechanistic details remain unclear, it is known that the helicase domain works in concert with the OBD to initially melt dsDNA in the AT-rich tracts. In SV40, the melted DNA is believed to be threaded through the double hexamer of TAg such that the two 3' ends leaving Site II (Site 1/2 in Py) pass through the centers of two opposing hexameric rings formed by the LT helicase domain. Once loaded, LT functions as an ATPase-driven DNA pump that also recruits cellular machinery (replication protein A, topoisomerase, and the polymerase alpha complex) for DNA replication (*322-329*). Sequence analysis shows that the MCV origin has a comparable arrangement of sequence motifs to the replication origins of Py subgroup

polyomaviruses (*55*). In contrast to the SV40 origin, which has a minimum, definable boundary, the replication functions of the origin of Py are more diffusely distributed (*330-333*). Despite similarities between MCV and SV40 origins, neither MCV nor SV40 T antigen initiate replication of the heterologous origins from the other virus (*279*).

In this study, we identify an MCV core origin and define the requirement for individual PS in LT-mediated replication that suggests the possibility of a more complex orchestration of LT seeding for MCV than the head-to-head double hexameric arrangement for SV40. Further, a single origin point mutation in a tumor-derived MCV strain at a critical PS outside of the canonical LT interaction region (Site II for SV40 and Site 1/2 for Py) abrogates MCV origin replication. We show that optimal LT initiation of MCV replication requires both viral sT protein expression and intact cellular Hsc70 binding by LT to fully support efficient viral DNA replication.

3.2 MATERIALS AND METHODS

3.2.1 Plasmids

Construction of genomic (TAg206.wt, TAg350, TAg339) and cDNA (57kT.wt) TAg expression plasmids were described previously (*279, 281*). For the LT cDNA constuct, cDNA was first amplified by PCR (*281*) followed by site directed mutagenesis to delete the 57kT exon 3 splice acceptor site using PCR primers 5'-CAC TTT TCC CCA AAA GCA AAT CTA AGA GAT TCC C-3' and 5'-GGG AAT CTC TTA GAT TTG CTT TTG GGG AAA AGT G-3'. To generate sT-eGFP, the open reading frame of sT was amplified from MCC350 (*55*) using primers (LT.*EcoR*V.S: CCG ATA TCA TGG ATT TAG TCC TAA ATA GG, sT.*Xho*I.AS: GGG CTC GAG TAG AAA AGG TGC AGA TGC AG) and cloned into pcDNA6/V5-HisB (Invitrogen) using *EcoR*V and *Xho*I restriction sites. The sT fragment was then transferred into pEGFP-N1 (Clontech) using the *Nhe*I and *Sac*II sites.

For DnaJ domain mutants of LT genomic constructs, D44H and D44N were generated by a QuikChange Lightning Site-Directed Mutagenesis Kit (Stratagene) using TAg206.wt (*279*) as a template and the following primer pairs: T.D44H(S) (5'-GCT TAA AGC ATC ACC CTC ATA AAG GGG GAA ATC C-3') and T.D44H(AS) (5'-GGA TTT CCC CCT TTA TGA GGG TGA TGC TTT AAG C-3'); T.D44N(S) (5'-GCT TAA AGC ATC ACC CTA ATA AAG GGG GAA ATC C-5') and T.D44N(AS) (5'-GGA TTT CCC CCT TTA TTA GGG TGA TGC TTT AAG C-3'). For LXCXK.D44N, primers T.D44N(S)

and T.D44N(AS) was used for PCR reaction using TAg206.wt.LXCXK (*279*) as a template.

MCV replication origin plasmids were amplified by PCR from MCC339 genomic DNA (GenBank # EU375804) with published primer sets (*278*) and cloned into pCR2.1 (Invitrogen).

3.2.2 Generation of Antibodies

Monoclonal antibodies, CM8E6 and CM2B4 (*281*), were generated by standard methods of immunizing mice with KLH-derivatized MDLVLNRKERREALC or CSRSRKPSSNASRGA peptide that correspond to the MCV TAg exon 1 and 2, respectively (Epitope Recognition Immunoreagent Core facility, University of Alabama).

3.2.3 MCV origin replication assay

Human embryonic kidney (HEK) 293 cells were maintained in DMEM supplemented with 10% FBS, 2 mM glutamine and penicillin/streptomycin. 293 Cells were transfected with MCV origin constructs and either empty vector or TAg expression vector by Lipofectamine 2000 (Invitrogen). Cells were harvested 48 h after transfection, lysed with TE/0.6% SDS buffer (10 mM Tris-HCl (pH 8.0), 1 mM EDTA and 0.6% SDS) for 10 min and then NaCl was added at a final concentration of 1 M. Lysates were centrifuged at 14,000 rpm for 30 min at 4°C to collect episomal DNA. After phenol-chloroform extraction, 5 μg of the collected DNA was double digested overnight with 10 units each of *Dpn*I and *BamH*I. Digested DNA was loaded on 0.8% agarose gel, transferred onto

nitrocellulose membrane, and subjected to Southern hybridization (*279*). Replication efficiency was detected by Southern hybridization with ^{32}P-labeled probe produced by PCR with primer pairs (Rep-S, 5'-GCC GCC AAG GAT CTG ATG-3'; pCR2.1-AS, 5'-CTG CGC AAG GAA CGC CCG TCG-3') and analyzed by PhosphorImager (Typhoon 9400, GE Healthcare) and ImageQuant software (GE Healthcare). All replication assays were performed at least twice and a representative experiment is shown. Expression levels for LT and sT-eGFP were confirmed in each transfection by immunoblotting using anti-V5 (Invitrogen), CM2B4, or anti-GFP (B-2) (SantaCruz).

3.2.4 Immunoprecipitation

293 cells were cotransfected with pCMV-myc/Hsc70 (*334*) and either pcDNA6/V5-His/lacZ plasmid (Invitrogen) or TAg plasmid (TAg206.wt, D44H and D44N) using Lipofectamine 2000 (Invitrogen). Cells were harvested 48 h after transfection, suspended in lysis buffer (50 mM Tris-HCl, 0.15 M NaCl, 1% Triton-X100, pH 7.4) supplemented with protease inhibitors. Precleared lysates were immunoprecipitated with either mouse monoclonal anti-c-myc (9E10) (SantaCruz) or rabbit anti-V5 (Bethyl) overnight at 4°C. Lysates were incubated with Protein A sepharose beads (Amersham) for 3 h at 4°C, collected and washed with lysis buffer. Beads were resuspended in 2×SDS loading buffer and proteins were separated by SDS/PAGE. Immunoblotting was performed with either anti-c-myc (SantaCruz) or anti-V5 (Invitrogen).

3.2.5 shRNA knockdown

Short hairpin RNA (shRNA) sequences targeting TAg (shT) and sT (shsT) alone were designed and inserted into a short hairpin RNA expressing plasmid pLKO.1-TRC (Addgene). Sequences for shT (sense strands, 5'-CCG GAA GAG AGG CTC TCT GCA AGC TCT CGA GAG CTT GCA GAG AGC CTC TCT TTT TTG-3') and shsT (sense strand, 5'-CCG GAA GTT GTC TCG CCA GCA TTG TTC AAG AGA CAA TGC TGG CGA GAC AAC TTT TTT TG-3') were cloned using *Age*I and *EcoR*I sites in the shRNA cassette of pLKO.1, respectively. A scrambled non-targeting short-hairpin RNA plasmid (scr) (Addgene) was used as control shRNA. For origin replication assay, 2 µg of TAg expression construct, 1 µg of origin construct were cotransfected with 2 µg of short hairpin construct into 293 cells grown in 6 well plate by Lipofectamine 2000 (Invitrogen). Cells were harvested and processed as described above.

3.2.6 Chromatin immunoprecipitation (ChIP)

TAg expression plasmids (TAg206.wt, TAg339, TAg350) or pcDNA6/V5-His empty vector (Invitrogen) were transfected with Ori339(97) or Ori350(97) plasmid into 293 cells using Lipofectamine 2000 (Invitrogen). Cells were cross-linked with 1% formaldehyde in PBS and DNA was sheared by sonication in lysis buffer (50 mM Tris (pH 8.0), 1% SDS, 10 mM EDTA (pH 8.0) with protease inhibitors). Cell lysates were diluted 10 times with dilution buffer (20 mM Tris (pH 8.0), 1 % Triton X-100, 2 mM EDTA (pH 8.0), 150 mM NaCl with protease inhibitors) and one third of diluted lysates was precleared with protein A sepharose (GE Healthcare)/ 2 µg of sonicated salmon sperm DNA

(Stratagene) for 2 h at 4°C. Cell lysates were incubated overnight at 4°C with anti-V5 (Bethyl) antibody and then with Protein A sepharose beads/2 µg salmon sperm DNA for 2 h at 4°C. Beads were washed 4 times with buffer I (20 mM Tris-HCl (pH 8.0), 150 mM NaCl, 1% Triton X-100, 2 mM EDTA, 0.1% SDS), buffer II (20 mM Tris-HCl (pH 8.0), 500 mM NaCl, 1% Triton X-100, 2 mM EDTA, 0.1% SDS), buffer III (10 mM Tris-HCl (pH 8.0), 500 mM LiCl, 1% NP40, 1% deoxycholate, 1 mM EDTA) and TE (10 mM Tris-HCl (pH 8.0), 1 mM EDTA). DNA was extracted with buffer (100 mM $NaHCO_3$, 1% SDS) and incubated at 65°C overnight to reverse cross-linking. DNA was purified and resuspended in distilled water followed by real time quantitative PCR (qPCR) performed with primers, Rep-S 5'-GCC GCC AAG GAT CTG ATG-3' and Rep-AS, 5'-GAG AAC CTG CGT GCA ATC-3' using Smart Cycler 5RX4Z01 (Cepheid) and SYBR GreenER qPCR SuperMix reagents (Invitrogen) according to manufacturer's instruction.

3.2.7 Molecular modeling

The model of the MCV origin-binding domains on DNA was generated in COOT (*335*). A homology model of the MCV TAg OBD on a fragment of double-stranded GAGGC-containing DNA was generated using the SV40 OBD structure (PDB code 2NCG) as a template. Copies of the MCV OBD model were placed on idealized B-form DNA with the MCV origin sequence by superimposing the GAGGC sequence within the homology model onto each of the GAGGC-like sites in the model of the origin. The figure shown was generated in Pymol (http://www.pymol.org).

3.3 RESULTS

3.3.1 The minimum MCV replication origin is defined by a 71 nucleotide genomic region

MCV is more closely related to the Py subgroup of polyomaviruses than to other human polyomaviruses or SV40 (*55*). We aligned the sequences of the MCV origin with presumptive origin sequences of SV40 and Py (**Figure 18A**). The common features of the core origin in the SV40 subgroup are the presence of the AT-rich tracts contributing to DNA melting (*321, 336*), flanked by a Site 1/2 region containing six GAGGC pentanucleotide repeats. An early promoter region containing additional GAGGC binding sites is also present. This region is required for Py virus replication but is dispensable for SV40 origin replication (*337-339*). The entire origin of MCV contains ten potential LT binding sequences (PS1-PS10, **Figure 20A**), six on one strand and four on the opposite strand. Eight of these pentanucleotides match the most common LT binding sequence 5'-GAGGC-3', while two, PS2 and PS3, in Site 1/2 have imperfect consensus sequences: 5'-G**G**GGC-3' and 5'-GAG**C**C-3', respectively.

To define the elements required for LT-mediated replication of MCV, deletions were generated for a tumor-derived MCV origin construct (Ori339(589), nt 4669 to 269) from MCV clone 339 (GenBank # EU375804) (**Figure 18A**). This origin fragment is perfectly conserved in most tumor and all nontumor-derived MCV strains thus far sequenced. Origin constructs were cloned into pCR2.1 (Invitrogen) and co-transfected

together with a full-length wild-type T antigen genomic expression construct (TAg206.wt, isolated from intestine tissue of a patient without MCC) into 293 cells. In this study, we refer to the genomic T antigen cassette as TAg, which expresses small T (sT) and 57kT proteins from alternatively spliced mRNAs in addition to LT protein (*279*). Origin replication was determined by Southern hybridization in which *Dpn*I-resistant (replicated) signal is normalized to *Dpn*I-sensitive (unreplicated) signal. In contrast to Py but similar to SV40, the MCV origin can be reduce to a discrete region such that constructs encompassing only an 80 bp origin show efficient replication by MCV TAg **(Figure 18B)**. Replication is completely abolished for a shorter 69 bp origin construct. The 80-bp fragment (nt. 5356-nt 48) contains, in addition to the AT-rich tract, eight of the identifiable LT binding PS (**Figure 18A**) indicating that PS9 and PS10 are not required for origin replication.

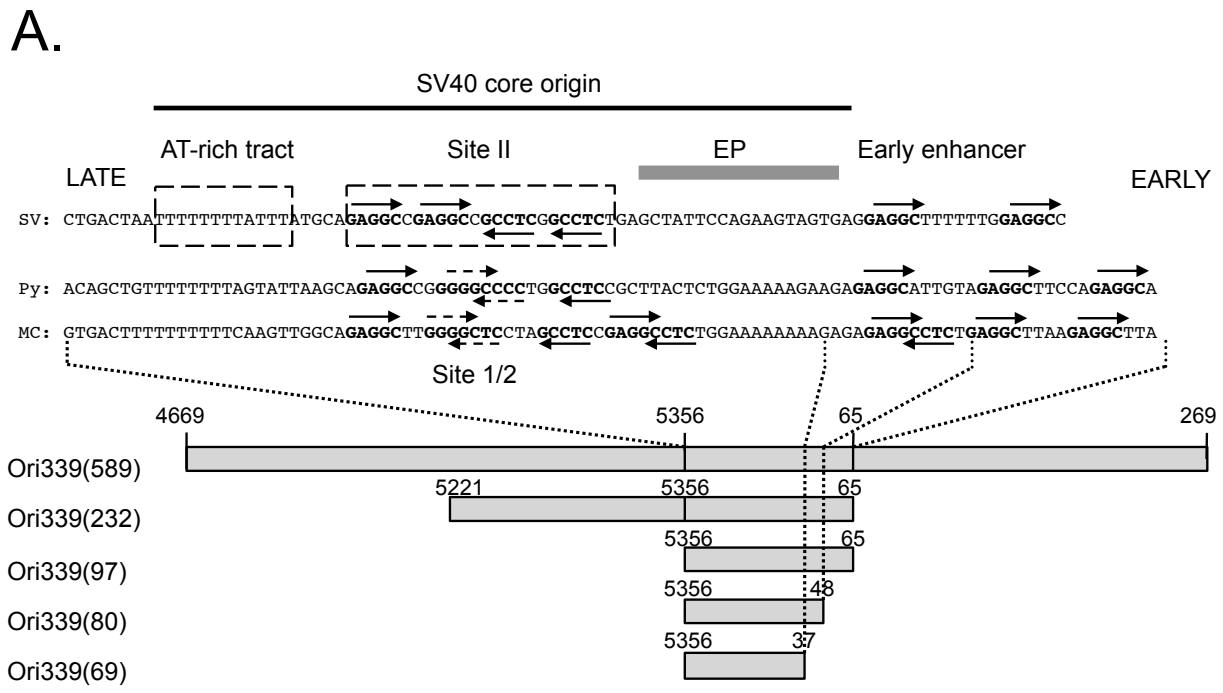

B.

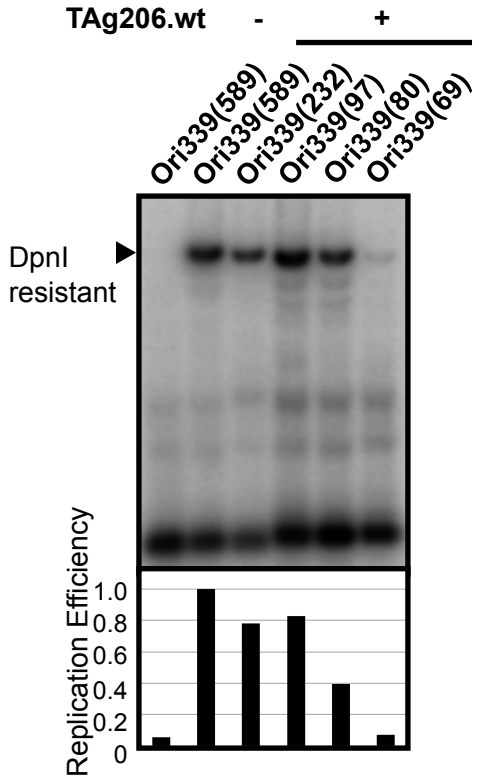

Figure 18. Mapping of the MCV core origin
(A) Comparison of the origin sequences among polyomavirus family. The straight and dotted arrow heads indicate complete (GAGGC) or incomplete pentanucleotide sequences (GXGGC, GAGXC) serving for LT binding sites, respectively. The origin of SV40 subgroup (GenBank# EF59667.1) consists of highly conserved region, including AT-rich tract on the late gene side, Site II GAGGC repeats, early palindrome (EP), and early enhancer region on the early gene side. MCV origin (GenBank# EU375804) is closely related to the origin of Py (GenBank# J02288). MCV origin constructs of different lengths (589 bp-69 bp) were cloned into pCR2.1 vector (Invitrogen) to identify the core origin sequence. (B) Deletion analysis of MCV origin. The origin constructs were cotransfected into 293 cells with either TAg206.wt or empty vector as a negative control and the replication from the MCV origin was analyzed by Southern blotting. The autoradiogram was quantified using ImageQuant software (GE Healthcare). The *Dpn*I sensitive DNA band was used as an internal standard for the amount of input DNA.

To define a minimal core origin, we successively truncated single-base pairs from the early and late sides of the 80 bp origin until replication was completely abolished (**Figure 19**). A significant decline in MCV replication efficiency occurs only after deletion of four of the ten thymidines in the polyT tract (dN70). This is in contrast to the SV40 origin which requires an intact polyT tract for efficient replication (*321*). MCV origin replication also declines sharply starting at the dC78 deletion that truncates PS8 on the early side of the origin. Thus, unlike Py, a minimal MCV core origin consisting of the 71-bp region from nucleotides 5364 through 47 can efficiently sustain LT-mediated DNA replication.

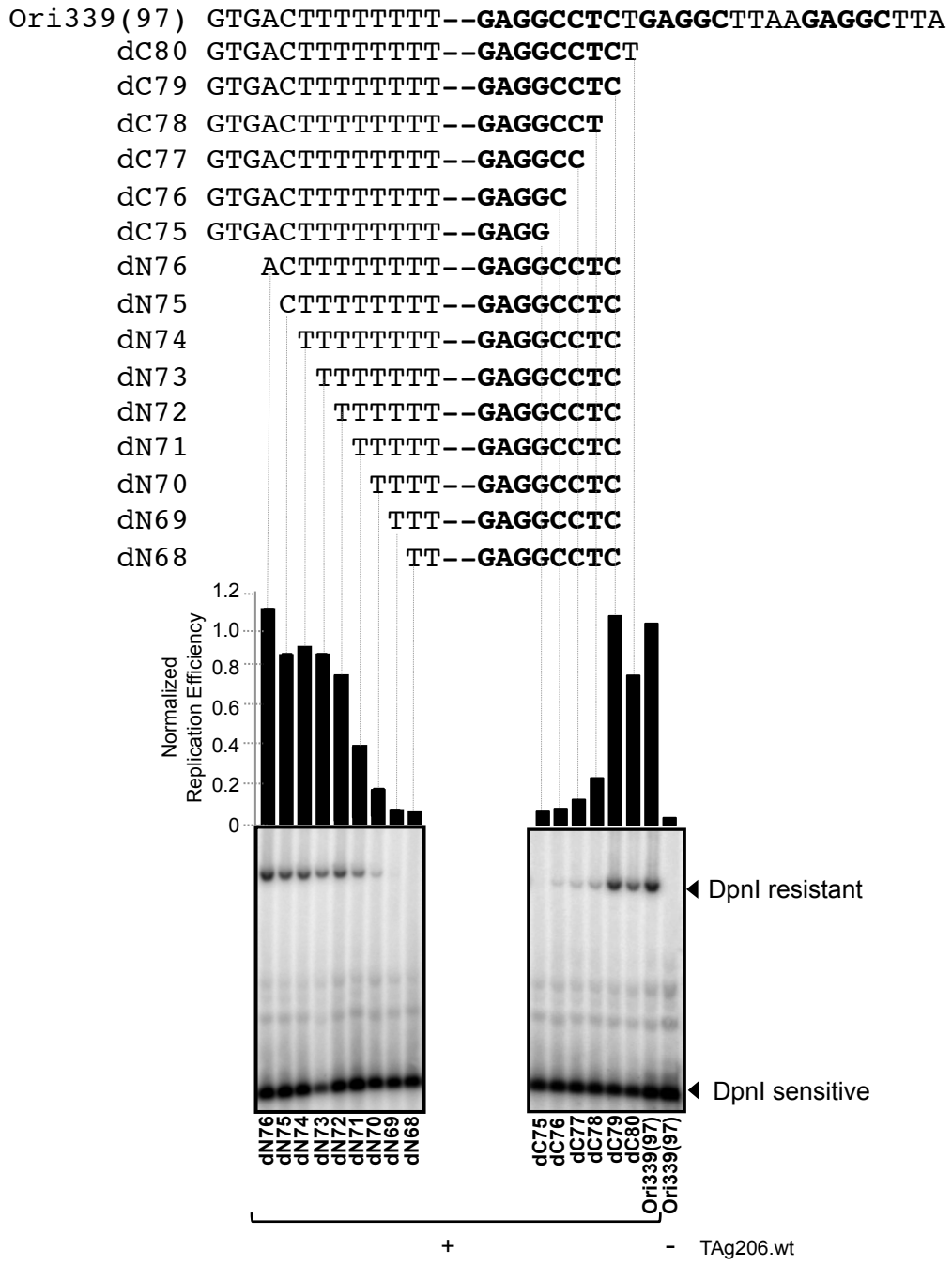

Figure 19. Definition of the minimal MCV core origin
Single-base pair deletions from both sides of the origin sequence (late-nt 5356, early-nt 48) were performed to define a minimal core origin. The expression level of TAg was observed by Western blotting (data not shown) and autoradiogram of replication was quantified as in **Fig. 1B** (middle panel).

3.3.2 Pentanucleotide requirements for MCV replication.

Four LT binding sites (**Figure 18A**) are present in the SV40 core origin, and all four pentanucleotides are necessary for origin DNA unwinding and replication events with pentanucleotides 1 and 3 needed for double hexamer formation (*340, 341*). These pentanucleotides are arranged on opposite strands allowing the double SV40 LT hexamer to form in a head-to-head orientation (*342*).

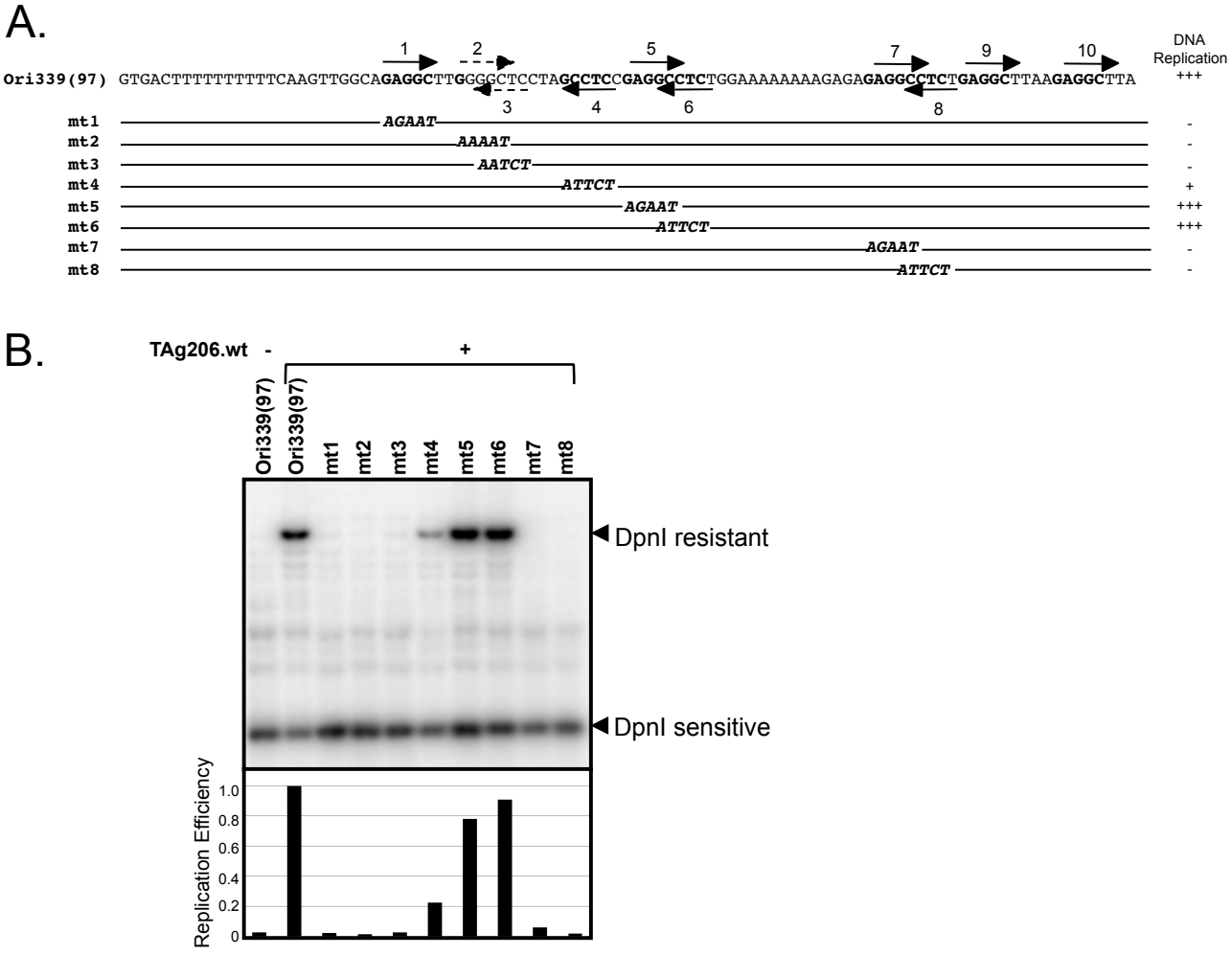

Figure 20. Pentanucleotide requirements
(A) Mutation of each pentanucleotide in 97-bp origin was generated by PCR-based direct mutagenesis (AT to GC) to define the essential pentanucleotides for MCV origin replication. Replication efficiency was examined by Southern blotting (B).

To determine whether a similar pentanucleotide arrangement is needed for MCV replication, mutations were introduced that disrupted all five nucleotides of pentanucleotide sequences PS1-8 in the 97-bp origin (**Figure 20A**). Mutations in three pentanucleotides within the region most analogous to Site II (PS1-4) (**Figure 18A**) and two pentanucleotides (PS7, 8) near the early enhancer region abolish replication. The PS4 mutant significantly diminishes replication. In contrast, PS5 and PS6 are dispensable (**Figure 20B**).

Since PS2 and PS3 partially overlap, as do PS7 and PS8, complete pentanucleotide substitutions affect overlapping elements because of shared nucleotides. We therefore investigated critical nucleotides in these four elements (PS 2, 3, 7, 8) by introducing single mutations to determine which of the overlapping PS sequences are essential (**Figure 21A**) as well as critical nucleotides in PS1. **Figure 21B** shows that single base pair mutations in three pentanucleotides (PS1, 2 and 7) impair efficient replication. In the non-consensus PS2 element, a single substitution mutation that reconstitutes a canonical GAGGC site remains competent for replication (**Figure 22B**). Single mutations unique to the PS3 site that do not overlap with the opposite strand PS2 have no effect on replication suggesting that PS2 is the critical LT binding element in this overlapping pair. A PS3 (S3-2C) mutation that creates the same head-to-head LT binding site as in the Py origin (GGGGCCCC) (**Figure 18A**) has no replication capacity (**Figure 22B**), indicating that the MCV LT replication complex may form assemblies on the DNA that are distinct from Py and SV40.

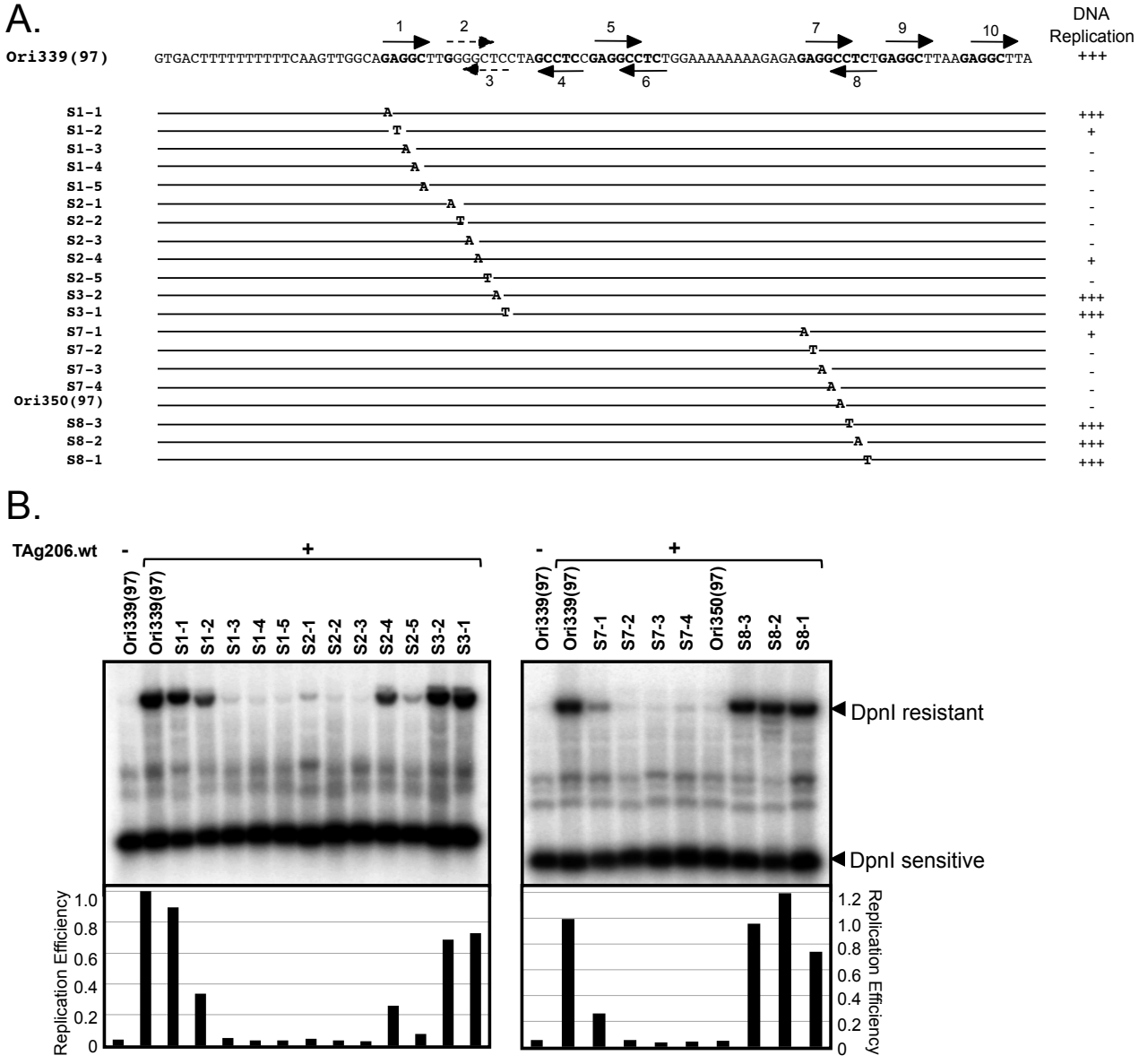

Figure 21. Single base pair mutational analysis of pentanucleotides
(A) Each sequence of Pentanucleotides 1, 2-3 and 7-8 was mutated by AT to GC substitutions to disrupt TAg binding site. To avoid reconstitution of T Ag binding site (5'-G(A/G)GGC-3') by mutation, AG to T substitutions were introduced in S7-2, S8-2, S2-2 and S3-2. (B) Southern blot results demonstrate that single base mutations in pentanucleotides 1, 2 and 7 can abolish replication efficiently indicating that these pentanucleotides sites are critical for MCV origin replication as a functional unit.

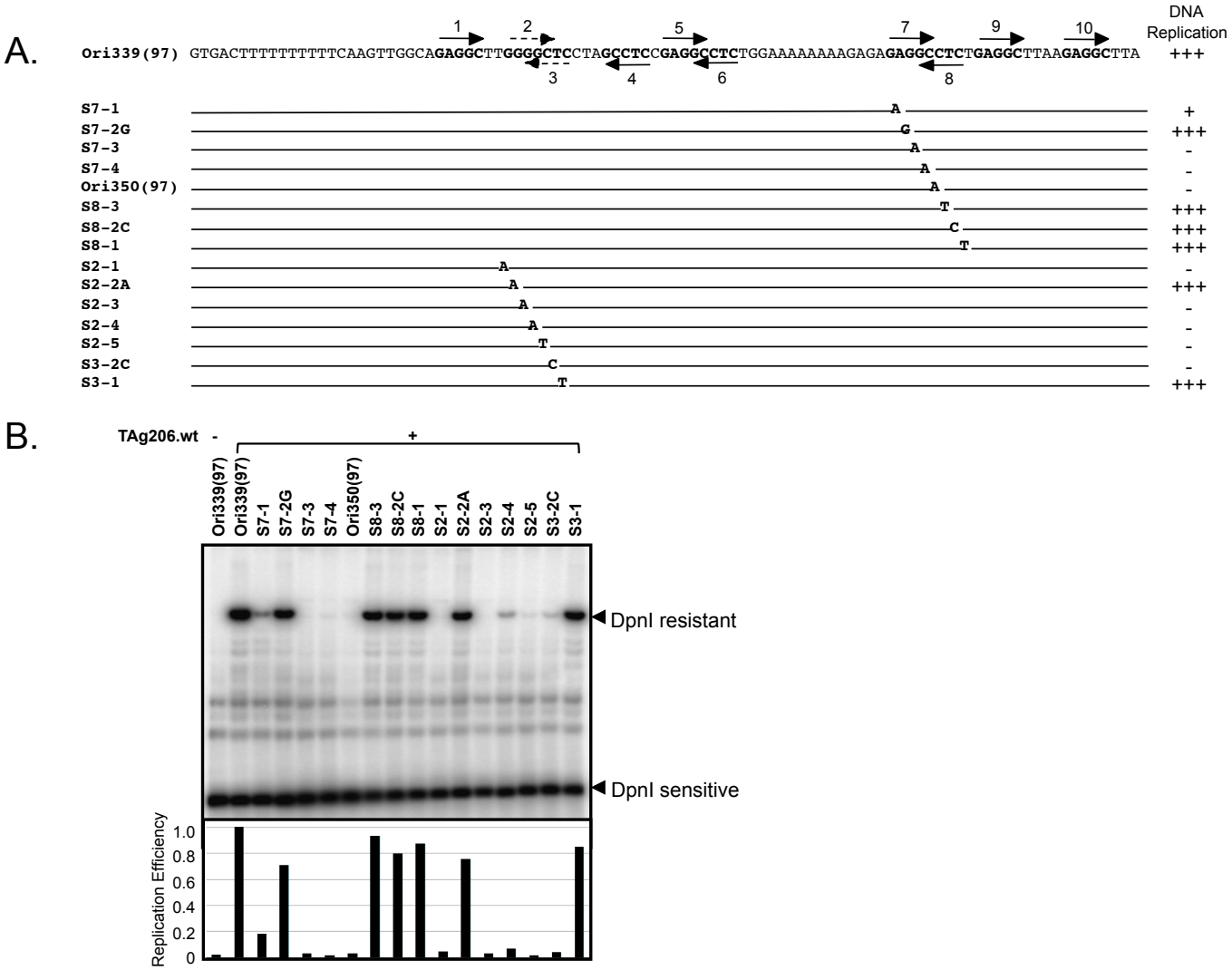

Figure 22. Reconstitution of pentanucleotide sequence to GAGGC
(A) In the non-consensus PS2 element (GGGGC), a single substitution mutation that reconstitutes a canonical GAGGC site (S2-2A) by A:T to G:C base pair substitutions remains competent for replication. (B) Southern hybridization results.

The importance of PS7 to MCV replication is illustrated by naturally arising mutations at the viral origin (Ori350(97) lane of **Figure 21B**). We sequenced MCV origins from one non-tumor tissue, 8 MCC tumors and 2 cell lines (*55*). Only the origin sequence from one tumor, MCV350 (GeneBank# EU375803), has a C to A substitution in position 5 of PS7 that also alters the sequence of the overlapping PS8. This natural mutation completely abrogates origin replication in the presence of TAg (**Figure 21B**). The TAg gene from this virus also possesses a TAg locus truncation mutation (*279*) that eliminates both the LT OBD and helicase domain.

3.3.3 Effects of Tumor-derived LT mutations on origin binding and replication

As shown here (**Figure 21B**), and described previously (*279*), tumor-derived MCV TAg is unable to initiate MCV origin replication due to truncating mutations in the LT protein. We compared origin-binding properties for wild-type LT protein (TAg206.wt) on the wild-type origin (Ori339(97)) and the mutated Ori350 (Ori350(97)), as well as mutant LT proteins from tumor derived viral strains (MCV339 and MCV350) (**Figure 23**). MCV339 LT protein retains the OBD but has a truncated helicase domain, whereas the MCV350 LT mutation eliminates both the OBD and helicase domains (*279*). Quantitative chromatin immunoprecipitation (ChIP) assays demonstrate that wild-type TAg206 efficiently binds to the wild-type origin Ori339 but binding to Ori350, possessing the PS7/PS8 mutation, is reduced ~50%. Origin-binding by MCV339 and MCV350 TAg proteins is comparable to vector alone controls for both viral origins suggesting that structural or enzymatic features of the MCV LT helicase domain are required for efficient recognition of the DNA element.

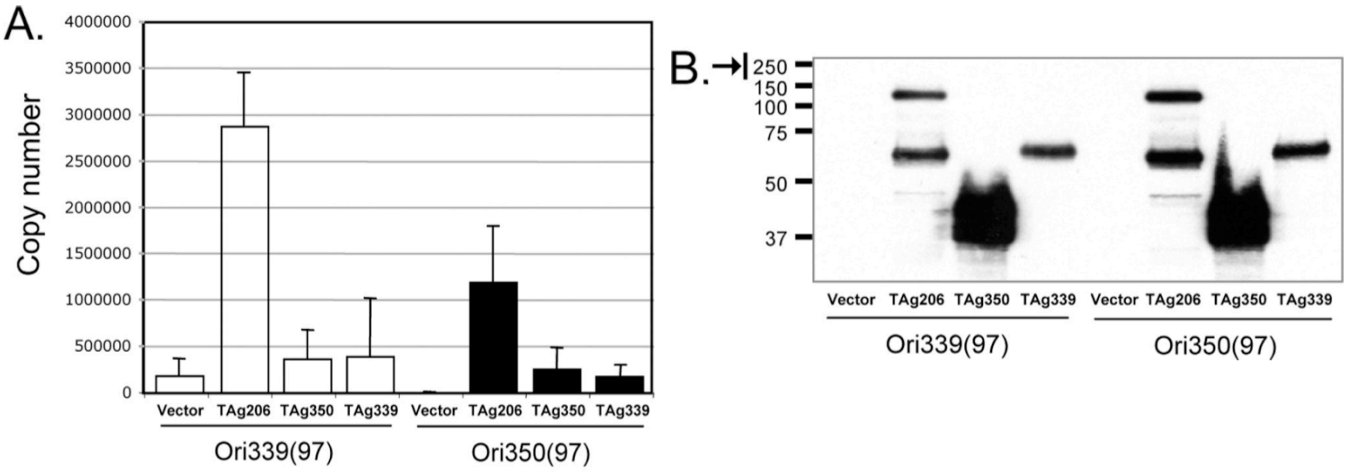

Figure 23. Chromatin immunoprecipitation (ChIP) analysis
(A) The binding efficiency of both non-tumor and tumor-derived TAg to MCV origin in vivo was examined using ChIP assay. The 97 bp origin-containing plasmid (Ori339(97) or Ori350(97)) and the TAg constructs from non-tumor (TAg206.wt) or tumor (TAg350, TAg339) tissues (*279*) were co-transfected into 293 cells and the binding of LT to the origin was investigated by quantitative PCR (qPCR). All experiments were repeated at least three times. Error bars indicate the standard deviation. (B) Immunoblot analysis confirming protein expression of TAg206, TAg350 and TAg339 using the LT specific antibody CM2B4.

Other factors influencing MCV replication

Four major TAg transcripts (T1-T4) have been identified using RACE and Northern blotting that correspond to LT, sT, and 57kT (*279*) (**Figure 24A**). The sT of MCV shares exon 1 with LT, which contains the conserved CR1 (LXXLL motif) and DnaJ (HPDK motif) domains, but lacks the LT OBD required for DNA recognition. The sT also encodes a PP2A binding site (CXCXXC) that is spliced out of LT and 57kT cDNAs. To test the effect of sT and other transcripts on viral origin replication, each cDNA transcript was cloned to express a unique TAg isoform. Each cDNA construct, singly and in combination, was then transfected into 293 cells to assess effects on origin replication. As seen in **Figure 24B**, LT cDNA expression alone is not sufficient for fully efficient replication, but replication efficiency is restored to that of the wild type genomic TAg by

coexpression of LT with sT. Coexpression of LT with 57kT does not increase replication over LT alone, and neither MCV sT nor 57kT individually have replication capacity.

To confirm the importance of sT in replication, we generated two short hairpin RNA (shRNA) constructs: shT targets all TAg transcripts and shsT targets only sT (**Figure 24A**) (*279*). We also generated a monoclonal antibody, CM8E6, directed against an exon 1 peptide shared by all TAg isoforms. Western blotting shows that shT down-regulates LT, sT, and 57kT protein expression as expected, whereas shsT only reduces sT expression (19 kDa) (**Figure 24C**). Knockdown of TAg proteins by either shT or shsT results in inhibition of origin replication compared to shScr control, confirming the functional importance of sT expression to MCV origin replication (**24D)**.

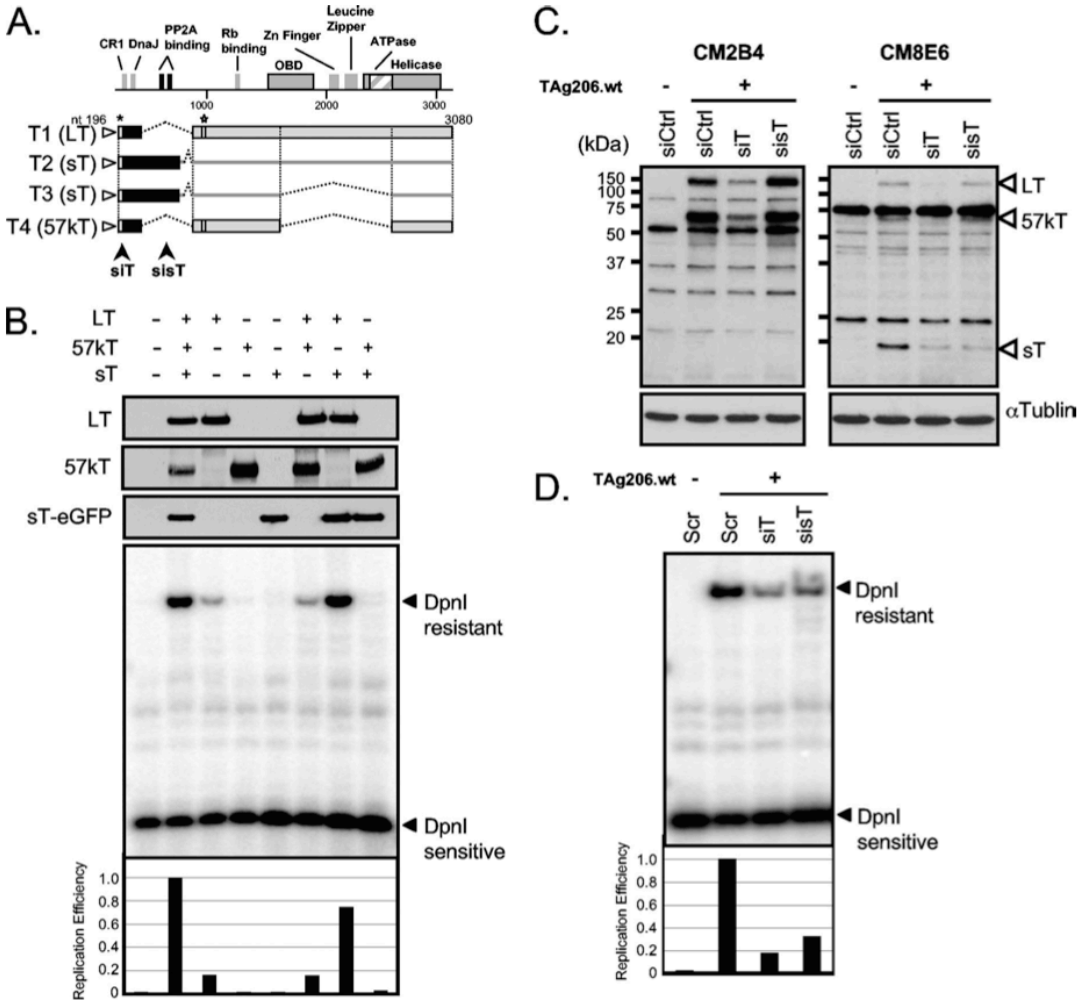

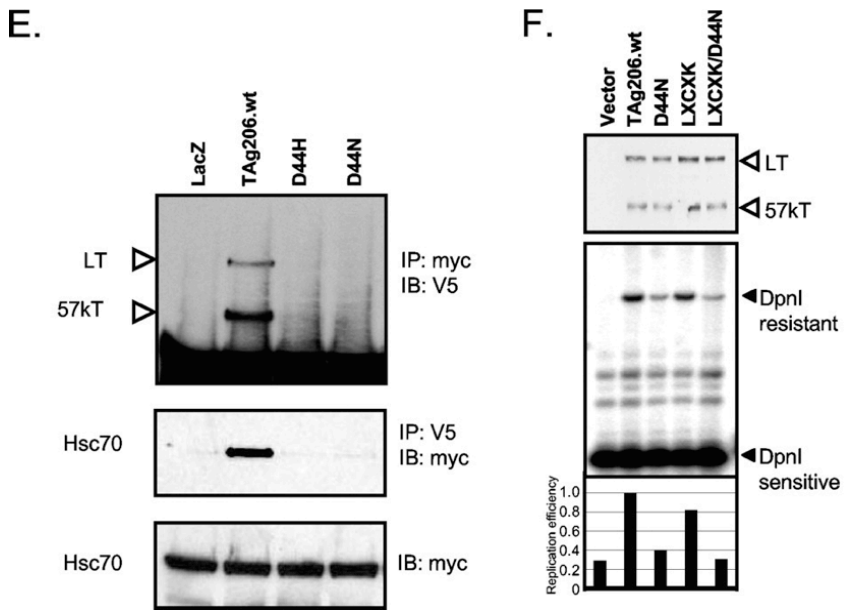

Figure 24. Other factors influencing MCV replication

(A) Alternative spliced products (T1-T4) of the early region give rise to large T (LT), small T (sT), and 57kT. Arrows indicate the position of shRNAs, shT and shsT. shT targets all TAg transcripts while shsT targets only sT transcripts. Asterisk and star show epitope sites of CM8E6 and CM2B4 antibodies, which detect LT/57kT/sT or LT/57kT proteins, respectively. The predicted MCV LT gene sequence retains all major conserved features of other polyomavirus LTs, including DnaJ, Rb-targeting, origin-binding, and helicase/ATPase domains. (B) LT, 57kT, and sT expression plasmids were cotransfected in combination into 293 cells to test contribution of origin replication. The genomic TAg construct (TAg206.wt) was used to express all three transcripts (LT, sT, 57kT). For the sT expression, EGFP fused sT expressing plasmid was used. Western blotting was performed to monitor the expression level of each transcript product using V5 antibody (Invitrogen) for LT and 57kT, and anti-GFP (SantaCruz) antibody for sT. Knockdown of LT, 57kT, and/or sT expression (C) and the effect on replication (D) by shRNA was examined. A scrambled non-targeting short-hairpin RNA plasmid (scr) was used as a control. Three specific bands (120, 57, 19 kDa) are detected by Western blotting using CM8E6 antibody in 293 cells transfected with genomic TAg expression constructs (TAg206.wt) (C, right panel). CM2B4 detected both ~120 kDa and ~57 kDa bands corresponding to the full-length LT and 57kT protein products, respectively (*281*) (C, left panel). (E) Interaction of TAg with Hsc70. To examine the interaction between TAg and Hsc70, Myc-tagged Hsc70 construct (pCMV-myc-Hsc70) was transfected into 293 cells with either V5-tagged wt TAg (TAg206.wt) or mt TAg (D44H, D44N). Lysates were immunoprecipitated with anti-myc or anti-V5 antibody and immunoblotted with anti-V5 or anti-myc antibody in a reciprocal way, respectively. The LacZ gene expressing vector, pcDNA6/V5-His/LacZ (Invitrogen) was used as a negative control for binding and 2% of the lysate was used for input control (~115 kDa). (F) Hsc70 binding to TAg promotes efficient viral replication. For the replication assay, TAg206.wt or mutants (Rb binding mutant, LXCXK; Hsc70 binding mutant, D44N; Rb/Hsc70 binding mutant, LXCXK/D44N) were cotransfected with MCV origin plasmid (Ori339(97)) into 293 cells. Replication efficiency was measured and quantified using ImageQuant (GE Healthcare).

Both MCV LT and sT contain DnaJ motifs encoded by exon 1 that are conserved among polyomaviruses and recruit interaction with chaperone heat-shock proteins (*343*). SV40 TAg association with Hsc70 (*344*) is mediated through the HPDK motif within the DnaJ domain (*334, 345*) which is required for efficient origin replication. We confirmed that this motif in MCV is a site for Hsc70 interaction by coimmunoprecipitation of V5-tagged wild-type (TAg206.wt) and DnaJ domain mutant (D44H and D44N) proteins with myc-tagged Hsc70 (**Figure 24E**).

To test whether Hsc70 interaction with MCV TAg is required for efficient viral DNA replication, wild type (TAg 206.wt) and the LT DnaJ mutant D44N were tested for origin replication using the Ori339(589) (**Figure 24F**). Mutation of the LT DnaJ domain markedly decreases origin replication compared to wild-type MCV TAg, whereas mutation of the MCV LT retinoblastoma-binding motif (LXCXE) does not, similar to results found for SV40 TAg (*334*). The MCV D44N LT mutant is less stable than wild-type MCV LT but enhanced expression to generate comparable levels of both proteins does not increase replication with the DnaJ-binding deficient protein (data not shown). In contrast, mutation of the DnaJ domain in sT has no effect on the ability of sT to enhance wild-type LT replication efficiency. In addition, mutation in the PP2A domain of sT abolishes its ability to enhance LT-mediate origin replication (**Figure 25**).

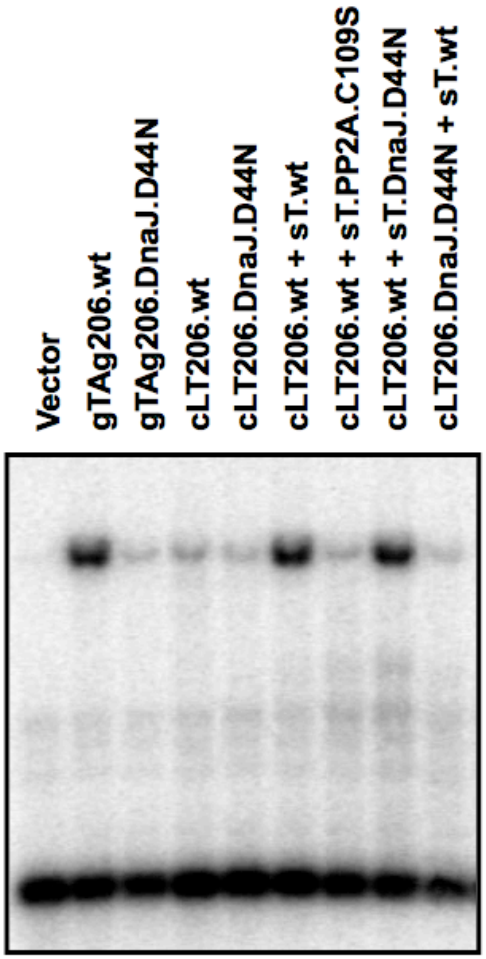

Figure 25. MCV origin replication assay with TAg mutants in DnaJ domain and PP2A binding site

The HPDK motif in the LT DnaJ domain was mutated (D44N) in constructs, gTAg206.wt, cLT206.wt and sT.wt. A PP2A binding site mutant of sT was generated by substituting Cys 109 to Ser. Origin plasmid (Ori339(97)) was cotransfected with wild type or various mutant TAgs into 293 cells and Southern blotting was performed. Mutation of the DnaJ domain in sT (sT.DnaJ.D44N) has no effect on wild-type LT replication efficiency. In contrast, the PP2A site mutant of sT (sT.PP2A.C109S) abolishes contribution of sT to enhance origin replication efficiency.

3.4 DISCUSSION

We find that a minimal MCV 71 bp core origin sequence is sufficient for TAg-directed DNA replication. Like other polyomaviruses, this MCV core origin contains three subdomains: an AT-rich tract, a LT-binding domain, and an early enhancer region. The AT-rich tract for SV40 directs DNA bending that may be a structural signal for LT binding (*321*). Adjacent to the AT-rich tract, pentanucleotides sequences are arranged as two pairs of imperfect repeat sequences (PS 1-4) inverted with respect to each other. These repeats are similar, but more closely spaced than those in SV40. Of these four, only three (PS1, PS2, and PS4) are required for origin replication. In addition to these three PS elements, the MCV origin has an additional LT binding site at PS7, which is required for origin replication and if disrupted, as found in a naturally-occurring tumor-derived strain, markedly reduces LT binding to the origin element in our quantitative ChIP assay and completely ablates origin replication. Mutational substitution analysis shows that even single point mutations on other essential PS also disrupt origin replication.

The origin binding domains of MCV, Py and SV40 are similar in sequence, and the residues shown to bind GAGGC pentamers are highly conserved in the three viruses. Sequence comparison reveals that the MCV OBD is 49% identical to Py and 48% identical to SV40 (data not shown). To better understand why MCV requires fewer GAGGC binding sites than other viruses for its replication, the crystal structure of the SV40 OBD on DNA was used to model the interaction of MCV TAg with the MCV origin.

As shown in **Figure 26**, the closely spaced PS sites also position the OBD of LT closely to one another. Given this proximity, it is likely that OBD-OBD interactions occur while apposing LT molecules are bound to the DNA. Such interactions are not observed in SV40, where the GAGGC sequences are farther separated, but they do occur in the more distantly related bovine papilloma virus (BPV) system (*346, 347*). In BPV, the analogous domain is part of the E1 protein and is not capable of recognizing its binding site without the help of the virally-encoded E2 protein. MCV origin recognition may share features of both SV40 and BPV.

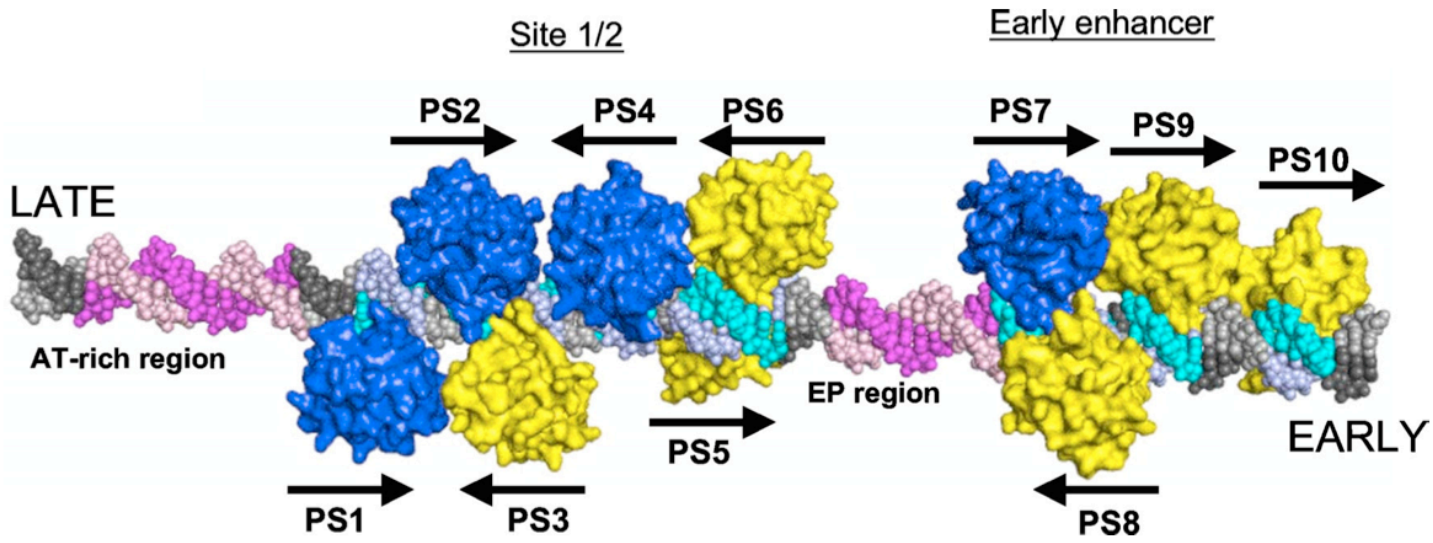

Figure 26. Model of the MCV OBDs on the MCV origin
A model of the MCV OBD was placed on each of the putative binding sites. OBDs positioned at the required PS1, PS2, PS4 and PS7 are shown in blue. The remainder are yellow. The GAGGC sequences are shown in cyan. The AT-rich tracts of DNA that flank Site 1/2 are shown in purple.

MCV is similar to SV40 in that replication does not require an E2-like protein, but like BPV, interactions among the OBDs may help stabilize the complex on the DNA, perhaps alleviating the need for well-formed binding sites at all positions. Based on our modeling, two sets of OBD-OBD interactions may occur on the DNA, both of which are

head-to-head interactions. The first is between the OBDs bound to PS2 and PS3, and the putative protein-protein interface involves amino acids within the major groove of the DNA. The second potential interaction involves residues well outside of the DNA-binding cleft and could occur between OBDs on PS1 and PS3 and between OBDs on PS2 and PS4.

We also examined non-origin factors related to viral replication efficiency. Previously, several studies using SV40, Py and JCV sT defective viruses or constructs have demonstrated that the absence of a functional sT reduces replication efficiency (*320, 348, 349*). In this report, we generated separate cDNA constructs for each early gene transcript product (LT, 57kT, sT) to clarify the role and contribution of sT in viral replication. We find that sT, but not 57kT, has a major role in enhancing LT mediated replication in MCV. The mechanism for sT replication enhancement in MCV remains poorly understood but it is likely that sT does not act directly in the LT-origin replication complex. Like other polyomavirus sT, MCV sT binds PP2A (*129*), a serine/threonine phosphatase critical to development, growth control and tumorigenesis (*350*). MCV sT might stimulate cell cycle entry through PP2A binding thus providing conditions for origin replication. Alternatively, sT expression might selectively affect the phosphorylation state of LT to enhance its binding affinity to the origin DNA binding site (*351, 352*). Intriguingly, both MCV LT and sT possess DnaJ domains that recruit Hsp70; while an intact LT DnaJ domain is required for efficient replication, an intact sT DnaJ domain is not. Site-directed mutagenesis of DnaJ domain residues reveals that this domain is necessary for LT and MT stability (*353*). We also find that MCV TAg DnaJ domain mutants are destabilized. While reduced protein expression may account

for some of the reduced activity of LT having DnaJ domain mutations, replication remains reduced even when the mutant protein is expressed at comparable levels to the wild-type protein.

The minimal replication origin of MCV provides a novel model for a defined genetic replication element. Our studies suggest that there is strong selective pressure within MCV-infected MCC tumors to eliminate independent viral DNA replication. Tumor-derived mutant MCV TAgs and origins may prove useful for structural and functional studies dissecting steps involved in TAg-dependent DNA replication.

4.0 MERKEL CELL CARCINOMA-DERIVED MERKEL CELL POLYOMAVIRUS T ANTIGEN INDUCES HUMAN CELL PROLIFERATION THROUGH ITS RB TARGETING DOMAIN BUT IS INSUFFICIENT TO TRANSFORM HUMAN FIBROBLASTS

Work described in this chapter is unpublished**.** Parts of the data presented here are in preparation for manuscript submission

with authors Anna Guastafierro, Masahiro Shuda, Huichen Feng, Yuan Chang and Patrick S. Moore.

A. Guastafierro, M. Shuda, and H. Feng contributed equally to this work. A. Guastafierro performed the generation of stable cell lines, cell-counting experiments, RNA isolation and microarray analysis, soft agar colony formation assays, FACS analysis and immunoblots. M. Shuda cloned the shRNA constructs used here and H. Feng analyzed microarray data and generated heat map images. All authors contributed to data interpretation and manuscript preparation.

4.1 INTRODUCTION

The study of tumor viruses has elucidated a large number of protein signaling networks that are involved in cancers of diverse cellular origins (*354, 355*). Despite the fact that oncogenic viruses cause only a small percentage of all human cancers, experimental models have defined gene elements required for human cell transformation by using viral oncogenes as tools to target specific combinations of intracellular pathways *in vitro* (*194*). The cancer phenotype is a multi-step process of genetic changes that lead to a loss of homeostasis in cellular mechanisms responsible for controlling diverse protein signaling networks. During this process normal cells acquire mutations that allow them to replicate indefinitely (immortalization), escape apoptosis, and promote cell cycle progression (*356*).

Hahn et al. described the creation of a human tumor cell by expressing simian vacuolating virus 40 (SV40) T antigens, as well as the telomerase catalytic subunit hTERT and oncogenic hRas (hRasV12) in BJ primary human fibroblasts (*357*). Immortalization of primary human cells can be achieved by hTERT expression, which elongates telomeres and therefore allows for an indefinite replicative lifespan of a cell (*358, 359*). SV40 large T antigen (LT) has been extensively studied and was crucial in the discovery of p53 as well as dissection of the Rb family pathways (*360, 361*). SV40 LT contains a conserved LXCXE motif, which can be found in a number of oncoproteins from other tumor viruses including HPV E7, adenovirus E1A and MCV LT (*55, 362*). The

LXCXE motif facilitates binding of Rb family members pRb, p107 and p130, which results in E2F-mediated cell cycle entry and progression (*362, 363*). In addition, SV40 LT binds to p53 through a C-terminal bi-partite binding site (*364*). This interaction has been shown to contribute to SV40 LT-mediated transformation of rodent cells not only by inactivating p53 transcriptional activity, but also by inducing a gain-of-function as a result of this interaction (*162*). In contrast, neither MCV full length LT nor tumor-derived truncated LT bind to p53 directly (*260*). SV40 small T antigen (sT) binds and perturbs the serine/threonine phosphatase PP2A through a conserved motif (*197, 365*). This interaction contributes to human cell transformation in combination with SV40 LT in human fibroblasts (*194*).

Recent data from our group shows that, in contrast to to SV40, MCV sT is capable of transforming rodent fibroblasts independent of its PP2A binding motif, as evaluated by soft agar as well as focus formation assays in Rat-1 and NIH3T3 cells (*129*). Neither MCV full length LT nor MCC-derived, truncated LT are capable of fully transforming rodent cells in these assays even though small cell aggregates are observed in soft agar. Nevertheless, tumor-derived MCV LT has growth promoting effects in both rodent as well as human fibroblasts (*260*). Most MCC tumors express both MCV LT as well as sT proteins, which indicates that both viral proteins are essential in MCC tumorigenesis (*129*).

In MCC tumors the MCV genome is clonally-integrated, which demonstrates that the viral integration event precedes tumor cell outgrowth, and therefore supports a causal relationship between the two processes (*55*). In addition to viral genome integration, all MCV genomes isolated from tumors have been shown to have truncating

deletions in the C-terminal ATPase/helicase domain of MCV LT, which is necessary for viral replication (*56*). Recent data from Cheng et al. demonstrates that the terminal exon 3 domain of LT, which is always deleted in MCC, has a growth inhibitory effect in human fibroblasts as well as MCV-positive MCC cells expressing a truncated LT (*260*). The mechanism that leads to this inhibitory activity of the C-terminus was recently associated with a DNA damage response resulting in p53 protein stabilization and phosphorylation, as well as downstream p21 activation in U2OS cells (*366*).

In this study, we show that tumor-derived MCV LT enhances human fibroblast proliferation in an LXCXE-dependent manner, and that MCV sT only minimally contributes to proliferation. In addition, we performed a microarray analysis, which indicates that G1/S phase transition regulators are specifically up-regulated by truncated LT, resulting in an increased percentage of cells entering S-phase. Additional expression of oncogenic hRasV12 and p53 knockdown in BJ-hTERT are required to induce soft agar colony formation in the presence of MCV sT; however, we did not observe soft agar colony formation in the presence of 339LT.

4.2 MATERIALS AND METHODS

4.2.1 Cell culture

The Merkel cell lines were grown in RPMI 1640 supplemented with 10% fetal calf serum. BJ and BJ-hTERT fibroblasts were grown in DMEM supplemented with 10% fetal calf serum, penicillin and streptomycin. All cells were grown at 37 °C in humidified air containing 5% CO_2.

4.2.2 Generation of stable cell lines

BJ-hTERT cells were infected with lentiviruses in the presence of 6ug/mL polybrene. Medium was changed after 24 hours, and antibiotic selection was added (puromycin = 1ug/mL; G418 = 400ug/mL; blasticidin = 5ug/mL) on day 3 after infection. Cells were grown under selection medium until all mock infected cells died.

4.2.3 Lentivirus production

Lentiviruses for pLKO knockdown as well as pLVX and pSMPUW overexpression constructs were produced in HEK293FT cells (Invitrogen) using pPax2 and pMD2.G helper constructs that were obtained from Addgene. At 3 days following transfection, virus supernatants were harvested and filtered through 0.45 µm pore size filters.

4.2.4 Overexpression and short hairpin RNA (shRNA) constructs

Overexpression constructs for 339LT, 339LT.LXCXK and sT were described previously. An shRNA sequences designed to target human cyclin E (shCyclinE: sense strand, 5'-CCT CCA AAG TTG CAC CAG TTT CTC GAG AAA CTG GTG CAA CTT TGG AGG TG -3') was cloned into AgeI and EcoRI sites of the pLKO.1.puro lentiviral vector. An shRNA designed to target to human p53 (shp53: sense strand, 5'- CAC CAT CCA CTA CAA CTA CAT CTC GAG ATG TAG TTG TAG TGG ATG GTG-3') was cloned into pLKO.1.neo lentiviral vector. The control pLKO.1 plasmid, having a scrambled non-targeting short-hairpin RNA sequence, was obtained from Addgene.

4.2.5 Cell counting and doubling time determination

To evaluate cell proliferation in different stable cell lines, cells were seeded in triplicates in 6 well plates at a density of 2.5 x 10^4 cells per well. Each day cells were counted in triplicates. Cells were treated with Trypsin (Millipore), collected, mixed with equal volume of Trypan blue (Lonza, 0.4%) and counted using a hemocytometer under the microscope. Doubling times were calculated using an exponential regression calculator (Roth V. 2006 http://www.doubling-time.com/compute.php)

4.2.6 Immunoblotting

Cells were lysed in radioimmunoprecipitation assay (RIPA) buffer containing 50mM Tris, 150 mM NaCl, 0.1% SDS, 0.5% Na Deoxycholate, 1% NP40, and protease inhibitors

(Complete cocktail, Roche, Indianapolis, IN). Lysates were kept on ice for 15 minutes, and then centrifuged 20,000 x g for 10 minutes at 4°C. Supernatants were mixed with 5X sodium dodecyl sulfate (SDS) loading dye, and denatured at 100°C for 5 minutes. Proteins were separated by SDS-polyacrylamide gel electrophoresis **(**PAGE), and transferred onto a Hybond-C nitrocellulose membrane (GE Healthcare). Viral proteins were detected using CM2B4 (LT), CM8E6 (sT), and CM5E1 (sT) antibodies as described before (*129, 254, 281, 290*). SV40 LT and sT were detected using the mouse monoclonal antibody Pab419 (Santa Cruz) at 1:1000. Cyclin E was detected using the rabbit polyclonal antibody C19 (Santa Cruz) at 1:1000. CDK2 was detected using the mouse monoclonal antibody clone SC-6248 (Santa Cruz) at 1:1000. Cyclin A was detected using the rabbit polyclonal antibody SC-596 (Santa Cruz) at 1:1000. Cyclin D1 was detected using the rabbit polyclonal antibody M20 (Santa Cruz) at 1:1000. p53 was detected using the mouse monoclonal antibody clone D-O1 (Santa Cruz) at 1:1000. p21 was detected using the mouse monoclonal antibody clone OP64 (Calbiochem) at 1:1000. Ras was detected using the rabbit monoclonal antibody clone 27H5 (Cell Signaling) at 1:1000. Alpha tubulin was detected with either the mouse monoclonal antibody clone B-5-1-2 (Sigma) at 1:10000, or with the rabbit monoclonal antibody clone 11H10 (Cell Signaling) at 1:2000. For secondary antibody detection the Odyssey Infrared Imaging system (LI-COR) was used with IRDye 680- or 800-conjugated secondary antibodies (1:8000 dilution, Rockland Immunochemicals). SV40 LT and sT were detected using the mouse monoclonal antibody Pab419 (Santa Cruz) at 1:1000.

4.2.7 Semi quantitative RT-PCR

RNA was extracted from BJ-hTERT stable cell lines using Trizol reagent (Invitrogen). RNA was DNaseI treated and cDNA was synthesized using SuperScript III First Strand Synthesis (Invitrogen). Primer sequences were as follows: Cyclin E (forward: AGTGCTACTGCCGCAGTATC; reverse: TGCTTCTTACCGCTCTGTGG), CDK2 (forward: ACAGCTGTGGACATCTGGAGC; reverse: GCTATCAGAGTCGAAGATGG), Cyclin D1 (forward: CCGTCCATGCGGAAGATC; reverse: GAAGACCTCCTCCTCGCACT), and GAPDH (forward: CTGCCCAGAACATCATCC; reverse: AGCCGTATTCATTGTCATACC). PCR reaction was performed using Taq polymerase (Invitrogen) for 30 cycles.

4.2.8 Soft agar assay

BJ-hTERT stable cell lines were trypsinized to single cells, counted, suspended in complete medium containing 0.3% agarose (Sigma-Aldrich), and seeded over a 0.6% agar layer in 6 well plates (2.5×10^4 cells/well) in triplicates. After 4 weeks, plates were photographed at a magnification of 100X.

4.2.9 Microarray

RNA was extracted from biological triplicate stable cell lines BJ-hTERT empty, 339LT, 339LT.LXCXK, and 339LT+sT using Trizol reagent (Invitrogen). RNA was DNaseI treated, and RNA integrity was assessed. For microarray analysis, RNA samples had to

have a RNA integrity number (RIN) of 6 or above. We used a Human HT-12 v4 Expression BeadChip from Illumina, which was processed at the University of Pittsburgh Genomics and Proteomics Core facility. Microarray data was normalized to total fluorescence intensity using cubic spline normalization. For multiple probes per gene, averages of all probes were used for individual gene analyses. All values used for analysis represent averages of three biological replicas. Standard deviations were calculated for genes that were detected with ≥3 probes.

4.3 RESULTS

4.3.1 The effect of MCV T antigens on BJ-hTERT proliferation

To test whether the proliferative effect of truncated MCV T antigens in human fibroblast cells depends on its LXCXE motif and whether sT contributes to this phenotype, we generated BJ-hTERT stable cells that express different combinations of MCV T antigen cDNA codon-optimized constructs by lentiviral transduction, and evaluated cell proliferation. We expressed a truncated MCV LT (339LT) previously described (*56*) (also see **Figures 11 and 34** for truncation pattern), and a LXCXK domain mutant of 339LT (339LT.LXCXK), which lacks RB-family pocket protein binding. 339LT was chosen because it represents one of the longest truncated MCV LT proteins described thus far. Protein expression of 339LT, 339LT.LXCXK, and sT was confirmed by immunoblot (**Figure 27A**). Cell counts over a 10-day period revealed that tumor-derived 339LT expression provides a significant growth advantage over empty vector control (**Figure 27B**). In addition, we observed that mutation of the LXCXE pocket protein-binding motif reverses this growth advantage, and MCV co-expression of sT slightly enhances proliferation of empty vector or 339LT expressing cells (**Figure 27B**). The doubling times and saturation densities of BJ-TERT stable cells reflect this LXCXE-dependent, growth promoting effect of tumor-derived 339LT (**Figure 27C**).

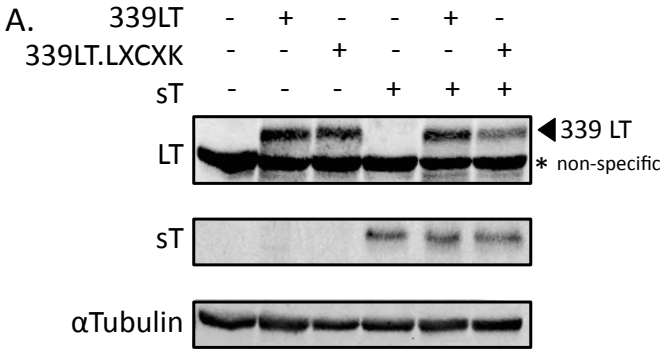

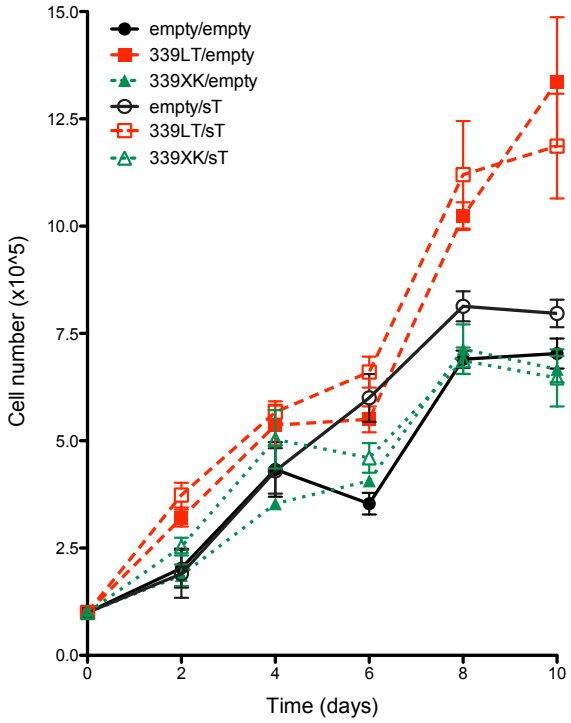

C.

Stable Cell Line	Doubling time (h)	Saturation Density*
Empty + empty	83.5	6.5 ± 1.2
339LT.LXCXK + empty	85.9	6.5 ± 1.5
339LT.LXCXK + sT	87.2	8.4 ± 1.5
Empty + sT	78.5	9.4 ± 1.2
339LT + sT	65.0	10.4 ± 0.9
339LT + empty	62.8	12.0 ± 3.3

* cell number x10^5 ± standard deviation

Figure 27. Tumor-derived MCV LT promotes human fibroblast proliferation through it LXCXE RB targeting domain
(A) Immunoblot analysis of BJ-hTERT stable cell lines was performed to detect truncated MCV 339 LT, 339 LT.LXCXK (339LT.XK) and sT using CM2B4 for 339LT and CM8E6 for sT detection. Tubulin blot serves as a loading control. (B) Proliferation assay of stable cell lines was performed twice in 10 % serum. This graph depicts one representative experiment of technical triplicates. (C) Doubling times Saturation densities of BJ-hTERT stable cell lines were measured on day 12 after seeding. Counts represent two replica in triplicates in a 6 well plate format.

4.3.2 Transformation assays

Given the strong proliferative effect of MCV T antigens, we evaluated whether MCV T antigens could be substituted for SV40 T antigens in the context of defined human cell transformation studies. Hahn et al. have previously identified elements capable of inducing human fibroblast transformation using SV40 LT (Rb and p53 inactivation;

possible gain of function due to p53 interaction), SV40 sT (PP2A inactivation), hRasV12, and hTERT (*316*). Since MCV LT does not bind p53 (*260*), we reasoned that p53 knockdown might be necessary in addition to MCV LT and sT as well as hRasV12 expression to transform BJ-hTERT cells.

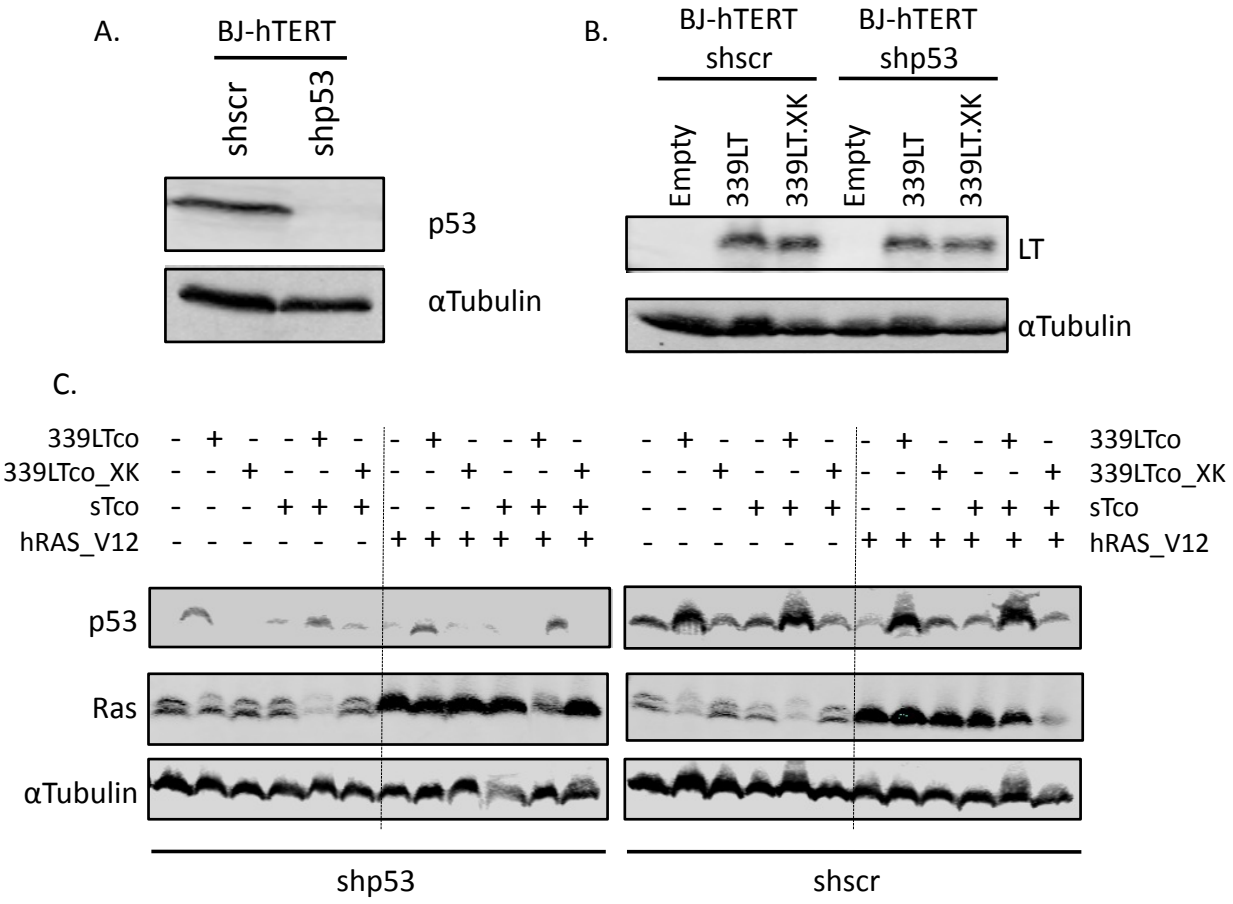

Figure 28. Generation of BJ-hTERT stable cell lines for transformation assays
(A) BJ-hTERT cells were infected with shscr and shp53 lentiviruses and selected to create stable cell lines. Immunoblot analysis using a p53 antibody shows knockdown efficiency. (B) BJ-hTERT shscr and shp53 stable cell lines were infected with empty, 339LT or 339LT.LXCXK (339LT.XK) lentiviruses and selected to create stable cell lines. LT expression was confirmed by immunoblotting using the CM2B4 antibody. (C) Stable cell lines used for soft agar seeding (Figure 30) were analyzed for p53 and Ras protein expression.

We created p53 knockdown BJ-TERT cell lines by lentiviral transduction of p53 shRNA. The p53 knockdown efficiency in our stably selected cell line is shown in **Figure 28A**. We infected the shp53 and shscr cell lines with lentivirus expressing MCV 339LT, MCV 339LT.LXCXK, or empty vector control (**Figure 28B**). After the antibiotic selection period, we infected each stable cell line with either empty vector or MCV sT expression lentivirus, followed by antibiotic selection and transient infection with lentivirus expressing either empty vector or hRasV12. We performed immunoblot analyses to confirm p53 knockdown and Ras protein expression in the resulting 24 different combinations of stable cell lines (**Figure 28C**). Endogenous Ras expression as well as ectopic hRasV12 expression varied between cell lines and p53 levels were slightly increased by 339LT expression in a LXCXE-dependent manner. To determine whether any of the oncogene combinations resulted in cell transformation, we performed a soft agar colony formation assay (**Figure 30**). As a positive control we seeded BJ-hTERT cells expressing SV40ER and hRasV12 in soft agar and observed large colony formation at 4 weeks (**Figure 29**). In the case of MCV T antigens, the results indicate that only BJ-hTERT fibroblast expressing hRasV12 and MCV sT in the presence of p53 knockdown form small soft agar colonies. Additional expression of 339LT did not result in colony formation (**Figure 30**).

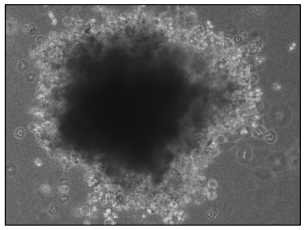

SV40ER + hRasV12

Figure 29. BJ-hTERT SV40ER and hRas stable cell line soft agar positive control
A BJ-hTERT stable cell line expressing the SV40 early region (ER) and hRasV12 was seeded in soft agar and photographed 4 weeks later at a magnification of 100X.

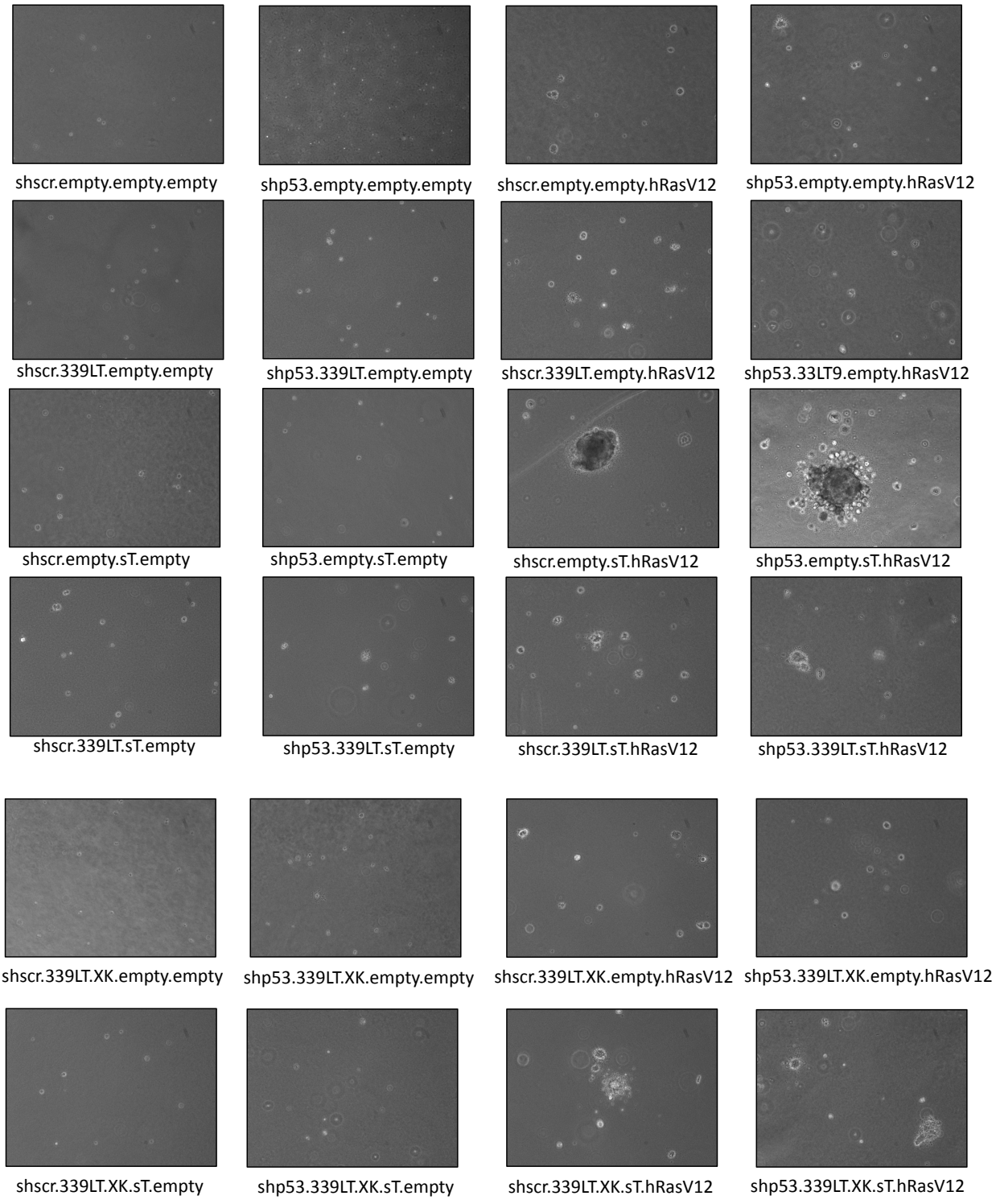

Figure 30. BJ-hTERT stable cells soft agar colony formation result
BJ-hTERT stable cell lines were seeded into soft agar at a density of 2.5x10^4 per 6 well plate well in triplicates. Pictures were taken 4 weeks after seeding at a magnification of 100X.

4.3.3 Microarray gene expression profile in BJ-TERT cells expressing MCV T antigens

To obtain mechanistic insights into the growth promoting effect of tumor-derived LT, we characterized the transcriptional gene profiles of the BJ-hTERT stable cells used in the cell proliferation studies (**Figure 27**). We performed a whole human microarray analysis using an Illumina-based Human BeadChip on three biological replicates of BJ-hTERT stable cell lines empty, 339LT, 339LT.LXCXK and 339LT+sT. To validate the integrity of our microarray, we analyzed a subset of E2F activated genes. As shown in **Figure 31**,

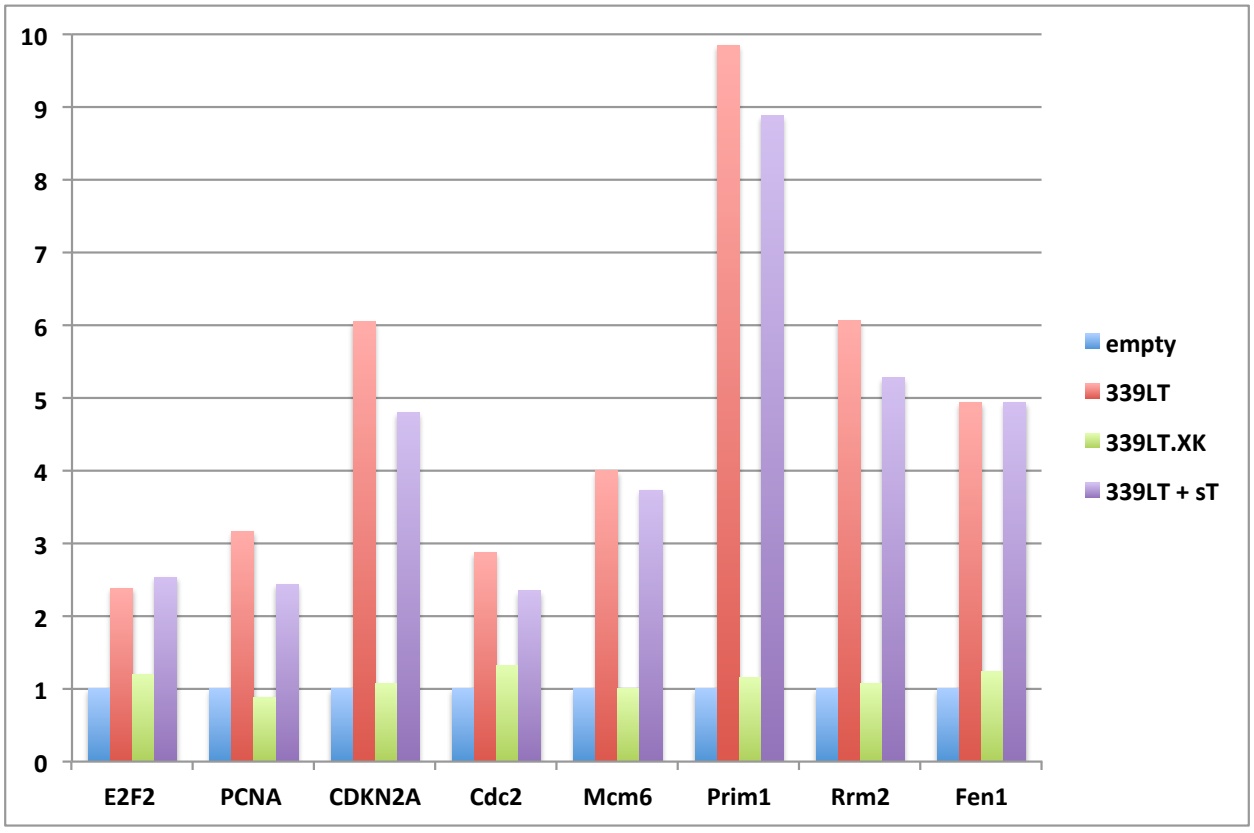

Figure 31. Microarray gene expression profile of E2F targets
Cubic spline normalized microarray expression data from biological triplicate averages for E2F target genes is represented as fold expression over empty control BJ-hTERT cells. Fold changes for E2F2 represent values from a single probe detection. Fold changes for all other genes shown here represent averages of 2 probes each.

this subset of E2F responsive genes is induced by 339LT expression in an LXCXE-dependent manner. This confirms that our microarray gene expression profile behaves accurately for gene changes already known to occur through LXCXE targeting.

We then plotted average gene expression values for each 339LT or 339LT.LXCXK against empty control and determined the number of up- and down-regulated genes in each case. This analysis reveals that 339LT expression has a significant affect on the cellular transcriptome in BJ-hTERT cells, with 549 probes up-regulated and 278 probes down-regulated over empty control (**Figure 32**). In contrast, mutation of the LXCXE motif results in a drastic reversal of this transcriptional modulation. 339LT.LXCXK cells have a transcriptional profile most closely resembling empty control cells, with only 23 probes up-regulated and 11 probes down-regulated (**Figure 32**). This highlights the notion that LT exhibits most of its transcriptional regulation through pocket protein binding and presumably E2F mediated transcription.

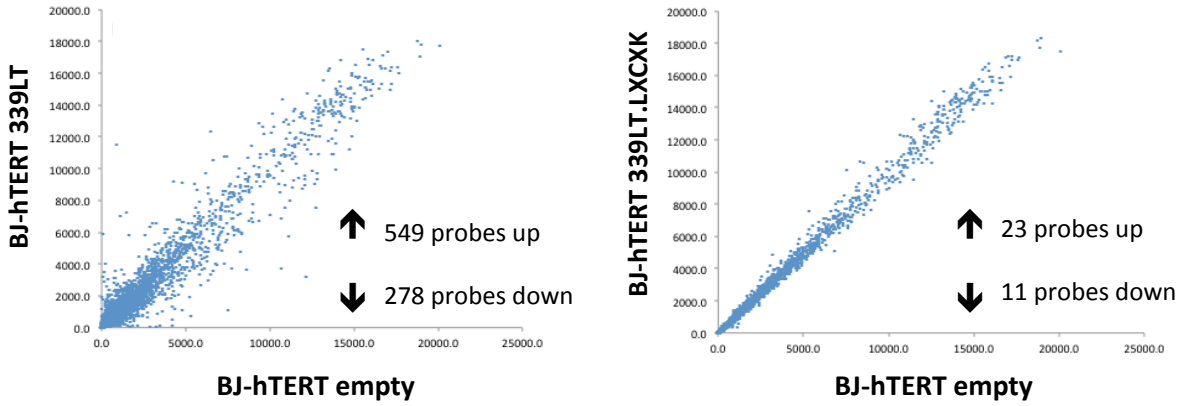

Figure 32. Transcriptome modulation by 339LT
Microarray data points from the 339LT or 339LT.LXCXK (339LT.XK) expressing BJ-hTERT cells were plotted against empty control. All data points represent averages of biological triplicates. Probes are considered up- or down-regulated if the fold change compared to empty is equal or greater to 2.

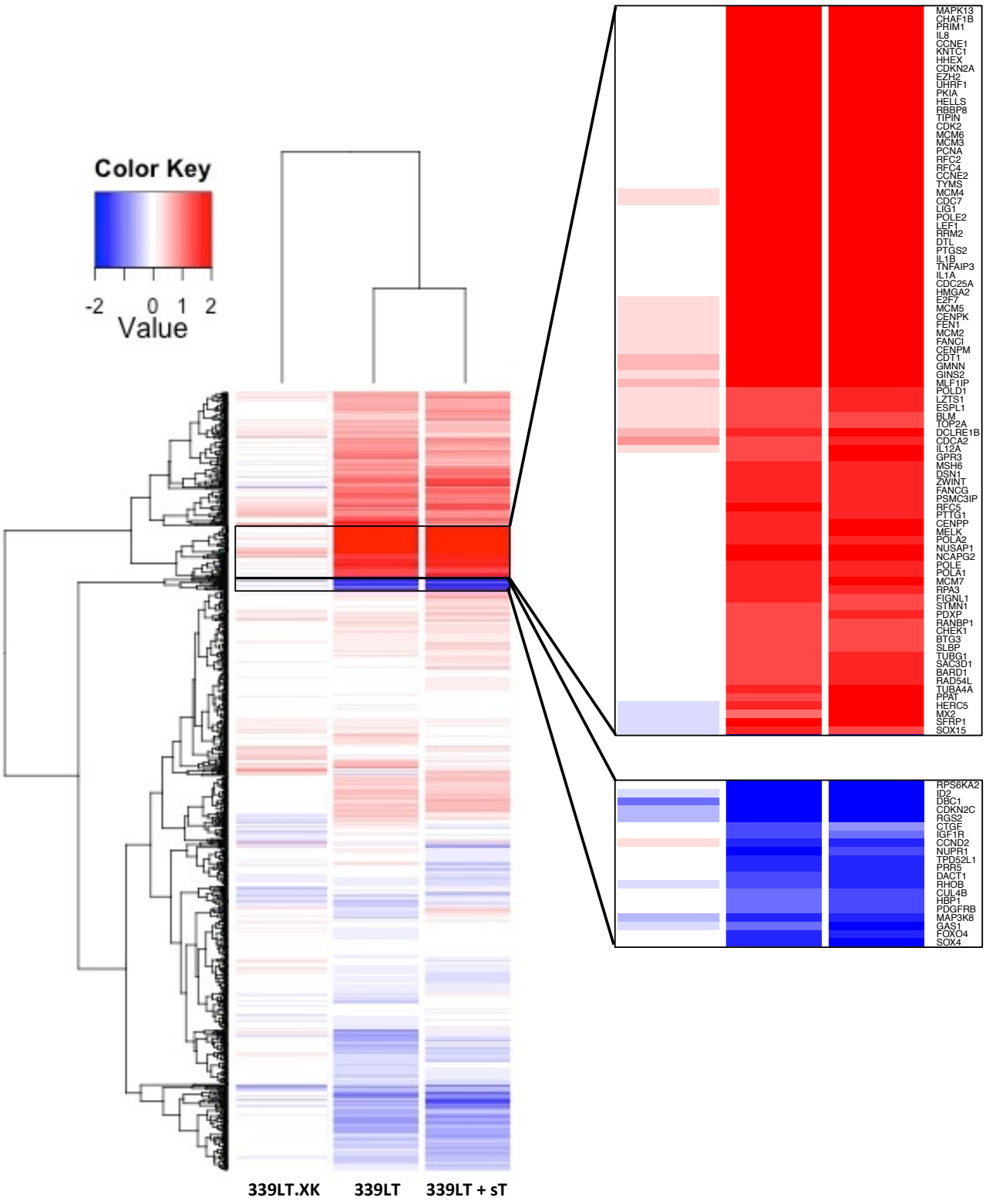

Figure 33. Heatmap of cell proliferation related genes
The heatmap was generated for cell proliferation related genes retrieved from Gene ontology (GO, http://www.geneontology.org/) and Kyoto Encyclopedia of Genes and Genomes database (KEGG, http://www.genome.jp/kegg) using R. Average intensities were calculated from biological triplicates after background subtraction and cubic spline normalization. The mock group was used as control to calculate ratios of transduction groups 339LT, 339LT.LXCXK, and 339LT+sT. Fold changes greater than 2 were considered as "2" for visualization comparison.

Next, we focused on pathways involved in cell proliferation. **Figure 33** shows a heat map of genes involved in controlling cellular proliferation and cell cycle regulation. The heatmap reveals a cluster of genes that is strongly regulated by tumor-derived LT, whereas 339LT.LXCXK only has a minimal effect on the transcription of these genes. Additional expression of sT did not greatly affect transcription of the majority of genes analyzed here. Zoomed-in regions highlight gene clusters that are up or down regulated by 339LT. Genes highlighted by the heatmap analysis (**Figure 33**) that are affected by 339LT expression include genes involved in a variety of biological functions related to cell cycle progression, DNA synthesis, mitosis, DNA repair, DNA damage response, embryonic development, differentiation and immune signaling (**Figure 33** and **Table 5**). In addition to genes required for cell proliferation and DNA replication, 339LT also induces or represses genes to regulate apoptosis or other forms of cell death **(Figure 33)**. Tumor necrosis factor alpha induced protein 3 (TNFAIP3) for example, which is known to be an inhibitor of programmed cell death, is increased 4.3 fold by 339LT according to our microarray data. In addition, the tumor protein D52-like 1 (TPD52L1), which positively regulates MAP3K5-induced apoptosis, is down-regulated 2.9 fold by 339LT expression. This data highlights the wide variety of genes that are modulated by 339LT to change the cellular milieu allowing for increased DNA replication without triggering an unfavorable response such as cell death.

Table 5. Biological functions affected by 339LT expression in BJ-hTERT

Biological Function	Genes regulated by 339LT*
G1/S transition	Cyclin E (CCNE1 and CCNE2) Ubiquitin-like with PHD and ring finger domain 1 (UHRF1) Cyclin-dependent kinase 2 (CDK2) Cell division cycle 7 (Cdc7) Cell division cycle 25A (Cdc25A) Deleted in bladder cancer 1 (DBC1) Growth arrest-specific 1 (GAS1) Cyclin-dependent kinase inhibitor 2C (CDKN2C/p18)
DNA replication machinery	Primase I (PRIMI) Minichromosome maitenance proteins (MCM2-7) Proliferating cell nuclear antigen (PCNA) Replication factor complex (RFC2,4) Thymidylate synthetase (TYMS) Ligase 1 (LIG1) Polymerase epsilon 2 (POLE2) Ribonucleotide reductase M2 (RRM2) Flap structure-specific endonuclease 1 (FEN1) Chromatin licensing and DNA replication factor 1 (CDT1) GINS complex subunit 2 (GINS2) Polymerase delta 1, catalytic subunit (POLD1) Topoisomerase (DNA) II alpha (TOP2A) Polymerase 2A (POL2A) Polymerase epsilon, catalytic subunit (POLE) Polymerase alpha 1, catalytic subunit (POLA1) Replication protein 3 (RPA3)
Mitosis and cytokinesis	Kinetochore associated 1 (KNTC1) Centromere protein K (CENPK) Centromere protein M (CENPM) MLF1 interacting protein 1 (MLF1IP) Extra spindle pole bodies homolog 1 (ESPL1) Cell division cycle associated 2 (CDCA2) MIND kinetochore complex component homolog (DSN1) ZW10 interactor, kinetochore protein (ZWINT) Centromere protein P (CENPP) Nucleolar and spindle associated protein 1 (NUSAP1) non-SMC condensin II complex, subunit G2 (NCAPG2) Pyridoxal phosphatase (PDXP) SAC3 domain containing 1 (SAC3D1) RAD54-like (RAD54L)
DNA damage and DNA repair	Retinoblastoma binding protein 8 (RBBP8) Fanconi anemia, complementation group I (FANCI) Fanconi anemia, complementation group G (FANCG) MutS homolog 6 (MSH6) Checkpoint kinase 1 (CHEK1) BRCA1 associated RING domain 1 (BARD1) RAD54-like (RAD54L)
Embryonic development and differentiation	Hematopoietically expressed homeobox (HHEX) Lymphoid enhancer binding factor 1 (LEF1) Secreted frizzled-related protein 1 (SFRP1) SRY box 15 (SOX15) Dapper, antagonist of beta catenin, homolog 1 (DACT1) Forkhead box O4 (FOXO4) SRY box 4 (SOX4
Immune signaling	Interleukin 8 (IL8) Interleukin 1 beta (IL1B) Interleukin 1 alpha (IL1A) Interleukin 12A (IL12A)

* Genes are considered regulated by 339LT if the average fold change from 3 biological replicates is greater or equal to 2 when compared to empty control

It is well known that E2F transcription factors induce genes involved in cell cycle entry. We therefore analyzed our data set for genes related to cell cycle regulation. **Table 6** lists fold changes of cell cycle regulatory genes that are changed greater than 2 fold in 339LT expressing BJ-hTERT cells in comparison with empty control cells. Cyclin E is the highest up-regulated gene of this group with a 9.9 fold induction (CCNE2) over empty BJ-hTERT. Cyclin-dependent kinase 2 (CDK2), which complexes with cyclin E to induce G1/S transition is up-regulated 3.8 fold over empty control (**Table 6**). Cell division cycle 25 A homolog (Cdc25A), which is also required for G1/S transition is up-regulated 2.9 fold in 339LT expressing cells (**Table 6**). Curiously, cyclin D2, which also acts to promote G1/S transition, is the highest down-regulated gene of this group (**Table 6**). Cyclin-dependent kinase inhibitor 2C (p18), which counteracts G1/S transition, is down-regulated 2.2 fold by 339LT. All gene changes listed in **Table 6** are LXCXEdependent, indicating the importance of LT pocket protein binding in modulating the cellular environment to promote S-phase entry.

Table 6. Cell cycle regulatory genes differentially regulated by 339LT

			Fold change**		
Regulation by 339LT	**Symbol**	**Entrez gene name**	**339 LT**	**339 LT_LXCXK**	**339 LT + sT**
up	**CCNE1**	cyclin E1	5.2 ± 3.1*	1.1 ± 0.3*	6.4 ± 4.0*
	CDKN2A	cyclin-dependent kinase inhibitor 2A (p16/p14)	4.4 ± 2.9*	1.1 ± 0.1*	3.6 ± 2.1*
	CCNE2	cyclin E2	4.1	1.1	5
	CDK2	cyclin-dependent kinase 2	3.8	1	3.5
	CDC25A	cell division cycle 25 homolog A (S. pombe)	2.9	0.9	3.8
	CDKN1A	cyclin-dependent kinase inhibitor 1A (p21, Cip1)	2.4	1.3	2.6
	E2F2	E2F transcription factor 2	2.4	1.2	2.5
down	**CCND2**	cyclin D2	0.3	1.2	0.4
	CDKN2C	cyclin-dependent kinase inhibitor 2C (p18, inhibits CDK4)	0.5	0.8	0.5

**** Average fold changes over empty control from biological triplicates for genes with >2 fold change in 339LT compared to control**
(Fold changes represent probe averages for genes detected by multiple probes (CCNE1 detected by 4 probes; CDKN2A detected by 3 probes; E2F2 detected by 1 probe; all other genes detected by 2 probes)
*** Standard deviation for genes detected by ≥3 individual probes during microarray analysis**

4.3.4 Confirmation of LXCXE-motif dependent up-regulation of cyclin E and CDK2 transcript levels

To validate the microarray result, which demonstrates up regulation of cyclin E and CDK2 transcripts (**Tables 5, 6**), we performed semi-quantitative RT-PCR on a panel of BJ-hTERT stable cell lines expressing different MCC-derived LTs (350, 339 and MKL-1 truncations, **Figure 34A**) and saw increased cyclin E and CDK2 transcript levels with all three truncated LT proteins (**Figure 34C**). Expression of an experimentally cloned LT construct that deletes LT sequence C-terminally from the start of the LXCXE motif (ΔLXCXE) or expression of 339LT.LXCXK show no change of cyclin E transcript levels compared to empty control (**Figure 34C**). Cyclin D1 transcripts, which showed no increase in our microarray analysis (data not shown), shows no consistent change across cell lines. GAPDH transcript levels serve as controls and are not significantly increased in the different stable cell lines (**Figure 34C**).

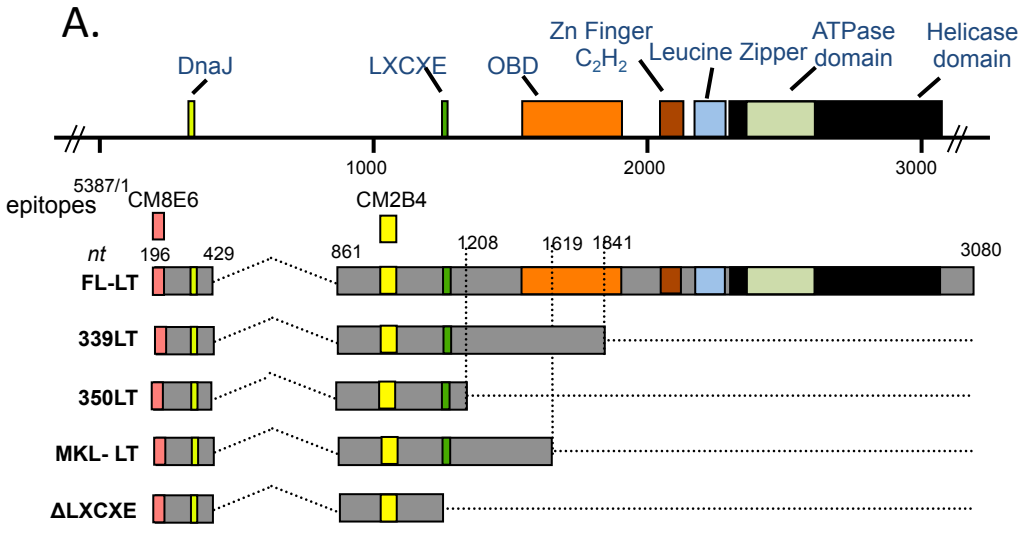

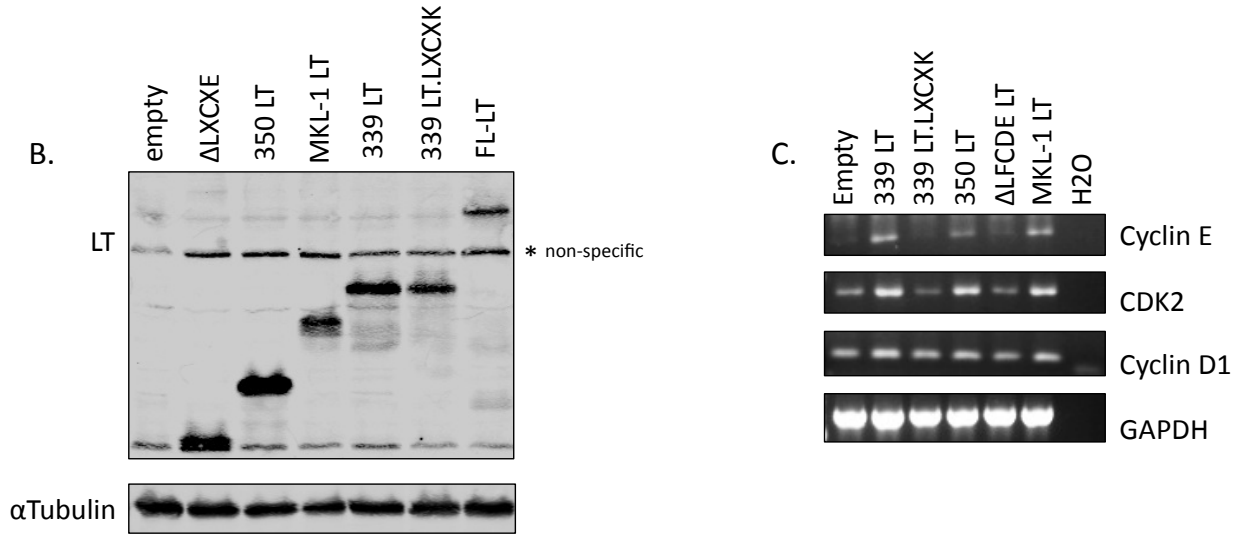

Figure 34. Semi quantitative RT-PCR analysis confirms up-regulation of cyclin E and CDK2 transcripts by tumor-derived LTs
(A) Diagram indicating different LT truncation constructs (ΔLXCXE, 339LT, 350LT and MKL-1 LT) as well as full length LT (FL-LT). (B) BJ-hTERT stable cell lines expressing different tumor-derived MCV LTs or the ΔLXCXE truncation mutant were immunoblotted for LT expression using the CM2B4 antibody as well as αTubulin as a loading control. (C) RT-PCR analysis of BJ-hTERT stable cell lines using cyclin E, CDK2 and cyclin D1 primer pairs. GAPDH was amplified as a housekeeping gene control.

4.3.5 Validation of increased Cyclin E and CDK2 protein expression in BJ-hTERT

To confirm that up-regulated Cyclin E and CDK2 transcripts in tumor LT expressing cells correlates with increased protein expression, we immunoblotted lysates from BJ-hTERT stable cell lines used for proliferation assays (**Figure 27**) and microarray analyses (**Figures 31-33**), and checked for cell cycle regulatory proteins. As published previously by our group (*367*), Cyclin E protein level is increased in an LXCXE-dependent manner by 339LT (**Figure 35A**). This increase is slightly enhanced by sT co-expression, and coincides with CDK2 protein induction (**Figure 35A**). Cyclin D1 and cyclin A protein levels are not significantly altered by 339LT expression (**Figure**

35A), which indicates that 339LT may act to specifically induce cyclinE/CDK2 complexes involved in the G1/S transition of the cell cycle.

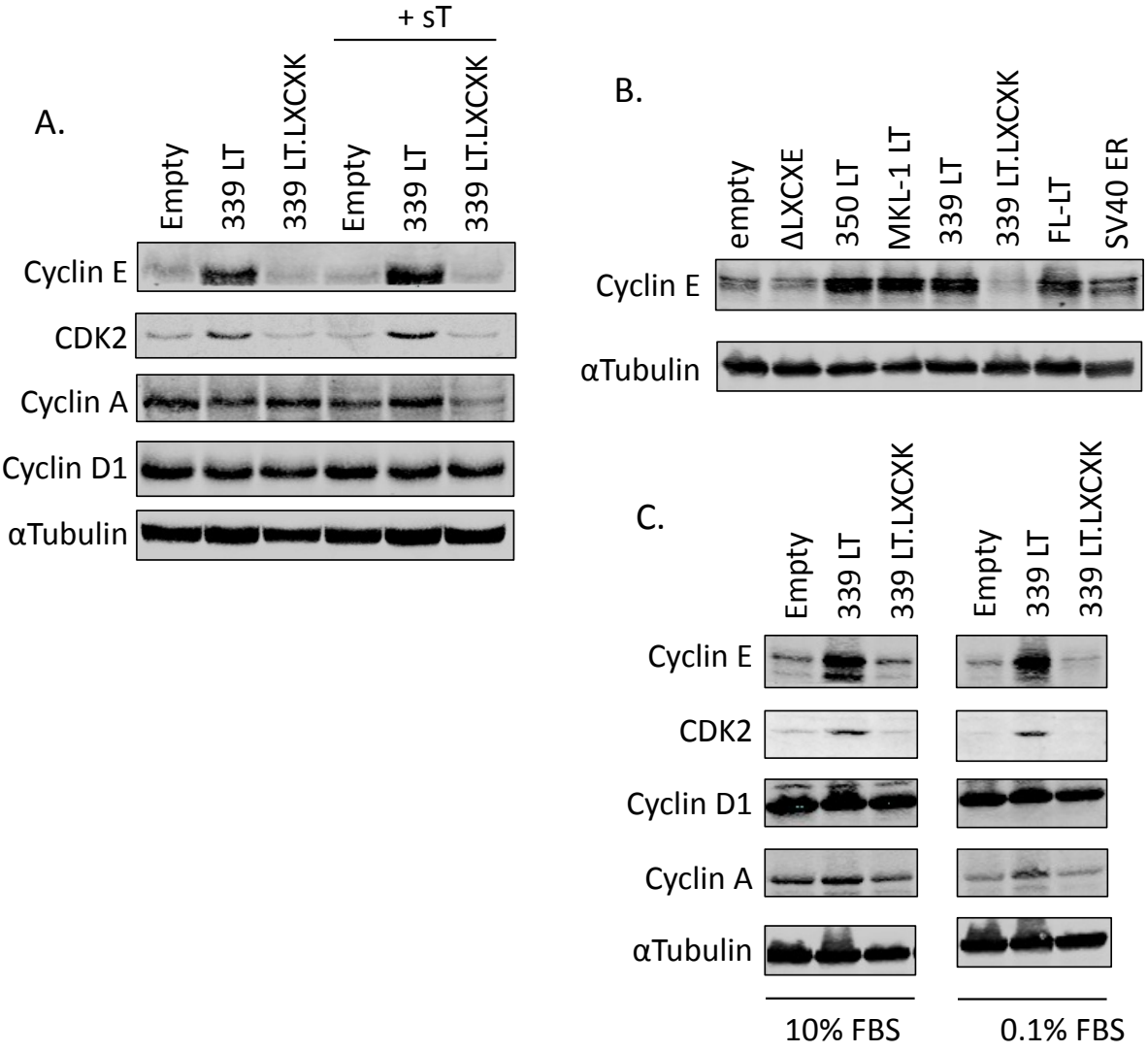

Figure 35. Cyclin E and CDK2 protein levels are preferentially up-regulated by tumor-derived MCV LT

(A) BJ-hTERT stable cell lines (lysates from Figure 27A) were analyzed for cell cycle regulatory proteins by immunoblot. (B) BJ-hTERT stable cells expressing truncated and full length LT (lysates from Figure 29B) as well as BJ-hTERT cells transiently transduced with SV40 ER were immunoblotted for cyclin E expression as well as αTubulin as a loading control. (C) BJ-hTERT stable cell lines grown in either 10% FBS or 0.1% FBS for 3 days were immunoblotted for expression of cell cycle regulators.

We then confirmed induction of cyclin E protein levels in the BJ-hTERT stable cell lines that express either full length LT (FL-LT) or different truncated LT proteins (350LT, MKL-1LT and 339LT) (**Figure 35A-B**). Stable expression of FL-LT did not increase cyclin E protein levels to the same extend as tumor-derived LTs (**Figure 35B**). Expression of the ΔLXCXE construct or 339LT.LXCXK shows no change in cyclin E protein compared to empty control (**Figure 35A-B**) consistent with microarray results. The SV40 early region (SV40 ER) was transiently transduced into BJ-hTERT by lentiviral infection and SV40 LT and sT protein levels were checked by immunoblot (data not shown). Interestingly, expression of SV40 ER, which also contains an LXCXE motif, did not alter cyclin E expression (**Figure 35B**). We also wanted to determine whether or not the effect of 339LT is seen in serum starvation conditions. After serum starving BJ-hTERT cells in 0.1% FBS, we confirmed up regulation of cyclin E and CDK2 even under nutrient deprivation (**Figure 35C**). Notably, the levels of cyclin A were also increased in 339LT expressing cells compared to empty and 339LT.LXCXK during serum starvation, which is not apparent during normal growth conditions (**Figure 35C**).

4.3.6 Cell cycle analysis of BJ-hTERT stable cells

To confirm functional consequences of up-regulated cyclin E and CDK2 levels we analyzed cell cycle profiles in BJ-hTERT 339LT as well as 339LT.LXCXK cells by BrDU incorporation as well as propidium iodide (PI) stain and compared them to empty control cells. Unsynchronized BJ-hTERT 339LT stable cells showed an increase in cells entering the cell cycle compared to empty and 339LT.LXCXK cells (**Figure 36**). This data supports the hypothesis that tumor-derived MCV LT induces S-phase entry in an LXCXE-dependent manner, presumably through increased cyclinE/CDK2 complexes.

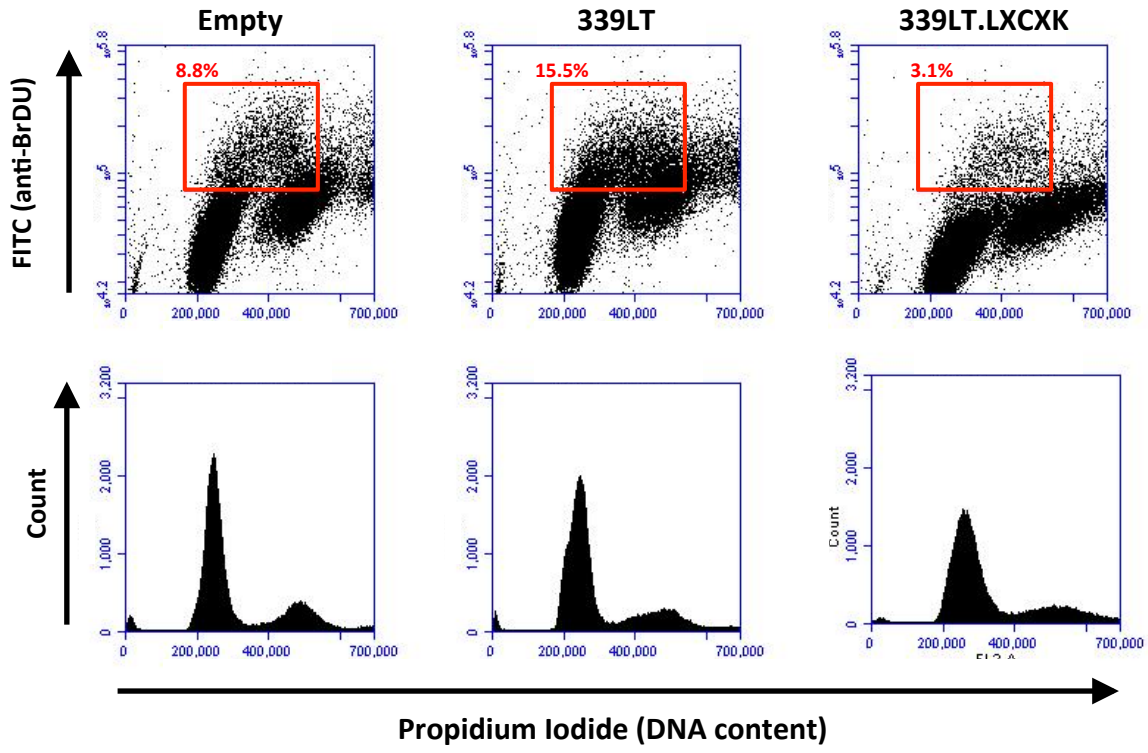

Figure 36. BJ-hTERT 339LT expressing cells show a greater percentage of cells entering the cell cycle
BJ-hTERT stable cell lines empty, 339LT and 339LT.LXCXK were analyzed for BrDU incorporation and PI staining by FACS. S-phase populations are indicated by red boxes in the top panel.

4.4 DISCUSSION

In this report, we further investigate the proliferative effect that tumor-derived MCV LT has on human fibroblast growth. Growth stimulation is dependent on LXCXE-mediated signaling, and increased by sT expression to a minimal extend. The growth promoting effect of tumor-derived MCV T antigen in human BJ-hTERT cells as well as mouse embryonic fibroblasts (MEFs) was reported previously (*260*), however, the contribution of the small T antigen isoform, as well as LXCXE dependence was not addressed. In addition, a recent report by Li et al. indicates that truncated LT does not have a growth promoting effect in U2OS cells (*366*), which may be due to the fact that U2OS is a transformed cancer cell line with oncogenic signaling already in place. Additional MCV LT expression therefore may not further increase the growth rate of this highly proliferative cell line. Li et al. did not observe a growth promoting effect of truncated MCV LT in MEFs (*366*), as was reported by Cheng et al. (*260*), however Li et al. did not express sT in addition to truncated LT, and this discrepancy in results may be due in part to sT expression. Therefore, sT may be critical in enhancing growth in rodent fibroblasts. This is supported by data demonstrating transforming activity of sT in Rat-1 cells (*129*). Our results indicating LXCXE-dependence for tumor-derived LT enhancement of growth proliferation are in line with a previous report indicating loss of MCV-positive MCC xenograft growth upon LXCXE mutation (*297*)

The fact that we do not observe soft agar colony formation in BJ-hTERT fibroblasts expressing 339LT, sT and hRasV12 in the context of p53 knockdown is most

likely due to insufficient hRasV12 transduction efficiency in this cell line (**Figure 36C**). Despite the fact that endogenous Ras levels are decreased in the presence of 339LT, the ectopically over-expressed hRasV12 is expressed strongly in most cell lines even in the presence of 339LT. Further investigations are needed to distinguish the effect that 339LT has on endogenous Ras or overexpressed hRasV12, and whether this has any effect on transformation.

When studying cumulative oncogenic events that lead to a transformed phenotype, it is important to keep in mind that the specific combination of oncogenic pathways that are deregulated in a cell and the specific cell type influence the ultimate fate of that cell. In contrast to SV40 T antigen mediated transformation, tumor-derived MCV LT may require a different combination of oncogenic hits to induce human fibroblast transformation. My findings emphasize further differences between SV40 LT and MCV LT and their modulation of the cellular milieu. In addition to MCV LT's possible inhibitory effect on Ras, SV40 induced human fibroblast transformation may also differ in that SV40 LT interaction with p53 has been indicated to contribute to transformation not only by inactivating p53, but also through a gain of function activity in rodent cells (*162*). Targeting of cellular proteins through the LCXCE motif also seems to differ in part between SV40 LT and MCV LT. While MCV tumor-derived LT induces cyclin E transcript and protein levels in an LXCXE-dependent manner, SV40 LT expression in BJ-hTERT cells does not result in cyclin E protein induction despite the presence of the LXCXE motif.

Microarray analysis reveals strong up-regulation of cell cycle regulators, with cyclin E and CDK2 among the top up-regulated genes in this group (**Table 6**). This

indicates that 339LT mainly modulates the cell cycle to promote G1/S transition. This is also supported by the fact that Cdc25A, which functions to regulate G1/S transition by dephosphorylating CDK2 (*368*), is also up-regulated in 339LT expressing cells (**Table 6**). In addition, the G1/S transition inhibitor p18 is down-regulated in BJ-hTERT 339LT cells (**Table 6**). D-type cyclins are known to partner with CDK4 or CDK 6 to phosphorylate RB family proteins resulting in E2F release to promote S-phase entry (*369*). Cyclin D2 is the highest down-regulated cell cycle regulator in 339LT expressing cells (**Table 6**), which could be explained by a negative feedback loop through p16 (CDKN2A), which is up-regulated by 339LT expression (**Table 6**). In addition, Cyclin D2 function may be compensated by Cyclins D1 and D3, which are unchanged in 339LT expressing cells compared to empty control cells (data not shown). However, D-type cyclin function in general may be dispensable in 339LT expressing cells, due to RB family proteins being bound to LT, freeing E2F transcription factors in the absence of RB phosphorylation through Cyclin D CDK4/6 complexes.

In addition to cell cycle regulators, our microarray analysis also identified other growth-promoting genes that are affected by by 339LT expression in BJ-hTERT cells, with especially high up-regulation of CXC family chemokines (data not shown). CXCL1, a CXC family chemokine that has been indicated in proliferation as well as migration (*370*), is highly up-regulated by 339LT (68 fold induction with single probe detection, data not shown). The highest up-regulated gene in the presence of 339LT in BJ-hTERT cells is IL-8, which is up-regulated 116 fold (average of 2 individual probes, data not shown) in an LXCXE-dependent manner. IL-8 is also a family member of the CXC chemokines that is known to stimulate cell proliferation and migration in various cell

types (*371, 372*). The proliferation and migration promoting effects of IL-8 is associated with EGFR transactivation as well as increased expression and activity of metalloproteinases (MMPs) (*373*), several of which are up-regulated in 339LT expressing cells as well (MMP1 = 18.4 fold induction from single probe detection, MMP3 = 4.3 fold induction from single probe detection; MMP7 = 2.5 fold induction from 2 probe detection). Like IL-8 up-regulation, induction of MMPs is LXCXE-dependent. Interestingly, a study reports that HPV 16 E6 induces IL-8 production and subsequent up-regulation of MMPs (*374*), indicating that this pathway may be commonly targeted by tumorviruses. However, we have not confirmed CXCL1, IL-8 or MMP transcriptional up-regulation by additional experimental techniques, and we do not know whether 339LT expressing BJ-hTERT cells secrete CXCL1 or IL-8. Future experimental analyses are needed to elucidate whether or not our microarray results can be validated and proven significant in MCV biology.

5.0 CONCLUSIONS AND PERSPECTIVES

5.1 MS-1 CELL LINE

In the pursuit to uncover novel features of MCV cell biology *in vitro*, we have developed the new MCV-positive MCC cell line MS-1, which provides a valuable tool for future studies related to this virus (described in chapter 2). MS-1 has clonally integrated MCV genome identical to the tumor biopsy from which it was derived with a tumor signature T antigen truncation. It exhibits markers characteristic for MCC in the clinic, and is tumorigenic in immunocompromised mice, which makes it a good candidate for preclinical chemotherapeutic studies (as described in Appendix B and C of this thesis).

5.2 MCV ORIGIN REPLICATION

As part of our quest to study MCV biology, we focused on several functions of the viral T antigen proteins that are either absent or conserved during MCC tumorigenesis. In chapter 3, we focused on aspects related to MCV genome replication, which is deleted in MCC-derived MCV genomes due to T antigen helicase domain truncations as well as origin point mutations. We identified domains required for efficient viral origin replication and defined a minimal core origin sequence of 71 nucleotides that is needed. We show

that the minimal origin region contains 4 essential GAGGC pentanucleotide sequences that are known to serve as LT binding sites in other polyomaviruses. The essential MCV pentanucleotide sequences however show a different orientation and spacing than is known for the well-studied SV40 and PyV origin sequences, which may provide the opportunity to study a unique origin replication mechanism in MCV. Further studies are needed to determine how LT forms a complex on the MCV origin, and whether or not it forms a double hexamer as other polyomaviral LTs do.

In addition to origin features required for MCV replication, we also evaluated non-origin viral functions. We find that sT expression is required for efficient origin replication by LT; however, additional experiments were needed to determine the precise mechanism by which sT expression contributes to replication. Subsequent studies by Kwun et al. (Cell Host & Microbe, in press) show that sT's PP2A targeting function is not necessary to enhance replication, but rather a sT domain responsible for stabilizing LT protein (LSD) is required. These results stand in conflict with data presented here, which indicate that a PP2A binding mutant of sT (C109S) is insufficient to promote origin replication. Further evaluation of the C109S sT mutant however demonstrated compromised protein stability as compared to wild-type sT protein, which may explain its lack of an enhancing effect on replication. Other PP2A mutants used in the follow-up study by Kwun et al. include R7A and L142A, which have comparable expression levels to wild-type sT and do not compromise sT's effect on replication. In addition, treatment with the PP2A inhibitor Okadaic acid also does not have any effect on sT-mediated enhancement of origin replication (data not shown). Kwun et al. show that sT stabilizes

LT protein by targeting the cellular ubiquitin ligase complex SCF^{Fbw7}, which targets LT for proteasomal degradation otherwise (Cell Host & Microbe, in press).

We also found that Hsc70 binding by LT through its J-domain is essential for its replication function. In SV40, the J domain is required for various functions including viral replication, as well as transformation, transcriptional activation, and virion assembly (*136*). It was discovered that instead of having a direct effect in which the J domain would recruit a Hsc70 homologue and facilitate viral DNA replication through physically rearranging the DNA replication machinery, the J domain acts indirectly through RB-family members and E2Fs (*136*). Published results support an indirect model of DnaJ domain functionality in replication, in which the DnaJ domain facilitates T antigen's interaction with RB family members in an ATP-dependent manner to promote E2F-mediated transcription to induce S-phase entry (*152*). Whether or not MCV LT mediated replication functions through a direct or an indirect mechanism remains to be uncovered. Future experiments are needed to investigate ATP dependence as well as the requirement to interact with RB family members to elucidate the role of the DnaJ domain in MCV replication.

5.3 PROLIFERATION AND TRANSFORMATION STUDIES

To further uncover mechanisms that lead to transformation, we investigate the role of tumor-derived MCV T antigens in the cellular environment. Chapter 4 focuses on one truncated LT, 339LT, which represents one of the longest tumor-derived MCV LT proteins identified in MCC tumors thus far. We show that 339LT expression promotes

human fibroblast (BJ-hTERT) proliferation in an LXCXE-dependent manner, and that sT only minimally contributes to this effect. Transformation studies presented here, which aimed to re-capitulate defined human transformation experiments performed by Hahn et al. (*316, 357*) in the context of SV40 T antigens, reveal that MCV T antigens do not transform BJ-hTERT cells. Additional knockdown of the tumor suppressor p53, as well as mitogenic hRasV12 expression resulted in small soft agar colony growth of cells expressing sT and hRasV12 in p53 knockdown conditions. In cells expressing p53 (shscr control cell line) that are transduced with sT and hRasV12, small soft agar colony formation was observed at 4 weeks (**Figure 30**); however, subsequent evaluation of soft agar plates at 8 weeks revealed degradation of the colonies (data not shown), indicating that p53 knockdown is required for soft agar colony maintenance.

Surprisingly, additional expression of 339LT did not result in soft agar colony growth in the presence of sT and hRasV12 (**Figure 30**). Protein expression analysis by immunoblotting however reveals that this result may be due to an insufficient transduction efficiency of hRasV12 in this particular cell line (condition shp53, 339LT, sT, hRasV12, **Figure 28**). In addition, endogenous Ras expression was consistently decreased in cells expressing 339LT (**Figure 28,** and **Appendix A**). Future studies are necessary to elucidate the effect that 339LT may have on endogenous Ras signaling. Since we utilized a pan-Ras antibody here, which detects N-, K-, and H-Ras, it would be important to perform additional analyses to distinguish endogenous expression between the different isoforms in the presence of 339LT to uncover mechanistic insight. Our microarray result indicates no difference in N-, K-, or H-Ras transcriptional expression in 339LT stable cells compared to empty controls (data not shown). Therefore, future

experiments may also include cyclohexamide treatment in order to determine whether or not 339LT has any effect on Ras protein turnover. It would also be beneficial to transduce a HA-tagged version of the hRasV12 to distinguish endogenous and ectopically expressed Ras by different antibodies, and determine the effect of 339LT on either. If 339LT shows no effect on hRasV12 overexpression in follow up experiments, it is necessary to repeat the experiment to ensure proper transduction efficiency of hRasV12 to be able to re-evaluate transformation under this condition (BJ-hTERT shp53, 339LT, sT, hRasV12).

Additional efforts aimed at defining genetic elements capable of transforming human fibroblasts in the context of MCV T antigen expression should also focus on different oncogenes that could replace hRasV12 expression in this set-up. Possible candidates include constitutively active forms of c-Myc or Akt, both of which are downstream targets of Ras-mediated signaling that promote oncogenesis (*375-377*).

Transduction of c-Myc in the presence of MCV T antigens represents a promising avenue for transformation studies, since sT has been shown to stabilize c-Myc protein levels by inihibiting its proteasomal degradation through SCF^{Fbw7} (Kwun et al., Cell host & Microbe, in press). In addition, Rat-1 transformation by sT is in part dependent on c-myc stabilization (unpublished data, Dr. Shuda). BJ-hTERT express rather low levels of c-myc, which are only slightly elevated by sT expression (unpublished data, Dr. Shuda); therefore higher, exogenous expression of c-myc may contribute to sT transforming activities in BJ-hTERT.

Expression of constitutively active Akt, may provide another genetic element to achieve human fibroblast transformation in the presence of MCV T antigens. MCV sT

has been shown to induce 4EBP-1 hyperphosphorylation, by an unknown mechanism, leading to Rat-1 transformation (*129*). It is clear that mTOR activity, which is a downstream target of Akt (*378*), is necessary for sT to induce transformation in this setting (*129*). If 339LT in fact does inhibit endogenous Ras signaling, this may affect downstream Akt activation, which in turn would lead to a loss of mTOR activity. Therefore, expression of activated Akt, may result in BJ-hTERT transformation in the presence of MCV T antigens.

Our microarray analysis revealed many additional pathways that are regulated by 339LT expression in BJ-hTERT cells. Several of these represent promising starting points in further investigating MCV biology in human fibroblasts. The highly up-regulated chemokine IL-8 has been implicated in proliferation and migration in several cell types. Further experiments that are needed to validate microarray results include RT-qPCR to confirm transcript up-regulation in the presence of 339LT, as well as ELISA analysis to confirm secretion of IL-8 by BJ-hTERT stable cell lines. If BJ-hTERT 339LT cells do secrete IL-8, it would be interesting to supply empty and BJ-hTERT 339.LXCXK cells with IL-8 in their medium to determine whether or not proliferation is induced. In addition, it would be possible to assay for an increased migratory potential of 339LT expressing cells, since IL-8 is known to promote metastasis through up-regulation of MMPs (*379*), some of which are also induced by 339LT. Therefore, performing matrigel invasion assays or gap closure assays would provide mechanistic insights into the migratory potential of 339LT expressing cells.

APPENDIX A

A.1 MOLECULAR FUN FACTS ABOUT BJ-HTERT STABLE CELL LINES

This section describes additional, unpublished data that was accumulated during experimental analyses of BJ-hTERT stable cell lines. Even though this data still leaves many questions unanswered, it presents interesting pieces of information on MCV LT effects on the cellular environment. Experimental methods are included in section 4.2 of this thesis. A. Guastafierro performed all experiments described in Appendix A. A. Guastafierro, M. Shuda, Y. Chang, and P.S. Moore interpreted the data.

A.1.1 Endogenous Ras protein levels are decreased in 339LT expressing BJ-hTERT human fibroblasts

Given the result that endogenous Ras and hRasV12 expression varied among the different BJ-hTERT stable cell lines with endogenous Ras always reduced in the presence of 339LT (**Figure 28C**), we checked Ras protein levels in our stable cell lines used for proliferation and microarray analyses (lysates used in **Figure 27**). We again observed decreased levels of endogenous Ras by MCV 339LT but not 339LT.XK (**Figure 37**). Interestingly, our microarray data did not reveal any transcriptional effect of 339LT expression on N-, K, or H-Ras (data not shown).

A previous report that analyzed the Ras/Raf/MEK/ERK signaling axis before MCV was discovered found that only two out of 44 MCC tumor samples showed downstream activation of this pathway by phospho-ERK IHC evaluation (*244*). In line with this data, our results indicate that MCV LT may inhibit endogenous Ras protein levels, which may result in downstream silencing of this pathway, but further studies are needed to demonstrate this. Nevertheless, the discovery of MCV in association with MCC, may provide an explanation for why this pathway, which is frequently activated in other skin cancers including melanoma (*243*), may not play a role in MCV-positive MCC tumors.

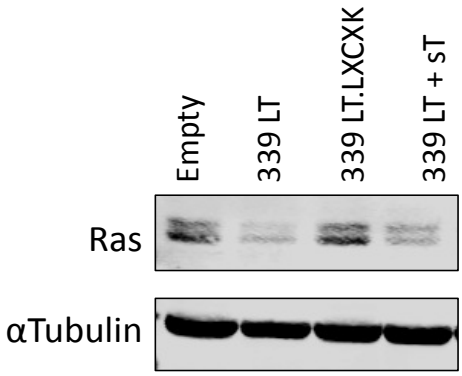

Figure 37. Endogenous Ras protein levels are decreased in the presence of 339LT
BJ-hTERT stable cells (lysates from Figure 27) were immunoblotted for endogenous Ras expression using an antibody that detects N-,K-, and H-Ras.

A.1.2 Tumor-derived MCV LT expression increases p53 protein levels resulting in p21 protein up-regulation in BJ as well as BJ-hTERT human fibroblasts

Unlicensed DNA replication due to increased cell cycle entry induced by oncogenes, such as cyclin E, have been shown to induce a DNA damage type response leading to enhanced p53 protein levels. This prompted us to evaluate p53 protein levels in the BJ-hTERT stable cell lines. We observed an increase in p53 protein levels in BJ-hTERT stable cells expressing 339LT but not the 339LT.LXCXK (**Figure 38A**). Addition of MCV sT expression did not alter p53 protein levels in the presence of 339LT. Knockdown of cyclin E resulted in a reversion of p53 protein to basal levels in BJ-hTERT cells. Knockdown of cyclin E was not complete in cells expressing 339LT, and showed higher residual levels in cells expressing both 339LT as well as sT **(Figure 38A**). We also checked p53 and p21 protein levels in BJ primary human fibroblasts, which have a lower basal expression level of p53 protein than BJ-hTERT fibroblasts (**Figure 38B**). We introduced 339LT as well as FL-LT, each with either an intact or mutated LXCXE motif, by transient lentiviral transduction. We observed increased levels of both p53 as well as the p53 downstream target p21 in the presence of 339LT as well as FL-LT (to a lesser extend) in an LXCXE-dependent manner (**Figure 38B**). We show that p21 induction is mediated through increased p53 protein since knocking down p53 reverses p21 protein up regulation (**Figure 38B**). We noticed that knockdown of p53 was less efficient in cells expressing 339LT, which results in residual p21 protein expression even under p53 knockdown conditions (**Figure 38B**). Transcriptional up-regulation of p21 in the presence of 339LT was confirmed by microarray results (**Table 6**). p53

transcripts are unchanged in 339LT expressing cells compared to empty control (data not shown).

We were struck by the result that tumor-derived 339LT increases p53 protein levels with subsequent p21 activation in human fibroblasts, while still enhancing cell cycle entry and promoting cell proliferation. In contrast, SV40 LT binds and stabilizes p53 protein levels without full p21 induction, circumventing cell cycle arrest (*380*). Another example of a viral protein that induces p53 mediated p21 protein level is HPV E7, which can initiate S-phase entry through cyclin E/CDK2 despite p21 up-regulation (*381*). Nevertheless, p53 regulates a wide range of genes other than p21 including transcriptional activation of genes involved in apoptosis.

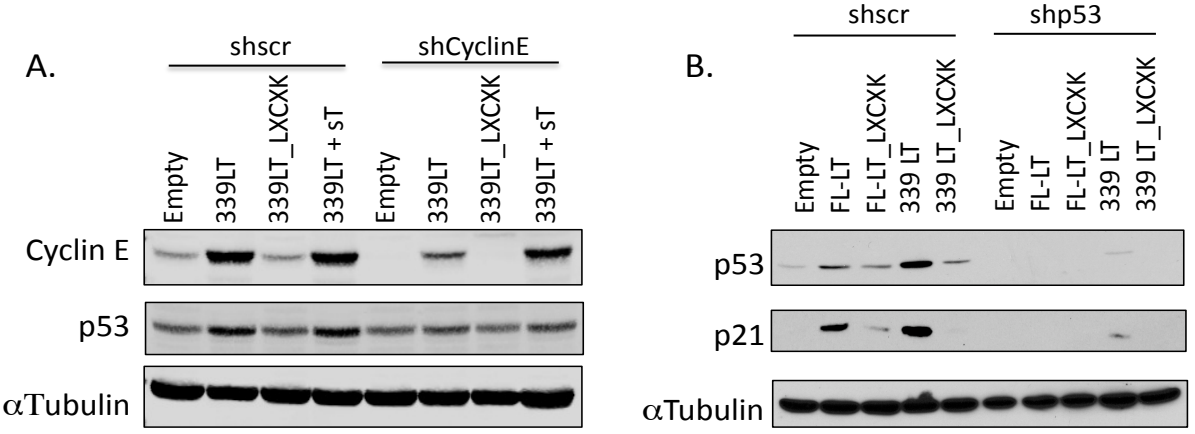

Figure 38. MCV LT stabilizes p53 protein levels resulting in p21 induction
(A) BJ-hTERT stable cell lines used for microarray analysis were transiently transduced with shscr or shCyclinE and immunoblotted for cyclin E, p53 and αTubulin as a loading control. (B) BJ fibroblast stable cells expressing full length (FL-) LT or tumor-derived 339 LT with either an intact or mutated LXCXE-motif were transiently transduced with shscr or shp53 lentivirus. Lysates were immunoblotted for LT (data not shown), p53, p21 and aTubulin as a loading control.

We therefore sought to analyze our microarray data for downstream p53 signaling pathways to determine whether p53 protein stabilization by 339LT results in up-regulation of p53 transcriptional targets other than p21. We analyzed 129 confirmed p53 target genes (*382*) from our microarray set, and only 14 genes (including p21) were transcriptionally affected greater than 2 fold by 339LT expression in BJ-hTERT fibroblasts. Out of these 14 genes we identified 3 genes that are typically repressed by p53 including cell division cycle 25 homolog C (Cdc25C), DNA (cytosine-5-)methyltransferase 1 (DNMT1), and immediate early response 3 (IER3); however, they were conversely activated in 339LT expressing cells (**Table 7**, top column). Discoidin domain receptor family member 1 (DKK1), Insulin-like growth factor binding protein 3 (IGFBP3), and matrix metallopeptidase 2 (MMP2) are genes usually activated by p53, but showed transcriptional repression by 339LT (**Table 7**, top column), indicating that out of the 14 p53 target genes de-regulated by 339 LT expression, only 7 genes were regulated in a way usually thought of by p53 (**Table 7**, bottom column). This indicates that even though p53 protein is induced in human fibroblasts, only selective target

Table 7. Microarray analysis of p53 transcriptional targets

				Average fold changes***		
Gene Name	**Short Description**	**Accesion #'s****	**p53 regulation**	**339 LT**	**339.LXCXK**	**339 LT + sT**
CDC25C	Cell division cycle 25 homolog C (S. pombe)	NM_001790.3; NM_022809.2; NM_001790.3	repressive	2.12 ± 0.81*	0.89 ± 0.21*	2.14 ± 0.72*
DKK1	Discoidin domain receptor family, member 1	NM_012242.2	activating	0.50	0.97	0.30
DNMT1	DNA (cytosine-5-) methyltransferase 1	NM_001379.1	repressive	2.96	1.02	2.89
IER3	Immediate eraly response 3	NM_003897.3	repressive	2.34	1.05	5.49
IGFBP3	Insulin-like growth factor binding protein 3	NM_000598.4; NM_001013398.1	activating	0.14	1.37	0.04
MMP2	Matrix metallopeptidase 2	NM_004530.2	activating	0.44	1.14	0.37
SCARA3	Scavenger receptor class A, member 3	NM_182826.1; NM_016240.2	unknown	4.12 ± 0.57*	1.02 ± 0.11*	2.95 ± 1.15*
CD82	CD82 molecule	NM_001024844.1; NM_002231.3	activating	3.48	1.00	4.59
CDKN1A, p21	Cyclin-dependent kinase inhibitor 1A (p21, Cip1)	NM_078467.1; NM_000389.2	activating	2.33	1.28	2.52
DDB2	Damage-specific DNA binding protein 2, 48kDa	NM_000107.1	activating	2.49	1.27	2.05
FANCC	Fanconi anemia complementation group C	NM_000136.2	activating	2.08	1.24	1.73
PCNA	Proliferating cell nuclear antigen	NM_182649.1; NM_002592.2	activating	2.98 ± 2.01*	0.94 ± 0.16*	2.11 ± 1.43*
SFN, 14-3-3sigma	stratifin	NM_006142.3	activating	2.11	0.64	1.70
TNFRSF10A, DR4	Tumor necrosis factor receptor superfamily 10 A	NM_003844.2	activating	2.23	1.11	2.43

*** Standard deviation for genes detected by 3 individual probes during microarray analysis**
**** Differential accession numbers corresponding to multiple probes are indicated**
***** Average fold changes of biological triplicates for genes with >2 fold change in 339 LT compared to control**

genes are transcriptionally regulated in response. The mechanism by which p53 mediated transcription is inhibited remains to be explored. The microarray dataset revealed that the gene encoding pituitary tumor-transforming 1 (PTTG1) is up-regulated 3.3 fold by 339LT expression. PTTG1 is known to stabilize p53 protein levels, while negatively regulate the transcriptional activity of p53 (*383, 384*), this may be a possible explanation of why p53 protein is enhanced in the presence of 339LT yet not fully transcriptionally active. In addition, we did not observe p53 Serine 15 phosphorylation in the presence of 339LT (data not shown), indicating limited p53 activation despite increased p53 protein levels in BJ-hTERT fibroblasts.

APPENDIX B

SURVIVIN IS A THERAPEUTIC TARGET IN MERKEL CELL CARCINOMA

Work described in Appendix B was published in Science Translational Medicine

Sci Transl Med. 2012 May 9;4(133):133ra56.

with authors Reety Arora, Masahiro Shuda, Anna Guastafierro, Huichen Feng, Tuna Toptan, Yanis Tolstov, Daniel Normolle, Laura L. Vollmer, Andreas Vogt, Alexander Dömling, Jeffrey L. Brodsky, Yuan Chang, and Patrick S. Moore

R. Arora and M. Shuda performed T antigen and survivin knock down experiments, immunoblots and cell cycle analysis. H. Feng performed DTS analysis. T. Toptan and R. Arora created stable cell lines and tested and confirmed protein expression by immunoblotting. R. Arora, Y. Tolstov, and L. Vollmer performed the drug screen. R. Arora tested individual drugs and performed cell titer glo studies. A. Guastafierro and R. Arora performed mouse xenograft experiments and qRT-PCR studies. D. Normolle performed xenograft tumor volume analysis. A. Vogt, J. Brodsky, and A. Dömling provided compounds and supervision on drug screen. R. Arora, Masahiro Shuda, A. Guastafierro, Y. Chang, and P.S. Moore interpreted the data and wrote the manuscript.

B.1 INTRODUCTION

By comparing digital transcriptome subtraction (DTS) deep-sequencing profiles, we found cellular survivin oncoprotein (*BIRC5a*) transcripts up-regulated seven-fold in virus-positive compared to virus-negative MCC tumors. MCV T antigen knock-down in MCV positive MCC cell lines decreased survivin mRNA and protein expression. Exogenously-expressed MCV large T antigen (LT) increased survivin protein expression in non-MCC primary cells. This required an intact retinoblastoma protein-targeting domain that activated survivin gene transcription as well as expression of other G1/S-phase proteins including E2F1 and Cyclin E. Survivin expression is critical to MCV-positive MCC cell survival and a small molecule survivin inhibitor, YM155, is a highly potent and selective agent for initiating irreversible, non-apoptotic, programmed MCV-positive MCC cell death. Of 1360 other chemotherapeutic and pharmacologically-active compounds screened *in vitro*, only bortezomib (Velcade) was found to be similarly potent, but not selective, for killing MCC cells. YM155 was nontoxic and halted MCV-positive MCC xenograft tumor growth in mice while bortezomib had significant toxicity and was not active *in vivo*. Xenograft tumors resumed growth once YM155 treatment was stopped suggesting that YM155 may be cytostatic rather than cytotoxic *in vivo*. Identifying the cellular circuits, such as survivin, that are targeted by tumor viruses can lead to rapid and rational identification of drug candidates for viral cancers that are otherwise difficult to treat.

B.2 MATERIALS AND METHODS

B.2.1 Cell culture

Seven Merkel cell carcinoma cell lines: MKL-1, MKL-2, MS-1, UISO, MCC13, MCC26 and WaGa (gift of Jurgen Becker); NCI-H69 small cell lung cancer cell line (ATCC); 293 human embryonic kidney cells (ATCC); U2OS osteosarcoma cell line (gift of Ole Gjoerup); BJhTERT immortalized foreskin fibroblast cell line (gift of Ole Gjoerup); and BJ primary foreskin fibroblasts (ATCC) were used to screen and evaluate the small molecules examined in this study. The Merkel cell lines and NCI-H69 were grown in RPMI 1640 supplemented with 10% fetal calf serum, penicillin and streptomycin at 37 °C in humidified air containing 5% CO_2. The remaining cell lines were grown in DMEM supplemented with 10% fetal calf serum.

B.2.2 Compounds

A total of 1,360 compounds were used in the screening survey (*232*): 1,280 compounds from LOPAC1280 library (Sigma Aldrich, accessed through University of Pittsburgh Drug Discovery Institute), 89 compounds from NCI's Approved Oncology Drug Set II (from The NCI/DTP Open Chemical Repository, http://dtp.cancer.gov), 6 LT ATPase inhibitors (MAL2-11B, MAL3-101, MAL2-51, DMT3084, bithionol and hexachlorophene (*385*)) and 4 compounds that target and inhibit p53 and MDM2 binding (Nutlin-3, YH264A, Y2H265A and KK_NW_16A (*386, 387*). 19 compounds that were in common between the LOPAC 1280 and the NCI Approved Oncology Drug Set II library were

screened twice with comparable results. NCI Approved Oncology Drug Set II, SV40 LT ATPase inhibitors and MDM2 inhibitors were reconstituted as recommended by supplier. YM155 (4,9-Dihydro-1-(2-methoxyethyl)-2-methyl-4,9-dioxo-3-(2-pyrazinylmethyl)-1H-naphth[2,3-d]imidazolium bromide) was purchased from Active Biochemicals Co. Ltd. (Hong Kong, China). Reconstituted compounds were diluted in cell culture media to obtain a 100x stock concentration prior to addition to cells. Doxorubicin (positive control) was obtained from Sigma-Aldrich and DMSO (negative control) was obtained from Fisher Bioreagents.

For EC50 measurements, dose-response curves were established for 17 drugs obtained individually in bulk stocks. Iodoacetamide (I1149), sanguarine chloride (S5890), NSC95397 (N1786), chelerythrine chloride (C2932), calmidazolium chloride (C3930), tetraethylthiuram disulfide (T1132), bay 11-7085 (B5681), quinacrine dihydrochloride (Q3251), ellipticine (E3380), amsacrine hydrochloride (A9809) and nutlin-3 (N6287) were purchased from Sigma Aldrich, USA. Mitoxantrone (NSC279836), daunorubicin HCl (NSC82151), valrubicin (NSC246131), topotecan HCl (NSC609699), teniposide (NSC122819) and bortezomib (NSC681239) were kindly provided by the NCI/DTP Open Chemical Repository, http://dtp.cancer.gov.

B.2.3 MKL-1 cytotoxicity screen

MKL-1 cells were seeded at a density of 6000 cells in 50 ml of medium per well (120 cells/ml) in opaque polypropylene 384-well microplates (#781080, Greiner Bio-One, Germany). Cells were incubated at 37°C in humidified air containing 5% CO_2 for 24 hours. Thereafter, 25 ml of medium containing 3X drug per well was added to the

plates, which were incubated for an additional 48 hours. Cell viability was measured using Cell Titer Glo (Promega) following manufacturer's instructions. The validity of Cell Titer Glo results in measuring cell viability was confirmed by trypan blue exclusion staining and WST-1 assays (Roche) in pilot studies.

The LOPAC1280 library was screened at a final concentration of 10 mM for each compound and the NCI library was screened at a final concentration of 1 mM for each compound. MAP-C (Titertek Instruments Inc) and Janus MDT (PerkinElmer Inc) were used for automated resuspension and the addition of LOPAC library drugs to assay plates. NCI library compounds were added to wells by manual pipetting.

Cell Titer Glo assays were performed in duplicate using 384 well plates, each containing 24 wells with 1% DMSO (negative control) and 32 wells with 200 mM doxorubicin (positive control). Screening results were evaluated on the basis of percentage cell survival normalized to the DMSO control (100%). Positive candidates were identified using a cut-off value of <10% cell survival. The average Z factor was 0.61 (range 0.34-0.74) for the LOPAC library screen and 0.82 for the NCI library screen (range 0.75-0.91).

B.2.4 Dose-response studies

Compounds that met the selection criteria < 10% cell survival were purchased or obtained in bulk from NCI/NIH Developmental Therapeutics Program. Serial drug dilutions from 10^{-4} M to 10^{-9} M were used on MCC and non-MCC cell lines. Cells were seeded into 384-well plates at 6000 cells in 50 ml of medium per well. After 24 hours, 25 ml of 3X drugs were added at increasing concentration to each well. Cell viability was

then measured using Cell Titer Glo (Promega) kit following manufacturer's instructions as described previously. Each drug concentration was tested in triplicate for each cell line and experiments were repeated twice. EC_{50} doses for the drugs were calculated using a four parameter logistic equation (GraphPad Prism).

B.2.5 Trypan blue dye exclusion assay

Cells were equally seeded and treated with YM155 for 48 hours. To quantitate cell death, cells were treated with Accutase (Millipore), collected, resuspended in PBS, mixed with equal volume of Trypan blue (Lonza, 0.4%) and counted using a hemocytometer under the microscope. Counting was performed three times, in triplicate.

B.2.6 Expression and shRNA lentivirus construction

To express codon optimized full-length MCV large T antigen, the gene was synthesized (DNA2.0) from the MCV-HF strain large T antigen sequence template (*254*) (GenBank ID: JF813003) and cloned into the lentiviral pLVX EF puro vector (*129*). Truncated tumor LT339 (representing the MCV339 strain, amino acid 1-455) and LT339.LXCXK were cloned by site-directed mutagenesis from the codon-optimized full-length LT into pSMPUW-hygro vector (Cell Biolabs Inc.) (*129*). MCV small T codon optimized was also cloned into the lentivirus vector. Cells were infected with lentiviruses in the presence of 1-4 mg/ml polybrene for 24 hours, followed by media change. Stable selection with

either puromycin (1 mg/ml) or hygromycin (200 mg/ml) was initiated 48 hours after infection.

shRNA for MCV T antigen knock-down was generated and used as previously described (*388*), we renamed shT1 in Houben et al. to panT1 in this study. To knock-down survivin gene expression, shRNA sequence (shsur1-5' ccggCCGCATCTCTACATTCAAGAACTCGAGTTCTTGAATGTAGAGATGCGGttttttg-3' and shsur2-5' ccggCCTTTCTGTCAAGAAGCAGTTCTCGAGAACTGCTTCTTGACAGAAAGGttttttg-3' (Lower cased nucleotides indicate linker sequences used for cloning)) was cloned into a pLKO.1puro lentiviral vector. shCntrl is a nontargeting shRNA negative control(*388*). Cells were infected with lentiviruses, washed after 24 hours and then harvested for immunoblotting six days after infection.

B.2.7 Immunoblotting

Cells were lysed in buffer (RIPA or 10mM Tris-HCl pH 8.0, 0.6% SDS) containing protease inhibitor cocktail (Roche). Lysates were electrophoresed in 10% SDS-PAGE, transferred to nitrocellulose membrane (Amersham) and reacted with specific antibodies CM2B4 (1:5000 dilution)(*281*), CM8E6 (1:500 dilution), cleaved PARP, cleaved caspase3, survivin, XIAP, p53, Bcl-2, Bax (1:1000 dilution, Cell Signalling Technologies), E2F1, cyclin E (1:1000 dilution, Santa Cruz Biotechnology), LC3 (1:1000 dilution, Novus Biologicals) or α-tubulin (1:5000 dilution, Sigma)) overnight at 4°C, followed by anti-mouse (1:5000 dilution, Amersham) or anti-rabbit IgG-HRP conjugates (1:3000 dilution, Cell signaling) for 1 hour at room temperature. Peroxidase activity was

detected using Western Lightning plus-ECL reagent (Perkin Elmer). For quantitative immunoblotting, Odyssey Infrared Imaging system (LI-COR) was used with IRDye 800-conjugated secondary antibodies (1:5000 dilution, Rockland Immunochemicals).

B.2.8 qRT-PCR

RNA was extracted from cell lysates using Trizol reagent (Invitrogen) and cDNA was synthesized using SuperScript III First Strand Synthesis (Invitrogen). Quantitative real-time PCR for survivin was performed on cDNA using the SYBR green method (based on manufacturer's protocol, Applied Biosystems). Primers used were 5'-CTGCCTGGCAGCCCTTT-3' (Forward) and 5'-CCTCCAAGAAGGGCCAGTTC-3' (reverse) for survivin (*389*) and 5'-CACTGGCTCGTGTGACAAGG-3' and 5'-CAGACCTACTGTGCGCCTACTTAA-3' for b-actin. The relative change in expression was calculated using the Pffal method (*390*) Experiments for MCC cell lines were repeated six times (2 biological repeats done in triplicate). Experiments for BJ cell lines were repeated six times (3 biological repeats done in duplicate). Mean and standard error of mean was calculated and plotted as column graphs for comparison.

B.2.9 Cell cycle analysis

MKL-1 cells were treated with Accutase (Millipore) to break clumps and then resuspended in fresh medium containing drug and treated for 12 hours. Bromodeoxyuridine (10 mM concentration) was added three hours before harvesting. Cells were then harvested and fixed in chilled 70% ethanol overnight. The cells were

then washed, resuspended in 200 ml of 2M HCl/Triton X (1%) and incubated for 30 mins at room temperature. Cells were centrifuged at 2000 rpm for 10 mins and neutralized in 200ml of 0.1M sodium tetraborate (pH 8.5). Cells were then washed, suspended in 20ml of PBS containing 0.5% tween20, 1% donkey serum and 2ml of anti-BrdU antibody (1:10 diution, BD Biosciences) and incubated overnight at 4°C. Cells were washed and incubated with secondary anti-mouse IgG Alexa488 (1:1000) for 1 hour at room temperature. Cells were washed, suspended in PBS containing 100mg/ml of RNase A, 50mg/ml of PI (propidium iodide) and 0,05% Triton X and incubated for 30 mins at 37°C in the dark and then analyzed using an Accuri C6 flow cytometer.

B.2.10 Cell death evaluation by CFDA and PI staining

After harvesting, cells were resuspended in 2 ml of PBS containing 4mg/ml PI (propidium iodide, Sigma) and 10 mM CFDA (Carboxy fluorescin diacetate, Invitrogen) at room temperature for 10 mins. Cells were then rinsed in 1X PBS and examined under the microscope. Quantitation was performed using ImageJ software.

B.2.11 Mouse xenograft studies

Compounds

For *in vivo* experiments, clinical-grade bortezomib (Velcade) was purchased from the University of Pittsburgh Cancer Institute Pharmacy and YM155 was purchased from Active Biochemicals Ltd. (Hong Kong, China). Compounds were dissolved in sterile 0.9% saline solution for administration to animals.

Animals

Six-week-old female triple immune-deficient NSG (NOD scid gamma) mice (Jackson Laboratory) were maintained in a specific pathogen-free environment at the Hillman Cancer Center Mouse Facility, University of Pittsburgh. All animal studies were conducted according to protocols approved by the Animal Ethics Committee of the University of Pittsburgh (IACUC Protocol # 1102226).

Xenograft Drug Treatments

MCC cells were checked for viability >90% by trypan blue staining resuspended in PBS (2×10^7 cells in 100 µl) and inoculated subcutaneously into the right flank of mice. Once tumors were palpable (2-4 weeks after injection), mice were assigned sequentially into receiving either bortezomib, YM-155 or saline treatment arms.

All treatments were delivered for three consecutive weeks. Bortezomib treatment was delivered subcutaneously twice weekly at 1 mg/kg per mouse. To avoid previously observed side effects, mice were given hydrogel (ClearH_2O) and kept at 30°C (using a heating blanket to heat up half of the cage) during bortezomib treatment. YM-155 (2 mg/kg) was given intraperitoneally on five consecutive days, followed by a two-day treatment-free interval. The control group received saline alone (21 mice on the same dosing schedule as bortezomib and 20 mice on the same dosing schedule as YM155. Day 19 was the last day of drug delivery for both schedules and hence the end of treatment. Caliper measurements of the longest perpendicular tumor diameters were performed every other day and tumor volumes were calculated using the formula: $(\text{width})^2 \times (\text{length}/2)$. Animals were sacrificed when tumors reached 2 cm in any dimension, >20% weight loss or when they became moribund. Survival was defined as

time from the first day of treatment until death/sacrifice.

Statistical analysis

Two-tailed paired Student's *t* test was used to analyze statistical differences in qRT-PCR results. Mouse survival curves were estimated using the Kaplan–Meier product-limit method and were compared using the log-rank test (GraphPad Software, La Jolla, CA). A piecewise linear hierarchical Bayesian model (*391*) was used to characterize differences in tumor volumes and growth between treatments.

Immunohistochemistry

Immunohistochemical staining of mouse tumor tissues was performed as previously described (*281*).

B.3 RESULTS

B.3.1 Survivin Expression in MCV-positive MCC

To identify pathways perturbed by MCV infection in MCC, we analyzed DTS datasets to identify cellular genes differentially regulated between MCV-positive and MCV-negative MCC (*55*). We compared 400,000 cellular transcripts from MCV-positive and MCV-negative MCC tumors and found 1096 of 11,531 (9.5%) genes elevated >3 fold for the MCV-positive compared to the MCV-negative library.

We next identified sixty-four genes using Gene Ontology (GO) gene definitions directly involved in programmed cell death or cell cycle regulation (**Figure 39A**). *BIRC5a* (Baculoviral inhibitor of apoptosis repeat-containing 5) mRNA encoding the survivin oncoprotein were increased 7 fold ($p=2.90xe^{-10}$) for virus-positive compared to virus-negative MCC tumors (**Figure 39A**). Other genes regulating programmed cell death, including TP53, cIAP2, XIAP, BAX, BCL2 and Caspase 3/6 transcripts, were not differentially expressed (**Figure 39A**). Notably, some genes including TRAF2 and PI3K were significantly reduced in virus-positive compared to virus-negative MCC tumor libraries.

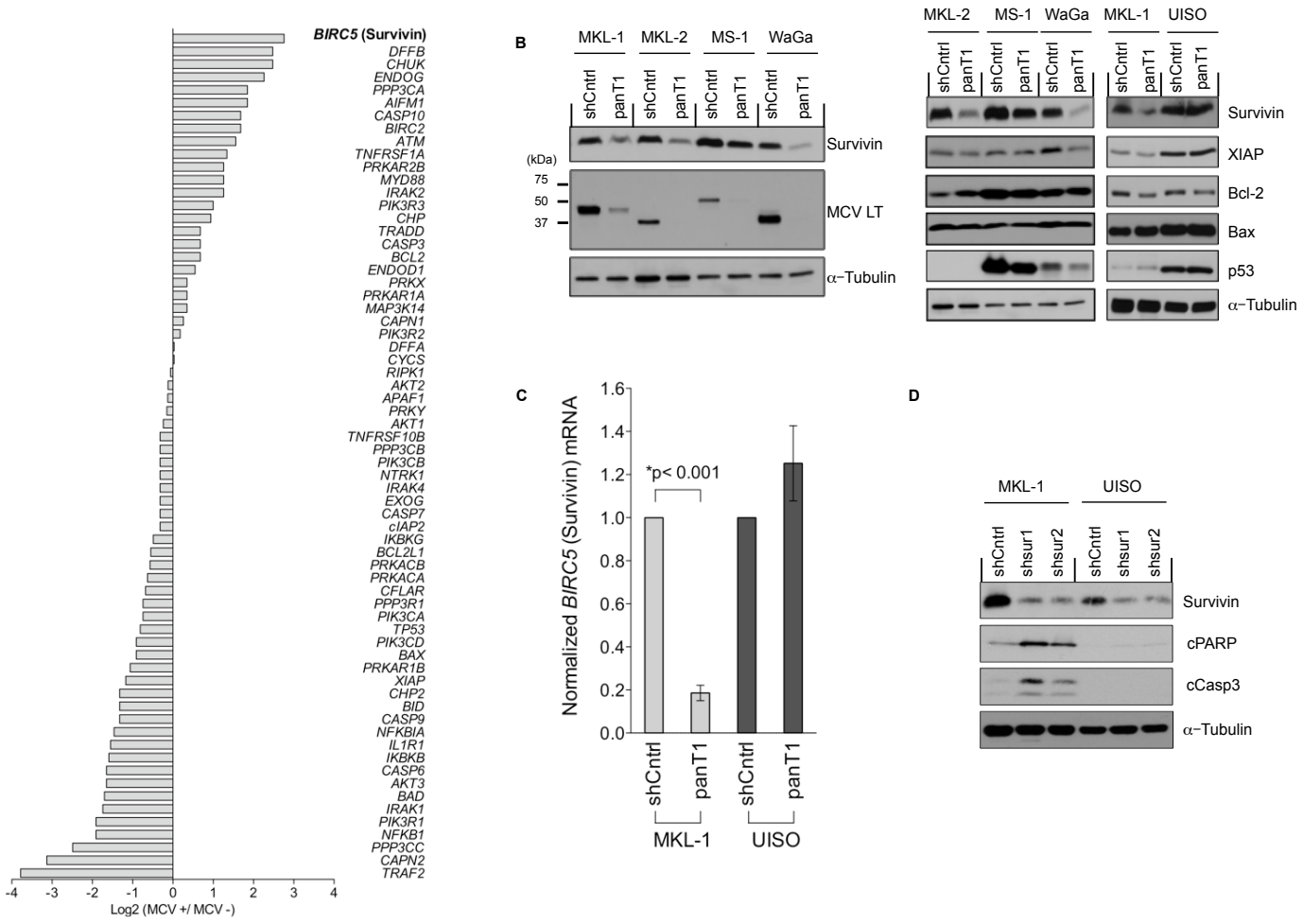

Figure 39. Survivin oncoprotein mRNA expression is increased in MCV-positive MCC
(**A**) DTS comparison of 64 genes involved in programmed cell death and cell cycle regulation, showing that survivin (*BIRC5*) mRNA transcripts (highlighted in bold) were seven-fold higher in a MCV-positive than an MCV-negative MCC DTS cDNA library. The relative expression of genes was normalized to total sequence reads for each MCC library (also see Table S1 for more details). (**B**) MCV T antigen is required for survivin expression. Lentiviral MCV T antigen exon1 knock-down (panT1) decreased survivin protein expression among four MCV-positive MCC cell lines (left panel). shCntrl is a scrambled shRNA control lentivirus. No consistent changes in XIAP, BCL-2, Bax or p53 protein levels are seen after MCV T antigen knock-down among MCC cell lines (right panel). MKL-1, MKL-2, MS-1 and WaGa are MCV positive and UISO is MCV negative. (**C**) MCV T antigen is required for survivin transcription. Survivin mRNA levels were reduced in MKL-1 but not UISO cells after T antigen knock-down indicating that T antigen acts survivin transcription. Survivin mRNA was measured by qRT-PCR and normalized to β-actin mRNA. The experiments were performed in triplicate and repeated two times (mean±SEM). (**D**) Survivin expression is required for MCV-positive MCC cell survival. Survivin was targeted for knock down with two shRNA lentiviral vectors, shsur1 and shsur2 in MKL-1 cells and UISO cells. MKL-1 cells initiate apoptosis after survivin knock-down, with increased expression of cleaved polyADP ribose polymerase (cPARP) and caspase 3 (cCasp3), whereas UISO cells are resistant to survivin knock down-induced apoptosis. a-Tubulin is used as a loading control.

B.3.2 MCV Large T Induces Survivin Through Retinoblastoma Protein Targeting

To determine if MCV T antigen increases survivin expression in MCC, we used a short-hairpin (shRNA) lentivirus (panT1) to perform RNAi targeting of the MCV T antigen exon1 sequence that selectively knocks down all MCV T antigen isoforms in MCC cells (*388*). MCV-positive MCC cells infected with this lentivirus undergo non-apoptotic cell death (necroptosis) when MCV oncoprotein expression is inhibited (*388*). MCV T antigen reduction correlated with survivin reduction in all MCV-positive MCC cell lines, but not in any of the MCV-negative cell lines (**Figure 39B**). The degree of survivin decrease with T antigen knock-down ranged from modest in MS-1 to near complete in WaGa cell lines (**Figure 39B**). This effect is at the level of transcription rather than translation since *BIRC5a* mRNA is significantly reduced by T antigen knock-down (**Figure 39C**).

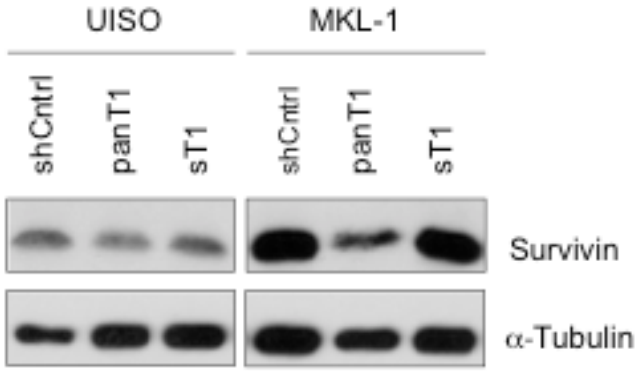

Figure 40. MCV sT knockdown in MCC cell lines does not affect survivin expression
UISO and MKL-1 cells infected with either sT1, which knocks down sT alone (Shuda *et al*., JCI 2011), or panT1 shRNA lentiviruses were immunoblotted for survivin and α-tubulin.

Use of an shRNA lentivirus that selectively targets only the small T antigen isoform (*129*), however, did not affect survivin expression (**Figure 40**), indicating that increased survivin transcription was dependent on MCV LT but not small T antigen (knock-down of LT alone is difficult due to the overlapping structure of the T antigen cistron). In contrast to survivin, no consistent changes in protein expression for p53, XIAP, Bcl-xL, Mcl-1, Bad, Bik, Bmf, Bim, Puma, Bcl-2 or Bax proteins (**Figure 39B** and ref. (*388*)) or for cleaved polyADP ribose polyomerase (PARP), cleaved caspase 3 or cleaved caspase 9 proteins was seen after panT1 knock down in MCV-positive cells. These results are consistent with our DTS findings suggesting that MCV T antigen selectively activates *BIRC5a* transcription. We next sought to determine the importance of survivin expression to survival of MCV-positive and MCV-negative MCC cells. Although only partial suppression of survivin expression was achieved by shRNA *BIRC5a* targeting, MCV-positive MKL-1 cells, but not MCV-negative UISO cells, underwent apoptosis (**Figure 39D**).

To confirm that LT is the MCV T antigen isoform responsible for survivin activation, we cloned and transduced a tumor-derived LT (LT339) cDNA into nontransformed, primary human BJ fibroblasts. Survivin protein levels increased three-fold when LT was expressed compared to the empty vector control (as measured by quantitative LICOR immunoblotting, **Figures 41A-B**). Also consistent with our knock-down experiments (**Figure 39C**), LT directly activates *BIRC5a* promoter transcription in BJ cells (**Figure 41C**). The LXCXE domain in LT responsible for sequestration of RB1 mediates survivin activation. Both cyclin E and E2F1, required for cell cycle S phase entry (*392*) are repressed by active RB1 and were used as markers for RB-regulated

gene expression. MCV LT339 activates expression of both cyclin E and E2F1 proteins in BJ cells whereas LT339 having a point mutation that prevents RB1 binding (changing LFCDE to LFCDK) (*279*) abolishes induction of cyclin E, E2F1 and survivin (**Figure 41A)**. MCV small T expressed alone in BJ cells did not increase survivin oncoprotein expression (data not shown) In contrast to primary BJ fibroblasts, we did not find that MCV LT markedly increased survivin expression in cell lines that had been already transformed, including 293HEK and U2OS cells (data not shown).

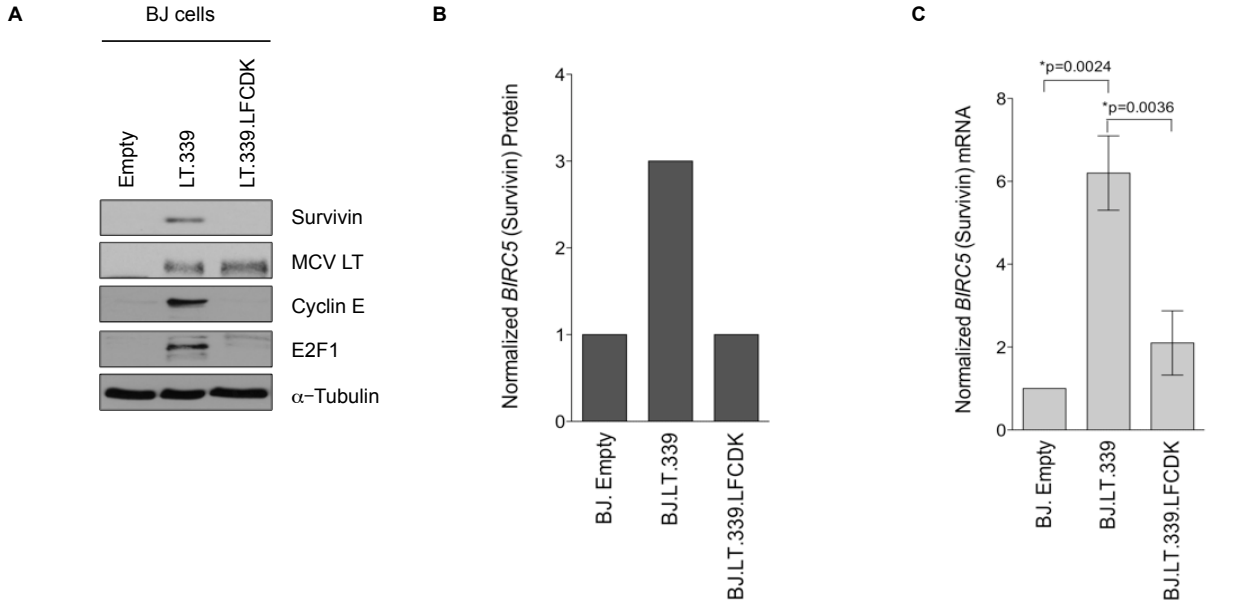

Figure 41. MCV LT induces survivin oncoprotein expression in primary BJ cells through its RB targeting domain

(A) BJ cells were transduced with either empty vector, a tumor-derived LT cDNA (LT.339) or an LT cDNA with an inactive RB binding domain (LT.339LFCDK). Immunoblotting reveals that MCV LT.339 induces survivin expression but LT.339LFCDK does not. A similar pattern is seen for other S phase cell cycle proteins such E2F1 and cyclin E that are also transcriptionally repressed by RB. (B) LICOR quantitative immunoblotting for survivin in (A), normalized to a-tubulin (arbitrary units). (C) Survivin mRNA levels increased in BJ cells expressing LT.339 protein but not in cells expressing the RB1 binding mutant LT.339LFCDK. BJ cells expressing either empty, LT.339 or LT.339LFCDK were serum starved for 48 hours and then harvested for RNA. Survivin mRNA was measured by qRT-PCR and normalized to β-actin mRNA. The experiments performed three times in duplicate (mean±SEM).

B.3.3 Survivin as a target for MCC chemotherapy

Given the apparent importance of MCV-induced survivin expression to MCC cell survival, we examined YM155, an imidazolium small molecule inhibitor of the survivin promoter that is currently undergoing Phase II trials for prostate cancer (*389, 393*). YM155 is both highly active and selective for inhibiting MCV-positive MCC cell growth in

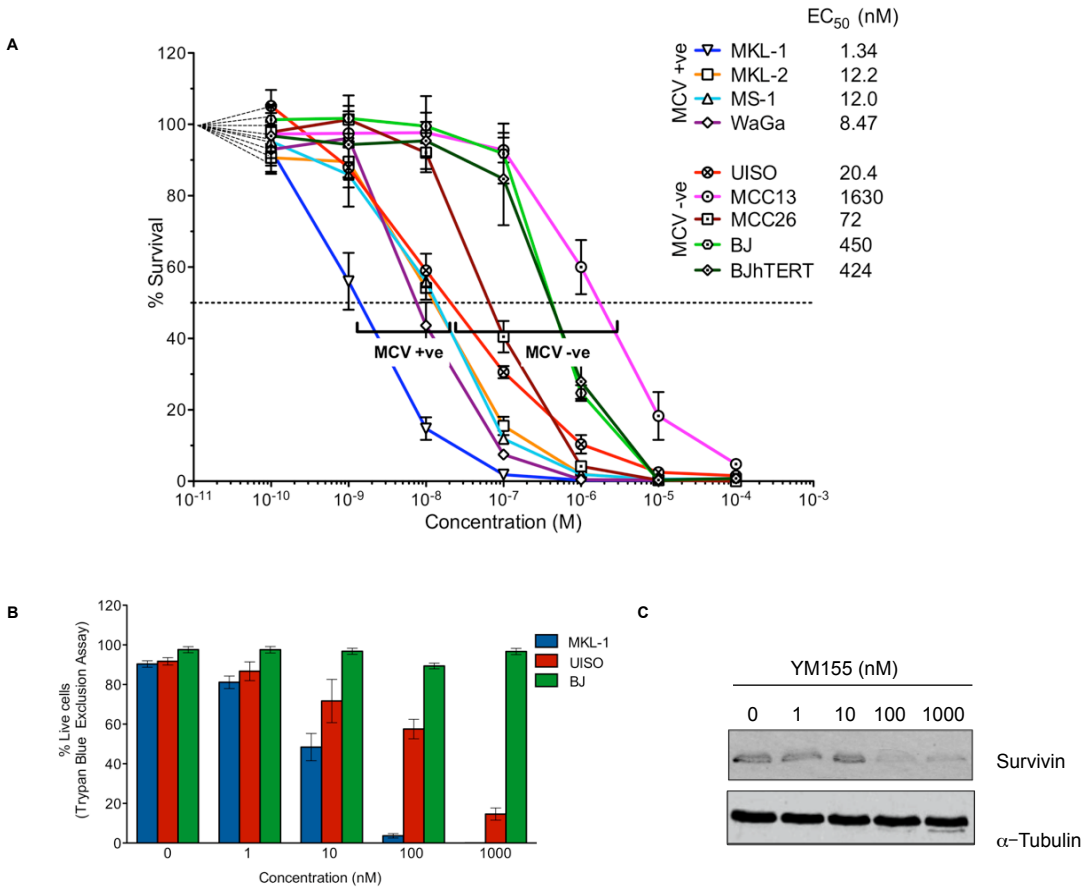

vitro as measured by Cell-Titer Glo assays (EC_{50} 1.34 nM to 12.2 nM) (**Figure 42A**).

Figure 42. The survivin promoter inhibitor YM155 inhibits MCV-positive MCC cell growth
(A) Dose-dependent growth curves at 48 h for YM155-treated cell lines. MCV-negative MCC13, BJ and BJhTERT cells showed relative resistance to YM155 treatment, whereas all MCV-positive cell lines (MKL-1, MKL-2, MS-1 and WaGa) were sensitive to YM155. MCV-negative UISO and MCC26 had intermediate sensitivity to the YM155. (B) Trypan blue vital dye exclusion assay showed dose-dependent cell killing at 48 h for MKL-1 cells (blue bars) whereas UISO cells (red bars) are relatively less sensitive and BJ cells (green bars) are resistant to YM155. (C)

Dose-dependent decrease in MKL-1 cell survivin protein expression after 12 h YM155 treatment.

MCV-negative MCC cell line growth is also inhibited by YM155 but this occurs at concentrations 1-2 orders of magnitude higher than for MCV-positive MCC cells. YM155 treatment for 48 hours at 10-100 nM preferentially killed MCV-positive MKL-1 compared to MCV-negative UISO cells as measured by trypan blue staining (**Figure 42B**). Survivin protein was reduced in MKL-1 cells after YM155 treatment, consistent with YM155's proposed mechanism of action in inhibiting the *BIRC5a* promoter (**Figure 42C**).

We next examined mechanisms of cell killing by YM155 in MCV-positive MCC cells (**Figure 43**). Survivin plays a role in mitotic progression and loss of survivin can lead to cell death through mitotic catastrophe in some tumor cells (*394*). MCV-positive MCC, however, are slowly cycling cells (doubling time of 3 days (*388*)) and do not undergo G1 arrest or G2/M pileup as would occur with mitotic checkpoint activation in rapidly cycling cells (**Figure 43A**, top panels). Instead, bromo-deoxyuridine (BrdU) incorporation into DNA reveals a profound inhibition of DNA synthesis by YM155. **Figure 43A** (boxes, bottom left panel) shows the normal inverted-U pattern for BrdU incorporation during S phase DNA synthesis in MKL-1 cells. When the topoisomerase I inhibitor camptothecin is added (**Figure 43A**, bottom right panel), accumulation of BrdU-positive cells in G1 and G2/M/G1-tetraploid becomes evident, and S phase incorporation is lost, consistent with repair polymerase activation during DNA damage response signaling. YM155 treatment, however, ablates BrdU incorporation (**Figure 31A**, center panel), most consistent with disruption of DNA replication forks and inhibition of new S phase and repair DNA synthesis, but not mitotic catastrophe.

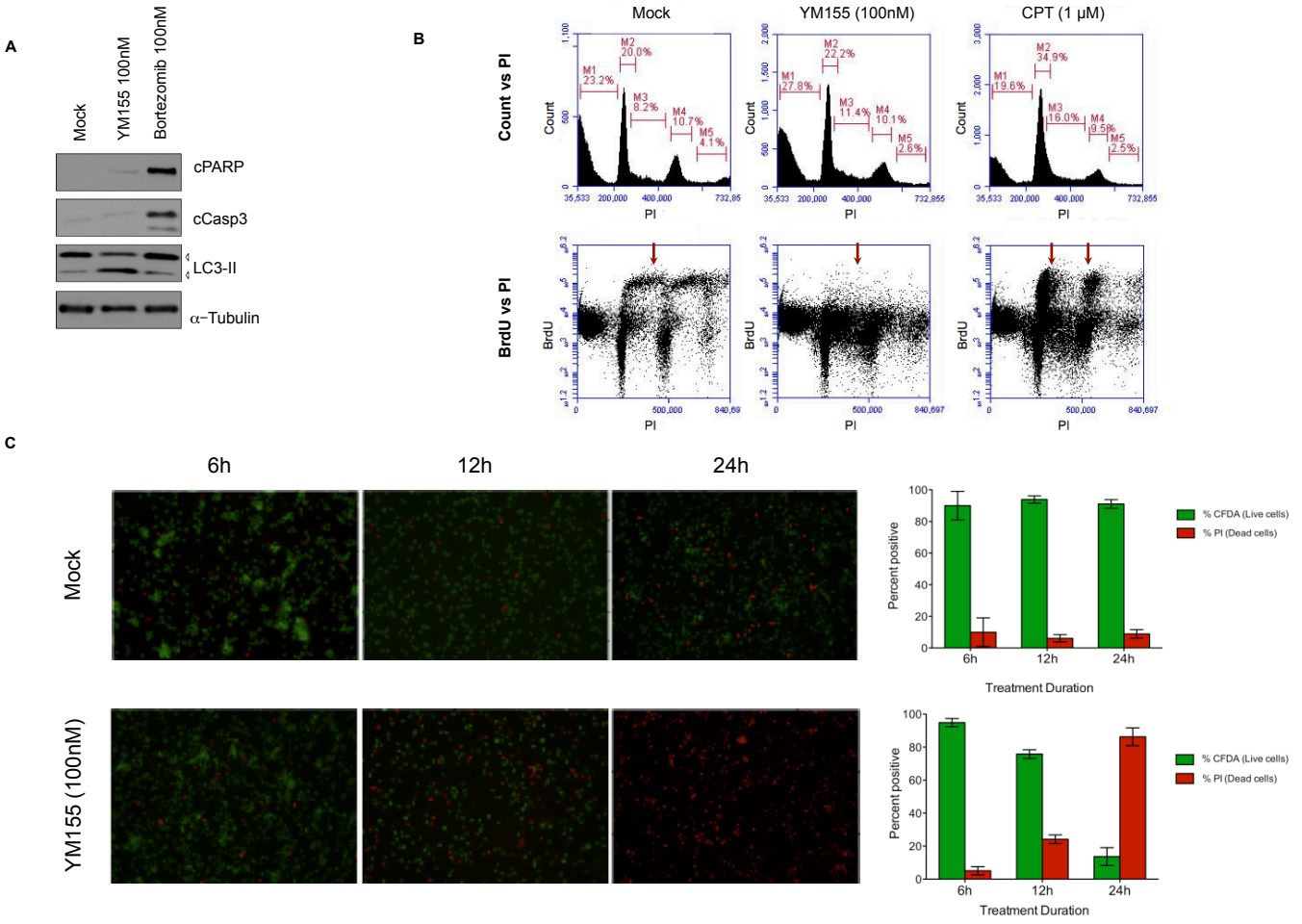

Figure 43. Cell death phenotype of MCV-positive MCC cells treated with YM155
(A) Cell cycle analysis reveals YM155 treated cells do not undergo mitotic catastrophe. MKL-1 cells were treated with DMSO, YM155 (100nM) and camptothecin (CPT, 1mM) for 12 h and then subjected to PI (upper panel) and BrdU staining (lower panel). Boxes show S phase BrdU incorporation without treatment, accumulation at G1 and G2/M/G1 tetraploid during CPT treatment, and near-complete loss of BrdU incorporation during YM155 treatment. Box a represents G1 phase, box b represents S phase and box c represents G2/M phase (B) YM155 induces nonapoptotic cell death associated with autophagy in MKL-1 cells. MKL-1 cells were treated with DMSO, YM155 (100nM) or bortezomib (100nM) and immunoblotted for (c) cleaved PARP, cCaspase 3, LC3 and a-tubulin. In contrast to YM155, the bortezomib proteasome inhibitor activates MKL-1 cell apoptosis (also see Fig S2). (C) YM155 treatment initiates programmed cell death within 12-24 hours after treatment. MKL-1 cells were co-stained with CFDA (green, live) and PI (red, dead). Column graphs (right panel) represent mean and range of % CFDA-positive (green) and % PI-positive cells (red).

YM155 treatment results in early commitment to nonapoptotic programmed cell death. No evidence of apoptosis was present, measured by caspase 3 and PARP cleavage (**Figure 43B**), when MKL-1 cells were treated with 100 nM YM155 for 48 hours, but YM155 did initiate LC3-II accumulation, a marker for cell autophagy (*395*). This is not due to loss of apoptosis pathway signaling since treatment with the proteasome inhibitor bortezomib (Velcade) activated PARP and caspase cleavage (**Figure 43B**). Commitment to YM155-dependent cell death occurs relatively quickly and irreversibly: when MKL-1 cells were treated with 100 nM YM155 for 3, 6 or 12 hours, followed by wash out with complete cell culture medium, only 51%, 3% and 1.8% of cells respectively, remained viable at 48 hours, as measured by trypan blue dye exclusion. This was confirmed by a cell viability assay using propidium iodide (PI, dead) and carboxyfluorescein diacetate (CFDA, alive) co-staining (**Figure 43C**). Twelve to 24 hours of 100 nM YM155 treatment causes MKL-1 cells to lose membrane integrity, becoming positive for PI and negative for CFDA staining.

To search for other MCC chemotherapeutics, we performed a two-stage cytotoxicity library screen on 1,360 pharmacologically-active drug compounds including 1,280 drugs from the Library of Pharmacologically Active Compounds (LOPAC) (Sigma Aldrich), 89 drugs from the National Cancer Institute's Approved oncology drug set II (19 compounds in common with LOPAC1280), 6 compounds targeting SV40 LT ATPase activity, and 4 compounds targeting MDM2 to activate p53. These compounds were screened at 10^{-5} M for >90% inhibition of MKL-1 cell growth in a Cell-Titer Glo assay (Promega). Notably, mTOR inhibitors (everolimus, rapamycin etc), antiviral compounds (ribavirin, acyclovir) and MDM-2 inhibitors active in other viral cancers (e.g.,

nutlin-3 (*396, 397*)) were not active in our screen (data not shown). This is consistent with previous findings that MCV loses replication activity (*279*) and activates cap-dependent translation downstream of mTOR in MCC tumor cells (*129*).

Eighteen (1.3%) of these 1360 drugs met our initial screening criterion for anti-MCC activity and were selected for secondary dose-dependent screening on MCV-positive and MCV-negative cell lines (**Table 8**). Only the proteasome-inhibitor bortezomib (*398*) was active in vitro at low doses with an EC_{50} of 1.3-13.2 nM; however, this activity was not selective for MCV-positive cells. Other agents, particularly topoisomerase I and II inhibitors, also inhibited MCC cell growth but were generally far less potent or had variable activity among different MCC cell lines (**Table 8**).

Table 8. EC_{50} (μM) concentrations for MCC cell lines

Drugs	MKL-1	MKL-2	MS-1	WaGa	UISO
PROTEASOME INHIBITOR					
Bortezomib	0.013	0.005	0.002	0.001	0.003
TOPOISOMERASE INHIBITORS					
Ellipticine	3.2	6.5	6.9	3.0	1.1
Amsacrine hydrochloride	0.11	3.0	7.5	0.25	2.6
Teniposide	0.010	2.8	3.0	0.026	7.3
Valrubicin	0.23	2.8	9.9	0.32	4.0
Mitoxantrone	0.006	1.3	1.6	0.014	0.97
Daunorubicin	0.015	0.086	0.15	0.018	1.4
Doxorubicin	0.21	0.022	0.37	0.022	0.25
Topotecan	0.028	0.43	0.62	0.015	0.17
OTHERS					
Iodoacetamide	0.29	0.30	0.64	0.37	2.5
Sanguinarine chloride	5.3	8.4	4.9	2.5	6.5
NSC 95397	1.2	1.5	1.8	0.73	2.8
Chelerythrine chloride	0.60	0.65	0.52	0.70	3.7
Calmidazolium chloride	2.2	1.7	2.1	2.1	2.0
Tetraethylthiuram disulfide	0.49	0.19	6.3	1.1	13
Bay 11-7085	1.4	1.7	2.7	1.2	4.5
Quinacrine dihydrochloride	5.1	4.6	4.9	5.2	7.1

B.3.4 Effect of YM155 on Human MCC Xenografts in Mice

We developed an MKL-1 xenograft model to test the *in vivo* efficacy of YM155 and bortezomib on human MCC in NOD scid gamma (NSG) mice. Subcutaneous injection of MKL-1 cells generates tumors that are positive for MCV LT and the MCC diagnostic marker CK20 (**Figure 44A**), and progress to endpoint (2 cm tumor diameter) within 2-4 weeks after tumors are first detected. We treated these mice with bortezomib, YM155 or saline for three weeks once tumors became palpable. Bortezomib was administered at levels effective on multiple myeloma xenografts (*399*) (1 mg/kg, twice-weekly subcutaneous injections). This did not significantly affect MCC tumor progression or volume compared to treatment with saline alone ($p=0.53$, log-rank test). Bortezomib administration at this level was associated with mouse lethargy and weight loss, requiring temporary use of heat blankets and Hydrogel (ClearH_2O) to prevent animal loss during initial treatment.

In contrast to bortezomib, YM155 (2 mg/kg, subcutaneous 5 times weekly) markedly delayed MKL-1 xenograft growth and significantly prolonged survival compared to either saline or bortezomib ($p<0.0001$, log-rank test, **Figures 44B-C**). This YM155 treatment regimen is the standard dosing for mouse xenograft experiments based on pharmacokinetic and treatment response studies of Nakahara et al. on six different human cancer xenografts (prostate, bladder, melanoma, breast and lung cancer) in mice and >100 human tumor cell lines (*229, 389, 400*). While 66.7-74.2% of bortezomib or saline-treated mice reached the euthanasia endpoint during the three-week treatment period, none of the YM155-treated mice reached this endpoint during treatment. Partial tumor regression occurred among some YM155-treated mice but all

tumors resumed growth once YM155 was stopped, indicating that a single 3-week treatment course was insufficient for tumor eradication (**Figure 44B**). For the majority of the mice, MKL-1 tumor volumes were unchanged or showed delayed growth during YM155 treatment, suggesting this drug may be cytostatic rather than cytocidal for MKL-1 xenografts (**Figure 44C**). YM155 was well-tolerated and no adverse effects or acute toxicities were noted. In smaller cohorts of mice bearing MS-1 (MCV-positive) and UISO (MCV-negative) cell xenografts, final tumor volumes for YM155-treated mice were 43-55% (median) of saline-treated control mice at the end of the three-week treatment period (**Figure 44D**).

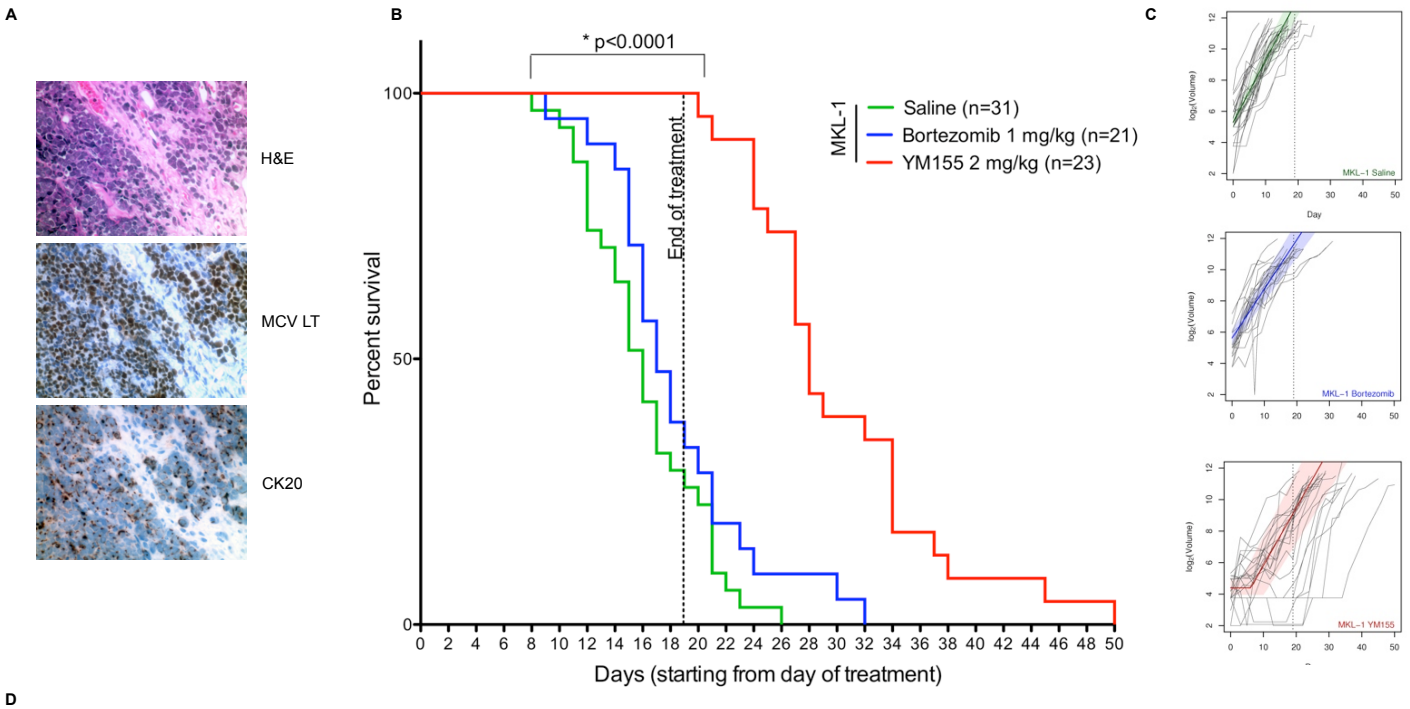

D

Cell line	Number of mice	Treatment	Day of termination			Tumor Volume day 19 (mm^3)		
			Average	Median	Range	Average	Median	Range
MS-1	5	Saline	34.6	34	26 -36	698.11	825	126-1080
	6	YM155	37	37.5	24 - 44	380.02	352	171-600
UISO	5	Saline	52.4	47	37 - 81	122.5	24.5	13.5-486
	5	YM155	53	54	41 -58	11.9	13.5	4-24.5

Figure 44. YM155 inhibits growth of MKL-1 xenografts in NSG mice
(A) MKL-1 xenograft tumors stained with hematoxylin and eosin, MCV LT (CM2B4 antibody) and CK20 (magnification 40X). (B) MKL-1 xenograft survival curves after drug treatment. Mice were subcutaneously injected with 20 million MKL-1 cells and assigned to a three-week drug treatment after tumors became palpable (see text). No significant difference was found between saline and bortezomib treatment. Tumor progression was significantly delayed by YM155, with none of the YM155-treated mice dying during treatment (up to day 19) compared to 23 of 31 (74%) saline and 14 of 21 (67%) bortezomib-treated mice. Tumor progression recurred for all YM155-treated mice once treatment was stopped. (C) Piecewise linear hierarchical Bayesian model for tumor volumes in treated mice (*391*) (see supplemental appendix for details). Colored lines show estimated central population tumor volumes with shaded regions representing 95% credible intervals. Actual tumor volumes (grey lines) for each mouse are shown for comparison. YM155 treatment retards tumor growth compared to saline or bortezomib treatment. (D) Table showing day of termination and tumor volumes for MS-1 and UISO xenograft mice treated with YM155 or saline.

B.4 DISCUSSION

We show here that discovery of a viral cause for most MCC in February 2008, followed by the description of the virus' oncogenes one year later, has now been used to rationally identify a survivin inhibitor that may have activity against this cancer. Our library screen of 1360 drugs, including the entire NCI Approved Oncology Drug Set II, confirmed that MCC is very chemoresistant and identified only one drug (bortezomib) that was highly active in vitro. Bortezomib however was not active *in vivo* against MCC xenografts. DTS, a quantitative cDNA deep sequencing method, not only identified MCV as a new human polyomavirus in MCC but also helped to uncover cell signaling pathways that are potential targets for MCV-positive MCC treatment.

Survivin, an inhibitor of apoptosis protein (IAP) family member (*401*), contributes to chemoresistance of melanoma (*402*) and is overexpressed in many cancers including MCC (*403*). It increases during non-neoplastic JC polyomavirus infection (*404*), and by SV40 LT through an E2F-regulated mechanism (*405, 406*). Our MCV T antigen knock-down and expression experiments confirm survivin to be activated by MCV LT's sequestration of RB-family transcription repressors. Survivin has pleiotropic activities in both preventing apoptosis and activating cell cycle entry (*407*). Our findings are consistent with retinoblastoma protein or other pocket proteins repressing survivin expression in primary cells (*405*), which can be relieved when MCV LT is expressed. MCV LT did not further increase survivin levels for transformed cells having the retinoblastoma protein pathway signaling blocked by mutation or E1A. MCV activation

of survivin through retinoblastoma protein targeting may typically serve to promote virus replication but is aberrantly activated during MCV-tumorigenesis (*10*).

YM155 is highly cytotoxic in vitro to MCV-positive MCC cells, causing these cells to initiate a necroptotic cell death routine. Loss of survivin is commonly linked to mitotic catastrophe in cancer cells (*408*); however, we did not find this to significantly contribute to MCC cell death. There was no distinct G1 or G2-M phase accumulation of cells during YM155 treatment and irreversible commitment to cell death occurs too quickly for most MCC cells to have an opportunity to transit the cell cycle. YM155 does increase LC3-II, implicating autophagy in YM155-induced cell death, but may reflect a consequence rather than a cause for cell death (*409*). Intriguingly, a very similar cell death phenotype occurs when T antigens are knocked down in MCV-positive MCC cells (*388*), whereas we found that knock-down of survivin alone causes apoptosis rather than necroptosis. As with YM155 treatment, this effect was predominant in an MCV-positive but not MCV-negative MCC cell line. Since knock-down of survivin causes apoptosis rather than necroptosis, we cannot exclude the possibility that YM155 targets other molecules in addition to survivin, or that different levels of survivin inhibition by YM155 and survivin knock-down result in different programmed cell death responses.

There are several important caveats to our current study. While YM155 was highly active in vitro, it was only cytostatic—not cytotoxic—in most mouse xenografts. Once YM155 treatment was stopped, tumors re-emerged in all of the treated mice. Either prolonged YM155 treatment or combined use with other drugs (e.g., bortezomib, topoisomerase inhibitors) may more effectively control MCC. YM155 was relatively nontoxic in our study, making it potentially more suitable for prolonged or combined

therapy. Practical limitations prevented us from extensively measuring YM155 activity on a variety of MCC cell line xenografts and we cannot exclude the possibility of resistance among other MCC. But it is encouraging that YM155 reduced tumor masses in two additional MCC xenografts, including one from a MCV-negative tumor. Finally, MCV sT (also expressed in MCC cells) increases cap-dependent protein translation (*129*), and could contribute to YM155 resistance through a transcription-independent mechanism of survivin induction (*410*).

DTS (*54*) is a useful method to discover (*55*) or exclude (*54*) viruses being present in human cancers. In this study, we show that DTS is also useful in measuring cellular gene expression by demonstrating that *BIRC5* transcription is activated in MCV-positive MCC. If carefully performed and rigorously analyzed, DTS data yields useful information even when no cancer viruses are discovered (*54*). Prior to discovery of MCV, few clues were available about the molecular causes for MCC (*411*). Now that MCV has been shown to be central to most MCC, rational targeting of survivin and other cellular pathways perturbed by MCV may lead to discovery of additional treatments that may be more effective and less toxic than current therapies.

APPENDIX C

RESPONSE OF MERKEL CELL POLYOMAVIRUS-POSITIVE MERKEL CELL CARCINOMA XENOGRAFTS TO YM155

The work described in Appendix C has been submitted to Cancer Research in July 2013

with authors Lindsay R. Dresang, Anna Guastafierro, Reety Arora, Daniel Normolle, Yuan Chang, and Patrick S. Moore

L.R. Dresang performed immunohistochemistry. L.R. Dresang and R. Arora performed CellTiter-Glo studies. L.R. Dresang, A. Guastafierro, and R. Arora performed mouse xenograft experiments. D. Normolle performed the statistical analyses of survival and tumor volume data. All authors interpreted the data and wrote the manuscript.

C.1 INTRODUCTION

We confirm here that YM155, a survivin suppressor, is cytotoxic to MCV-positive MCC cells *in vitro* at nanomolar levels. Mouse survival was significantly improved for NOD-Scid-Gamma mice treated with YM155 in a dose and duration dependent manner for 3 of 4 MCV-positive MCC xenografts. One MCV-positive MCC xenograft (MS-1) failed to significantly respond to YM155, which corresponds with *in vitro* dose-response activity. Combination treatment of YM155 with other chemotherapeutics resulted in additive but not synergistic cell killing of MCC cell lines *in vitro*. These results suggest that survivin targeting is a promising therapeutic approach for most but not all MCV-positive MCCs.

C.2 MATERIALS AND METHODS

C.2.1 Cell Lines and Tissue Culture

The MCC cell lines MKL-1 (*412*), MS-1 (*265*), MKL-2 (*234*), and WaGa (gift of J. Becker) (*297*) were cultured in RPMI 1640 with 10% fetal calf serum, and primary human fibroblasts, BJ (American Type Culture Collection), were cultured in Dulbecco's modified Eagle's medium with 10% fetal calf serum, as described previously (*232, 265*). All cells were maintained at 37°C in humidified air containing 5% CO_2.

C.2.2 NOD-Scid-Gamma Mice

The animals used for these studies are as described previously (*232*). NSG female mice (*413*), strain #005557 (Jackson Laboratory), were received at 6-weeks of age and maintained in a specific, pathogen-free environment at the Hillman Cancer Center Mouse Facility, University of Pittsburgh, for at least one week prior to cell line injection. All animal studies were performed with approval from the Animal Ethics Committee of the University of Pittsburgh (Institutional Animal Care and Use Committee Protocol #12020149).

C.2.3 Xenografts and Treatment

MCC xenografts were generated as previously described (Appendix B (*232*)). MCC cell lines were optimally grown at >90% cell viability as determined by trypan blue dye exclusion. MCC cells were washed with phosphate-buffered saline (PBS) and resuspended at $2x10^7$cells per 100uL in PBS and injected into the right flanks of NSG mice. Treatment regimens began as individual animals developed palpable tumors (~2mm x 2mm), as outlined in **Figure 45**. All treatments followed a five day on, two day off regimen of daily intraperitoneal (I.P.) injections. Three-week treatments ended on day 19 of I.P. injection. Continuous treatments were carried out until the animals reached the experimental endpoint. The experimental endpoint was evaluated by tumor burden, with at least one measurable diameter of 20mm, or by the presence of multiple signs of distress (respiratory rate elevation, wheezing, hypothermia, behavioral changes, inactivity, >20% weight loss, vertebral protrusion, or ruffled fur). Saline-treated mice were injected with a fixed volume of 100uL 0.9% Sodium Chloride USP Normal Saline (Nurse Assist) per injection. YM155 was administered at either 2mg/kg, 4mg/kg, or 6mg/kg, resuspended in 0.9% Sodium Chloride USP Normal Saline and filter sterilized. Tumor volumes were measured three times weekly and at the time of euthanization according to the following formula: $width^2$ x (length ÷ 2). Mouse weights were monitored at least once per week throughout the experiment. Observations, including weight measurements, were recorded daily on an individual mouse basis if signs of distress were observed.

C.2.4 Statistical Analysis of Survival and Tumor Volume Data

Mixed-effects ANOVA was used for batch-adjusted times to 50% survival per cell line and treatment group, with 95% confidence intervals. Pairwise comparisons between treatments or between cell lines were estimated (with 95% confidence intervals) by linear contrasts on the estimated ANOVA parameters . Between-batch variation was taken into account for all analyses. Tumor volumes were assessed for differential growth across treatment groups using an extension to the piecewise linear hierarchical Bayesian model that accounts for batch effects (*391*). All analyses were performed using SAS (SAS Institute), R (R Development Core Team) and JAGS software. Average tumor growth kinetics with 95% confidence intervals were estimated as described previously (*232*). Briefly, a delay in tumor growth (or re-growth) is estimated by a hinge point, called nadir, where the volume at nadir (α) is expressed as a $\log_2$(volume) and the time at nadir (ρ) is expressed in days. An initial decrease in growth is estimated as β_1, where $\log_2(\text{volume}) = \alpha+\beta_1*(\rho\text{-day})$. Final increase in tumor growth is estimated as β_2, where $\log_2(\text{volume}) = \alpha+\beta_2*(\text{day}-\rho)$. These four parameters are estimated for each animal and for each treatment and cell line.

C.2.5 Immunohistochemistry

Immunohistochemistry was performed as described previously (*57*). Tumor and/or normal mouse tissue was cut to size for optimal formalin infusion (10% neutral-buffered solution; Sigma) for at least 24hrs prior to paraffin embedding. Paraffin embedding, preparation of unstained slides, and H&E processing was performed by Research

Histology Services at the Thomas E. Starzl Transplantation Institute core facilities at the University of Pittsburgh. Unstained slides were baked at 60°C for 1hr under vacuum. Deparaffinization continued with xylene treatment (2-3 incubations, 10min). Slides were gradually rehydrated moving from 100% ethanol (2 incubations, 10min), to 95% ethanol (2 incubations, 10min), to 80% ethanol with agitation, to 70% ethanol with agitation, and finally moving to deionized water. Slides were treated with 3% hydrogen peroxide to quench endogenous peroxidases, rinsed several times with deionized water, and then placed in 1mM EDTA pH8.0 for heat-induced epitope retrieval (125°C for 3min and 15s, followed by 90°C for 15s). After 45-60min of gradual cooling, slides were briefly rinsed several times with deionized water, rinsed with TBS (68mM NaCl, 10mM Tris pH7.5), treated with Protein Block (DAKO) for 5min, and then incubated with CM2B4 (*57*) primary antibody (diluted 0.5-1.5ug/mL) for 30min (PBS pH7.4, 1% BSA, 0.1% gelatin, 0.5% Triton-X-100, 0.05% sodium azide). Slides were washed 3 times with agitation in TBS. Secondary mouse-HRP antibody (Mouse Envision Polymer; DAKO) was incubated on the slides for 30min. Slides were again washed 3 times with agitation in TBS. Colorimetric detection with 3,3-diaminobenzidine and chromagen was quenched with deionized water. Slides were counter-stained with Mayer's hemotoxylin, Lillie's modification (DAKO), rinsed several times in tap water, blued in 1% lithium carbonate, rinsed several times in tap water, and then dehydrated through 95% ethanol (twice with agitation) to 100% ethanol (twice with agitation). Slides were incubated twice in xylene for 5min and coverslips were adhered using Permount (Fisher Scientific).

C.2.6 Chemotherapeutic Compounds

YM155 was purchased from Active Biochemicals Ltd. Docetaxel, carboplatin, etoposide, topotecan HCl, and bortezomib were provided by the NCI/DTP Open Chemical Repository (http://dtp.cancer.gov).

C.2.7 Dose-Response Studies

Dose-response studies were performed as previously described (*232*). Briefly, 6000 cells were seeded per well in 384 well plates at a volume of 50uL and allowed to incubate overnight at 37°C in a 5% CO_2 humidified chamber. A log range of drug concentrations from 10^{-4} to 10^{-10} was resuspended in culture medium (with or without a fixed amount of YM155) at 3X concentration and then added at a volume of 25uL. After 48 hours further incubation in a humidified chamber, cells were treated with 25uL CellTiter-Glo Luminescent reagent (Promega) and cell viability was measured as per manufacturer's instructions. No-drug control wells served as normalization controls per cell line. Each concentration per cell line was plated in triplicate. Three or more biological replicates per cell line were tested with YM155 alone, two or more biological replicates were tested with all other single drugs, and combination studies were tested independently with either 1nM YM155 or 3nM YM155, with representative analysis at 3nM YM155 combination shown. Empty wells were used to separate different cell lines and treatment groups to reduce error from luminescent bleed-over. EC50 values were calculated from a four-parameter logistic equation fit to the surviving proportions of cells per dose.

C.3 RESULTS

C.3.1 MCV-positive MCC cell line xenograft model experimental outline

NSG mice were injected with MCV-positive MCC cell lines **(Figure 45A)** and were monitored for tumor growth, weight, and overall health. Once palpable tumors were detected **(Figure 45B)**, NSG mice were intraperitoneally (I.P.) injected (once per day for five days, followed by two days of rest) with either saline treatment, 2mg/kg YM155 treatment for three weeks, or were continuously treated with YM155 (2mg/kg or 4mg/kg) until the tumor attained a diameter of 20mm or the mouse exhibited multiple signs of distress **(Figure 45C)**.

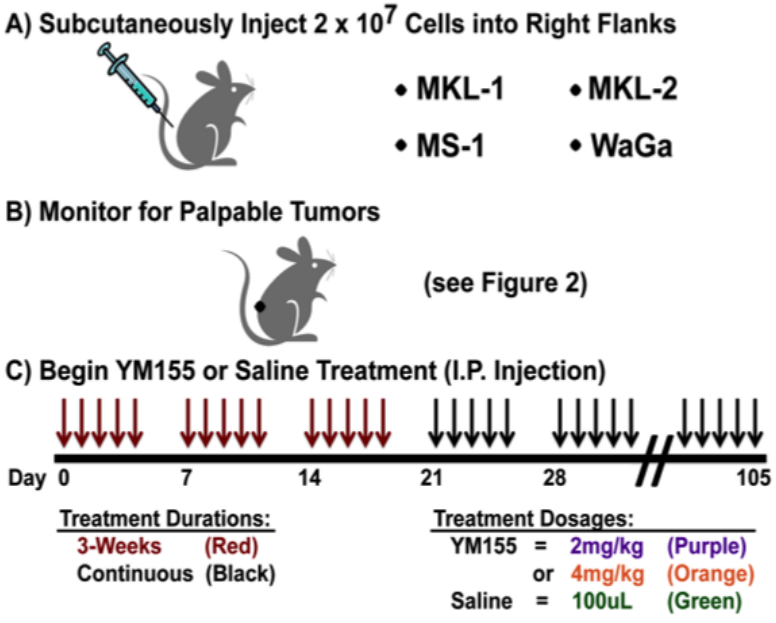

Figure 45. MCC mouse xenograft treatment groups and experimental outline
(A) NSG mice were subcutaneously injected in the right flank with $2x10^7$ MCV-positive, MCC cells (MKL-1, MS-1, WaGa, or MKL-2). (B) NSG mice were monitored for palpable tumors (~2mm x 2mm) to determine start of treatment. (C) Mice with palpable tumors were randomly assigned to either saline treatment, YM155 treatment for 3-weeks at 2mg/kg, YM155 continuous treatment at 2mg/kg, or YM155 continuous treatment at 4mg/kg. Each week of treatment consisted of a single intraperitoneal injection per day for 5 days, followed by 2 days of rest.

YM155 at 6mg/kg was tested in two mice, but both mice had >20% weight loss and additional signs of distress (ruffled fur, inactivity, and behavioral changes) within the first week of treatment and were euthanized (as per Institutional Animal Care and Use Committee protocol #12020149). Mice receiving saline treatment or YM155 treatment at 2mg/kg do not lose weight **(Figure 46A and 46B, respectively)** or show signs of distress, whereas mice receiving YM155 at 4mg/kg lose weight **(Figure 46C)** and display minimal signs of distress (only ruffled fur, normal behavior). This toxicity dissipates after the first 1-2 weeks of treatment **(Figure 46C)**. Thus, 4mg/kg YM155 is the maximum tolerated dose in NSG mice when administered by single daily I.P. injection.

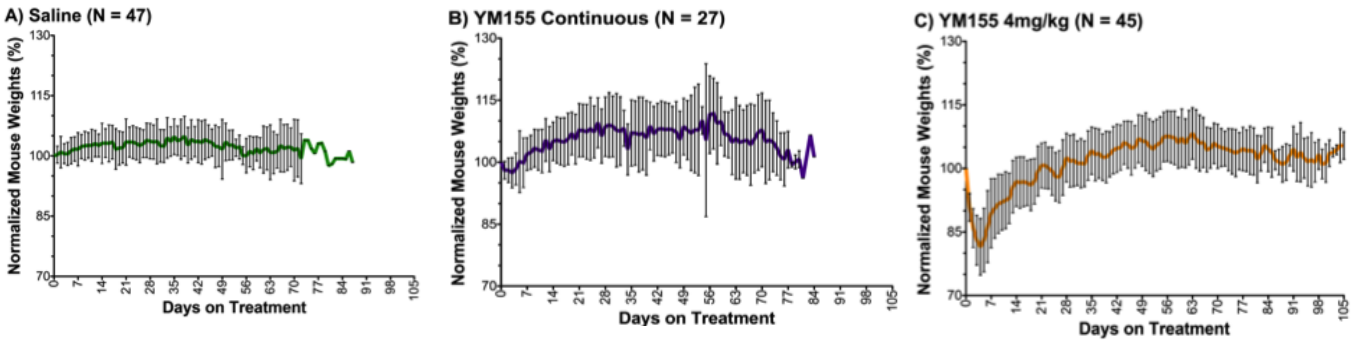

Figure 46. Mouse weights on saline and YM155 treatment groups
Average mouse weights with standard deviations are reported according to treatment regimen, where weights were normalized to day zero of treatment (100%): (A) mouse weights on saline, continuous-treatment (green line); (B) mouse weights on YM155, continuous-treatment (purple line); and (C) mouse weights on YM155 double-dose, continuous-treatment (orange line). Mouse weights were adjusted to remove the weight of tumors prior to normalization. Weights from mice with significant liver metastases were not included as metastatic-tumor weights could not be determined during the course of treatment.

C.3.2 Survival of mice with MCC xenografts is prolonged by increasing YM155 duration of treatment, as well as by increasing the dosage of YM155, in a cell line dependent manner

Estimated mean survival times with 95% confidence intervals are presented in **Figure 47A** according to treatment group and cell line. Batch variations from independent replicates per treatment group and cell line were taken into account for the reported statistical analyses. **Figure 47B** shows a Kaplan-Meier survival curve for MKL-1 xenografts treated for a single 3-week course (2mg/kg YM155) or continuously until sacrifice (data from this figure include mice treated in preliminary studies, Appendix B (*232*)). Extending the duration of YM155 treatment prolongs survival (relative to saline or 3-week treatment, $P<0.0001$; **Figure 47B**), which is prolonged further by doubling the YM155 dose to 4mg/kg (relative to all treatment arms, $P<0.0001$; **Figure 47B**). The EC50 values for YM155 *in vitro* range from 1.3nM to 12nM for different MCV-positive MCC cell lines (*232*); MKL-1 and MS-1 are at opposite ends of this range, respectively. MS-1 was tested in mice to assess the degree of response to YM155 *in vivo*. Mice were treated with either saline, 2mg/kg YM155 continuously, or 4mg/kg YM155 continuously. In contrast to MKL-1, **Figure 47C** shows that MS-1 does not significantly respond to YM155 treatment *in vivo*, despite extended duration of treatment or increased dosage. This is in contrast to two other MCV-positive MCC cell lines, WaGa and MKL-2 **(Figures 47D-E)**. Both WaGa and MKL-2 xenografts responded to YM155 (4mg/kg) relative to saline treatment ($P=0.0034$ and $P<0.0001$, respectively; **Figure 47D-E**).

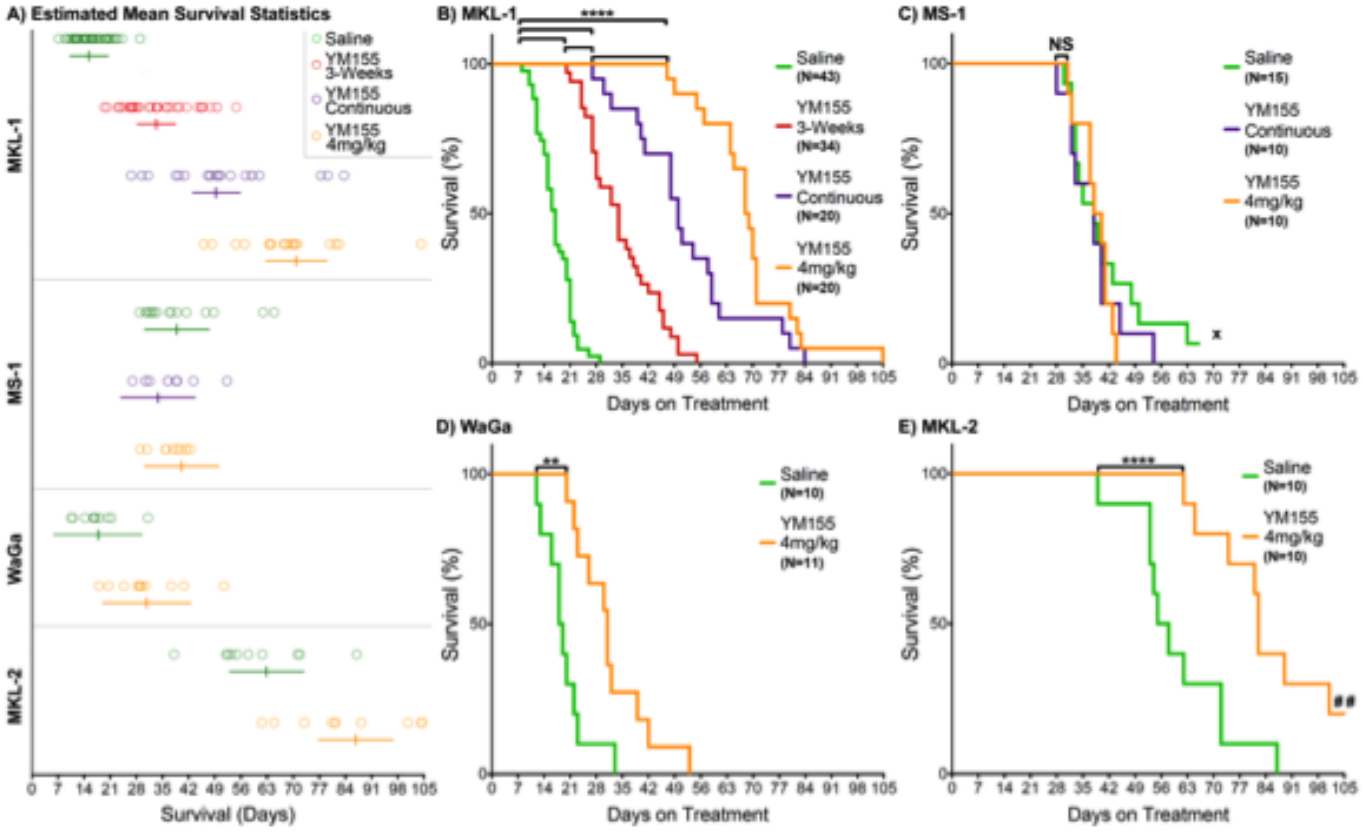

Figure 47. Survival of various MCC xenograft models on different treatments
(A) Estimated survival means and 95% confidence intervals are reported along compressed survival summaries per cell line and treatment arm, where open circles correspond survival of individual mice. (B) Mice with MKL-1 xenografts exhibit significantly prolonged survival (****P < 0.0001) on any of the three YM155 treatment groups (3-weeks at 2mg/kg = red; continuous treatment at 2mg/kg = purple; continuous treatment at 4mg/kg = orange) relative to saline treatment (green). Increasing the duration of YM155 treatment from 3-weeks to continuous treatment at the 2mg/kg dose significantly prolongs survival (****P < 0.0001). Increasing the dose of YM155 from 2mg/kg to 4mg/kg on continuous treatment significantly prolongs survival (****P < 0.0001). (C) Mice with MS-1 xenografts do not exhibit prolonged survival with YM155 continuous treatment (either at 2mg/kg or 4mg/kg) relative to saline treatment (NS = not significant). One mouse on saline treatment spontaneously regressed for over 5-weeks and was euthanized early (as indicated by x). (D) Mice with WaGa xenografts exhibit significantly prolonged survival (**P = 0.0034) with continuous YM155 treatment at 4mg/kg relative to saline treatment. (E) Mice with MKL-2 xenografts exhibit significantly prolonged survival (****P < 0.0001) with continuous YM155 treatment at 4mg/kg relative to saline treatment. Two mice did not reach the final 20mm tumor dimension by day 105 and were euthanized early (as indicated by ##).

C.3.3 Tumor shrinkage and delay of re-growth (regression), and/or slower growth rate is observed upon YM155 treatment (relative to saline) in three of four MCC xenografts

Tumor volume data analysis reveals that the delay of tumor re-growth was significant in all YM155 treatment arms of mice with MKL-1 xenografts **(Figure 48A)**, relative to saline: 2mg/kg YM155 treatment for three weeks (8.6±2.5 days); 2mg/kg continuous YM155 treatment (15.8.6±3.2 days); and 4mg/kg continuous YM155 treatment (29.9±4.0 days) **(Table 9)**. The delay in re-growth was significantly greater in the 4mg/kg arm than the 2mg/kg arm ($P<0.05$). After the initial delay, final tumor growth rate of MKL-1 xenografts in mice treated continuously with YM155 (2mg/kg or 4mg/kg) was slower than mice treated with YM155 for 3-weeks or mice treated with saline (both P-values <0.05). Final tumor growth rates in mice treated continuously at either 2mg/kg or 4mg/kg doses were comparable **(Table 9)**.

Table 9. Average tumor growth kinetics

Cell Line	Treatment	Alpha (α)	Std. Err. (α)	95% C.I. (α)	Beta-1 (β1)	Std. Err. (β1)	95% C.I. (β1)	Beta-2 (β2)	Std. Err. (β2)	95% C.I. (β2)	Rho (ρ)	Std. Err. (ρ)	95% C.I. (ρ)	>20% Reg. (*)
MKL-1	Saline	4.633	0.496	(3.530 , 5.735)	0.962	0.060	(0.832 , 1.092)	0.455	0.041	(0.363 , 0.546)	-1.294	2.413	(-6.489, 3.900)	N/A
MKL-1	YM155 3-Weeks	2.552	0.498	(1.454 , 3.650)	0.602	0.061	(0.472 , 0.732)	0.426	0.042	(0.334 , 0.517)	8.628	2.501	(3.379 , 13.878)	(8, 35)
MKL-1	YM155 Continuous	1.847	0.593	(0.599 , 3.094)	0.370	0.078	(0.209 , 0.530)	0.207	0.053	(0.095 , 0.318)	15.751	3.229	(9.092 , 22.409)	(5, 37)
MKL-1	YM155 4mg/kg	-0.474	0.735	(-1.989, 1.041)	0.168	0.098	(-0.036, 0.372)	0.208	0.067	(0.066 , 0.349)	29.889	3.977	(21.415, 38.362)	(3, 50)
MKL-2	Saline	1.929	0.957	(-0.166, 4.024)	0.781	0.119	(0.529 , 1.033)	0.176	0.081	(-0.001, 0.353)	5.940	4.815	(-4.249, 16.130)	N/A
MKL-2	YM155 4mg/kg	-0.443	0.957	(-2.538, 1.652)	0.562	0.119	(0.310 , 0.814)	0.158	0.081	(-0.019, 0.335)	12.449	4.815	(2.260 , 22.639)	(2, 51)
MS-1	Saline	1.972	0.860	(-0.006, 3.950)	0.845	0.100	(0.623 , 1.066)	0.282	0.069	(0.123 , 0.440)	2.355	3.975	(-6.333, 11.042)	N/A
MS-1	YM155 Continuous	1.822	0.957	(-0.273, 3.917)	0.695	0.119	(0.442 , 0.947)	0.308	0.081	(0.131 , 0.485)	1.965	4.815	(-8.225, 12.154)	N/A
MS-1	YM155 4mg/kg	1.544	0.957	(-0.551, 3.638)	0.861	0.119	(0.609 , 1.113)	0.278	0.081	(0.101 , 0.455)	1.040	4.815	(-9.150, 11.229)	N/A
WaGa	Saline	4.321	1.176	(1.554 , 7.088)	0.941	0.133	(0.637 , 1.245)	0.495	0.092	(0.275 , 0.714)	0.000	5.190	(-11.73, 11.731)	N/A
WaGa	YM155 4mg/kg	4.619	1.168	(1.856 , 7.382)	0.933	0.131	(0.630 , 1.235)	0.275	0.091	(0.056 , 0.495)	0.000	5.090	(-11.64, 11.645)	N/A

α = Log2 Tumor Volume at Nadir; β1 = Pre-Nadir Slope (Decreasing); β2 = Post-Nadir Slope (Increasing); ρ = Time at Nadir; Reg. = Regression; Std. Err. = Standard Error; C.I. = Confidence Interval; N/A = Not Applicable

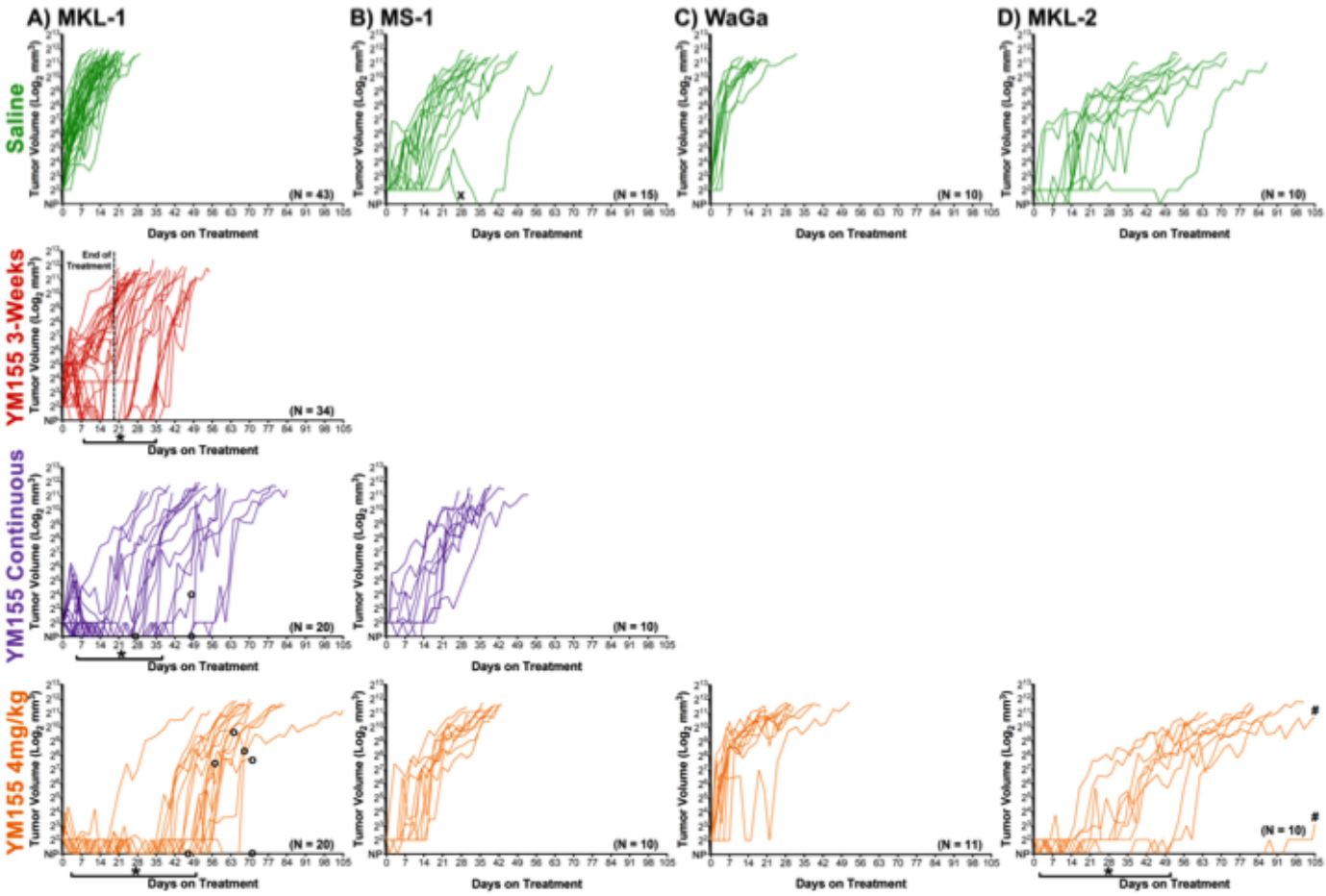

Figure 48. Tumor volume response to YM155 is dose, duration, and cell line dependent
Tumor volumes (mm^3) are reported on a Log_2 scale according to treatment group. Non-palpable (NP) tumors are indicated at baseline corresponding to tumor regression. **(A)** Tumor volumes of MKL-1 xenografts undergo an initial regression period with YM155 treatment where >20% of mice lack palpable tumors (as indicated by *****), which is extended with increased dose and duration of YM155 treatment. Overall tumor growth rate is reduced with increased YM155 duration and dosage. A total of 9 mice were euthanized before a diameter of 20mm was measured on the primary tumor due to distress associated with liver metastasis (as indicated by **o**). (**B)** Tumor volumes of MS-1 xenografts are unaffected by YM155 treatment. A spontaneous regression was observed on saline treatment (as indicated by **x**). (**C)** Tumor volumes of WaGa xenografts do not undergo an initial regression, but have a reduced growth rate. (**D)** Tumor volumes of MKL-2 xenografts undergo an initial regression period with YM155 treatment where >20% of mice lack palpable tumors (as indicated by *****). Overall tumor growth rate is reduced on YM155 treatment relative to saline treatment. Two mice did not reach the final 20mm tumor dimension by day 105 (as indicated by **#**).

There was no shrinkage in tumor volume, delay of tumor re-growth, or reduction in growth rate observed in mice with MS-1 xenografts comparing saline treatment to

YM155 treatment at either 2mg/kg or 4mg/kg **(Figure 48B and Table 8)**. WaGa xenografts in mice treated continuously with 4mg/kg YM155 grew slower than mice treated with saline (P<0.05), but there was no evidence of initial tumor shrinkage or delay of re-growth in these mice **(Figure 48C and Table 8)**. There was evidence of initial tumor shrinkage in YM155-treated mice with MKL-1 **(Figure 48A)** and MKL-2 **(Figure 48D)** xenografts (all P-values <0.05), but the absolute amount of shrinkage was small **(Table 8)**. The delay of tumor re-growth was significantly longer in mice with MKL-1 xenografts than in mice with MKL-2 xenografts (P<0.05); tumor shrinkage and delayed tumor re-growth correlate with a regression period in which >20% of mice no longer had palpable tumors **(Table 6, Figure 48A** and **D, mared by asterisks)**. However, all mice were eventually euthanized due to progressive disease. Thus, while YM155 continuous treatment at 4mg/kg prolongs survival in NSG mice with three of the four MCC xenografts, this treatment regimen does not eradicate tumor cells.

C.3.4 MCV-positive MCC xenograft mouse models develop metastases at different locations in a cell line dependent manner

MKL-1, MS-1, and WaGa cell lines are each derived from metastatic lesions (*265, 276, 412*); the site of MKL-2 derivation is unknown. Common sites of metastasis include skin, lymph nodes, liver, lung, bone, and brain (reviewed by Eng *et al*. (*414*)). Autopsy was performed on each mouse reaching experimental endpoint to assess the metastatic capability of each cell line in our mouse xenograft models. Mice with MKL-1, MS-1, or MKL-2 xenografts developed at least one or more metastases. LT-staining of primary

xenograft tumors was confirmed for at least one mouse per treatment group, per cell line (data not shown). Metastatic lesions also stained positive for LT, confirming a MCC origin **(Figures 49 and 50).**

MCC metastases occurred in the liver of 18/117 mice with MKL-1 xenografts; this subset corresponds to 27% of MKL-1-injected mice that survive past day 25. Diameters of metastatic lesions were highly variable. In 9/117 instances, liver metastasis resulted in distress requiring euthanization of mice before primary tumor diameters of 20mm were measured **(Figure 48A, marked by open circles)**. Both MKL-1 xenograft primary tumors **(Figure 49A-B)** and liver metastases **(Figure 49C-D)** contain nuclear staining for MCV-LT. Dual MKL-2 metastases occurred along the urogenital tract in 1/20 mice with separate lesion diameters of 12mm and 13mm. LT-staining in urogenital metastases was similar to staining of MKL-2 xenograft primary tumors **(50A-D)**. MKL-2-derived MCV-LT is truncated prior to the nuclear localization signal (*265*), thus staining for LT is not restricted to the nucleus as with MKL-1 or MS-1. In one instance, a MS-1 primary tumor regressed spontaneously under saline treatment for more than 5 weeks **(Figure 48B, marked by x)**, but autopsy revealed a 3mm-diameter subcutaneous metastasis on the abdomen. This metastasis was confirmed to stain for MCV-LT, similar to MS-1 xenograft primary tumors **(Figure 50E-H)**. Local invasion to surrounding tissues within the abdominal cavity, resulting in tumors of ~30mm diameter, was also observed in three MS-1 xenografts. WaGa xenograft primary tumors stain positive for LT **(Figure 50I-J)**. WaGa-derived MCV-LT is truncated within the NLS thus staining of LT is not restricted to the nucleus. WaGa-injected mice did not develop any metastases.

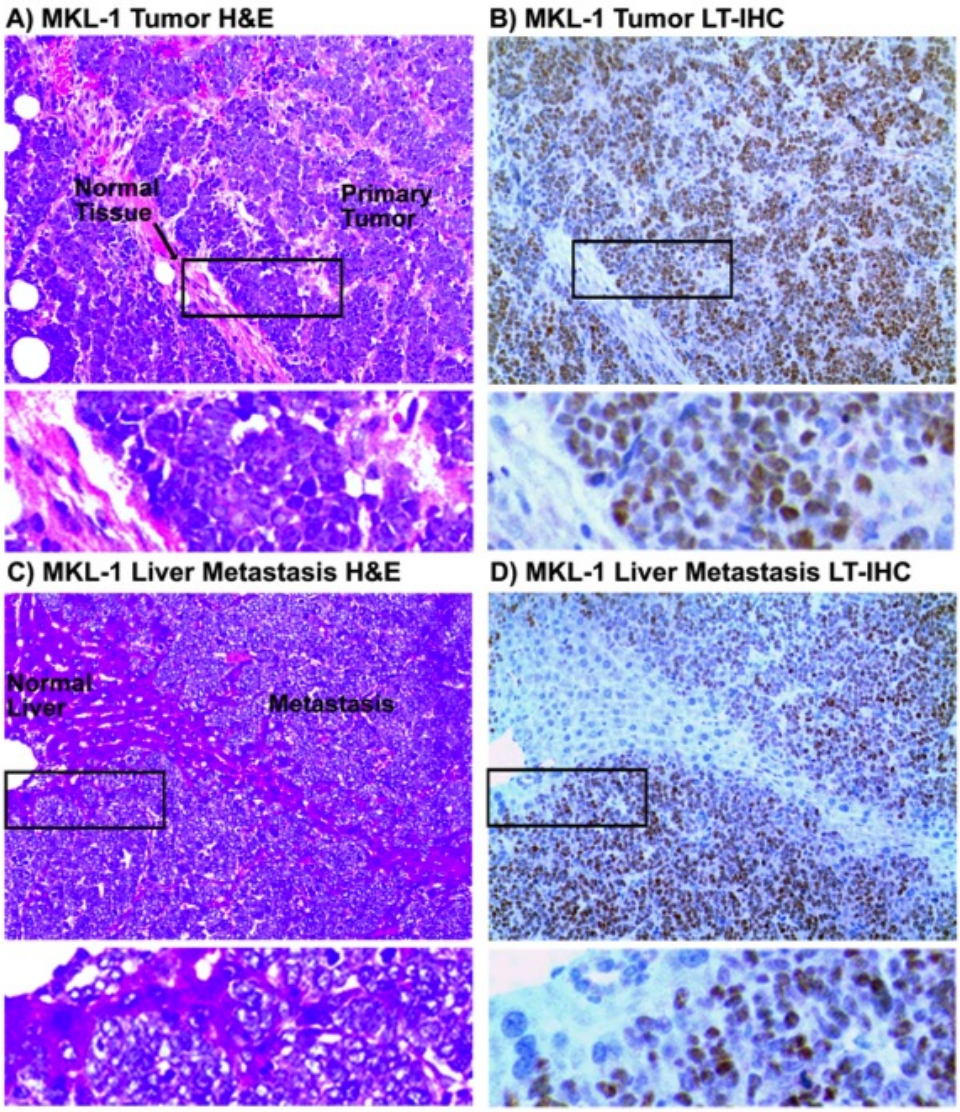

Figure 49. Immunohistochemistry of MCV LT in a MKL-1 xenograft tumor and liver metastasis

Shown are paired hemotoxylin & eosin (H&E) stained slides and adjacent sections stained with CM2B4, the MCV-LT antibody (LT-IHC), in mice with MKL-1 xenografts: (**A)** MKL-1 xenograft primary tumor, H&E; (**B)** MKL-1 xenograft primary tumor, LT-IHC; (**C)** MKL-1 xenograft liver metastasis, H&E; and (**D)** MKL-1 xenograft liver metastasis, LT-IHC. MKL-1 cells contains nuclear staining of LT, consistent with an intact nuclear localization signal (NLS). Original magnification = 200X; insets = 600X.

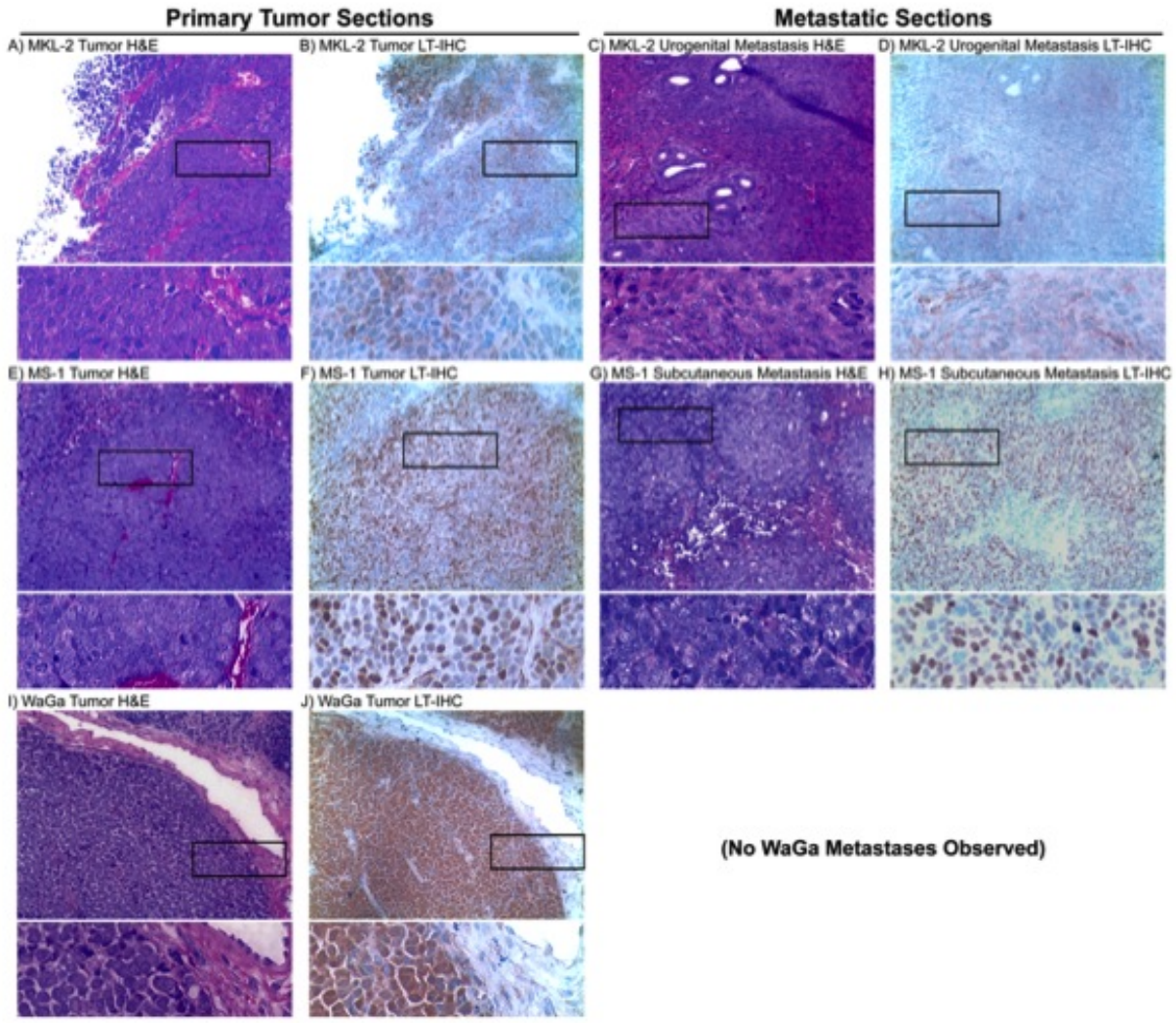

Figure 50. Immunohistochemistry of MCV LT in various MCC xenograft tumors and metastases

Shown are paired hemotoxylin & eosin (H&E) stained slides and adjacent sections stained with CM2B4, the MCV-LT antibody (LT-IHC), in mice with MCC xenografts: (**A)** MKL-2 xenograft primary tumor, H&E; (**B)** MKL-2 xenograft primary tumor, LT-IHC; (**C)** MKL-2 xenograft urogenital metastasis, H&E; (**D)** MKL-2 xenograft urogenital metastasis, LT-IHC; (**E)** MS-1 xenograft primary tumor, H&E; (**F)** MS-1 xenograft primary tumor, LT-IHC; (**G)** MS-1 xenograft subcutaneous metastasis, H&E; (**H)** MS-1 xenograft subcutaneous metastasis, LT-IHC; **I)** WaGa xenograft primary tumor, H&E; and (**J)** WaGa xenograft primary tumor, LT-IHC. MS-1 cells contain nuclear staining of LT, consistent with an intact nuclear localization signal (NLS). Both MKL-2 and WaGa lack an intact NLS, thus LT staining is not restricted to the nucleus. Original magnification = 200X; insets = 600X.

C.3.5 Combination drug treatments with YM155 act additively, but not synergistically, to reduce MCC cell line viability *in vitro*

YM155 was tested alone **(Figure 51A)** and in combination with other chemotherapeutic agents to identify a treatment strategy that may kill MCC cells synergistically. Bortezomib, docetaxel, carboplatin, etoposide, and topotecan were tested alone or in combination with a fixed concentration of YM155 **(Figure 51B-I).** Bortezomib is a proteasomal inhibitor that has been shown previously to efficiently kill MCC cells at sub-micromolar concentrations **(*232*)**. However, primary human fibroblasts, BJ, are also efficiently killed by bortezomib treatment **(Figure 51B-C)**. Docetaxel was previously tested in melanoma xenografts with YM155 to induce cancer-specific mitotic catastrophe and cell death (*415*). Docetaxel treatment does not decrease cell viability of MCC cell lines **(Figure 51D-E)**. Carboplatin, a platinum-based chemotherapeutic, also does not decrease cell viability of MCC cell lines (data not shown). Etoposide, a topoisomerase type II inhibitor, with or without carboplatin (data not shown), decreases cell viability of MCC cell lines at micromolar concentrations **(Figure 51F-G)**. Topotecan, a topoisomerase type I inhibitor, decreases cell viability at sub-micromolar concentrations **(Figure 51H-I)**. However, none of these chemotherapeutic agents decrease cell viability of MCC cells in a synergistic manner when combined with YM155—the effect is merely additive.

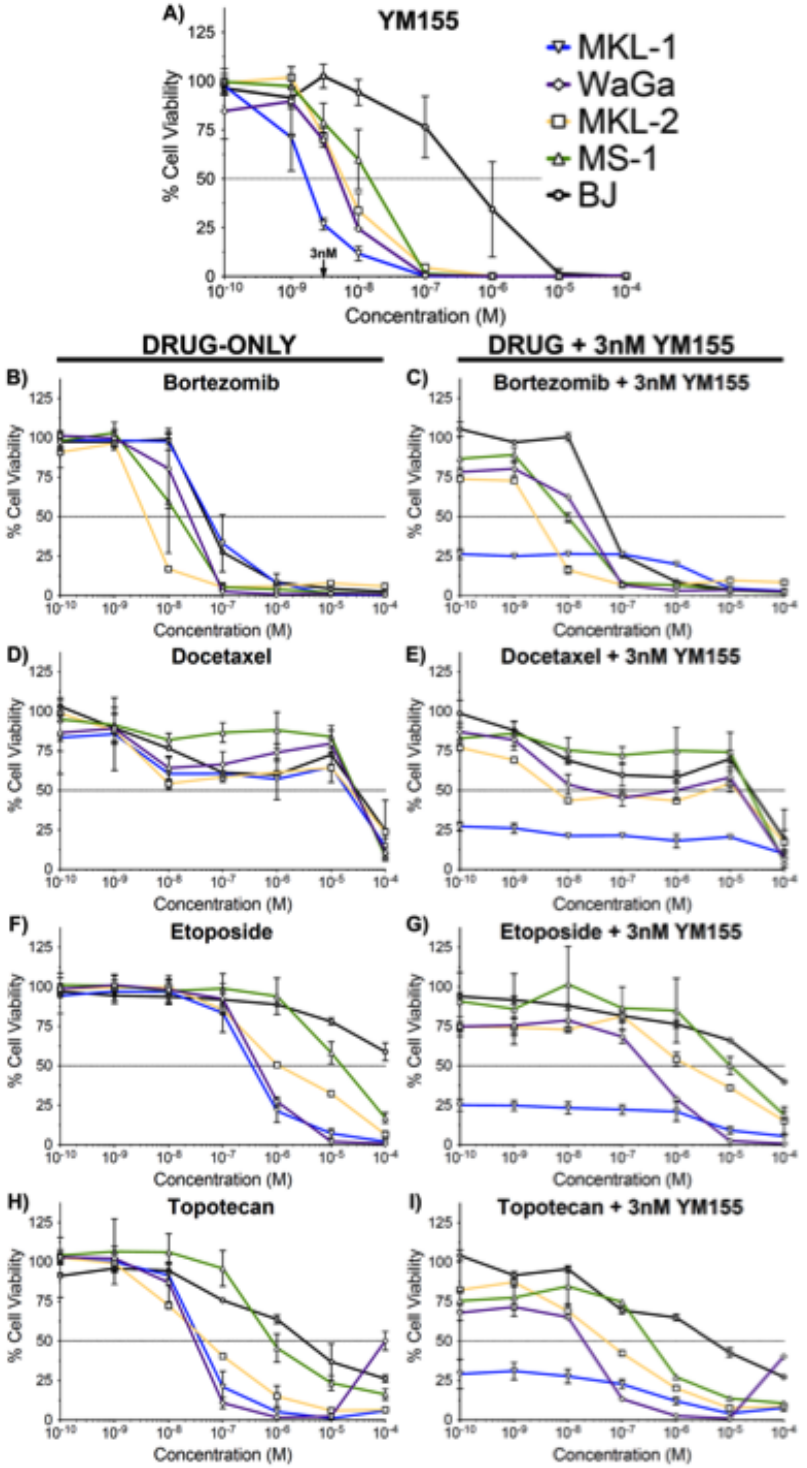

Figure 51. Various chemotherapeutics induce MCC cell death in an additive, but not synergistic manner, when combined with YM155 *in vitro*

CellTiter-GLO assays were performed using multiple MCC cell lines as well as the control primary human fibroblast, BJ. Corresponding EC50 curves are shown for the following chemotherapeutic agents and drug combinations: (**A)** YM155; (**B)** Bortezomib; (**C)** Bortezomib + 3nM YM155; (**D)** Docetaxel; (**E)** Docetaxel + 3nM YM155; (**F)** Etoposide; (**G)** Etoposide + 3nM YM155 (**H)** Topotecan; and (**I)** Topotecan + 3nM YM155.

C.4 DISCUSSION

In this study we assessed the sensitivity of four MCV-positive MCCs to YM155. Three of the four xenografts responded to YM155 treatment. YM155 efficacy is enhanced by extending the duration of treatment as well as by increasing YM155 dosage. However, the degree of YM155 efficacy is cell line dependent. Response to YM155 *in vivo* reflects YM155 response *in vitro* **(Figure 51A)**; WaGa and MKL-2 xenografts respond to YM155 treatment intermediately to MKL-1 and MS-1 when assessing *in vivo* estimated survival data between YM155 double-dose treatment and saline treatment and they also have intermediate EC50 values determined from *in vitro* cell viability data **(Figure 51A)**. MKL-1 is the most sensitive to YM155 both *in vivo* and *in vitro*, whereas MS-1 is the least sensitive to YM155 *in vitro* and does not respond to YM155 *in vivo*.

For MCC xenografts, regression, growth rate, and even metastatic escape are highly cell line dependent. Liver metastasis was only observed with MKL-1 xenografts, and metastasis was only observed after survival was significantly prolonged with YM155 treatment. While WaGa does not undergo regression or even tumor shrinkage upon YM155 treatment, survival was significantly prolonged relative to saline treatment owing to a reduced tumor growth rate. Why MCC xenografts stop responding to YM155 treatment and what determines overall response to YM155 for a given MCC cell line remains unknown.

Previous studies using MCV-positive MCC cell lines identified bortezomib as a potent *in vitro* chemotherapeutic, but not *in vivo* (*232*). Topoisomerase type I and type II

inhibitors were also shown to induce death of MCC cell lines (*232*). Although we again verified *in vitro* efficacy of bortezomib, etoposide, and topotecan, none of these agents act synergistically with YM155 treatment—the effect is only additive. However, this may not exclude the possibility that combination therapy of topoisomerase inhibitors with YM155 will prove beneficial in future studies.

YM155 administered by single daily I.P. injection has a maximum-tolerated dose of 4mg/kg. No toxicity was observed at the 2mg/kg dose **(Figure 47B)**. In the clinic YM155 is administered by continuous intravenous (I.V.) injection and is tolerated up to 8mg/kg (*416*). YM155 has previously been shown to have a 50% clearance by 12 hours from a single injection (*417*), whereas continuous injection maintains YM155 in the circulation for an extended period of time (*416*). Continuous injection also seems to alleviate the degree of toxicity observed at higher doses of YM155 (*400*). Combining these facts with the notion that YM155 was tested in our studies using severely immunocompromised mice, we are optimistic that YM155 treatment will be met with greater success in the clinic.

BIBLIOGRAPHY

1. R. T. Javier, J. S. Butel, The history of tumor virology. *Cancer Res* **68**, 7693 (Oct 1, 2008).
2. P. K. Vogt, Peyton Rous: homage and appraisal. *Faseb J* **10**, 1559 (Nov, 1996).
3. P. Rous, A Sarcoma of the Fowl Transmissible by an Agent Separable from the Tumor Cells. *J Exp Med* **13**, 397 (Apr 1, 1911).
4. L. Gross, A filterable agent, recovered from Ak leukemic extracts, causing salivary gland carcinomas in C3H mice. *Proc Soc Exp Biol Med* **83**, 414 (Jun, 1953).
5. L. Gross, Presence of leukemic agent in normal testes and ovaries of young mice of Ak line. *Acta Haematol* **10**, 18 (Jul, 1953).
6. M. A. Epstein, B. G. Achong, Y. M. Barr, Virus Particles in Cultured Lymphoblasts from Burkitt's Lymphoma. *Lancet* **1**, 702 (Mar 28, 1964).
7. Proceedings of the IARC Working Group on the Evaluation of Carcinogenic Risks to Humans. Epstein-Barr Virus and Kaposi's Sarcoma Herpesvirus/Human Herpesvirus 8. Lyon, France, 17-24 June 1997. *IARC Monogr Eval Carcinog Risks Hum* **70**, 1 (1997).
8. B. E. Griffin, Epstein-Barr virus (EBV) and human disease: facts, opinions and problems. *Mutation research* **462**, 395 (Apr, 2000).
9. G. L. Kelly, A. B. Rickinson, Burkitt lymphoma: revisiting the pathogenesis of a virus-associated malignancy. *Hematology Am Soc Hematol Educ Program*, 277 (2007).
10. W. Henle, V. Diehl, G. Kohn, H. Zur Hausen, G. Henle, Herpes-type virus and chromosome marker in normal leukocytes after growth with irradiated Burkitt cells. *Science* **157**, 1064 (Sep 1, 1967).
11. D. N. Fredericks, D. A. Relman, Sequence-based identification of microbial pathogens: a reconsideration of Koch's postulates. *Clin Microbiol Rev* **9**, 18 (Jan, 1996).
12. A. B. Hill, The Environment and Disease: Association or Causation? *Proc R Soc Med* **58**, 295 (May, 1965).
13. B. S. Blumberg, H. J. Alter, S. Visnich, A "New" Antigen in Leukemia Sera. *Jama* **191**, 541 (Feb 15, 1965).
14. B. S. Blumberg, J. S. Friedlaender, A. Woodside, A. I. Sutnick, W. T. London, Hepatitis and Australia antigen: autosomal recessive inheritance of susceptibility to infection in humans. *Proc Natl Acad Sci U S A* **62**, 1108 (Apr, 1969).
15. A. M. Prince, An antigen detected in the blood during the incubation period of serum hepatitis. *Proc Natl Acad Sci U S A* **60**, 814 (Jul, 1968).
16. B. S. Blumberg *et al.*, The relation of infection with the hepatitis B agent to primary hepatic carcinoma. *Am J Pathol* **81**, 669 (Dec, 1975).

17. E. B. Buynak *et al.*, Vaccine against human hepatitis B. 1976. *Jama* **276**, 1793 (Dec 11, 1996).
18. M. R. Hilleman, Critical overview and outlook: pathogenesis, prevention, and treatment of hepatitis and hepatocarcinoma caused by hepatitis B virus. *Vaccine* **21**, 4626 (Dec 1, 2003).
19. S. M. Feinstone, A. Z. Kapikian, R. H. Purceli, Hepatitis A: detection by immune electron microscopy of a viruslike antigen associated with acute illness. *Science* **182**, 1026 (Dec 7, 1973).
20. A. Martin, S. M. Lemon, Hepatitis A virus: from discovery to vaccines. *Hepatology* **43**, S164 (Feb, 2006).
21. C. Seeger, W. S. Mason, Hepatitis B virus biology. *Microbiol Mol Biol Rev* **64**, 51 (Mar, 2000).
22. M. Seifer, M. Hohne, S. Schaefer, W. H. Gerlich, In vitro tumorigenicity of hepatitis B virus DNA and HBx protein. *J Hepatol* **13 Suppl 4**, S61 (1991).
23. B. Bressac, M. Kew, J. Wands, M. Ozturk, Selective G to T mutations of p53 gene in hepatocellular carcinoma from southern Africa. *Nature* **350**, 429 (Apr 4, 1991).
24. I. C. Hsu *et al.*, Mutational hotspot in the p53 gene in human hepatocellular carcinomas. *Nature* **350**, 427 (Apr 4, 1991).
25. Q. L. Choo *et al.*, Isolation of a cDNA clone derived from a blood-borne non-A, non-B viral hepatitis genome. *Science* **244**, 359 (Apr 21, 1989).
26. H. M. Temin, S. Mizutani, RNA-dependent DNA polymerase in virions of Rous sarcoma virus. *Nature* **226**, 1211 (Jun 27, 1970).
27. D. Baltimore, RNA-dependent DNA polymerase in virions of RNA tumour viruses. *Nature* **226**, 1209 (Jun 27, 1970).
28. B. J. Poiesz *et al.*, Detection and isolation of type C retrovirus particles from fresh and cultured lymphocytes of a patient with cutaneous T-cell lymphoma. *Proc Natl Acad Sci U S A* **77**, 7415 (Dec, 1980).
29. M. Popovic, G. Lange-Wantzin, P. S. Sarin, D. Mann, R. C. Gallo, Transformation of human umbilical cord blood T cells by human T-cell leukemia/lymphoma virus. *Proc Natl Acad Sci U S A* **80**, 5402 (Sep, 1983).
30. M. Popovic *et al.*, Isolation and transmission of human retrovirus (human t-cell leukemia virus). *Science* **219**, 856 (Feb 18, 1983).
31. M. S. Reitz, Jr., B. J. Poiesz, F. W. Ruscetti, R. C. Gallo, Characterization and distribution of nucleic acid sequences of a novel type C retrovirus isolated from neoplastic human T lymphocytes. *Proc Natl Acad Sci U S A* **78**, 1887 (Mar, 1981).
32. M. Robert-Guroff *et al.*, Natural antibodies to human retrovirus HTLV in a cluster of Japanese patients with adult T cell leukemia. *Science* **215**, 975 (Feb 19, 1982).
33. R. C. Gallo, History of the discoveries of the first human retroviruses: HTLV-1 and HTLV-2. *Oncogene* **24**, 5926 (Sep 5, 2005).
34. Y. Hinuma *et al.*, Adult T-cell leukemia: antigen in an ATL cell line and detection of antibodies to the antigen in human sera. *Proc Natl Acad Sci U S A* **78**, 6476 (Oct, 1981).
35. M. Matsuoka, K. T. Jeang, Human T-cell leukaemia virus type 1 (HTLV-1) infectivity and cellular transformation. *Nat Rev Cancer* **7**, 270 (Apr, 2007).
36. M. Matsuoka, K. T. Jeang, Human T-cell leukemia virus type 1 (HTLV-1) and leukemic transformation: viral infectivity, Tax, HBZ and therapy. *Oncogene* **30**, 1379 (Mar 24, 2011).

37. M. Boshart *et al.*, A new type of papillomavirus DNA, its presence in genital cancer biopsies and in cell lines derived from cervical cancer. *Embo J* **3**, 1151 (May, 1984).
38. M. Durst, L. Gissmann, H. Ikenberg, H. zur Hausen, A papillomavirus DNA from a cervical carcinoma and its prevalence in cancer biopsy samples from different geographic regions. *Proc Natl Acad Sci U S A* **80**, 3812 (Jun, 1983).
39. H. zur Hausen, Papillomaviruses and cancer: from basic studies to clinical application. *Nat Rev Cancer* **2**, 342 (May, 2002).
40. A. Beby-Defaux, C. Plouzeau-Jayle, G. Agius, [Papillomaviruses under spotlight: the birth of a cancer vaccine]. *Pathol Biol (Paris)* **55**, 313 (Sep, 2007).
41. D. R. Brown *et al.*, The impact of quadrivalent human papillomavirus (HPV; types 6, 11, 16, and 18) L1 virus-like particle vaccine on infection and disease due to oncogenic nonvaccine HPV types in generally HPV-naive women aged 16-26 years. *J Infect Dis* **199**, 926 (Apr 1, 2009).
42. H. zur Hausen, Papillomaviruses causing cancer: evasion from host-cell control in early events in carcinogenesis. *J Natl Cancer Inst* **92**, 690 (May 3, 2000).
43. C. B. Woodman, S. I. Collins, L. S. Young, The natural history of cervical HPV infection: unresolved issues. *Nature reviews. Cancer* **7**, 11 (Jan, 2007).
44. L. Cancian, A. Hansen, C. Boshoff, Cellular origin of Kaposi's sarcoma and Kaposi's sarcoma-associated herpesvirus-induced cell reprogramming. *Trends in cell biology*, (May 17, 2013).
45. E. Martro *et al.*, Risk factors for human Herpesvirus 8 infection and AIDS-associated Kaposi's sarcoma among men who have sex with men in a European multicentre study. *Int J Cancer* **120**, 1129 (Mar 1, 2007).
46. Y. Chang *et al.*, Identification of herpesvirus-like DNA sequences in AIDS-associated Kaposi's sarcoma. *Science* **265**, 1865 (1994).
47. P. S. Moore, Y. Chang, KSHV: forgotten but not gone. *Blood* **117**, 6973 (Jun 30, 2011).
48. E. Cesarman, Y. Chang, P. S. Moore, J. W. Said, D. M. Knowles, Kaposi's sarcoma-associated herpesvirus-like DNA sequences in AIDS-related body-cavity-based lymphomas. *N Engl J Med* **332**, 1186 (May 4, 1995).
49. J. Soulier *et al.*, Kaposi's sarcoma-associated herpesvirus-like DNA sequences in multicentric Castleman's disease. *Blood* **86**, 1276 (Aug 15, 1995).
50. V. E. Gould, R. Moll, I. Moll, I. Lee, W. W. Franke, Neuroendocrine (Merkel) cells of the skin: hyperplasias, dysplasias, and neoplasms. *Laboratory investigation; a journal of technical methods and pathology* **52**, 334 (Apr, 1985).
51. Z. Halata, M. Grim, K. I. Bauman, Friedrich Sigmund Merkel and his "Merkel cell", morphology, development, and physiology: review and new results. *The anatomical record. Part A, Discoveries in molecular, cellular, and evolutionary biology* **271**, 225 (Mar, 2003).
52. E. A. Engels, M. Frisch, J. J. Goedert, R. J. Biggar, R. W. Miller, Merkel cell carcinoma and HIV infection. *Lancet* **359**, 497 (Feb 9, 2002).
53. J. F. Buell *et al.*, Immunosuppression and Merkel cell cancer. *Transplantation proceedings* **34**, 1780 (Aug, 2002).
54. H. Feng *et al.*, Human transcriptome subtraction by using short sequence tags to search for tumor viruses in conjunctival carcinoma. *J. Virol.* **81**, 11332 (Oct, 2007).
55. H. Feng, M. Shuda, Y. Chang, P. S. Moore, Clonal integration of a polyomavirus in human Merkel cell carcinoma. *Science* **319**, 1096 (Feb 22, 2008).

56. M. Shuda *et al.*, T antigen mutations are a human tumor-specific signature for Merkel cell polyomavirus. *Proc Natl Acad Sci U S A* **105**, 16272 (Oct 21, 2008).
57. M. Shuda *et al.*, Human Merkel cell polyomavirus infection I. MCV T antigen expression in Merkel cell carcinoma, lymphoid tissues and lymphoid tumors. *Int J Cancer* **125**, 1243 (Sep 15, 2009).
58. D. L. Poulin, J. A. DeCaprio, Is there a role for SV40 in human cancer? *J Clin Oncol* **24**, 4356 (Sep 10, 2006).
59. S. E. Stewart, B. E. Eddy, N. Borgese, Neoplasms in mice inoculated with a tumor agent carried in tissue culture. *J Natl Cancer Inst* **20**, 1223 (Jun, 1958).
60. S. E. Stewart, Neoplasms in mice inoculated with cell-free extracts or filtrates of leukemic mouse tissues. II. Leukemia in hybrid mice produced by cell-free filtrates. *J Natl Cancer Inst* **16**, 41 (Aug, 1955).
61. S. E. Stewart, Neoplasms in mice inoculated with cell-free extracts or filtrates of leukemic mouse tissues. I. Neoplasms of the parotid and adrenal glands. *J Natl Cancer Inst* **15**, 1391 (Apr, 1955).
62. B. E. Eddy, G. S. Borman, G. E. Grubbs, R. D. Young, Identification of the oncogenic substance in rhesus monkey kidney cell culture as simian virus 40. *Virology* **17**, 65 (May, 1962).
63. B. H. Sweet, M. R. Hilleman, The vacuolating virus, S.V. 40. *Proc Soc Exp Biol Med* **105**, 420 (Nov, 1960).
64. B. Kuska, SV40: working the bugs out of the polio vaccine. *J Natl Cancer Inst* **89**, 283 (Feb 19, 1997).
65. N. Shivapurkar *et al.*, Presence of simian virus 40 DNA sequences in human lymphomas. *Lancet* **359**, 851 (Mar 9, 2002).
66. M. Carbone *et al.*, SV40-like sequences in human bone tumors. *Oncogene* **13**, 527 (Aug 1, 1996).
67. D. J. Bergsagel, M. J. Finegold, J. S. Butel, W. J. Kupsky, R. L. Garcea, DNA sequences similar to those of simian virus 40 in ependymomas and choroid plexus tumors of childhood. *N Engl J Med* **326**, 988 (Apr 9, 1992).
68. M. Carbone *et al.*, Simian virus 40-like DNA sequences in human pleural mesothelioma. *Oncogene* **9**, 1781 (Jun, 1994).
69. F. Lopez-Rios, P. B. Illei, V. Rusch, M. Ladanyi, Evidence against a role for SV40 infection in human mesotheliomas and high risk of false-positive PCR results owing to presence of SV40 sequences in common laboratory plasmids. *Lancet* **364**, 1157 (Sep 25-Oct 1, 2004).
70. K. V. Shah, SV40 and human cancer: a review of recent data. *Int J Cancer* **120**, 215 (Jan 15, 2007).
71. H. D. Strickler *et al.*, Simian virus 40 and pleural mesothelioma in humans. *Cancer epidemiology, biomarkers & prevention : a publication of the American Association for Cancer Research, cosponsored by the American Society of Preventive Oncology* **5**, 473 (Jun, 1996).
72. S. de Sanjose *et al.*, Lack of serological evidence for an association between simian virus 40 and lymphoma. *Int J Cancer* **104**, 522 (Apr 20, 2003).
73. E. A. Engels *et al.*, Case-control study of simian virus 40 and non-Hodgkin lymphoma in the United States. *J Natl Cancer Inst* **96**, 1368 (Sep 15, 2004).

74. R. P. Viscidi *et al.*, Serological cross-reactivities between antibodies to simian virus 40, BK virus, and JC virus assessed by virus-like-particle-based enzyme immunoassays. *Clin Diagn Lab Immunol* **10**, 278 (Mar, 2003).
75. V. Bouvard *et al.*, Carcinogenicity of malaria and of some polyomaviruses. *The lancet oncology* **13**, 339 (Apr, 2012).
76. L. L. Emerson, H. M. Carney, L. J. Layfield, J. R. Sherbotie, Collecting duct carcinoma arising in association with BK nephropathy post-transplantation in a pediatric patient. A case report with immunohistochemical and in situ hybridization study. *Pediatric transplantation* **12**, 600 (Aug, 2008).
77. D. Geetha, B. C. Tong, L. Racusen, J. S. Markowitz, W. H. Westra, Bladder carcinoma in a transplant recipient: evidence to implicate the BK human polyomavirus as a causal transforming agent. *Transplantation* **73**, 1933 (Jun 27, 2002).
78. M. Narayanan *et al.*, BK virus associated renal cell carcinoma: case presentation with optimized PCR and other diagnostic tests. *American journal of transplantation : official journal of the American Society of Transplantation and the American Society of Transplant Surgeons* **7**, 1666 (Jun, 2007).
79. S. Loghavi, S. Bose, Polyomavirus infection and urothelial carcinoma. *Diagnostic cytopathology* **39**, 531 (Jul, 2011).
80. J. Y. Kausman, G. R. Somers, D. M. Francis, C. L. Jones, Association of renal adenocarcinoma and BK virus nephropathy post transplantation. *Pediatr Nephrol* **19**, 459 (Apr, 2004).
81. J. R. Abend, M. Jiang, M. J. Imperiale, BK virus and human cancer: innocent until proven guilty. *Seminars in cancer biology* **19**, 252 (Aug, 2009).
82. T. Dalianis, H. H. Hirsch, Human polyomaviruses in disease and cancer. *Virology* **437**, 63 (Mar 15, 2013).
83. S. D. Gardner, A. M. Field, D. V. Coleman, B. Hulme, New human papovavirus (B.K.) isolated from urine after renal transplantation. *Lancet* **1**, 1253 (Jun 19, 1971).
84. B. L. Padgett, D. L. Walker, G. M. ZuRhein, R. J. Eckroade, B. H. Dessel, Cultivation of papova-like virus from human brain with progressive multifocal leucoencephalopathy. *Lancet* **1**, 1257 (Jun 19, 1971).
85. T. Allander *et al.*, Identification of a third human polyomavirus. *J Virol* **81**, 4130 (Apr, 2007).
86. A. M. Gaynor *et al.*, Identification of a novel polyomavirus from patients with acute respiratory tract infections. *PLoS Pathog* **3**, e64 (May 4, 2007).
87. J. M. Kean, S. Rao, M. Wang, R. L. Garcea, Seroepidemiology of human polyomaviruses. *PLoS pathogens* **5**, e1000363 (Mar, 2009).
88. N. L. Nguyen, B. M. Le, D. Wang, Serologic evidence of frequent human infection with WU and KI polyomaviruses. *Emerging infectious diseases* **15**, 1199 (Aug, 2009).
89. T. Dalianis, T. Ramqvist, K. Andreasson, J. M. Kean, R. L. Garcea, KI, WU and Merkel cell polyomaviruses: a new era for human polyomavirus research. *Seminars in cancer biology* **19**, 270 (Aug, 2009).
90. R. M. Schowalter, D. V. Pastrana, K. A. Pumphrey, A. L. Moyer, C. B. Buck, Merkel cell polyomavirus and two previously unknown polyomaviruses are chronically shed from human skin. *Cell Host Microbe* **7**, 509 (Jun 25, 2010).

91. E. J. Duncavage, J. D. Pfeifer, Human polyomaviruses 6 and 7 are not detectable in Merkel cell polyomavirus-negative Merkel cell carcinoma. *Journal of cutaneous pathology* **38**, 790 (Oct, 2011).
92. E. van der Meijden *et al.*, Discovery of a new human polyomavirus associated with trichodysplasia spinulosa in an immunocompromized patient. *PLoS Pathog* **6**, e1001024 (2010).
93. M. R. Matthews, R. C. Wang, R. L. Reddick, V. A. Saldivar, J. C. Browning, Viral-associated trichodysplasia spinulosa: a case with electron microscopic and molecular detection of the trichodysplasia spinulosa-associated human polyomavirus. *Journal of cutaneous pathology* **38**, 420 (May, 2011).
94. E. van der Meijden *et al.*, Seroprevalence of trichodysplasia spinulosa-associated polyomavirus. *Emerging infectious diseases* **17**, 1355 (Aug, 2011).
95. B. H. Tan, K. J. Busam, Virus-associated Trichodysplasia spinulosa. *Advances in anatomic pathology* **18**, 450 (Nov, 2011).
96. S. Kazem *et al.*, Trichodysplasia spinulosa is characterized by active polyomavirus infection. *J Clin Virol* **53**, 225 (Mar, 2012).
97. N. Scuda *et al.*, A novel human polyomavirus closely related to the african green monkey-derived lymphotropic polyomavirus. *J Virol* **85**, 4586 (May, 2011).
98. F. Trusch *et al.*, Seroprevalence of human polyomavirus 9 and cross-reactivity to African green monkey-derived lymphotropic polyomavirus. *The Journal of general virology* **93**, 698 (Apr, 2012).
99. J. T. Nicol *et al.*, Seroprevalence and cross-reactivity of human polyomavirus 9. *Emerging infectious diseases* **18**, 1329 (Aug, 2012).
100. E. A. Siebrasse *et al.*, Identification of MW polyomavirus, a novel polyomavirus in human stool. *J Virol* **86**, 10321 (Oct, 2012).
101. C. B. Buck *et al.*, Complete genome sequence of a tenth human polyomavirus. *J Virol* **86**, 10887 (Oct, 2012).
102. G. Yu *et al.*, Discovery of a novel polyomavirus in acute diarrheal samples from children. *PLoS One* **7**, e49449 (2012).
103. E. S. Lim *et al.*, Discovery of STL polyomavirus, a polyomavirus of ancestral recombinant origin that encodes a unique T antigen by alternative splicing. *Virology* **436**, 295 (Feb 20, 2013).
104. S. Korup *et al.*, Identification of a novel human polyomavirus in organs of the gastrointestinal tract. *PLoS One* **8**, e58021 (2013).
105. T. Chen *et al.*, Serological evidence of Merkel cell polyomavirus primary infections in childhood. *J Clin Virol* **50**, 125 (Feb, 2011).
106. E. A. Siebrasse *et al.*, Human polyomaviruses in children undergoing transplantation, United States, 2008-2010. *Emerging infectious diseases* **18**, 1676 (Oct, 2012).
107. R. J. Rockett *et al.*, Detection of Novel Polyomaviruses, TSPyV, HPyV6, HPyV7, HPyV9 and MWPyV in Feces, Urine, Blood, Respiratory Swabs and Cerebrospinal Fluid. *PLoS One* **8**, e62764 (2013).
108. Y. Ito, N. Spurr, B. E. Griffin, Middle T antigen as primary inducer of full expression of the phenotype of transformation by polyoma virus. *J Virol* **35**, 219 (Jul, 1980).
109. M. I. Riley, W. Yoo, N. Y. Mda, W. R. Folk, Tiny T antigen: an autonomous polyomavirus T antigen amino-terminal domain. *J Virol* **71**, 6068 (Aug, 1997).

110. J. Zerrahn, U. Knippschild, T. Winkler, W. Deppert, Independent expression of the transforming amino-terminal domain of SV40 large I antigen from an alternatively spliced third SV40 early mRNA. *Embo J* **12**, 4739 (Dec, 1993).
111. P. W. Trowbridge, R. J. Frisque, Identification of three new JC virus proteins generated by alternative splicing of the early viral mRNA. *J Neurovirol* **1**, 195 (Jun, 1995).
112. S. Raghava, K. M. Giorda, F. B. Romano, A. P. Heuck, D. N. Hebert, SV40 Late Protein VP4 Forms Toroidal Pores To Disrupt Membranes for Viral Release. *Biochemistry* **52**, 3939 (Jun 4, 2013).
113. R. C. Liddington *et al.*, Structure of simian virus 40 at 3.8-A resolution. *Nature* **354**, 278 (Nov 28, 1991).
114. T. Stehle, Y. Yan, T. L. Benjamin, S. C. Harrison, Structure of murine polyomavirus complexed with an oligosaccharide receptor fragment. *Nature* **369**, 160 (May 12, 1994).
115. U. Neu, K. Woellner, G. Gauglitz, T. Stehle, Structural basis of GM1 ganglioside recognition by simian virus 40. *Proc Natl Acad Sci U S A* **105**, 5219 (Apr 1, 2008).
116. B. Tsai *et al.*, Gangliosides are receptors for murine polyoma virus and SV40. *Embo J* **22**, 4346 (Sep 1, 2003).
117. J. A. Low, B. Magnuson, B. Tsai, M. J. Imperiale, Identification of gangliosides GD1b and GT1b as receptors for BK virus. *J Virol* **80**, 1361 (Feb, 2006).
118. G. F. Elphick *et al.*, The human polyomavirus, JCV, uses serotonin receptors to infect cells. *Science* **306**, 1380 (Nov 19, 2004).
119. K. D. Erickson, R. L. Garcea, B. Tsai, Ganglioside GT1b is a putative host cell receptor for the Merkel cell polyomavirus. *J Virol* **83**, 10275 (Oct, 2009).
120. U. Neu *et al.*, Structures of Merkel cell polyomavirus VP1 complexes define a sialic acid binding site required for infection. *PLoS pathogens* **8**, e1002738 (2012).
121. R. M. Schowalter, D. V. Pastrana, C. B. Buck, Glycosaminoglycans and sialylated glycans sequentially facilitate Merkel cell polyomavirus infectious entry. *PLoS pathogens* **7**, e1002161 (Jul, 2011).
122. X. Z. a. X. J. Ellen Fanning, in *DNA Tumor Viruses*. (Springer Science, 2009).
123. S. Eash, K. Manley, M. Gasparovic, W. Querbes, W. J. Atwood, The human polyomaviruses. *Cell Mol Life Sci* **63**, 865 (Apr, 2006).
124. E. Fanning, K. Zhao, SV40 DNA replication: from the A gene to a nanomachine. *Virology* **384**, 352 (Feb 20, 2009).
125. P. Taneja *et al.*, Timed interactions between viral and cellular replication factors during the initiation of SV40 in vitro DNA replication. *Biochem J* **407**, 313 (Oct 15, 2007).
126. C. Schneider, K. Weisshart, L. A. Guarino, I. Dornreiter, E. Fanning, Species-specific functional interactions of DNA polymerase alpha-primase with simian virus 40 (SV40) T antigen require SV40 origin DNA. *Mol Cell Biol* **14**, 3176 (May, 1994).
127. D. Ahuja, M. T. Saenz-Robles, J. M. Pipas, SV40 large T antigen targets multiple cellular pathways to elicit cellular transformation. *Oncogene* **24**, 7729 (Nov 21, 2005).
128. Y. Gluzman, B. Ahrens, SV40 early mutants that are defective for viral DNA synthesis but competent for transformation of cultured rat and simian cells. *Virology* **123**, 78 (Nov, 1982).
129. M. Shuda, H. J. Kwun, H. Feng, Y. Chang, P. S. Moore, Human Merkel cell polyomavirus small T antigen is an oncoprotein targeting the 4E-BP1 translation regulator. *J Clin Invest* **121**, 3623 (Sep, 2011).

130. L. Raptis, H. Lamfrom, T. L. Benjamin, Regulation of cellular phenotype and expression of polyomavirus middle T antigen in rat fibroblasts. *Mol Cell Biol* **5**, 2476 (Sep, 1985).
131. S. H. Ali, J. A. DeCaprio, Cellular transformation by SV40 large T antigen: interaction with host proteins. *Semin Cancer Biol* **11**, 15 (Feb, 2001).
132. J. M. Pipas, Common and unique features of T antigens encoded by the polyomavirus group. *J Virol* **66**, 3979 (Jul, 1992).
133. J. S. Butel, J. A. Lednicky, Cell and molecular biology of simian virus 40: implications for human infections and disease. *J Natl Cancer Inst* **91**, 119 (Jan 20, 1999).
134. L. V. Crawford *et al.*, Characterization of the complex between SV40 large T antigen and the 53K host protein in transformed mouse cells. *Cold Spring Harb Symp Quant Biol* **44 Pt 1**, 179 (1980).
135. D. P. Lane, L. V. Crawford, T antigen is bound to a host protein in SV40-transformed cells. *Nature* **278**, 261 (Mar 15, 1979).
136. C. S. Sullivan, J. M. Pipas, T antigens of simian virus 40: molecular chaperones for viral replication and tumorigenesis. *Microbiol Mol Biol Rev* **66**, 179 (Jun, 2002).
137. D. Ahuja, A. V. Rathi, A. E. Greer, X. S. Chen, J. M. Pipas, A structure-guided mutational analysis of simian virus 40 large T antigen: identification of surface residues required for viral replication and transformation. *J Virol* **83**, 8781 (Sep, 2009).
138. S. H. Ali, J. S. Kasper, T. Arai, J. A. DeCaprio, Cul7/p185/p193 binding to simian virus 40 large T antigen has a role in cellular transformation. *J Virol* **78**, 2749 (Mar, 2004).
139. M. Cotsiki *et al.*, Simian virus 40 large T antigen targets the spindle assembly checkpoint protein Bub1. *Proc Natl Acad Sci U S A* **101**, 947 (Jan 27, 2004).
140. Z. L. Fei, C. D'Ambrosio, S. Li, E. Surmacz, R. Baserga, Association of insulin receptor substrate 1 with simian virus 40 large T antigen. *Mol Cell Biol* **15**, 4232 (Aug, 1995).
141. A. Srinivasan *et al.*, The amino-terminal transforming region of simian virus 40 large T and small t antigens functions as a J domain. *Mol Cell Biol* **17**, 4761 (Aug, 1997).
142. H. Stubdal *et al.*, Inactivation of pRB-related proteins p130 and p107 mediated by the J domain of simian virus 40 large T antigen. *Mol Cell Biol* **17**, 4979 (Sep, 1997).
143. P. Yaciuk, M. C. Carter, J. M. Pipas, E. Moran, Simian virus 40 large-T antigen expresses a biological activity complementary to the p300-associated transforming function of the adenovirus E1A gene products. *Mol Cell Biol* **11**, 2116 (Apr, 1991).
144. N. L. Lill, M. J. Tevethia, R. Eckner, D. M. Livingston, N. Modjtahedi, p300 family members associate with the carboxyl terminus of simian virus 40 large tumor antigen. *J Virol* **71**, 129 (Jan, 1997).
145. J. A. DeCaprio *et al.*, SV40 large tumor antigen forms a specific complex with the product of the retinoblastoma susceptibility gene. *Cell* **54**, 275 (Jul 15, 1988).
146. A. M. Helt, D. A. Galloway, Mechanisms by which DNA tumor virus oncoproteins target the Rb family of pocket proteins. *Carcinogenesis* **24**, 159 (Feb, 2003).
147. L. Marcos-Villar *et al.*, Kaposi's sarcoma-associated herpesvirus lana2 protein interacts with the pocket proteins and inhibits their sumoylation. *Oncogene*, (Jan 14, 2013).
148. L. Litovchick, L. A. Florens, S. K. Swanson, M. P. Washburn, J. A. DeCaprio, DYRK1A protein kinase promotes quiescence and senescence through DREAM complex assembly. *Genes & development* **25**, 801 (Apr 15, 2011).
149. P. Stiegler, A. De Luca, L. Bagella, A. Giordano, The COOH-terminal region of pRb2/p130 binds to histone deacetylase 1 (HDAC1), enhancing transcriptional repression of the E2F-dependent cyclin A promoter. *Cancer Res* **58**, 5049 (Nov 15, 1998).

150. P. An, M. T. Saenz Robles, J. M. Pipas, Large T antigens of polyomaviruses: amazing molecular machines. *Annual review of microbiology* **66**, 213 (2012).
151. J. Y. Lin, J. A. DeCaprio, SV40 large T antigen promotes dephosphorylation of p130. *J Biol Chem* **278**, 46482 (Nov 21, 2003).
152. C. S. Sullivan, P. Cantalupo, J. M. Pipas, The molecular chaperone activity of simian virus 40 large T antigen is required to disrupt Rb-E2F family complexes by an ATP-dependent mechanism. *Mol Cell Biol* **20**, 6233 (Sep, 2000).
153. A. V. Rathi, M. T. Saenz Robles, P. G. Cantalupo, R. H. Whitehead, J. M. Pipas, Simian virus 40 T-antigen-mediated gene regulation in enterocytes is controlled primarily by the Rb-E2F pathway. *J Virol* **83**, 9521 (Sep, 2009).
154. S. Y. Fuchs, V. Adler, T. Buschmann, X. Wu, Z. Ronai, Mdm2 association with p53 targets its ubiquitination. *Oncogene* **17**, 2543 (Nov 12, 1998).
155. C. A. Brady *et al.*, Distinct p53 transcriptional programs dictate acute DNA-damage responses and tumor suppression. *Cell* **145**, 571 (May 13, 2011).
156. H. M. Sheppard, S. I. Corneillie, C. Espiritu, A. Gatti, X. Liu, New insights into the mechanism of inhibition of p53 by simian virus 40 large T antigen. *Mol Cell Biol* **19**, 2746 (Apr, 1999).
157. M. Scheffner, B. A. Werness, J. M. Huibregtse, A. J. Levine, P. M. Howley, The E6 oncoprotein encoded by human papillomavirus types 16 and 18 promotes the degradation of p53. *Cell* **63**, 1129 (1990).
158. P. R. Yew, A. J. Berk, Inhibition of p53 transactivation required for transformation by adenovirus early 1B protein. *Nature* **357**, 82 (May 7, 1992).
159. F. Tiemann, W. Deppert, Stabilization of the tumor suppressor p53 during cellular transformation by simian virus 40: influence of viral and cellular factors and biological consequences. *J Virol* **68**, 2869 (May, 1994).
160. D. I. Linzer, A. J. Levine, Characterization of a 54K dalton cellular SV40 tumor antigen present in SV40-transformed cells and uninfected embryonal carcinoma cells. *Cell* **17**, 43 (1979).
161. R. Zhao *et al.*, The transcriptional program following p53 activation. *Cold Spring Harb Symp Quant Biol* **65**, 475 (2000).
162. A. Hermannstadter, C. Ziegler, M. Kuhl, W. Deppert, G. V. Tolstonog, Wild-type p53 enhances efficiency of simian virus 40 large-T-antigen-induced cellular transformation. *J Virol* **83**, 10106 (Oct, 2009).
163. M. Herzig, M. Novatchkova, G. Christofori, An unexpected role for p53 in augmenting SV40 large T antigen-mediated tumorigenesis. *Biological chemistry* **380**, 203 (Feb, 1999).
164. D. R. Borger, J. A. DeCaprio, Targeting of p300/CREB binding protein coactivators by simian virus 40 is mediated through p53. *J Virol* **80**, 4292 (May, 2006).
165. K. S. Campbell *et al.*, DnaJ/hsp40 chaperone domain of SV40 large T antigen promotes efficient viral DNA replication. *Genes & development* **11**, 1098 (May 1, 1997).
166. A. J. Berk, Recent lessons in gene expression, cell cycle control, and cell biology from adenovirus. *Oncogene* **24**, 7673 (Nov 21, 2005).
167. N. G. Iyer, H. Ozdag, C. Caldas, p300/CBP and cancer. *Oncogene* **23**, 4225 (May 24, 2004).
168. R. Eckner *et al.*, Association of p300 and CBP with simian virus 40 large T antigen. *Mol Cell Biol* **16**, 3454 (Jul, 1996).

169. D. L. Poulin, A. L. Kung, J. A. DeCaprio, p53 targets simian virus 40 large T antigen for acetylation by CBP. *J Virol* **78**, 8245 (Aug, 2004).
170. G. A. Horwitz *et al.*, Adenovirus small e1a alters global patterns of histone modification. *Science* **321**, 1084 (Aug 22, 2008).
171. R. Ferrari *et al.*, Epigenetic reprogramming by adenovirus e1a. *Science* **321**, 1086 (Aug 22, 2008).
172. G. Chinnadurai, Opposing oncogenic activities of small DNA tumor virus transforming proteins. *Trends Microbiol* **19**, 174 (Apr, 2011).
173. A. Sarikas, X. Xu, L. J. Field, Z. Q. Pan, The cullin7 E3 ubiquitin ligase: a novel player in growth control. *Cell Cycle* **7**, 3154 (Oct, 2008).
174. J. S. Kasper, H. Kuwabara, T. Arai, S. H. Ali, J. A. DeCaprio, Simian virus 40 large T antigen's association with the CUL7 SCF complex contributes to cellular transformation. *J Virol* **79**, 11685 (Sep, 2005).
175. H. Okabe *et al.*, A critical role for FBXW8 and MAPK in cyclin D1 degradation and cancer cell proliferation. *PLoS One* **1**, e128 (2006).
176. X. Xu *et al.*, The CUL7 E3 ubiquitin ligase targets insulin receptor substrate 1 for ubiquitin-dependent degradation. *Mol Cell* **30**, 403 (May 23, 2008).
177. P. Meraldi, P. K. Sorger, A dual role for Bub1 in the spindle checkpoint and chromosome congression. *Embo J* **24**, 1621 (Apr 20, 2005).
178. S. Boichuk, L. Hu, J. Hein, O. V. Gjoerup, Multiple DNA damage signaling and repair pathways deregulated by simian virus 40 large T antigen. *J Virol* **84**, 8007 (Aug, 2010).
179. O. V. Gjoerup *et al.*, Surveillance mechanism linking Bub1 loss to the p53 pathway. *Proc Natl Acad Sci U S A* **104**, 8334 (May 15, 2007).
180. T. DeAngelis, J. Chen, A. Wu, M. Prisco, R. Baserga, Transformation by the simian virus 40 T antigen is regulated by IGF-I receptor and IRS-1 signaling. *Oncogene* **25**, 32 (Jan 5, 2006).
181. Y. Yu, J. C. Alwine, Interaction between simian virus 40 large T antigen and insulin receptor substrate 1 is disrupted by the K1 mutation, resulting in the loss of large T antigen-mediated phosphorylation of Akt. *J Virol* **82**, 4521 (May, 2008).
182. M. Prisco *et al.*, Nuclear translocation of insulin receptor substrate-1 by the simian virus 40 T antigen and the activated type 1 insulin-like growth factor receptor. *J Biol Chem* **277**, 32078 (Aug 30, 2002).
183. A. Lassak *et al.*, Insulin receptor substrate 1 translocation to the nucleus by the human JC virus T-antigen. *J Biol Chem* **277**, 17231 (May 10, 2002).
184. J. H. Lee, T. T. Paull, ATM activation by DNA double-strand breaks through the Mre11-Rad50-Nbs1 complex. *Science* **308**, 551 (Apr 22, 2005).
185. X. Wu *et al.*, SV40 T antigen interacts with Nbs1 to disrupt DNA replication control. *Genes Dev* **18**, 1305 (Jun 1, 2004).
186. D. M. Koepp *et al.*, Phosphorylation-dependent ubiquitination of cyclin E by the SCFFbw7 ubiquitin ligase. *Science* **294**, 173 (Oct 5, 2001).
187. M. Welcker *et al.*, The Fbw7 tumor suppressor regulates glycogen synthase kinase 3 phosphorylation-dependent c-Myc protein degradation. *Proc Natl Acad Sci U S A* **101**, 9085 (Jun 15, 2004).
188. A. S. Nateri, L. Riera-Sans, C. Da Costa, A. Behrens, The ubiquitin ligase SCFFbw7 antagonizes apoptotic JNK signaling. *Science* **303**, 1374 (Feb 27, 2004).

189. G. Wu *et al.*, SEL-10 is an inhibitor of notch signaling that targets notch for ubiquitin-mediated protein degradation. *Mol Cell Biol* **21**, 7403 (Nov, 2001).
190. M. Welcker, B. E. Clurman, The SV40 large T antigen contains a decoy phosphodegron that mediates its interactions with Fbw7/hCdc4. *J Biol Chem* **280**, 7654 (Mar 4, 2005).
191. B. Turk, A. Porras, M. C. Mumby, K. Rundell, Simian virus 40 small-t antigen binds two zinc ions. *J Virol* **67**, 3671 (Jun, 1993).
192. M. J. Sleigh, W. C. Topp, R. Hanich, J. F. Sambrook, Mutants of SV40 with an altered small t protein are reduced in their ability to transform cells. *Cell* **14**, 79 (May, 1978).
193. S. Mungre *et al.*, Mutations which affect the inhibition of protein phosphatase 2A by simian virus 40 small-t antigen in vitro decrease viral transformation. *J Virol* **68**, 1675 (Mar, 1994).
194. W. C. Hahn *et al.*, Enumeration of the simian virus 40 early region elements necessary for human cell transformation. *Mol Cell Biol* **22**, 2111 (Apr, 2002).
195. A. A. Sablina, W. C. Hahn, SV40 small T antigen and PP2A phosphatase in cell transformation. *Cancer Metastasis Rev* **27**, 137 (Jun, 2008).
196. E. Sontag, Protein phosphatase 2A: the Trojan Horse of cellular signaling. *Cell Signal* **13**, 7 (Jan, 2001).
197. D. C. Pallas *et al.*, Polyoma small and middle T antigens and SV40 small t antigen form stable complexes with protein phosphatase 2A. *Cell* **60**, 167 (Jan 12, 1990).
198. Y. Chen *et al.*, Structural and biochemical insights into the regulation of protein phosphatase 2A by small t antigen of SV40. *Nature structural & molecular biology* **14**, 527 (Jun, 2007).
199. O. Gjoerup, Y. Chang, Update on human polyomaviruses and cancer. *Advances in cancer research* **106**, 1 (2010).
200. E. Yeh *et al.*, A signalling pathway controlling c-Myc degradation that impacts oncogenic transformation of human cells. *Nature cell biology* **6**, 308 (Apr, 2004).
201. J. J. Zhao *et al.*, Human mammary epithelial cell transformation through the activation of phosphatidylinositol 3-kinase. *Cancer cell* **3**, 483 (May, 2003).
202. P. Rodriguez-Viciana, C. Collins, M. Fried, Polyoma and SV40 proteins differentially regulate PP2A to activate distinct cellular signaling pathways involved in growth control. *Proc Natl Acad Sci U S A* **103**, 19290 (Dec 19, 2006).
203. E. Sontag *et al.*, The interaction of SV40 small tumor antigen with protein phosphatase 2A stimulates the map kinase pathway and induces cell proliferation. *Cell* **75**, 887 (Dec 3, 1993).
204. E. Sontag, J. M. Sontag, A. Garcia, Protein phosphatase 2A is a critical regulator of protein kinase C zeta signaling targeted by SV40 small t to promote cell growth and NF-kappaB activation. *Embo J* **16**, 5662 (Sep 15, 1997).
205. M. T. Saenz Robles, J. M. Pipas, T antigen transgenic mouse models. *Seminars in cancer biology* **19**, 229 (Aug, 2009).
206. R. L. Brinster *et al.*, Transgenic mice harboring SV40 T-antigen genes develop characteristic brain tumors. *Cell* **37**, 367 (Jun, 1984).
207. M. T. Saenz Robles, H. Symonds, J. Chen, T. Van Dyke, Induction versus progression of brain tumor development: differential functions for the pRB- and p53-targeting domains of simian virus 40 T antigen. *Mol Cell Biol* **14**, 2686 (Apr, 1994).

208. H. S. Symonds, S. A. McCarthy, J. Chen, J. M. Pipas, T. Van Dyke, Use of transgenic mice reveals cell-specific transformation by a simian virus 40 T-antigen amino-terminal mutant. *Mol Cell Biol* **13**, 3255 (Jun, 1993).
209. S. A. McCarthy, H. S. Symonds, T. Van Dyke, Regulation of apoptosis in transgenic mice by simian virus 40 T antigen-mediated inactivation of p53. *Proc Natl Acad Sci U S A* **91**, 3979 (Apr 26, 1994).
210. H. Symonds *et al.*, p53-dependent apoptosis in vivo: impact of p53 inactivation on tumorigenesis. *Cold Spring Harb Symp Quant Biol* **59**, 247 (1994).
211. K. Simin *et al.*, pRb inactivation in mammary cells reveals common mechanisms for tumor initiation and progression in divergent epithelia. *PLoS biology* **2**, E22 (Feb, 2004).
212. S. H. Kim, K. A. Roth, C. M. Coopersmith, J. M. Pipas, J. I. Gordon, Expression of wild-type and mutant simian virus 40 large tumor antigens in villus-associated enterocytes of transgenic mice. *Proc Natl Acad Sci U S A* **91**, 6914 (Jul 19, 1994).
213. J. A. Markovics *et al.*, Intestinal dysplasia induced by simian virus 40 T antigen is independent of p53. *J Virol* **79**, 7492 (Jun, 2005).
214. A. V. Rathi, M. T. Saenz Robles, J. M. Pipas, Enterocyte proliferation and intestinal hyperplasia induced by simian virus 40 T antigen require a functional J domain. *J Virol* **81**, 9481 (Sep, 2007).
215. A. Xiao, H. Wu, P. P. Pandolfi, D. N. Louis, T. Van Dyke, Astrocyte inactivation of the pRb pathway predisposes mice to malignant astrocytoma development that is accelerated by PTEN mutation. *Cancer cell* **1**, 157 (Mar, 2002).
216. R. Hill, Y. Song, R. D. Cardiff, T. Van Dyke, Heterogeneous tumor evolution initiated by loss of pRb function in a preclinical prostate cancer model. *Cancer Res* **65**, 10243 (Nov 15, 2005).
217. M. Bennoun *et al.*, The amino-terminal region of SV40 large T antigen is sufficient to induce hepatic tumours in mice. *Oncogene* **17**, 1253 (Sep 10, 1998).
218. S. M. Maricich *et al.*, Merkel cells are essential for light-touch responses. *Science* **324**, 1580 (Jun 19, 2009).
219. M. E. Spurgeon, P. F. Lambert, Merkel cell polyomavirus: a newly discovered human virus with oncogenic potential. *Virology* **435**, 118 (Jan 5, 2013).
220. A. Van Keymeulen *et al.*, Epidermal progenitors give rise to Merkel cells during embryonic development and adult homeostasis. *The Journal of cell biology* **187**, 91 (Oct 5, 2009).
221. N. J. Ball, G. Tanhuanco-Kho, Merkel cell carcinoma frequently shows histologic features of basal cell carcinoma: a study of 30 cases. *J Cutan Pathol* **34**, 612 (Aug, 2007).
222. M. Bobos, P. Hytiroglou, I. Kostopoulos, G. Karkavelas, C. S. Papadimitriou, Immunohistochemical distinction between merkel cell carcinoma and small cell carcinoma of the lung. *Am J Dermatopathol* **28**, 99 (Apr, 2006).
223. V. Koljonen, Merkel cell carcinoma. *World journal of surgical oncology* **4**, 7 (2006).
224. R. W. Miller, C. S. Rabkin, Merkel cell carcinoma and melanoma: etiological similarities and differences. *Cancer epidemiology, biomarkers & prevention : a publication of the American Association for Cancer Research, cosponsored by the American Society of Preventive Oncology* **8**, 153 (Feb, 1999).
225. M. P. Pulitzer, B. D. Amin, K. J. Busam, Merkel cell carcinoma: review. *Advances in anatomic pathology* **16**, 135 (May, 2009).

226. B. Lemos, P. Nghiem, Merkel cell carcinoma: more deaths but still no pathway to blame. *J Invest Dermatol* **127**, 2100 (Sep, 2007).
227. P. J. Allen *et al.*, Merkel cell carcinoma: prognosis and treatment of patients from a single institution. *Journal of clinical oncology : official journal of the American Society of Clinical Oncology* **23**, 2300 (Apr 1, 2005).
228. A. A. Sarnaik, M. H. Lien, P. Nghiem, C. K. Bichakjian, Clinical recognition, diagnosis, and staging of merkel cell carcinoma, and the role of the multidisciplinary management team. *Current problems in cancer* **34**, 38 (Jan-Feb, 2010).
229. B. D. Lemos *et al.*, Pathologic nodal evaluation improves prognostic accuracy in Merkel cell carcinoma: analysis of 5823 cases as the basis of the first consensus staging system. *Journal of the American Academy of Dermatology* **63**, 751 (Nov, 2010).
230. D. Mercer, P. Brander, K. Liddell, Merkel cell carcinoma: the clinical course. *Annals of plastic surgery* **25**, 136 (Aug, 1990).
231. C. K. Bichakjian *et al.*, Merkel cell carcinoma: critical review with guidelines for multidisciplinary management. *Cancer* **110**, 1 (Jul 1, 2007).
232. R. Arora *et al.*, Survivin is a therapeutic target in Merkel cell carcinoma. *Science translational medicine* **4**, 133ra56 (May 9, 2012).
233. J. H. Leonard, P. Leonard, J. H. Kearsley, Chromosomes 1, 11, and 13 are frequently involved in karyotypic abnormalities in metastatic Merkel cell carcinoma. *Cancer Genet Cytogenet* **67**, 65 (May, 1993).
234. M. Van Gele *et al.*, Combined karyotyping, CGH and M-FISH analysis allows detailed characterization of unidentified chromosomal rearrangements in Merkel cell carcinoma. *Int J Cancer* **101**, 137 (Sep 10, 2002).
235. K. G. Paulson *et al.*, Array-CGH reveals recurrent genomic changes in Merkel cell carcinoma including amplification of L-Myc. *J Invest Dermatol* **129**, 1547 (Jun, 2009).
236. A. Ziegler *et al.*, Mutation hotspots due to sunlight in the p53 gene of nonmelanoma skin cancers. *Proc Natl Acad Sci U S A* **90**, 4216 (May 1, 1993).
237. S. Popp, S. Waltering, C. Herbst, I. Moll, P. Boukamp, UV-B-type mutations and chromosomal imbalances indicate common pathways for the development of Merkel and skin squamous cell carcinomas. *Int J Cancer* **99**, 352 (May 20, 2002).
238. M. Van Gele *et al.*, Mutation analysis of P73 and TP53 in Merkel cell carcinoma. *Br J Cancer* **82**, 823 (Feb, 2000).
239. H. N. Ananthaswamy, W. E. Pierceall, Molecular alterations in human skin tumors. *Progress in clinical and biological research* **376**, 61 (1992).
240. J. Carr, R. M. Mackie, Point mutations in the N-ras oncogene in malignant melanoma and congenital naevi. *The British journal of dermatology* **131**, 72 (Jul, 1994).
241. M. Jafari *et al.*, Analysis of ras mutations in human melanocytic lesions: activation of the ras gene seems to be associated with the nodular type of human malignant melanoma. *Journal of cancer research and clinical oncology* **121**, 23 (1995).
242. A. Lassacher, E. Heitzer, H. Kerl, P. Wolf, p14ARF hypermethylation is common but INK4a-ARF locus or p53 mutations are rare in Merkel cell carcinoma. *J Invest Dermatol* **128**, 1788 (Jul, 2008).
243. H. Davies *et al.*, Mutations of the BRAF gene in human cancer. *Nature* **417**, 949 (Jun 27, 2002).
244. R. Houben *et al.*, Absence of classical MAP kinase pathway signalling in Merkel cell carcinoma. *J Invest Dermatol* **126**, 1135 (May, 2006).

245. S. Liu, T. Daa, K. Kashima, Y. Kondoh, S. Yokoyama, The Wnt-signaling pathway is not implicated in tumorigenesis of Merkel cell carcinoma. *J Cutan Pathol* **34**, 22 (Jan, 2007).
246. B. L. Swick, L. Ravdel, J. E. Fitzpatrick, W. A. Robinson, Merkel cell carcinoma: evaluation of KIT (CD117) expression and failure to demonstrate activating mutations in the C-KIT proto-oncogene - implications for treatment with imatinib mesylate. *Journal of cutaneous pathology* **34**, 324 (Apr, 2007).
247. M. M. Kennedy, K. Blessing, G. King, K. M. Kerr, Expression of bcl-2 and p53 in Merkel cell carcinoma. An immunohistochemical study. *The American Journal of dermatopathology* **18**, 273 (Jun, 1996).
248. A. Plettenberg, J. Pammer, E. Tschachler, Merkel cells and Merkel cell carcinoma express the BCL-2 proto-oncogene. *Experimental dermatology* **5**, 102 (Apr, 1996).
249. T. L. Benjamin, Polyoma virus: old findings and new challenges. *Virology* **289**, 167 (Oct 25, 2001).
250. I. K. Sariyer, A. S. Saribas, M. K. White, M. Safak, Infection by agnoprotein-negative mutants of polyomavirus JC and SV40 results in the release of virions that are mostly deficient in DNA content. *Virology journal* **8**, 255 (2011).
251. S. Nomura, G. Khoury, G. Jay, Subcellular localization of the simian virus 40 agnoprotein. *J Virol* **45**, 428 (Jan, 1983).
252. J. J. Carter *et al.*, Identification of an overprinting gene in Merkel cell polyomavirus provides evolutionary insight into the birth of viral genes. *Proc Natl Acad Sci U S A*, (Jul 11, 2013).
253. D. V. Pastrana *et al.*, Quantitation of human seroresponsiveness to Merkel cell polyomavirus. *PLoS Pathog* **5**, e1000578 (Sep, 2009).
254. H. Feng *et al.*, Cellular and viral factors regulating Merkel cell polyomavirus replication. *PLoS One* **6**, e22468 (2011).
255. G. J. Seo, L. H. Fink, B. O'Hara, W. J. Atwood, C. S. Sullivan, Evolutionarily conserved function of a viral microRNA. *J Virol* **82**, 9823 (Oct, 2008).
256. C. S. Sullivan, A. T. Grundhoff, S. Tevethia, J. M. Pipas, D. Ganem, SV40-encoded microRNAs regulate viral gene expression and reduce susceptibility to cytotoxic T cells. *Nature* **435**, 682 (Jun 2, 2005).
257. G. J. Seo, C. J. Chen, C. S. Sullivan, Merkel cell polyomavirus encodes a microRNA with the ability to autoregulate viral gene expression. *Virology* **383**, 183 (Jan 20, 2009).
258. S. Lee *et al.*, Identification and validation of a novel mature microRNA encoded by the Merkel cell polyomavirus in human Merkel cell carcinomas. *J Clin Virol* **52**, 272 (Nov, 2011).
259. C. Martel-Jantin *et al.*, Genetic variability and integration of Merkel cell polyomavirus in Merkel cell carcinoma. *Virology* **426**, 134 (May 10, 2012).
260. J. Cheng, O. Rozenblatt-Rosen, K. G. Paulson, P. Nghiem, J. A. Decaprio, Merkel cell polyomavirus large T antigen has growth-promoting and inhibitory activities. *J Virol* **87**, 6118 (Jun, 2013).
261. M. Schmitt, U. Wieland, A. Kreuter, M. Pawlita, C-terminal deletions of Merkel cell polyomavirus large T-antigen, a highly specific surrogate marker for virally induced malignancy. *Int J Cancer* **131**, 2863 (Dec 15, 2012).
262. A. Kassem *et al.*, Frequent detection of Merkel cell polyomavirus in human Merkel cell carcinomas and identification of a unique deletion in the VP1 gene. *Cancer Res* **68**, 5009 (Jul 1, 2008).

263. X. Liu *et al.*, Merkel cell polyomavirus large T antigen disrupts lysosome clustering by translocating human Vam6p from the cytoplasm to the nucleus. *J Biol Chem* **286**, 17079 (May 13, 2011).
264. N. Fischer, J. Brandner, F. Fuchs, I. Moll, A. Grundhoff, Detection of Merkel cell polyomavirus (MCPyV) in Merkel cell carcinoma cell lines: cell morphology and growth phenotype do not reflect presence of the virus. *Int J Cancer* **126**, 2133 (May 1, 2010).
265. A. Guastafierro *et al.*, Characterization of an early passage Merkel cell polyomavirus-positive Merkel cell carcinoma cell line, MS-1, and its growth in NOD scid gamma mice. *Journal of virological methods* **187**, 6 (Jan, 2013).
266. H. C. Laude *et al.*, Distinct merkel cell polyomavirus molecular features in tumour and non tumour specimens from patients with merkel cell carcinoma. *PLoS pathogens* **6**, e1001076 (2010).
267. X. Sastre-Garau *et al.*, Merkel cell carcinoma of the skin: pathological and molecular evidence for a causative role of MCV in oncogenesis. *The Journal of pathology* **218**, 48 (May, 2009).
268. U. Wieland, C. Mauch, A. Kreuter, T. Krieg, H. Pfister, Merkel cell polyomavirus DNA in persons without merkel cell carcinoma. *Emerging infectious diseases* **15**, 1496 (Sep, 2009).
269. Y. L. Tolstov *et al.*, Human Merkel cell polyomavirus infection II. MCV is a common human infection that can be detected by conformational capsid epitope immunoassays. *Int J Cancer* **125**, 1250 (Sep 15, 2009).
270. J. J. Carter *et al.*, Association of Merkel cell polyomavirus-specific antibodies with Merkel cell carcinoma. *J Natl Cancer Inst* **101**, 1510 (Nov 4, 2009).
271. A. Touze *et al.*, Generation of Merkel cell polyomavirus (MCV)-like particles and their application to detection of MCV antibodies. *J Clin Microbiol* **48**, 1767 (May, 2010).
272. L. Ren *et al.*, WU and KI polyomavirus present in the respiratory tract of children, but not in immunocompetent adults. *J Clin Virol* **43**, 330 (Nov, 2008).
273. S. Bialasiewicz, S. B. Lambert, D. M. Whiley, M. D. Nissen, T. P. Sloots, Merkel cell polyomavirus DNA in respiratory specimens from children and adults. *Emerg Infect Dis* **15**, 492 (Mar, 2009).
274. M. Loyo *et al.*, Quantitative detection of Merkel cell virus in human tissues and possible mode of transmission. *Int J Cancer* **126**, 2991 (Jun 15, 2010).
275. S. Bofill-Mas, J. Rodriguez-Manzano, B. Calgua, A. Carratala, R. Girones, Newly described human polyomaviruses Merkel cell, KI and WU are present in urban sewage and may represent potential environmental contaminants. *Virology journal* **7**, 141 (2010).
276. R. Houben *et al.*, Merkel cell polyomavirus-infected Merkel cell carcinoma cells require expression of viral T antigens. *J Virol* **84**, 7064 (Jul, 2010).
277. R. Houben *et al.*, An intact retinoblastoma protein-binding site in Merkel cell polyomavirus large T antigen is required for promoting growth of Merkel cell carcinoma cells. *Int J Cancer* **130**, 847 (Feb 15, 2012).
278. H. J. Kwun *et al.*, The minimum replication origin of merkel cell polyomavirus has a unique large T-antigen loading architecture and requires small T-antigen expression for optimal replication. *J Virol* **83**, 12118 (Dec, 2009).
279. M. Shuda *et al.*, T antigen mutations are a human tumor-specific signature for Merkel cell polyomavirus. *Proc. Natl. Acad. Sci. USA* **105**, 16272 (Oct 21, 2008).

280. P. Coursaget, M. Samimi, J. T. Nicol, C. Gardair, A. Touze, Human Merkel cell polyomavirus: virological background and clinical implications. *APMIS : acta pathologica, microbiologica, et immunologica Scandinavica* **121**, 755 (Aug, 2013).
281. M. Shuda *et al.*, Human merkel cell polyomavirus infection I. MCV T antigen expression in merkel cell carcinoma, lymphoid tissues and lymphoid tumors. *Int. J. Cancer* **doi:10.1002/ijc.24510**, (2009).
282. A. Touze *et al.*, High levels of antibodies against merkel cell polyomavirus identify a subset of patients with merkel cell carcinoma with better clinical outcome. *Journal of clinical oncology : official journal of the American Society of Clinical Oncology* **29**, 1612 (Apr 20, 2011).
283. K. Bhatia, J. J. Goedert, R. Modali, L. Preiss, L. W. Ayers, Immunological detection of viral large T antigen identifies a subset of Merkel cell carcinoma tumors with higher viral abundance and better clinical outcome. *Int J Cancer* **127**, 1493 (Sep 1, 2010).
284. M. Van Gele *et al.*, Gene-expression profiling reveals distinct expression patterns for Classic versus Variant Merkel cell phenotypes and new classifier genes to distinguish Merkel cell from small-cell lung carcinoma. *Oncogene* **23**, 2732 (Apr 8, 2004).
285. D. N. Carney *et al.*, Establishment and identification of small cell lung cancer cell lines having classic and variant features. *Cancer Res* **45**, 2913 (Jun, 1985).
286. A. F. Gazdar, D. N. Carney, M. M. Nau, J. D. Minna, Characterization of variant subclasses of cell lines derived from small cell lung cancer having distinctive biochemical, morphological, and growth properties. *Cancer Res* **45**, 2924 (Jun, 1985).
287. J. H. Leonard, P. Dash, P. Holland, J. H. Kearsley, J. R. Bell, Characterisation of four Merkel cell carcinoma adherent cell lines. *Int J Cancer* **60**, 100 (Jan 3, 1995).
288. S. T. Rosen *et al.*, Establishment and characterization of a neuroendocrine skin carcinoma cell line. *Laboratory investigation; a journal of technical methods and pathology* **56**, 302 (Mar, 1987).
289. K. Krasagakis *et al.*, Growth and characterization of a cell line from a human primary neuroendocrine carcinoma of the skin (Merkel cell carcinoma) in culture and as xenograft. *J Cell Physiol* **187**, 386 (Jun, 2001).
290. Y. L. Tolstov *et al.*, Human merkel cell polyomavirus infection II. MCV is a common human infection that can be detected by conformational capsid epitope immunoassays. *Int. J. Cancer* **doi:10.1002/ijc.24509**, (2009).
291. J. K. Chan *et al.*, Cytokeratin 20 immunoreactivity distinguishes Merkel cell (primary cutaneous neuroendocrine) carcinomas and salivary gland small cell carcinomas from small cell carcinomas of various sites. *The American journal of surgical pathology* **21**, 226 (Feb, 1997).
292. W. Goessling, P. H. McKee, R. J. Mayer, Merkel cell carcinoma. *J Clin Oncol* **20**, 588 (Jan 15, 2002).
293. A. J. Hanly, G. W. Elgart, M. Jorda, J. Smith, M. Nadji, Analysis of thyroid transcription factor-1 and cytokeratin 20 separates merkel cell carcinoma from small cell carcinoma of lung. *J Cutan Pathol* **27**, 118 (Mar, 2000).
294. X. Sastre-Garau *et al.*, Merkel cell carcinoma of the skin: pathological and molecular evidence for a causative role of MCV in oncogenesis. *J. Pathol.* **218**, 48 (May, 2009).
295. T. Nakamura *et al.*, Nuclear localization of Merkel cell polyomavirus large T antigen in Merkel cell carcinoma. *Virology* **398**, 273 (Mar 15, 2010).

296. H. C. Laude *et al.*, Distinct merkel cell polyomavirus molecular features in tumour and non tumour specimens from patients with merkel cell carcinoma. *PLoS Pathog* **6**, (2010).
297. R. Houben *et al.*, An intact retinoblastoma protein-binding site in Merkel cell polyomavirus large T antigen is required for promoting growth of Merkel cell carcinoma cells. *Int J Cancer*, (Mar 16, 2011).
298. C. T. Wetzels *et al.*, Ultrastructural proof of polyomavirus in Merkel cell carcinoma tumour cells and its absence in small cell carcinoma of the lung. *PLoS One* **4**, e4958 (2009).
299. O. Jansen *et al.*, Endovascular therapy of arteriovenous fistulae with electrolytically detachable coils. *Neuroradiology* **41**, 951 (Dec, 1999).
300. M. P. Jansen *et al.*, Morphologically normal, CD30-negative B-lymphocytes with chromosome aberrations in classical Hodgkin's disease: the progenitor cell of the malignant clone? *J Pathol* **189**, 527 (Dec, 1999).
301. B. Jansen *et al.*, Farnesylthiosalicylic acid inhibits the growth of human Merkel cell carcinoma in SCID mice. *J Mol Med (Berl)* **77**, 792 (Nov, 1999).
302. H. Schlagbauer-Wadl *et al.*, Bcl-2 antisense oligonucleotides (G3139) inhibit Merkel cell carcinoma growth in SCID mice. *J Invest Dermatol* **114**, 725 (Apr, 2000).
303. J. H. Hooijberg *et al.*, Antifolate resistance mediated by the multidrug resistance proteins MRP1 and MRP2. *Cancer Res* **59**, 2532 (Jun 1, 1999).
304. M. Gerritsen, J. A. Jansen, J. A. Lutterman, Performance of subcutaneously implanted glucose sensors for continuous monitoring. *Neth J Med* **54**, 167 (Apr, 1999).
305. R. M. Benbow, J. Zhao, D. D. Larson, On the nature of origins of DNA replication in eukaryotes. *Bioessays* **14**, 661 (Oct, 1992).
306. C. N. Cole, S. D. Conzen, *Polyomavirinae: the viruses and their replication, p.2141-2174. In D.M. Knipe and P.M. Howley (ed.), Fields Virology* K. D. Field BN, Howley PM, Ed., (Lippincott-Raven Publishers, Piladelphia, PA, 2001), pp. 2141-2174.
307. D. Rio, A. Robbins, R. Myers, R. Tjian, Regulation of simian virus 40 early transcription in vitro by a purified tumor antigen. *Proc. Natl. Acad. Sci. USA* **77**, 5706 (Oct, 1980).
308. K. Cowan, P. Tegtmeyer, D. D. Anthony, Relationship of replication and transcription of Simian Virus 40 DNA. *Proc. Natl. Acad. Sci. USA* **70**, 1927 (Jul, 1973).
309. R. Tjian, T antigen binding and the control of SV40 gene expression. *Cell* **26**, 1 (Oct, 1981).
310. R. M. Myers, D. C. Rio, A. K. Robbins, R. Tjian, SV40 gene expression is modulated by the cooperative binding of T antigen to DNA. *Cell* **25**, 373 (Aug, 1981).
311. S. L. Spence, J. M. Pipas, Simian virus 40 large T antigen host range domain functions in virion assembly. *J. Virol.* **68**, 4227 (Jul, 1994).
312. S. L. Spence, J. M. Pipas, SV40 large T antigen functions at two distinct steps in virion assembly. *Virology* **204**, 200 (Oct, 1994).
313. E. Fanning, R. Knippers, Structure and function of simian virus 40 large tumor antigen. *Annu. Rev. Biochem.* **61**, 55 (1992).
314. A. Srinivasan *et al.*, The amino-terminal transforming region of simian virus 40 large T and small t antigens functions as a J domain. *Mol. Cell. Biol.* **17**, 4761 (Aug, 1997).
315. N. Bouck, N. Beales, T. Shenk, P. Berg, G. di Mayorca, New region of the simian virus 40 genome required for efficient viral transformation. *Proc. Natl. Acad. Sci. USA* **75**, 2473 (May, 1978).

316. W. C. Hahn *et al.*, Enumeration of the simian virus 40 early region elements necessary for human cell transformation. *Mol. Cell. Biol.* **22**, 2111 (Apr, 2002).
317. L. S. Chang, S. Pan, M. M. Pater, G. Di Mayorca, Differential requirement for SV40 early genes in immortalization and transformation of primary rat and human embryonic cells. *Virology* **146**, 246 (Oct 30, 1985).
318. L. S. Chang, M. M. Pater, N. I. Hutchinson, G. di Mayorca, Transformation by purified early genes of simian virus 40. *Virology* **133**, 341 (Mar, 1984).
319. A. Porras *et al.*, A novel simian virus 40 early-region domain mediates transactivation of the cyclin A promoter by small-t antigen and is required for transformation in small-t antigen-dependent assays. *J. Virol.* **70**, 6902 (Oct, 1996).
320. C. Prins, R. J. Frisque, JC virus T' proteins encoded by alternatively spliced early mRNAs enhance T antigen-mediated viral DNA replication in human cells. *J. Neurovirol.* **7**, 250 (Jun, 2001).
321. S. Deb, A. L. DeLucia, A. Koff, S. Tsui, P. Tegtmeyer, The adenine-thymine domain of the simian virus 40 core origin directs DNA bending and coordinately regulates DNA replication. *Mol. Cell. Biol.* **6**, 4578 (Dec, 1986).
322. G. Meinke *et al.*, The crystal structure of the SV40 T-antigen origin binding domain in complex with DNA. *PLoS Biol.* **5**, e23 (Feb, 2007).
323. D. Li *et al.*, Structure of the replicative helicase of the oncoprotein SV40 large tumour antigen. *Nature* **423**, 512 (May 29, 2003).
324. M. C. San Martin, C. Gruss, J. M. Carazo, Six molecules of SV40 large T antigen assemble in a propeller-shaped particle around a channel. *J. Mol. Biol.* **268**, 15 (Apr 25, 1997).
325. G. Meinke, P. A. Bullock, A. Bohm, Crystal structure of the simian virus 40 large T-antigen origin-binding domain. *J. Virol.* **80**, 4304 (May, 2006).
326. A. Kumar *et al.*, Model for T-antigen-dependent melting of the simian virus 40 core origin based on studies of the interaction of the beta-hairpin with DNA. *J. Virol.* **81**, 4808 (May, 2007).
327. H. Liu, Y. Shi, X. S. Chen, A. Warshel, Simulating the electrostatic guidance of the vectorial translocations in hexameric helicases and translocases. *Proc. Natl. Acad. Sci. USA* **106**, 7449 (May 5, 2009).
328. X. Jiang *et al.*, Structural mechanism of RPA loading on DNA during activation of a simple pre-replication complex. *EMBO J.* **25**, 5516 (Nov 29, 2006).
329. M. Valle, X. S. Chen, L. E. Donate, E. Fanning, J. M. Carazo, Structural basis for the cooperative assembly of large T antigen on the origin of replication. *J. Mol. Biol.* **357**, 1295 (Apr 7, 2006).
330. C. Prives *et al.*, DNA sequence requirements for replication of polyomavirus DNA in vivo and in vitro. *Mol. Cell. Biol.* **7**, 3694 (Oct, 1987).
331. A. Cowie, R. Kamen, Multiple binding sites for polyomavirus large T antigen within regulatory sequences of polyomavirus DNA. *J. Virol.* **52**, 750 (Dec, 1984).
332. A. Cowie, R. Kamen, Guanine nucleotide contacts within viral DNA sequences bound by polyomavirus large T antigen. *J. Virol.* **57**, 505 (Feb, 1986).
333. A. Scheller, C. Prives, Simian virus 40 and polyomavirus large tumor antigens have different requirements for high-affinity sequence-specific DNA binding. *J. Virol.* **54**, 532 (May, 1985).

334. K. S. Campbell *et al.*, DnaJ/hsp40 chaperone domain of SV40 large T antigen promotes efficient viral DNA replication. *Genes Dev.* **11**, 1098 (May 1, 1997).
335. P. Emsley, K. Cowtan, Coot: model-building tools for molecular graphics. *Acta Crystallogr. D Biol. Crystallogr.* **60**, 2126 (Dec, 2004).
336. J. A. Borowiec, J. Hurwitz, Localized melting and structural changes in the SV40 origin of replication induced by T-antigen. *EMBO J.* **7**, 3149 (Oct, 1988).
337. Y. C. Peng, N. H. Acheson, Polyomavirus large T antigen binds cooperatively to its multiple binding sites in the viral origin of DNA replication. *J. Virol.* **72**, 7330 (Sep, 1998).
338. S. J. Triezenberg, W. R. Folk, Essential nucleotides in the polyomavirus origin region. *J. Virol.* **51**, 437 (Aug, 1984).
339. I. Weichselbraun, G. Haider, E. Wintersberger, Optimal replication of plasmids carrying polyomavirus origin regions requires two high-affinity binding sites for large T antigen. *J. Virol.* **63**, 961 (Feb, 1989).
340. F. B. Dean *et al.*, Simian virus 40 (SV40) DNA replication: SV40 large T antigen unwinds DNA containing the SV40 origin of replication. *Proc. Natl. Acad. Sci. USA* **84**, 16 (Jan, 1987).
341. S. Deb *et al.*, The T-antigen-binding domain of the simian virus 40 core origin of replication. *J. Virol.* **61**, 2143 (Jul, 1987).
342. W. S. Joo *et al.*, Purification of the simian virus 40 (SV40) T antigen DNA-binding domain and characterization of its interactions with the SV40 origin. *J. Virol.* **71**, 3972 (May, 1997).
343. F. U. Hartl, Molecular chaperones in cellular protein folding. *Nature* **381**, 571 (Jun 13, 1996).
344. E. T. Sawai, J. S. Butel, Association of a cellular heat shock protein with simian virus 40 large T antigen in transformed cells. *J. Virol.* **63**, 3961 (Sep, 1989).
345. Q. Sheng *et al.*, The DnaJ domain of polyomavirus large T antigen is required to regulate Rb family tumor suppressor function. *J. Virol.* **71**, 9410 (Dec, 1997).
346. E. J. Enemark, G. Chen, D. E. Vaughn, A. Stenlund, L. Joshua-Tor, Crystal structure of the DNA binding domain of the replication initiation protein E1 from papillomavirus. *Mol. Cell* **6**, 149 (Jul, 2000).
347. E. J. Enemark, A. Stenlund, L. Joshua-Tor, Crystal structures of two intermediates in the assembly of the papillomavirus replication initiation complex. *EMBO J.* **21**, 1487 (Mar 15, 2002).
348. M. C. Chen, D. Redenius, F. Osati-Ashtiani, M. M. Fluck, Enhancer-mediated role for polyomavirus middle T/small T in DNA replication. *J. Virol.* **69**, 326 (Jan, 1995).
349. C. Cicala *et al.*, Simian virus 40 small-t antigen stimulates viral DNA replication in permissive monkey cells. *J. Virol.* **68**, 3138 (May, 1994).
350. V. Janssens, J. Goris, Protein phosphatase 2A: a highly regulated family of serine/threonine phosphatases implicated in cell growth and signalling. *Biochem. J.* **353**, 417 (Feb 1, 2001).
351. S. I. Yang *et al.*, Control of protein phosphatase 2A by simian virus 40 small-t antigen. *Mol. Cell. Biol.* **11**, 1988 (Apr, 1991).
352. C. Prives, The replication functions of SV40 T antigen are regulated by phosphorylation. *Cell* **61**, 735 (Jun 1, 1990).

353. K. A. Whalen, R. de Jesus, J. A. Kean, B. S. Schaffhausen, Genetic analysis of the polyomavirus DnaJ domain. *J. Virol.* **79**, 9982 (Aug, 2005).
354. J. S. Butel, Viral carcinogenesis: revelation of molecular mechanisms and etiology of human disease. *Carcinogenesis* **21**, 405 (Mar, 2000).
355. M. E. McLaughlin-Drubin, K. Munger, Viruses associated with human cancer. *Biochim Biophys Acta* **1782**, 127 (Mar, 2008).
356. D. Hanahan, R. A. Weinberg, Hallmarks of cancer: the next generation. *Cell* **144**, 646 (Mar 4, 2011).
357. W. C. Hahn *et al.*, Creation of human tumour cells with defined genetic elements. *Nature* **400**, 464 (Jul 29, 1999).
358. S. E. Artandi, R. A. DePinho, Telomeres and telomerase in cancer. *Carcinogenesis* **31**, 9 (Jan, 2010).
359. J. W. Shay, W. E. Wright, Ageing and cancer: the telomere and telomerase connection. *Novartis Found Symp* **235**, 116 (2001).
360. J. A. DeCaprio, How the Rb tumor suppressor structure and function was revealed by the study of Adenovirus and SV40. *Virology* **384**, 274 (Feb 20, 2009).
361. L. J. Hofseth, S. P. Hussain, C. C. Harris, p53: 25 years after its discovery. *Trends Pharmacol Sci* **25**, 177 (Apr, 2004).
362. A. Dahiya, M. R. Gavin, R. X. Luo, D. C. Dean, Role of the LXCXE binding site in Rb function. *Mol Cell Biol* **20**, 6799 (Sep, 2000).
363. H. M. Chan, L. Smith, N. B. La Thangue, Role of LXCXE motif-dependent interactions in the activity of the retinoblastoma protein. *Oncogene* **20**, 6152 (Sep 27, 2001).
364. W. Lilyestrom, M. G. Klein, R. Zhang, A. Joachimiak, X. S. Chen, Crystal structure of SV40 large T-antigen bound to p53: interplay between a viral oncoprotein and a cellular tumor suppressor. *Genes Dev* **20**, 2373 (Sep 1, 2006).
365. U. S. Cho *et al.*, Structural basis of PP2A inhibition by small t antigen. *PLoS Biol* **5**, e202 (Aug, 2007).
366. J. Li *et al.*, Merkel Cell Polyomavirus Large T Antigen Disrupts Host Genomic Integrity and Inhibits Cellular Proliferation. *J Virol*, (Jun 12, 2013).
367. R. Arora *et al.*, Survivin is a therapeutic target in Merkel cell carcinoma. *Sci Transl Med* **4**, 133ra56 (May 9, 2012).
368. L. Busino, M. Chiesa, G. F. Draetta, M. Donzelli, Cdc25A phosphatase: combinatorial phosphorylation, ubiquitylation and proteolysis. *Oncogene* **23**, 2050 (Mar 15, 2004).
369. R. Koyama-Nasu *et al.*, The critical role of cyclin D2 in cell cycle progression and tumorigenicity of glioblastoma stem cells. *Oncogene*, (Sep 10, 2012).
370. C. Bolitho, M. A. Hahn, R. C. Baxter, D. J. Marsh, The chemokine CXCL1 induces proliferation in epithelial ovarian cancer cells by transactivation of the epidermal growth factor receptor. *Endocr Relat Cancer* **17**, 929 (Dec, 2010).
371. Y. Itoh *et al.*, IL-8 promotes cell proliferation and migration through metalloproteinase-cleavage proHB-EGF in human colon carcinoma cells. *Cytokine* **29**, 275 (Mar 21, 2005).
372. A. Li, S. Dubey, M. L. Varney, B. J. Dave, R. K. Singh, IL-8 directly enhanced endothelial cell survival, proliferation, and matrix metalloproteinases production and regulated angiogenesis. *J Immunol* **170**, 3369 (Mar 15, 2003).
373. M. Jovanovic, I. Stefanoska, L. Radojcic, L. Vicovac, Interleukin-8 (CXCL8) stimulates trophoblast cell migration and invasion by increasing levels of matrix metalloproteinase (MMP)2 and MMP9 and integrins alpha5 and beta1. *Reproduction* **139**, 789 (Apr, 2010).

374. M. Y. Shiau *et al.*, Human papillomavirus up-regulates MMP-2 and MMP-9 expression and activity by inducing interleukin-8 in lung adenocarcinomas. *PLoS One* **8**, e54423 (2013).
375. R. Sears *et al.*, Multiple Ras-dependent phosphorylation pathways regulate Myc protein stability. *Genes Dev* **14**, 2501 (Oct 1, 2000).
376. V. K. Rajasekhar *et al.*, Oncogenic Ras and Akt signaling contribute to glioblastoma formation by differential recruitment of existing mRNAs to polysomes. *Mol Cell* **12**, 889 (Oct, 2003).
377. P. T. Wan *et al.*, Mechanism of activation of the RAF-ERK signaling pathway by oncogenic mutations of B-RAF. *Cell* **116**, 855 (Mar 19, 2004).
378. N. Hay, N. Sonenberg, Upstream and downstream of mTOR. *Genes Dev* **18**, 1926 (Aug 15, 2004).
379. M. Luca *et al.*, Expression of interleukin-8 by human melanoma cells up-regulates MMP-2 activity and increases tumor growth and metastasis. *Am J Pathol* **151**, 1105 (Oct, 1997).
380. M. Kohli, T. J. Jorgensen, The influence of SV40 immortalization of human fibroblasts on p53-dependent radiation responses. *Biochem Biophys Res Commun* **257**, 168 (Apr 2, 1999).
381. M. N. Ruesch, L. A. Laimins, Initiation of DNA synthesis by human papillomavirus E7 oncoproteins is resistant to p21-mediated inhibition of cyclin E-cdk2 activity. *J Virol* **71**, 5570 (Jul, 1997).
382. T. Riley, E. Sontag, P. Chen, A. Levine, Transcriptional control of human p53-regulated genes. *Nat Rev Mol Cell Biol* **9**, 402 (May, 2008).
383. J. A. Bernal, A. Hernandez, p53 stabilization can be uncoupled from its role in transcriptional activation by loss of PTTG1/securin. *J Biochem* **141**, 737 (May, 2007).
384. J. A. Bernal *et al.*, Human securin interacts with p53 and modulates p53-mediated transcriptional activity and apoptosis. *Nat Genet* **32**, 306 (Oct, 2002).
385. S. P. Seguin *et al.*, High-throughput screening identifies a bisphenol inhibitor of SV40 large T antigen ATPase activity. *Journal of biomolecular screening* **17**, 194 (Feb, 2012).
386. A. Czarna *et al.*, Robust generation of lead compounds for protein-protein interactions by computational and MCR chemistry: p53/Hdm2 antagonists. *Angewandte Chemie* **49**, 5352 (Jul 19, 2010).
387. G. M. Popowicz *et al.*, Structures of low molecular weight inhibitors bound to MDMX and MDM2 reveal new approaches for p53-MDMX/MDM2 antagonist drug discovery. *Cell Cycle* **9**, 1104 (Mar 15, 2010).
388. R. Houben *et al.*, Merkel cell polyomavirus-infected Merkel cell carcinoma cells require expression of viral T antigens. *J Virol* **84**, 7064 (Jul, 2010).
389. T. Nakahara *et al.*, YM155, a novel small-molecule survivin suppressant, induces regression of established human hormone-refractory prostate tumor xenografts. *Cancer Res* **67**, 8014 (Sep 1, 2007).
390. M. W. Pfaffl, A new mathematical model for relative quantification in real-time RT-PCR. *Nucleic Acids Res* **29**, e45 (May 1, 2001).
391. L. Zhao *et al.*, Bayesian hierarchical changepoint methods in modeling the tumor growth profiles in xenograft experiments. *Clinical cancer research : an official journal of the American Association for Cancer Research* **17**, 1057 (Mar 1, 2011).
392. K. Ohtani, J. DeGregori, J. R. Nevins, Regulation of the cyclin E gene by transcription factor E2F1. *Proc Natl Acad Sci U S A* **92**, 12146 (Dec 19, 1995).

393. T. Iwasa *et al.*, Marked anti-tumour activity of the combination of YM155, a novel survivin suppressant, and platinum-based drugs. *British journal of cancer* **103**, 36 (Jun 29, 2010).
394. S. P. Tu *et al.*, Suppression of survivin expression inhibits in vivo tumorigenicity and angiogenesis in gastric cancer. *Cancer Res* **63**, 7724 (Nov 15, 2003).
395. D. J. Klionsky, A. M. Cuervo, P. O. Seglen, Methods for monitoring autophagy from yeast to human. *Autophagy* **3**, 181 (May-Jun, 2007).
396. G. Sarek *et al.*, Reactivation of the p53 pathway as a treatment modality for KSHV-induced lymphomas. *J Clin Invest* **117**, 1019 (Apr, 2007).
397. C. E. Petre, S. H. Sin, D. P. Dittmer, Functional p53 signaling in Kaposi's sarcoma-associated herpesvirus lymphomas: implications for therapy. *J Virol* **81**, 1912 (Feb, 2007).
398. H. Einsele, Bortezomib. *Recent results in cancer research. Fortschritte der Krebsforschung. Progres dans les recherches sur le cancer* **184**, 173 (2010).
399. R. LeBlanc *et al.*, Proteasome inhibitor PS-341 inhibits human myeloma cell growth in vivo and prolongs survival in a murine model. *Cancer Res* **62**, 4996 (Sep 1, 2002).
400. T. Nakahara *et al.*, Broad spectrum and potent antitumor activities of YM155, a novel small-molecule survivin suppressant, in a wide variety of human cancer cell lines and xenograft models. *Cancer science* **102**, 614 (Mar, 2011).
401. G. Ambrosini, C. Adida, D. C. Altieri, A novel anti-apoptosis gene, survivin, expressed in cancer and lymphoma. *Nature medicine* **3**, 917 (Aug, 1997).
402. H. Takeuchi, D. L. Morton, D. Elashoff, D. S. Hoon, Survivin expression by metastatic melanoma predicts poor disease outcome in patients receiving adjuvant polyvalent vaccine. *Int J Cancer* **117**, 1032 (Dec 20, 2005).
403. J. Kim, J. M. McNiff, Nuclear expression of survivin portends a poor prognosis in Merkel cell carcinoma. *Modern pathology : an official journal of the United States and Canadian Academy of Pathology, Inc* **21**, 764 (Jun, 2008).
404. S. Pina-Oviedo *et al.*, Effects of JC virus infection on anti-apoptotic protein survivin in progressive multifocal leukoencephalopathy. *Am J Pathol* **170**, 1291 (Apr, 2007).
405. Y. Jiang, H. I. Saavedra, M. P. Holloway, G. Leone, R. A. Altura, Aberrant regulation of survivin by the RB/E2F family of proteins. *J Biol Chem* **279**, 40511 (Sep 24, 2004).
406. D. Raj, T. Liu, G. Samadashwily, F. Li, D. Grossman, Survivin repression by p53, Rb and E2F2 in normal human melanocytes. *Carcinogenesis* **29**, 194 (Jan, 2008).
407. D. C. Altieri, Survivin in apoptosis control and cell cycle regulation in cancer. *Prog Cell Cycle Res* **5**, 447 (2003).
408. R. Zhang *et al.*, Survivin knockdown by short hairpin RNA abrogates the growth of human hepatocellular carcinoma xenografts in nude mice. *Cancer gene therapy* **17**, 275 (Apr, 2010).
409. G. Kroemer, G. Marino, B. Levine, Autophagy and the integrated stress response. *Molecular cell* **40**, 280 (Oct 22, 2010).
410. A. N. Santhanam *et al.*, Role of 3'UTRs in the translation of mRNAs regulated by oncogenic eIF4E--a computational inference. *PLoS One* **4**, e4868 (2009).
411. B. Lemos, P. Nghiem, Merkel cell carcinoma: more deaths but still no pathway to blame. *J Invest Dermatol* **127**, 2100 (Sep, 2007).

412. S. T. Rosen *et al.*, Establishment and characterization of a neuroendocrine skin carcinoma cell line. *Laboratory investigation; a journal of technical methods and pathology* **56**, 302 (Mar, 1987).
413. L. D. Shultz *et al.*, Human lymphoid and myeloid cell development in NOD/LtSz-scid IL2R gamma null mice engrafted with mobilized human hemopoietic stem cells. *J Immunol* **174**, 6477 (May 15, 2005).
414. T. Y. Eng *et al.*, A comprehensive review of the treatment of Merkel cell carcinoma. *American journal of clinical oncology* **30**, 624 (Dec, 2007).
415. K. Yamanaka *et al.*, Antitumor activity of YM155, a selective small-molecule survivin suppressant, alone and in combination with docetaxel in human malignant melanoma models. *Clinical cancer research : an official journal of the American Association for Cancer Research* **17**, 5423 (Aug 15, 2011).
416. T. Satoh *et al.*, Phase I study of YM155, a novel survivin suppressant, in patients with advanced solid tumors. *Clinical cancer research : an official journal of the American Association for Cancer Research* **15**, 3872 (Jun 1, 2009).
417. T. Minematsu *et al.*, Pharmacokinetics, distribution and excretion of YM155 monobromide, a novel small-molecule survivin suppressant, in male and pregnant or lactating female rats. *Biopharmaceutics & drug disposition* **33**, 160 (Apr, 2012).